

**University of Strathclyde,
Department of Electronic and Electrical Engineering,
Glasgow, United Kingdom**

Development of an Ambient Temperature Alkaline Electrolyser
for Integrating with the Electrical Grid and Renewable Energy
Systems

By

Tamunosaki Graham Douglas

In partial fulfilment for the award of Doctor of Philosophy

April 2013

Supervised by: Prof. Andrew Cruden

Copyright Statement

This thesis is the result of the author's original research. It has been composed by the author and has not been previously submitted for examination which has led to the award of a degree.

The copyright of this thesis belongs to the author under the terms of the United Kingdom Copyright Acts as qualified by University of Strathclyde Regulation 3.50. Due acknowledgment must always be made of the use of any material contained in, or derived from, this thesis.

22/04/2013

X Tamunosaki Graham Dou...

Tamunosaki Graham Douglas
PhD

Signed Signed by: Tamunosaki Graham Douglas

Date 22nd April 2013

Acknowledgments

I would like to thank Prof. Andrew Cruden for the guidance, criticism, and supervision during this PhD study. Also, my thanks go to Prof. Peter Hall, Prof. David Infield and Dr. Amitava Roy for their useful advice which contributed to shape this thesis.

A special thank you to Mr. David Daubney of the EEE workshop, who was directly involved in the fabrication of the cell that was used for this research. “Without you this wouldn’t have happened”.

I also appreciate my PhD colleague, Mahdi Kiaee for the useful conversation that contributed to identify the novelty of this work.

I appreciate the financial support for this project from the UK EPSRC SuperGen-Delivery of Sustainable Hydrogen (DOSH2) consortium. <http://supergendosh2.wordpress.com/>

Most of all, I dedicate this thesis to Sylvia, for the encouragements and love. Also, a heartfelt gratitude to my family and friends for the love, support and encouragement during this period of my PhD study.

Abstract

Electrolytic hydrogen production from an alkaline electrolyser is considered a promising energy storage technology that integrates renewable energy sources such as wind, solar, wave and tidal energy with the electrical grid. Hydrogen energy systems consisting of conventional temperature (at 80°C) alkaline electrolysers have been widely demonstrated by industry and their collaborators in academic institutions to minimise dependence on fossil fuels especially in the transport sector and thus help to ultimately reduce carbon emissions. However, the conventional temperature alkaline electrolysers are limited in terms of reliability, dynamic and fast-response operation when powered by renewable energy sources. Also, cost and safety concerns are barriers to decentralise and distribute the technology. As a result of this adds to the scepticism about the feasibility of a so called future 'hydrogen economy'.

In this PhD study, an ambient temperature (at 23°C) alkaline electrolyser was investigated as part of a future integrated renewable energy system and compared with existing conventional temperature alkaline electrolyser system. The ambient temperature alkaline electrolyser is identified as a low-cost, reliable, and safe technology that is suitable for dynamic, intermittent, continuous and fast-response operation with renewable energy sources and the electrical grid. This also means the ambient temperature alkaline electrolyser is capable of wider operational range at 5%-100% of rated electrical power and faster response time in less than 1 second when powered by renewable energy sources. The auxiliary equipment are significantly reduced in the operation of ambient temperature alkaline electrolyser thereby reducing the cost of hydrogen and oxygen production and also making the technology reliable and safe for portable, stationary, transport and renewable energy system applications.

Equally important is the capability of the alkaline electrolyser to efficiently convert electricity and water into hydrogen and oxygen. This is demonstrated by DC polarisation and Electrochemical Impedance Spectroscopy (EIS) analysis of the alkaline electrolyser. EIS is used to determine resistance and capacitance which are

basic electrical circuit elements of the alkaline electrolyser, and thus provides useful knowledge to the electrical engineer who is interested in modelling and optimisation of alkaline electrolysers as electrical loads.

Additionally, the thesis provides a systematic approach to fabricating and characterising the electrodes for the ambient temperature alkaline electrolyser that is powered directly by either renewable energy sources such as wind turbine or the electrical grid. As such, EIS has become invaluable to characterise the electrodes based on exchange current density and corrosion rates. The objective is not only to enhance energy efficiency of the cell but to develop low-cost and durable electrodes.

During this PhD work the electrodes have been characterised in an ‘open-system’ and flow-cell alkaline electrolyser. The ‘open-system’ simulates the monopolar tank-type alkaline electrolyser cell, and consists of stainless steel coated with nickel and molybdenum (SS-Ni-Mo) electro-catalyst that enhances the efficiencies for hydrogen and oxygen production. The flow-cell alkaline electrolyser has the unique advantage of modularity because the electrodes can be configured in either monopolar or bi-polar filter press arrangements. The flow-cell alkaline electrolyser is manifolded in order to capture the hydrogen and oxygen product gases that can be subsequently utilised in an alkaline fuel cell to essentially generate back electricity. It is demonstrated in this research work that, through electro-catalysis, appropriate cell design and good electrochemical engineering, efficiency and durability of the ambient temperature alkaline electrolyser can be enhanced by about 13 % and 50 % respectively.

Preface

This thesis is organised into nine (9) chapters. Chapter 1 deals with an analysis of existing energy sources in the UK and identifies the need to develop alternative and sustainable energy sources. It attempts to identify the important role of electrolytic hydrogen within the UK energy mix and its impact on economic growth. For this reason the benefits of hydrogen and oxygen energy systems are described. However, the technical challenges of conventional temperature alkaline electrolyser are identified and highlighted as the scope for this research.

Chapter 2 describes the basic principles of thermodynamics and electrochemistry of the alkaline electrolyser. It also provides an introduction to electrochemical impedance spectroscopy (EIS) of alkaline electrolysers. The ambient temperature alkaline electrolyser was compared with the conventional temperature alkaline electrolyser based on operational system, efficiency and cost, thereby identifying the scope to develop a low-cost, dynamic, robust and fast-response alkaline electrolyser that can be integrated directly with renewable energy sources. The basic principles of advanced electrolyser cell design and electrode kinetics are also treated in this Chapter.

Chapter 3 deals with comparing the electrodes in an ambient temperature and conventional temperature alkaline electrolysers. It demonstrates methods of determining electrical resistance, exchange current density, and corrosion rates of the electrode.

Chapters 4, 5 and 6 demonstrate systematic approaches to develop and characterise the electrodes for the ambient temperature alkaline electrolyser that is powered directly by either renewable energy sources or the electrical grid.

Chapter 7 describes the construction of monopolar flow-cell and multi-cell alkaline electrolysers that were developed by the author. The experience of characterising the electrode in the flow-cell and multi-cell alkaline electrolysers is also discussed in this chapter.

Chapter 8 deals with modelling of cell overvoltages and corrosion rates of the electrode in the ambient temperature and conventional temperature alkaline electrolyzers.

Chapter 9 deals with general conclusion of the thesis as well as highlighting the author's novel contributions to the field of the alkaline electrolyser.

Table of Contents

Title Page.....	i
Copyright Statement.....	ii
Acknowledgments.....	iii
Abstract.....	iv
Preface.....	vi
Table of Contents.....	viii
List of Figures.....	xiii
List of Tables.....	xxii
Nomenclature.....	xxvi

1.0 Hydrogen Production by Water Electrolysis: The way forward towards a Sustainable UK Energy Economy1

1.1 An Economic Case for Electrolytic Hydrogen.....	1
1.2 Alkaline Electrolysers for Decentralised and Distributed Generation of Renewable Energy.....	9
1.3 Sizing of the Electrolysers and Hydrogen Production Cost.....	14
1.4 Nuclear-based Hydrogen from Alkaline Electrolysers.....	15
1.5 Comparison of Alkaline Electrolyser and PEM Electrolyser for Dynamic Operation with Renewable Energy Systems.....	17
1.6 The Strategy for Developing Highly Efficient Alkaline Electrolyser Cells and Objectives of PhD Research.....	19
1.6.1 Objectives of PhD Research.....	23

2.0 Recent Progress in the Research and Development of Alkaline Electrolyser Technology and Review of Literature.....25

2.1 Basics of Alkaline Electrolyser Technology.....	25
2.2 Comparison of Efficiency of the Ambient and Conventional Temperature Alkaline Electrolysers.....	27
2.3 Electrical Double-Layer Capacitance and Electrode Kinetics.....	33
2.3.1 Hydrogen Evolution Reaction (<i>HER</i>) and Oxygen Evolution Reaction (<i>OER</i>) Mechanisms on the Electrode.....	35
2.3.2 Corrosion of the Electrode during Electrolysis and open-circuit.....	39
2.4 Introduction to Electrochemical Impedance Spectroscopy (EIS) of Alkaline Electrolysers.....	39
2.5 Comparison of Operational Costs for the Ambient and Conventional Temperature Alkaline Electrolysers.....	44
2.6 Cell Design, Configuration and Geometry.....	56
2.6.1 Cell Geometry.....	59
2.7 Efficiency and Corrosion Rates of Electrode Materials in the Conventional and Ambient Temperature Alkaline Electrolysers.....	62
2.7.1 Research Trends on Electrode and Electro-catalyst Materials....	64
2.8 Conclusion of Chapter.....	73

3.0 Comparative Thermal Investigation of the Electrode and Catalyst in a Conventional Alkaline Electrolyser.....74

3.1 Background and Theory.....	74
3.2 Experimental Measurements.....	76
3.3 Discussion of the Results: Investigation of the Electrode Metal and Catalyst in Variable Power of operation.....	80
3.4 Investigation of the Electrodes under Intermittent Electrical Power of operation.....	87
3.5 Investigation of the Electrode and Catalyst in a Flow-Cell Alkaline Electrolyser.....	88

3.6 Conclusion of Chapter.....	92
4.0 Fabrication and Characterisation of the Electrode.....	93
4.1 Background.....	93
4.1.1 Physical Dimensions and Electrical Resistance of SS.....	93
4.2 Experimental Measurements.....	94
4.3 Discussion of the Results.....	95
4.3.1 Kinetic Efficiency under Variable Electrical Power of Operation.....	95
4.3.2 Etching of the Electrode and Kinetic Efficiency under Variable Electrical Power of Operation.....	101
4.3.3 Stability under Intermittent Electrical Power of Operation...	107
4.3.4 Stability under Constant Electrical Power of Operation.....	109
4.3.4.1 <i>OER</i> and <i>HER</i> Production Rates on the Electrode.....	115
4.4 Conclusion of Chapter.....	131
5.0 Fabrication and Characterisation of the Electro-Catalyst.....	132
5.1 Materials for Electrodeposition of Ni-Mo Catalyst on the SS mesh (type 304).....	132
5.2 SS-Ni-Mo(1) Developed at pH 4.0.....	134
5.2.1 Kinetic Efficiency under Variable Electrical Power of Operation.....	135
5.2.2 Stability under Intermittent Electrical Power of Operation.....	137
5.2.3 Stability under Constant Electrical Power of Operation.....	138
5.3 SS-Ni-Mo(2) Developed at pH 5.0.....	147
5.3.1 Kinetic Efficiency under Variable Electrical Power of Operation.....	148
5.3.2 Stability under Intermittent Electrical Power of Operation.....	150

5.3.3 Stability under Constant Electrical	
Power of Operation.....	151
5.4 Comparison of Electro-Catalyst Activity and Effect of pH.....	158
5.4.1 Effect of pH on Electro-Catalyst Activity.....	160
5.5 Conclusion of Chapter.....	161

6.0 Development of SS-Ni-Mo Electro-Catalyst for the Ambient Temperature Alkaline Electrolyser.....162

6.1 Introduction.....	162
6.2 Efficiency of Electro-catalyst for Hydrogen and Oxygen Production	162
6.3 Stability of the Electro-catalyst.....	166
6.4 Experimental.....	167
6.5 Discussion of the Results.....	169
6.6 Conclusion of Chapter.....	181

7.0 Construction of the Flow-Cell Ambient Temperature Alkaline Electrolyser for Characterising the Electrode.....183

7.1 Introduction and Description of Cell Components.....	183
7.1.1 Electrode Compartment.....	183
7.1.2 Electrolyte Compartment.....	187
7.1.3 End Plates and Cell Assembly.....	189
7.2 Experimental Measurements and Discussion of the Results.....	191
7.2.1 Monopolar Flow-cell Configuration.....	191
7.2.2 Bi-polar Multi-cell Configuration.....	194
7.3 Open-circuit Voltage of the Alkaline Electrolyser.....	199
7.4 Conclusion of Chapter.....	202

8.0 Modelling of Concentration Polarisation and Corrosion Rate of the Electrode.....	203
8.1 Background	203
8.2 Research Problem and Hypothesis.....	205
8.3 Diffusion Model Theory and Assumptions.....	206
8.4 Modelling of Corrosion Rates of the Electrode on Open-circuit.....	209
8.5 Experimental Set-up and Discussion of the Results.....	213
8.5.1 Efficiency of Cell in Variable Power of Operation.....	213
8.5.2 Determination of Corrosion Rate of the Electrode	219
8.6 Water Replenishment and Conductivity of KOH Electrolyte.....	221
8.7 Conclusion of Chapter.....	222
9.0 General Conclusions and Future Scope of Research.....	223
9.1 General Conclusions and Contributions to Field.....	223
9.1.1 Operational Temperature of the Alkaline Electrolyser.....	224
9.1.1.1 Sustainable Hydrogen and Oxygen Production.....	224
9.1.1.2 Dynamic Operation with Renewable Energy Sources.....	225
9.1.1.3 Operational and Maintenance Cost Investment.....	225
9.1.1.4 Degradation of Electrode and Electro-Catalysts.....	226
9.1.1.5 Efficiency and Stability of Electrode and Electro-Catalyst.....	226
9.1.2 Fabrication and Characterisation of Electrode and Electro-Catalyst Materials.....	227
9.1.3 Concentration Polarisation and Corrosion Rate of Electrodes.....	227
9.2 Future Scope of Research.....	228
9.2.1 Electro-Catalyst Development.....	228
9.2.2 Optimisation of Cell Design and Operation.....	228
References.....	230
Appendix A: List of Publications, Posters and Presentations.....	243

Appendix B: How to Calculate Geometric Surface Area of the Mesh Electrode and Electrical Resistance of the Wires.....245

List of Figures

Chapter 1

Figure 1-1 Oil price.....2

Figure 1-2 Current UK energy sources.....3

Figure 1-3 Currently installed Wind/Hydrogen energy systems utilising alkaline electrolyzers.....10

Figure 1-4 Proposed Wind/Hydrogen and Oxygen energy systems utilising alkaline electrolyzers.....13

Figure 1-5 Hydrogen selling price produced by electrolyzers of various capacities..... 14

Figure 1-6 Schematic diagram of a nuclear-hydrogen system..... 16

Figure 1-7 Commercial target for low-cost hydrogen.....20

Figure 1-8 Electrode concept selection.....21

Figure 1-9 A typical effect of higher operating temperature to reduce overvoltages of the alkaline electrolyser cell.....21

Figure 1-10 Strategy for electrode efficiency improvement.....22

Chapter 2

Figure 2-1 Schematic of the alkaline electrolyser cell.....25

Figure 2-2: Cell potential for hydrogen production by water electrolysis as a function of temperature.....29

Figure 2-3 Schematic illustration of the cell resistances.....31

<i>Figure 2-4 Schematic of the electrolytic double-layer in the alkaline electrolyser.....</i>	<i>33</i>
<i>Figure 2-5 Electrochemical circuit of the alkaline electrolyser on open-circuit.....</i>	<i>34</i>
<i>Figure 2-6 Schematic of EIS measurement.....</i>	<i>40</i>
<i>Figure 2-7 Equivalent circuit model for the ideal alkaline electrolyser.....</i>	<i>42</i>
<i>Figure 2-8 (A) Nyquist plot showing impedance, (B) Bode plot showing phase angle Frequency and magnitude of impedance.....</i>	<i>43</i>
<i>Figure 2-9 Optimised system operation for hydrogen production from the conventional temperature alkaline electrolyser.....</i>	<i>45</i>
<i>Figure 2-10 Electrolytic production of hydrogen and oxygen from the ambient temperature alkaline electrolyser.....</i>	<i>48</i>
<i>Figure 2-11 Hydrogen and Oxygen Energy System utilising the ambient temperature alkaline electrolyser.....</i>	<i>50</i>
<i>Figure 2-12 Microgeneration application of the ambient temperature alkaline electrolyser.....</i>	<i>51</i>
<i>Figure 2-13 Schematic diagram of the monopolar cell design.....</i>	<i>56</i>
<i>Figure 2-14 Schematic diagram of the bi-polar cell design.....</i>	<i>57</i>
<i>Figure 2-15 Schematic illustration of bi-polar filter-press cell construction.....</i>	<i>59</i>
<i>Figure 2-16 Schematic illustration of zero-gap cell construction.....</i>	<i>59</i>
<i>Figure 2-17 Comparison of electrode metal cost.....</i>	<i>62</i>
<i>Figure 2-18 Potential-pH (Pourbaix) diagram for steel (Fe-H₂O) at 100°C and comparison of the corrosion areas (HFeO₂⁻) at 25°C and 100°C.....</i>	<i>63</i>
<i>Figure 2-19 Temperature dependence of the electrical conductivity of aqueous solution of KOH and NaOH.....</i>	<i>64</i>
<i>Figure 2-20 Electrode efficiency by Bailleux and comparison with commercial target.....</i>	<i>65</i>
<i>Figure 2-21 Electrode efficiency by Balej and comparison with commercial target.....</i>	<i>66</i>

<i>Figure 2-22 Electrode efficiency by Ganley and comparison with commercial target.....</i>	<i>67</i>
<i>Figure 2-23 Electrode efficiency by Weikang and comparison with commercial target.....</i>	<i>71</i>
<i>Figure 2-24 Electrode efficiency by Amitava and comparison with commercial target.....</i>	<i>72</i>
Chapter 3	
<i>Figure 3-1 Schematic representation for DC and EIS measurements of the alkaline electrolyser cell.....</i>	<i>77</i>
<i>Figure 3-2 Image of the open-system alkaline electrolyser cell.....</i>	<i>78</i>
<i>Figure 3-3 Image of the open-system alkaline electrolyser cell under the fume hood.....</i>	<i>79</i>
<i>Figure 3-4 (A) HER and OER polarisation of the electrode metals in the ambient and conventional temperature alkaline electrolyzers: (B) Tafel relation.....</i>	<i>80</i>
<i>Figure 3-5 Nyquist impedance plot for electrode metals in the ambient and conventional temperature alkaline electrolyzers.....</i>	<i>82</i>
<i>Figure 3-6 (A) HER and OER polarisation on the electrode metal and catalyst in the ambient and conventional alkaline electrolyzers: (B) Tafel relation.....</i>	<i>84</i>
<i>Figure 3-7 Nyquist impedance for electrode metal and catalyst in the ambient and conventional temperature alkaline electrolyzers.....</i>	<i>86</i>
<i>Figure 3-8 Stability of Ni mesh under intermittent electrical power supply; (A) at 23 °C, (B) at 80 °C and (C) Applied current load profile.....</i>	<i>87</i>
<i>Figure 3-9 Stability of SS mesh under intermittent electrical power supply: (A) at 23 °C, (B) at 80 °C. (C) Applied current load profile.....</i>	<i>88</i>
<i>Figure 3-10 Image of the flow-cell ambient alkaline electrolyser which consist of the SS mesh electro-catalyst.....</i>	<i>89</i>
<i>Figure 3-11 Polarisation of the SS mesh and Ni-Mo catalyst in the flow-cell ambient alkaline electrolyser</i>	<i>90</i>

<i>Figure 3-12 Nyquist impedance plot for the SS mesh and Ni-Mo catalyst in the flow-cell ambient alkaline electrolyser.....</i>	<i>91</i>
--	-----------

Chapter 4

<i>Figure 4-1 Comparison of the kinetic efficiency of SS mesh and SS sheet electrode metals;A. DC polarisation, B. Tafel relation.....</i>	<i>96</i>
--	-----------

<i>Figure 4-2 Nyquist impedance comparison of SS mesh and SS sheet.....</i>	<i>96</i>
---	-----------

<i>Figure 4-3 Kinetic efficiency of SS mesh: A. DC polarisation,B. Tafel relation.....</i>	<i>97</i>
--	-----------

<i>Figure 4-4 Nyquist impedance for OER on SS mesh</i>	<i>98</i>
--	-----------

<i>Figure 4-5 Nyquist impedance for HER on SS mesh.....</i>	<i>99</i>
---	-----------

<i>Figure 4-6 Comparison of kinetic efficiency of SS mesh (types 304 and 316): A.DC polarisation, B. Tafel relation.....</i>	<i>100</i>
--	------------

<i>Figure 4-7 Comparison of Nyquist impedance on SS mesh (types 304 and 316)...</i>	<i>100</i>
---	------------

<i>Figure 4-8 Comparison of kinetic efficiency of etched-SS mesh (type 304) and ordinary SS mesh (type 304). A. DC polarisation, B. Tafel relation</i>	<i>102</i>
--	------------

<i>Figure 4-9 Comparison of Nyquist impedance on etched-SS mesh (type 304) and ordinary SS mesh (type 304).....</i>	<i>103</i>
---	------------

<i>Figure 4-10 Comparison of kinetic efficiency of etched -SS mesh (type 316) and ordinary SS mesh-type 316. A. DC polarisation, B. Tafel relation.....</i>	<i>104</i>
---	------------

<i>Figure 4-11 Comparison of Nyquist impedance on etched SS mesh (type 316) and ordinary SS mesh (type 316) etched.....</i>	<i>105</i>
---	------------

<i>Figure 4-12 Comparison of kinetic efficiency of etched SS sheet and ordinary SS sheet: A. DC polarisation, B. Tafel relation.....</i>	<i>106</i>
--	------------

<i>Figure 4-13 Comparison of Nyquist impedance on etched SS sheet and ordinary SS sheet.....</i>	<i>107</i>
--	------------

<i>Figure 4-14 Comparison of open-circuit test on: A. SS mesh (type 304) B. SS sheet, C. applied current load.....</i>	<i>108</i>
--	------------

<i>Figure 4-15 Continuous electrolysis at 200mA/cm² on the SS mesh: Inset shows applied current load.....</i>	<i>109</i>
--	------------

<i>Figure 4-16 Comparison of polarisation on SS mesh before and after continuous electrolysis.....</i>	<i>110</i>
--	------------

<i>Figure 4-17 Comparison of Nyquist impedance on the SS mesh before and after continuous electrolysis.....</i>	<i>111</i>
<i>Figure 4-18 Continuous electrolysis at 190mA/cm² on the SS sheet; inset shows applied current load.....</i>	<i>112</i>
<i>Figure 4-19 Comparison of polarisation on the SS sheet before and after continuous electrolysis.....</i>	<i>113</i>
<i>Figure 4-20 Comparison of Nyquist impedance on the SS sheet before and after continuous electrolysis.....</i>	<i>114</i>
<i>Figure 4-21 OER at 2V for 4 hours on SS mesh; inset shows applied voltage.....</i>	<i>115</i>
<i>Figure 4-22 Nyquist impedance before and after OER at 2V for 12 hours on SS mesh.....</i>	<i>116</i>
<i>Figure 4-23 OER at 2V for 2 hours on SS mesh; inset shows applied voltage.....</i>	<i>117</i>
<i>Figure 4-24 Nyquist impedance before and after OER at 2V for 2 hours on SS mesh.....</i>	<i>118</i>
<i>Figure 4-25 HER at -2V for 2 hours on SS mesh; inset shows applied voltage.....</i>	<i>119</i>
<i>Figure 4-26 Nyquist impedance before and after HER at -2V for 2 hours on SS mesh.....</i>	<i>120</i>
<i>Figure 4-27 OER at 2V for 2 hours on SS sheet; inset shows applied.....</i>	<i>121</i>
<i>Figure 4-28 Nyquist impedance before and after OER at 2V for 2 hours on SS sheet.....</i>	<i>122</i>
<i>Figure 4-29 HER at -2V for 2 hours on SS sheet.....</i>	<i>123</i>
<i>Figure 4-30 Nyquist impedance before and after HER at -2V for 2 hours on SS sheet.....</i>	<i>124</i>
<i>Figure 4-31 OER at 200mA/cm² for 2 hours on SS mesh.....</i>	<i>125</i>
<i>Figure 4-32 HER at -200mA/cm² for 2 hours on SS mesh.....</i>	<i>126</i>
<i>Figure 4-33 Nyquist impedance before and after OER at 200mA/cm² for 2 hours on the SS mesh.....</i>	<i>127</i>
<i>Figure 4-34 Nyquist impedance before and after HER at -200mA/cm² for 2 hours on SS mesh.....</i>	<i>127</i>
<i>Figure 4-35 OER at 190mA/cm² for 2 hours on SS sheet.....</i>	<i>128</i>

<i>Figure 4-36 HER at -190mA/cm² for 2 hours on SS sheet.....</i>	<i>129</i>
<i>Figure 4-37 Nyquist impedance before and after OER at 190mA/cm² for 2 hours on SS sheet.....</i>	<i>130</i>
<i>Figure 4-38 Nyquist impedance before and after HER at -190mA/cm² for 2 hours on SS sheet.....</i>	<i>131</i>

Chapter 5

<i>Figure 5-1 SEM micrographs: A. uncoated SS mesh, B. SS-Ni-Mo (1), C. SS-Ni-Mo (1) magnified view.....</i>	<i>134</i>
<i>Figure 5-2 Comparison of kinetic efficiency of SS-Ni-Mo (1) and SS mesh: A. Polarisation relation, B. Tafel relation.....</i>	<i>135</i>
<i>Figure 5-3 Nyquist impedance comparison of impedance of SS-Ni-Mo (1) and SS mesh.....</i>	<i>136</i>
<i>Figure 5-4 Nyquist impedance on SS-Ni-Mo (1) at varying potentials: A. Nyquist plot, B. Bode plot.....</i>	<i>137</i>
<i>Figure 5-5 Open-circuit test on SS-Ni-Mo (1).....</i>	<i>138</i>
<i>Figure 5-6 OER at 2V for 2 hours on SS-Ni-Mo (1).....</i>	<i>139</i>
<i>Figure 5-7 Nyquist Impedance before and after OER at 2V for 2 hours on SS-Ni-Mo(1).....</i>	<i>140</i>
<i>Figure 5-8 HER at -2V for 2 hours on SS-Ni-Mo (1).....</i>	<i>141</i>
<i>Figure 5-9 Nyquist impedance before and after HER at -2V for 2 hours on SS-Ni-Mo (1).....</i>	<i>142</i>
<i>Figure 5-10 OER at 200 mA/cm² for 2 hours on SS-Ni-Mo (1).....</i>	<i>143</i>
<i>Figure 5-11 HER at -200 mA/cm² for 2 hours on SS-Ni-Mo (1).....</i>	<i>143</i>
<i>Figure 5-12 Impedance before and after OER at 200mA/cm² for 2 hours on SS-Ni-Mo (1): A. Nyquist plot, B. Bode plot.....</i>	<i>144</i>
<i>Figure 5-13 Nyquist Impedance before and after HER at -200mA/cm² for 2 hours on SS-Ni-Mo (1).....</i>	<i>145</i>
<i>Figure 5-14 SEM micrographs: A. SS-Ni-Mo (1) before electrolysis, B. SS-Ni-Mo (1) after electrolysis, C. SS-Ni-Mo (1) after electrolysis magnified view.....</i>	<i>146</i>

<i>Figure 5-15 SEM micrographs: A. uncoated SS mesh, B. SS-Ni-Mo (2), C. SS-Ni-Mo (2) magnified view.....</i>	<i>148</i>
<i>Figure 5-16 Comparison of kinetic efficiency of SS-Ni-Mo (2) and SS mesh; A. Polarisation relation, B. Tafel relation.....</i>	<i>149</i>
<i>Figure 5-17 Nyquist impedance comparison of SS-Ni-Mo (2) and SS mesh.....</i>	<i>150</i>
<i>Figure 5-18 Open-circuit test on SS-Ni-Mo (2).....</i>	<i>151</i>
<i>Figure 5-19 OER at 2V for 2 hours on SS-Ni-Mo (2).....</i>	<i>152</i>
<i>Figure 5-20 Nyquist impedance before and after OER at 2V for 2 hours on SS-Ni-Mo (2).....</i>	<i>153</i>
<i>Figure 5-21 HER at -2V for 2 hours on SS-Ni-Mo (2).....</i>	<i>154</i>
<i>Figure 5-22 Nyquist impedance before and after HER at -2V for 2 hours on SS-Ni-Mo (2).....</i>	<i>155</i>
<i>Figure 5-23 OER at 129 mA/cm² for 2 hours on SS-Ni-Mo (2).....</i>	<i>156</i>
<i>Figure 5-24 HER at 163 mA/cm² for 2 hours on SS-Ni-Mo (2); Inset shows applied current load.....</i>	<i>157</i>
<i>Figure 5-25 Impedance before and after HER at 129 mA/cm² for 2 hours on SS-Ni-Mo (2): A. Nyquist plot, B. Bode plot.....</i>	<i>158</i>
<i>Figure 5-26 DC polarisation of SS-Ni-Mo: (A) Polarisation comparison for apparent activity, (B).Tafel comparison for apparent activity.....</i>	<i>160</i>
 Chapter 6	
<i>Figure 6-1 Equivalent circuit model for a smooth electrode surface in contact with electrolyte.....</i>	<i>164</i>
<i>Figure 6-2 Equivalent circuit model for a rough electrode in contact with electrolyte.....</i>	<i>164</i>
<i>Figure 6-3 Schematic illustration of fabrication and characterisation procedure for the SS-Ni-Mo.....</i>	<i>168</i>
<i>Figure 6-4 SEM image of SS mesh (A) and SS-Ni-Mo (B).....</i>	<i>169</i>
<i>Figure 6-5 Magnified SEM image of SS-Ni-Mo.....</i>	<i>169</i>
<i>Figure 6-6 Steady-state polarisation: (A) and Tafel polarisation (B) for SS mesh and SS-Ni-Mo electrocatalysts.....</i>	<i>171</i>

<i>Figure 6-7 Nyquist impedance comparison for SS mesh and SS-Ni-Mo electrocatalyst.....</i>	<i>172</i>
<i>Figure 6-8 Nyquist (A) and Bode (B) impedance for SS mesh at anodic potentials.....</i>	<i>173</i>
<i>Figure 6-9 Nyquist (A) and Bode (B) impedance for SS mesh at cathodic potentials.....</i>	<i>174</i>
<i>Figure 6-10 Nyquist (A) and Bode (B) impedance for SS-Ni-Mo at anodic potentials.....</i>	<i>176</i>
<i>Figure 6-11 Nyquist (A) and Bode (B) impedance for SS-Ni-Mo at cathodic potentials.....</i>	<i>176</i>
<i>Figure 6-12 Stability of SS-Ni-Mo under intermittent electrolysis at 200mA/cm² for up to 3 cycles for the HER(A) and OER(B).....</i>	<i>178</i>
<i>Figure 6-13 Stability of SS-Ni-Mo under continuous electrolysis at 200mA/cm² for the OER (A); Steady-state polarisation for the OER on SS-Ni-Mo (B) and Nyquist impedance for the OER on SS-Ni-Mo(C).....</i>	<i>179</i>
<i>Figure 6-14 Continuous electrolysis on SS-Ni-Mo at 200mA/cm² for the HER for up to 24 hours.....</i>	<i>180</i>
<i>Figure 6-15 Steady-state polarisation for the HER on SS-Ni-Mo (B); Nyquist impedance for the HER on SS-Ni-Mo.....</i>	<i>180</i>
<i>Figure 6-16 SEM images of SS-Ni-Mo: (A) before electrolysis and (B) after electrolysis.....</i>	<i>181</i>
 Chapter 7	
<i>Figure 7-1 Electrode compartment in the alkaline electrolyser cell.....</i>	<i>184</i>
<i>Figure 7-2 Technical drawing of electrode compartment-part 1 of the alkaline electrolyser cell.....</i>	<i>185</i>
<i>Figure 7-3 Technical drawing of electrode compartment-part 2 of the alkaline electrolyser cell.....</i>	<i>186</i>
<i>Figure 7-4 Electrolyte compartment in the alkaline electrolyser cell.....</i>	<i>187</i>
<i>Figure 7-5 Technical drawing of electrolyte compartment of the alkaline electrolyser cell.....</i>	<i>188</i>
<i>Figure 7-6 End plates and cell assembly.....</i>	<i>189</i>

<i>Figure 7- 7: Technical drawing of end plate of the alkaline electrolyser cell.....</i>	<i>190</i>
<i>Figure 7-8 Polarisation of SS electrode in the monopolar flow-cell alkaline electrolyser.....</i>	<i>192</i>
<i>Figure 7-9 Nyquist impedance of SS electrode in the monopolar flow-cell alkaline electrolyser.....</i>	<i>193</i>
<i>Figure 7-10 Nyquist impedance on the SS electrode in the monopolar flow-cell alkaline electrolyser at varying potentials.....</i>	<i>194</i>
<i>Figure 7-11 Image of the ‘bi-polar’ multi-cell alkaline electrolyser.....</i>	<i>195</i>
<i>Figure 7-12 Schematic illustration of the bi-polar multi-cell alkaline electrolyser.....</i>	<i>196</i>
<i>Figure 7-13 Schematic illustration of the flow-cell alkaline electrolyser that is constructed with ‘point-wise’ current collection.....</i>	<i>197</i>
<i>Figure 7-14 Image of the flow-cell alkaline electrolyser constructed with point-wise current collection.....</i>	<i>198</i>
<i>Figure 7-15 Polarisation of the flow-cell alkaline electrolyser constructed with point-wise current-collection.....</i>	<i>198</i>
<i>Figure 7-16 Nyquist impedance on the flow-cell alkaline electrolyser constructed with point-wise current collection.....</i>	<i>199</i>
<i>Figure 7-17 OCV of the Flow-Cell alkaline electrolyser at: A. 16 minutes of charging, B. 33 minutes of charging, C. 41 minutes of charging.....</i>	<i>200</i>
<i>Figure 7-18 OCV of the flow-cell alkaline electrolyser at discharge time of 3 minutes recorded continuously.....</i>	<i>200</i>
<i>Figure 7-19 Nyquist impedance of the flow-cell alkaline electrolyser at OCV.....</i>	<i>201</i>

Chapter 8

<i>Figure 8-1 Model prediction of concentration polarisation for the electrolyser cell operated in 30% KOH at 293K, and approximately zero-gap bi-polar cell geometry.....</i>	<i>205</i>
<i>Figure 8-2 Behaviour of the alkaline electrolyser on open-circuit and dynamic power input.....</i>	<i>210</i>

<i>Figure 8-3 Showing the thermometer and stirring rod that was used for the experiment.....</i>	<i>213</i>
<i>Figure 8-4 Polarisation of SS electrodes separated by 3cm distance in 30% KOH with stirring of electrolyte using 2cm rod: A. polarisation B. Tafel relation.....</i>	<i>214</i>
<i>Figure 8-5 Nyquist impedance on SS electrode separated by 3cm distance in 30% KOH with stirring of electrolyte using 2cm rod.....</i>	<i>215</i>
<i>Figure 8-6 Polarisation of SS electrode at 1mm separation gap with stirring of electrolyte solution using 4cm rod.....</i>	<i>216</i>
<i>Figure 8-7 Nyquist impedance on SS electrode with stirring of electrolyte solution</i>	<i>217</i>
<i>Figure 8-8 Polarisation of SS electrode at different separation distance.....</i>	<i>218</i>
<i>Figure 8-9 Nyquist impedance of SS electrode at different separation distance.....</i>	<i>219</i>
<i>Figure 8-10 Comparison of Nyquist impedance of SS electrode on open-circuit and during electrolysis.....</i>	<i>220</i>
<i>Figure 8-11 Effect of excess water replenishment in the alkaline electrolyser.....</i>	<i>221</i>

List of Tables

Chapter 1

<i>Table 1-1 Key assumptions on hydrogen and fuel cell applications by 2020 in the EU and comparison with similar assumption in the US and Japan</i>	<i>5</i>
<i>Table 1-2 Overview of wind/hydrogen systems installed worldwide.....</i>	<i>9</i>
<i>Table 1-3 Size and capacities of current commercial alkaline electrolyzers.....</i>	<i>15</i>
<i>Table 1-4 Comparison of the commercial alkaline electrolyzers and PEM electrolyzers.....</i>	<i>18</i>

Chapter 2

<i>Table 2-1 Comparison of thermodynamic voltages of the ambient and conventional temperature alkaline electrolyzers.....</i>	<i>28</i>
<i>Table 2-2 Commercial data for the conventional temperature single-cell alkaline electrolyzers.....</i>	<i>45</i>

<i>Table 2-3 Assumptions for feedstock and utility requirement for the conventional temperature single-cell alkaline electrolyzers.....</i>	<i>46</i>
<i>Table 2-4 Operational and hydrogen production costs for the conventional temperature single-cell alkaline electrolyzers.....</i>	<i>46</i>
<i>Table 2-5 Assumed data for the ambient temperature single cell alkaline electrolyser.....</i>	<i>52</i>
<i>Table 2-6 Assumptions for feedstock and utility for the ambient temperature ‘single cell’ alkaline electrolyser.....</i>	<i>52</i>
<i>Table 2-7 Operational costs for the ambient temperature alkaline electrolyzers.....</i>	<i>53</i>
<i>Table 2-8 Production costs for the ambient temperature alkaline electrolyzers.....</i>	<i>53</i>
<i>Table 2-9: Comparison of the ambient and conventional temperature alkaline electrolyzers.....</i>	<i>55</i>
<i>Table 2-10 Data for the industrial alkaline electrolyzers.....</i>	<i>56</i>
<i>Table 2-11 Comparison of monopolar and bi-polar cell designs.....</i>	<i>58</i>
<i>Table 2-12 Comparison of different membrane types used in the alkaline electrolyser.....</i>	<i>61</i>
<i>Table 2-13 Composition of plating solution for Ni-Mo catalyst prepared by Luciana et-al.....</i>	<i>70</i>

Chapter 3

<i>Table 3-1 Summary of HER activity of investigated cathode electrodes in the conventional temperature alkaline electrolyser.....</i>	<i>74</i>
<i>Table 3-2 Summary of kinetic parameters for the electrode metals in the ambient and conventional temperature alkaline electrolyser.....</i>	<i>81</i>
<i>Table 3-3 Resistance, exchange current density and corrosion rates for the electrode metals in the ambient and conventional temperature alkaline electrolyser.....</i>	<i>83</i>
<i>Table 3 4 Summary of kinetic parameters for the electrode metal and catalyst in the ambient and conventional temperature alkaline electrolyser.....</i>	<i>85</i>

<i>Table 3-5 Resistance, exchange current density and corrosion rates for the electrode and catalyst in the ambient and conventional temperature alkaline electrolyser.....</i>	<i>86</i>
---	-----------

Chapter 4

<i>Table 4-1 Physical and electrical properties of the SS electrode metal.....</i>	<i>94</i>
<i>Table 4-2 Summary of hydrogen and oxygen production rates on SS mesh.....</i>	<i>124</i>
<i>Table 4-3 Summary of hydrogen and oxygen production rates on SS smooth sheet.....</i>	<i>124</i>

Chapter 5

<i>Table 5-1 Comparison of physico-chemical properties of the electrodeposited SS mesh.....</i>	<i>133</i>
<i>Table 5-2 Comparison of surface roughness factors for SS-Ni-Mo electrocatalyst.....</i>	<i>159</i>
<i>Table 5-3 Hydrogen and Oxygen production rates on SS-Ni-Mo electro-catalyst.....</i>	<i>161</i>

Chapter 6

<i>Table 6-1 Physico-chemical characteristics of the prepared SS-Ni-Mo.....</i>	<i>169</i>
<i>Table 6-2 Tafel parameters for SS mesh and SS-Ni-Mo electrocatalyst.....</i>	<i>172</i>
<i>Table 6-3 Resistance and capacitance of SS mesh.....</i>	<i>175</i>
<i>Table 6-4 Resistance and capacitance of SS-Ni-Mo electrocatalyst.....</i>	<i>177</i>

Chapter 7

<i>Table 7-1 Specifications of the ‘single-cell’ alkaline electrolyser</i>	<i>191</i>
--	------------

Chapter 8

Table 8-1 Summary of polarisation results for the SS-type 316 electrode at 1mm separation gap.....216

Table 8-2 Summary of EIS measurements and corrosion rates of the SS electrode at 1mm separation distance.....220

Nomenclature

Symbol	Definition
A	Area of electrode in square centimeter (cm^2)
A_{real}	Real active area of electrode (cm^2)
$A_{geometric}$	Geometric active area of electrode (cm^2)
A_{SI}	Area of electrode in square meter (m^2)
a	Molecular weight in gram per mole (g/mol)
C_{OH}	Concentration of hydroxyl ions near the electrode surface in mol per cubic meter (mol/m^3)
C_{O_2}	Concentration of oxygen gas bubbles near the electrode in mol per cubic meter (mol/m^3)
C_{dl}	Double-layer capacitance in Farad per square centimeter (F/cm^2)
C_p	Heat capacity of water in Joules per gram Kelvin (J/gK)
d	Distance of separation between electrodes in centimeter (cm)
D_{OH}	Diffusion co-efficient of aqueous hydroxyl ions in square meter per second (m^2/sec)
E_{act}	Activation over-voltage in Volts (V)
E_{ohmic}	Ohmic over-voltage in Volts (V)
$E^{\circ}_{cathode}$	Standard cathode half-cell potential in Volts (V)
E°_{anode}	Standard anode half-cell potential in Volts (V)
E_{cell}	Cell potential in Volts (V)
$E_{electrode}$	Electrode potential in Volts (V)
E°_{cell}	Standard reversible cell potential in Volts (V)
E_{Rev}	Reversible voltage in Volts (V)
E_{therm}	Thermoneutral voltage in Volts (V)
F	Faraday's constant in Coloumb per mol (96,500 C/mol)
GW	Gigawatt
G°	Gibb's free energy in Joules per mol (J/mol)
h	Height of electrode in meters (m)
i	Current in Amperes (A)
i_a	Anode current density in Amperes per square centimeter (A/cm^2)

Symbol	Definition
i_o	Exchange current density in Amperes per square centimeter (A/cm^2)
i_c	Cathode current density in Amperes per square centimeter (A/cm^2)
I_{app}	Applied current in Amperes (A)
I_L	Leakage current in Amperes (A)
i_L	Limiting current in Amperes (A)
j	Imaginary unit ($\sqrt{-1}$)
J	Current density in Amperes per square centimeter (A/cm^2)
J_{corr}	Corrosion rate and current density in Amperes per square centimeter (A/cm^2)
J_{OH}	Flux of hydroxyl ions in mol per square meter per second ($mol/m^2 \cdot sec$)
J_{O_2}	Flux of oxygen in mol per square meter per second ($mol/m^2 \cdot sec$)
kWh/kg	KiloWatt-hour per kilogram
kg/hr	Kilogram per hour
kg/yr	Kilogram per year
kW	KiloWatt
kWh / Nm^2	KiloWatt hour per normal square meter
kAm^{-2}	Kilo amperes per square meter
KOH	Potassium hydroxide
K_e	Electrochemical equivalent of the alloy ($\sim m/A \text{ hr} / dm^2$)
L	Distance between adjacent wires of the electrode mesh or length of electrode in meter (m)
MWh	MegaWatt-hour
MPa	MegaPascal
m	Mass in grams (g)
n	Number of equivalent electrons transferred
N	Number of moles of electrolysed species in mol (mol)
P	Co-efficient of CPE
R	Gas constant in Joules per mol per Kelvin ($J/mol \cdot K$)
R_Ω or R_s	Ohmic resistance in Ohms ()
R_P	Polarisation or reaction resistance in Ohms ()

Symbol	Definition
R_1	Electrical resistance in Ohms ()
R_{anode}	Anode resistance in Ohms ()
R_{cathode}	Cathode resistance in Ohms ()
$R_{\text{bubble H}_2}$	Resistance of hydrogen bubbles in Ohms ()
$R_{\text{bubble O}_2}$	Resistance of oxygen bubbles in Ohms ()
R_f	Surface roughness factor in Ohms ()
R_{membrane}	Membrane resistance in Ohms ()
R_{ions}	Transport resistance of ions in Ohms ()
T_K	Absolute temperature in Kelvin (K)
T	CPE constant ($\Omega^{-1} s^P$)
T_e	Thickness of deposit (~m)
t	Time of electrolysis in seconds (sec)
t_E	Thickness of the electrode in centimeters (cm)
t_e	Time of electrodeposition (hr)
V	Electrode surface potential in Volts (V)
x_d	Diffusion layer thickness in meters (m)
Z_{CPE}	Impedance of constant phase element in Ohms ()
Z''	Imaginary impedance in Ohms ()
Z_{Ohmic}	Ohmic impedance in Ohms ()
$Z_{\text{Polarisation}}$	Polarisation impedance in Ohms ()
	Electrode overpotential in Volts (V)
r	Charge transfer co-efficient of electrode
S	Tafel parameter in Volts per decade of current (V/dec)

Symbol Definition

a	Anode Tafel constant in Volts per decade of current (V/dec)
c	Cathode Tafel constant in Volts per decade of current (V/dec)
c	Concentration over-potential in Volts (V)
a_{anode}	Anode over-potential in Volts (V)
c_{cathode}	Cathode over-potential in Volts (V)
c_{cell}	Cell over-potential in Volts (V)
$y_{\text{electrode}}$	Electrode over-potential in Volts (V)
y_{ELEC}	Efficiency of electrolysis (%)
...	Resistivity in Ohm meter (Ω -m)
... membrane	Resistivity of membrane in Ohm meter (Ω -m)
U_{heater}	Energy consumption in heater (kWh)
Y_{heater}	Heating cost in US dollar per hour (\$/hour)
$H_{H_2O}(T)$	Enthalpy of water in Joules per mol (J/mol) at a specific temperature in Kelvin
H°	Standard enthalpy (heat content) in Joules per mol (J/mol)
S°	Standard entropy in Joules per Kelvin per mol (J/K/mol)
X_{H_2O}	Water flow rate in kilogram per hour (kg/hr)
$Y_{\text{electricity}}$	Electricity consumption cost in US dollar per hour (\$/hr)
$Y_{\text{heat exchanger}}$	Heat exchanger electricity consumption cost in US dollar per hour (\$/hr)
$Q_{\text{heat exchanger}}$	Heat supplied to heat exchanger in Joules (J)
$U_{\text{heat exchanger}}$	Energy consumption in heat exchanger (kWh)
$X_{H_2O/KOH}$	Aqueous KOH electrolyte flow rate in kilogram per hour (kg/hr)
$Y_{\text{demineralised water}}$	Demineralised water consumption cost in US dollar per hour (\$/hr)
Y_{Total}	Total operational cost in US dollar per hour (\$/hr)
\$/kWh	US dollar per kiloWatt-hour
\$/kg	US dollar per kilogram
\tilde{S}	Angular frequency of AC impedance (rad s^{-1})
\ddagger	Time constant (sec)

Symbol**Definition** $Y_{\text{electricity for H}_2 \text{ production}}$

Electricity consumption for hydrogen production

 $Y_{\text{electricity for O}_2 \text{ production}}$

Electricity consumption for oxygen production

 $Y_{\text{cost for H}_2 \text{ production}}$

Total cost for hydrogen production

 $Y_{\text{cost for O}_2 \text{ production}}$

Total cost for oxygen production

Chapter 1

Hydrogen Production by Water Electrolysis: The way forward towards a Sustainable UK Energy Economy

This chapter deals with the role of electrolytic hydrogen as an energy carrier in the UK energy economy. As the UK government plans to increase renewable energy capacity on the electrical grid, [1-2] energy storage technologies will be needed for integrating with the electrical grid. Alkaline electrolyzers are suitable for energy storage applications. However, reducing cost, improving reliability and flexibility of the alkaline electrolyser still remain a big challenge [3-5]. The conventional operating conditions of alkaline electrolyser have indeed limited its dynamic and robust applications [6, 7]. The ambient temperature alkaline electrolyser¹ however is capable for flexible, low-cost, reliable and dynamic operation as it is equally suitable for hydrogen and oxygen production.

1.1 An Economic Case for Electrolytic Hydrogen

There is uncertainty over energy security of fossil fuels. Predicted limited supply of available fossil fuel reserves in oil-rich countries such as Saudi Arabia, and increasing energy demand in developing countries such as China and India have raised concerns over limited global oil and gas supplies by the year 2050 [8]. Political tensions in the Middle East and in some African countries have caused the oil price to rise by \$ 80 per barrel from the year 2009 record low (Figure 1-1) [9]. As a result many countries, including Britain, face the economic risk of inflation. In fact some analysts [8] have claimed that the oil price reaching the \$120 price mark is the specific ‘danger point’ at which the cost of oil can influence total global economic output by more than 5.5 %.

¹ The ambient temperature alkaline electrolyser is an alkaline electrolyser that is operated without external heating of the electrolyte solution at 23°C. In contrast, the conventional temperature alkaline electrolyser requires external heating of the electrolyte solution at about 80°C.



Figure 1-1 Oil price in \$/barrel vs. year; Courtesy of money week [10]

For the UK economy, the fear is that the rising price of crude oil will accelerate inflation which is already double the monetary policy committee's 2% target at 4% [8] resulting in dampened growth. The contraction in growth is expected to cause tax receipts of £ 1b lower in 2011 and £ 1.3b in 2012 [8]. However, higher oil and gas revenues from sales of North Sea crude oil and gas outputs as well as VAT receipts are expected to offset the gross domestic product effect.

As shown in Figure 1-2, 90% of UK energy sources are derived from fossil fuels, most of which is natural gas that is utilised for electricity and heating applications [11]. About 40% of the liquefied natural gas (LNG) is imported from countries such as Norway, Qatar and Nigeria [12]. In 2010 alone UK gas usage as a proportion of all fossil fuels has increased by 20% from 1990 levels [13], and efforts to replace existing coal-fired power stations with additional gas turbine generating plants will likely increase the UK overall gas utilisation by as much as 80% in the years ahead.

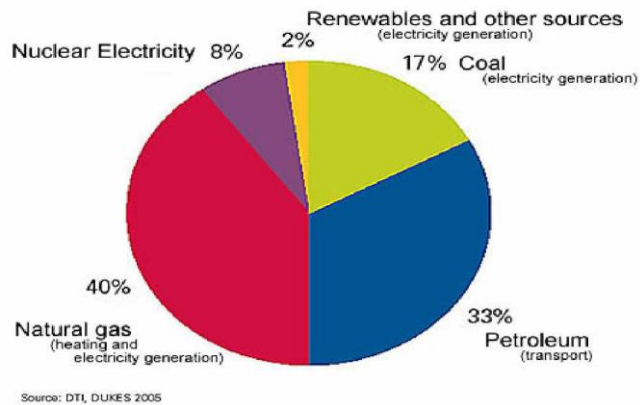


Figure 1-2 Current UK energy sources; Courtesy of DTI [1]

Carbon dioxide (CO₂) represents about 84 % of the UK's man-made greenhouse gas emissions [13] and in recent years the energy supply sector has decreased its CO₂ gas emissions by 23 % due to increased natural gas usage for electricity generation. A unit of coal produces more CO₂ emission than a unit of natural gas [13]. So electricity generated by the combustion of natural gas is relatively cleaner technology compared to combustion of coal or oil. However, CO₂ emissions have increased by about 13 % from the residential sector due to increased use of LNG during severe winter conditions. In general, the statistics for the UK energy economy does indicate heavy reliance on LNG in the years ahead. Sadly, the North Sea gas production is declining by more than 3 % due to depletion in the Continental Shelf Reserves [2].

The economic implications for over-reliance on imported LNG could be both external and internal affecting the UK energy economy. The external implications include: increasing energy demand in China and India, volatile political tension in the Middle East and oil-rich African countries and price fluctuations in oil and gas supply. The internal implication could be increasing unemployment as a result of losing about £100bn investment opportunities in the renewable energy sector [14].

Hydrogen is considered a very promising alternative to LNG for electricity and heat generation [15]. Currently, large-scale hydrogen is produced by steam methane reforming (SMR) which contributes about 95 % of hydrogen in the global market and efforts are made to reduce the cost of this hydrogen down to \$3/kg or \$1/kg in order to produce hydrogen in larger-scale for the 'hydrogen economy' [16].

However, the hydrogen could be contaminated with oxides of carbon, even as trace as 0.01% of carbon oxides [16], the hydrogen could only be directly utilised for industrial purposes such as petroleum refining. This means the hydrogen cannot be used directly in fuel cells for electricity and heat generation because the cell components can become contaminated and degrade quite easily. Attempts to purify the hydrogen by carbon capture sequestration [17] have yet to be realised as this technology requires significant cost investments and can impart negatively on the environment. Also, if natural gas is converted into hydrogen and the demand for natural gas continues to grow in other market, the natural gas reserve will decrease even more and the supply will be put under pressure. This could result in increased natural gas prices.

Electrolytic hydrogen that is produced from a renewable energy resource is sustainable as long as the feedstock is non-fossil fuel (in this case electricity from renewable sources). Electrolysis of water has the economic advantage of local hydrogen production [18] which allows for the introduction of renewable energy to the transport sector [19], energy security and the benefit of an infrastructure that is based upon distributed energy generation [20]. Electrolytic hydrogen is considered an energy vector for renewable resources thereby providing the potent link between sustainable energy technologies and a sustainable energy economy that is generally placed under the umbrella term of ‘hydrogen economy’[20-21].

Already some of the countries in Europe, US, Canada and Japan are at the forefront of developing cleaner and sustainable energy technologies. The European Fuel Cell and Hydrogen Association [22], German National Organisation for Hydrogen and Fuel Cell Technologies (German NOW) [23], US Department of Energy (US DoE) [24], Canadian Hydrogen and Fuel Cell Association [25] and Japanese World Energy Network (WE-NET) [26] are examples of national hydrogen and fuel cells programs. The international RD&D² programmes on hydrogen and fuel cell technologies provide a policy framework for setting-up targets and milestones in order to commercialise hydrogen as an energy carrier. In particular, the US DoE hydrogen

² Research, Development and Deployment

program [24] is structured with pre-defined milestones and ‘go no go’ decision points that are set to 2015, when progress will be assessed and decisions on large-scale commercialisation of hydrogen technology will be made accordingly.

The Japanese programme also has a major ‘go no go’ decision point set for 2015 and the European programme has the target of 2020 for future market penetration of hydrogen technology. Table 1-1 provides a comparison of the EU targets for hydrogen commercialisation and those of the Japanese and the US programmes. It shows the EU is more optimistic in developing hydrogen and fuel cell technologies for portable and combined heat and power applications. However, it is not clear whether government funding on hydrogen programmes will continue beyond 2015 since current RD&D efforts are yet to demonstrate the viability of the so called ‘hydrogen economy’ which still require significant cost investment for storage and delivery of the hydrogen.

Table 1-1 Key assumptions on hydrogen and fuel cell applications by 2020 in the EU and comparison with similar assumption in the US and Japan (adapted from M.Contestabile [27])

	Portable Fuel Cells for handheld electronic devices	Portable Generators & Early markets	Stationary Fuel Cells For Combined Heat and Power (CHP) applications	Road Transport
EU H ₂ /FC units sold per year projection 2020	~250 million	~ 100,000 per year (~1 GW)	100,000 to 200,000 per year (2-4 GW)	0.4 million to 1.8 million per year
EU cumulative sales projections until 2020	n.a	~600,000 (~6 GW)	400,000 to 800,000 (8-16 GW)	1-5 million
EU expected 2020 market status	Established	Established	Growth	Mass market roll-out
Japan METI cumulative sales targets 2020	n.a	n.a	10 GW	5 million
US DoE sales targets 2012	n.a	0.5 GW	n.a	n.a

Electrolytic hydrogen technology that uses electricity from renewable energy sources such as solar, wind, marine energy, etc is currently considered a promising route to sustainable hydrogen production [3-7]. In particular, electrolytic hydrogen provides a niche commercial market for a clean, indigenous and sustainable energy supply in the UK energy economy. Energy security will be assured since water and renewable energy resources such as wind, wave and tidal power are already abundant in the UK. Also, the education sector will be expanded to empower a renewed workforce and thereby create job opportunities in the renewable sector.

An important application of electrolytic hydrogen is as an energy carrier. The specific energy (in J/kg or J/l) of liquid hydrogen is 60 % more than LNG because of the light weight of elemental hydrogen [20]. Thus the hydrogen could potentially be used as a storage and transport medium for electricity that is generated from intermittent renewable resource such as wind, wave and tidal power. Gaseous hydrogen that is compressed at about 700 bars in tube cylinders has almost equal volumetric energy density with LNG. However, the technology for hydrogen storage is currently expensive as it requires about 40 % of the inherent energy content of the hydrogen to compress the gas and still results in a large storage capacity for stationary or automotive fuel applications [20].

The alkaline electrolyser converts electricity and water into pure hydrogen and oxygen thereby allowing production of hydrogen that can be stored and transported as an energy carrier. Alkaline electrolysers are already a mature technology that has a high energy efficiency of up to 75 % of High Heating Value (HHV³) [28] and utilises relatively low cost non-noble metal electrode materials such as nickel (Ni), molybdenum (Mo) and aqueous potassium hydroxide (KOH) electrolyte. For this reason, alkaline electrolysers are preferred compared to proton exchange membrane (PEM) electrolysers and solid oxide electrolysers to produce pure hydrogen and oxygen in commercial quantities [3, 6, 29].

³ The higher heating value is useful for calculating heating values for hydrogen fuel where condensation of the reaction products is practical, for example using hydrogen in gas fired-boiler for space heating applications

The electricity consumption in conventional temperature alkaline electrolyzers contributes to about 60 % -80 % of the cost of hydrogen. The conventional alkaline electrolyzers require auxiliary sub-systems such as heat exchangers and heaters that consume additional electricity in order to operate at the temperature of 70-80 °C (343-353 K) for low-cost hydrogen production.

Already there are proposals to further increase the efficiency of the alkaline electrolyser by operating at a higher temperature (i.e. above 80 °C or 353 K). In a study conducted in Denmark, [28] it was estimated that the cost of hydrogen is reduced by about 10 % by increasing the electrical efficiency of the alkaline electrolyser from the current 75 % to 100 % which is achieved at a cell operating voltage of about 1.48 V. The limited reduction in the cost of hydrogen in spite of 25 % increase in electrical energy efficiency has not limited research for a more efficient electrolyser since this is profitable for the people in the business of producing and selling hydrogen for energy storage applications and as chemical feedstock raw material. It is therefore no surprise that plans are made for large-scale production of hydrogen from alkaline electrolyzers in re-fuelling and dispensing stations [30] worldwide.

The UK government has planned to increase, from the current 2 % to 15 % of its renewable energy capacity by 2020 [1-2]. About 70 % of the projected 30 GW installed renewable energy capacity is anticipated to come from offshore wind turbines, which means in the foreseeable future the UK electrical grid network is likely to be characterised with large amounts of intermittent electricity that is generated from the wind turbines. Renewable electricity generation is favourable compared with other generation sectors as they have the advantage of low or no fuel costs and invulnerability to any penalty imposed on carbon emissions. For this reason, owners of renewable generation equipment may continue to enjoy government subsidy [31]. However, the price paid to renewable generators may also suffer if the operators are unable to deliver reliably according to efficiency and cost [32].

One remedy to this situation is to develop the technology that can efficiently convert renewable electricity into other forms of energy sources. An alkaline electrolyser and alkaline fuel cell system is potentially suited for *efficient energy conversion, energy storage and distribution of renewable electricity* as it offers high specific energy storage density at relatively low-cost investments [33] compared with the other forms of energy storage such as batteries and pumped-hydro. Alkaline electrolysers convert water and electricity into hydrogen and oxygen gases that can be stored as energy sources, distributed and converted back into electricity in alkaline fuel cells. Already there are a number of successful demonstration projects that have showcased the possibility to integrate the alkaline electrolyser with renewable energy systems [3-5, 34-35]. However, the limited reliability and flexibility of conventional temperature alkaline electrolysers have not justified this technology for energy storage applications. The conventional temperature alkaline electrolysers usually have operational range within 20% to 100% of their rated electrical capacity [3,5,34-35], which limits dynamic and/or continuous (steady-state) operation with renewable energy systems. Also, the conventional temperature alkaline electrolysers require significant auxiliary equipment which increase cost and make the technology not flexible for portable, stationary and transport applications. Therefore the aims of this thesis are:

- To analyse renewable energy systems consisting of alkaline electrolyser that is integrated with the electrical grid and renewable energy sources, and thereby identify scope for improving performance of the alkaline electrolyser.
- To investigate methods of reducing cost of hydrogen and oxygen production from the alkaline electrolyser.
- To investigate methods of improving reliability of the alkaline electrolyser for dynamic, intermittent and continuous (stead-state) operation with the electrical grid that is integrated with renewable energy sources.
- To investigate methods of enhancing efficiency, durability and robustness of the alkaline electrolyser.
- To investigate methods of improving flexibility of the alkaline electrolyser for portable, stationary and transport applications.

1.2 Alkaline Electrolysers for Decentralised and Distributed Generation of Renewable Energy

The renewable energy systems that are integrated with electrolysers are based on stand-alone systems and electrical grid connected systems. Table 1-2 gives a list of the best known installed hydrogen energy projects globally:

Table 1-2 Overview of wind/hydrogen systems installed worldwide

Year of installation	Location	Name of Project	Type of Electrolyser
2000	ENEA Research centre Cassicia,Italy	Prototype wind/electrolyser testing system for stand-alone operation [5].	10kW alkaline electrolyser
2001	University of Quebec,Trios-Rivere's Canada	Renewable system based on hydrogen for remote applications [36].	5kW alkaline electrolyser
2004	Utsira Island, Norway	Wind/electrolyser demonstration system for stand-alone operation by Statoil-Hydro [35].	50kW alkaline electrolyser
2004	West Beacon Farm, Loughborough, UK	Electrical-grid integrated renewable energy/electrolyser system by the Hydrogen And Renewable Integration (HARI) project team [3].	36kW alkaline electrolyser.
2005	Unst,Shetland island,UK	Wind/electrolyser system for stand-alone operation by PURE Energy [37].	Not exactly stated
2006	NREL,Golden,Colorado, USA	Electrical-grid integrated renewable energy/electrolyser system [38].	6kW PEM electrolyser
2007	Pico Truncado,Argentina	Wind/electrolyser system for stand-alone operation by CNEA [39].	6kW PEM electrolyser
2007	Keratea,Greece	Electrical-grid integrated wind/electrolyser system by the Centre For Renewable Energy Sources (CRES) [40].	25kW alkaline electrolyser

Notable amongst the renewable projects are the autonomous wind/hydrogen system that was developed by Statoil-Hydro [35] for the community on the island of Utsira (Norway), and the wind/hydrogen system that was developed by the HARI project

team for the West Beacon Farm in Loughborough (UK). These two major renewable energy systems have a similar concept that is illustrated in Figure 1-3, whereby the conventional temperature alkaline electrolyser was utilised to convert excess renewable electricity and water into hydrogen and oxygen. The oxygen is sometimes stored or vented to the atmosphere, but the hydrogen is usually stored and later utilised alongside air in the fuel cell to generate electricity when it is needed. In other words, the conventional temperature alkaline electrolyser was essentially utilised to produce hydrogen as part of a long-term energy storage medium.

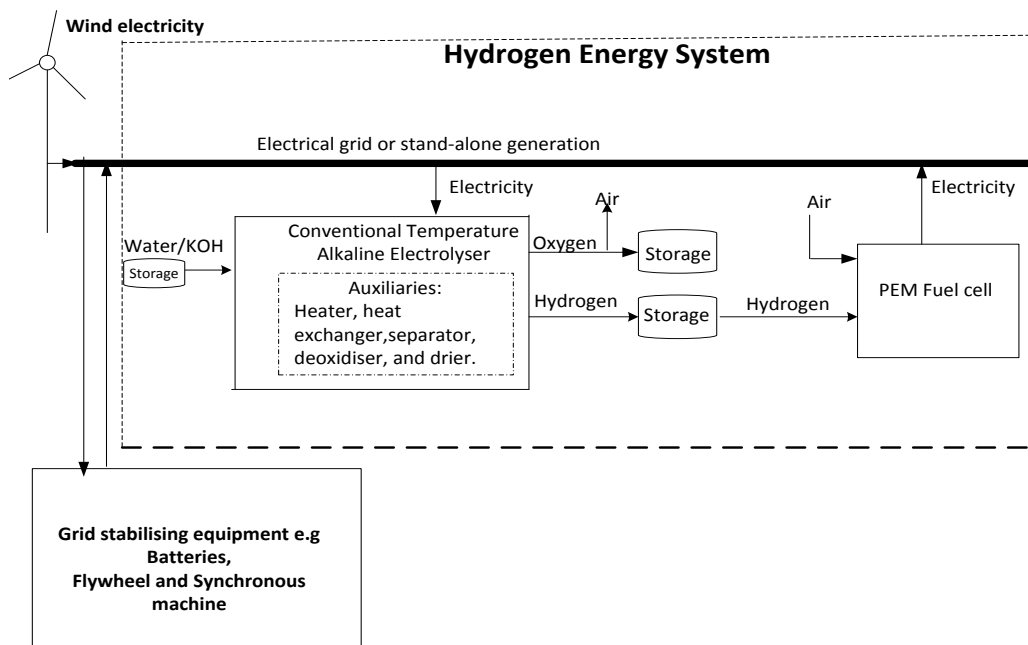


Figure 1-3 An illustration of currently installed Wind/Hydrogen energy systems utilising alkaline electrolysers

However, the limited operational ranges of conventional temperature alkaline electrolysers, the expensive requirement for storage and distribution of the hydrogen and low-round trip energy conversion efficiency are three main barriers to the sustainability of hydrogen energy systems. The conventional temperature alkaline electrolyser has limited operational ranges within 20 % to 100 % of rated capacity [3,35]. The high minimum input power (20 % of rated power) that is required means that the electrolyser and its auxiliary units have to be properly sized in order to allow

for continuous and dynamic operation with the wind energy supply. Part of the available electric load is used for heating purposes especially in remote communities where there is lack of access to other heat sources. As a consequence, the conventional temperature alkaline electrolyser was not in operation most of the time when there was either a power deficit or excess power from the wind turbines. For example in both the HARI and Utsira projects, the alkaline electrolyser was turned on/off several times due to power shortages from the wind turbines that were below the minimum operational limit or excess power from the wind turbines that was above the maximum operational limit. Grid stabilising equipment such as batteries, flywheel and synchronous machines were used most of the time for energy storage applications. During the periods of sufficient wind power however, it took more than 30 minutes [35] to turn on the electrolyser from stand-by mode into full operational mode. The increased start-up time is partly due to nitrogen purging that is normally done when the electrolyser is in stand-by mode and the requirement to maintain the optimum temperature of the stack by continued heating and cooling of electrolyte [3,35].

The technology for hydrogen storage also requires significant capital and operational cost investments. The project that was undertaken at CRES [40] has demonstrated that the hydrogen can be stored in metal hydride tanks in order to reduce storage capacity and ultimately achieve the DoE target [20]. However, the metal hydrides were made of rare earth metals such as lanthanum and cerium which are expensive and will require major scientific and technological breakthrough to commercialise. It is no wonder some experts are not optimistic about the so called ‘hydrogen economy’ due to a lack of affordable hydrogen storage and distribution infrastructure.

Also, the need for storage of hydrogen brings the issue of safety into consideration. The lower explosion limit (LEL) of hydrogen mixed with air or oxygen is 4 %, therefore care would be taken to avoid leakage of hydrogen from tanks or tube cylinders that are located especially in residential areas. The hydrogen is stored in steel tanks below ground at the hydrogen filling station in Porsgrunn [41]. However, storing hydrogen in vehicles poses danger in case there is hydrogen leakage that can cause explosion.

The hydrogen energy system is also limited due to low-round trip energy conversion efficiency⁴ [42]. The round-trip efficiency for an alkaline electrolyser and PEM fuel cell system is within 32 %-42% [43]. The round-trip efficiency is relatively low due to unreliability of the PEM fuel cells⁵. For example the Utsira PEM fuel cell [35] had severe problems of degradation that has made it impossible to reliably convert the hydrogen and air into electricity when it is needed. Apparently, as illustrated in Figure 1-3, oxygen that is produced from the alkaline electrolyser was not stored and air was used instead to operate the fuel cells. Oxygen from air could likely be contaminated with oxides of carbon which can accelerate deterioration of the synthetic polymer membranes in PEM fuel cells, or even formation of potassium carbonate which ‘poisons’ the electrodes in alkaline fuel cells [43].

Oxygen is required as an oxidant in a fuel cell. The oxygen is sometimes vented to atmosphere in conventional temperature alkaline electrolysers because the operators are mainly concerned to produce hydrogen that can also be used as chemical feedstock raw material. However, in the case of producing hydrogen for energy conversion, say from wind energy then the oxygen that is produced from the alkaline electrolyser should be stored and utilised as well. The production ratio (2:1) of hydrogen and oxygen respectively is the same as needed for the back conversion, and fuel cells operated with pure oxygen (instead of air which contains only 21 % oxygen) can perform with higher efficiency up to 70 % because of faster electrode reactions [43].

Alkaline electrolyser and alkaline fuel cell systems are capable of converting water and renewable electricity into pure hydrogen and oxygen that can be converted back into electricity when it is needed most. For example the hydrogen and oxygen product gases that are produced from the alkaline electrolyser can be directly utilised in the alkaline fuel cell to generate back electricity as shown in Figure 1-4. This will

⁴ The round trip energy conversion efficiency is the product of efficiencies of electrolyser and fuel cell. E.g. electrolyser efficiency of 71% x fuel cell efficiency of 45% = round-trip efficiency of 32%

⁵ A fuel cell is an electrochemical device that works as the reverse of electrolysers by combining gaseous hydrogen and oxygen to form electricity, water and heat

eliminate additional processing cost for the produced gases and allow for short or long-term energy storage and for distribution of renewable energy to off-grid locations. The hydrogen and oxygen energy system is potentially attractive to increase the round trip-energy efficiency by least 4.5 % compared with hydrogen and air energy system [44]. Further, the ambient temperature alkaline electrolyser can be utilised in the hydrogen and oxygen energy system to improve reliability, and flexibility at relatively lower cost, because by operating at the ambient temperature auxiliary equipment as well as auxiliary electricity consumption are minimised.

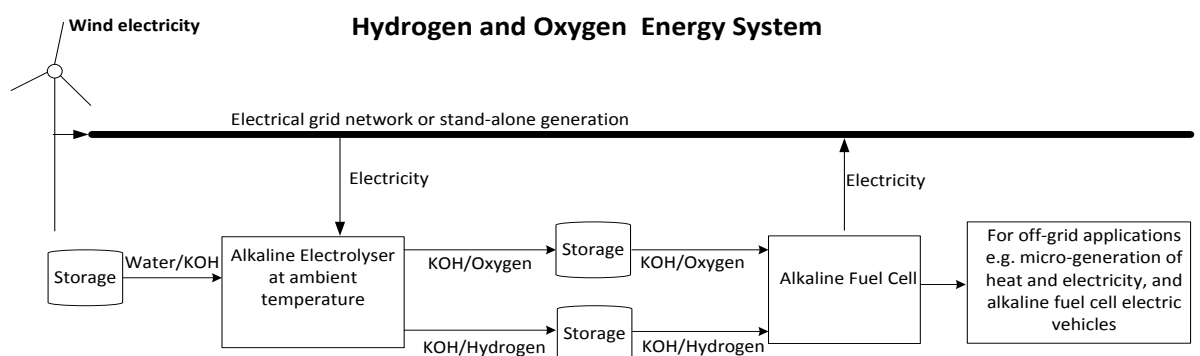


Figure 1-4 Proposed Wind/Hydrogen and Oxygen energy systems utilising alkaline electrolysers

The benefits of alkaline electrolysers for short or long-term energy storage applications and for distributing renewable electricity to off-grid locations cannot be overemphasised. The alkaline electrolyser can be utilised in renewable energy systems as energy storage medium and together with the alkaline fuel cell they can provide sustainable energy supply for off-grid/remote locations [35, 37, 45]. Moreover, the alkaline electrolyser offers the best alternative energy source to decarbonise the transport sector and promote development of fuel cell electric vehicles. Electric vehicles are not only important to decarbonise the transport sector and to reduce carbon emissions, but are also promising technologies that can be integrated with the electrical grid as flexible electrical load demand. A combination of alkaline electrolyser and alkaline fuel cell is a regenerative alkaline fuel cell that is relatively low cost and has significantly higher energy density compared with

batteries such as lithium ion, nickel-metal hydride, and lead-acid, and super capacitors for electricity generation in electric vehicles. As the energy density is increased, driving range of the electric vehicle can be extended. Hence, the alkaline electrolyser can be utilised as sustainable energy source to produce hydrogen and oxygen for alkaline fuel cell electric vehicles.

1.3 Sizing of the Electrolysers and Hydrogen Production Cost

The commercially available alkaline electrolysers are mostly large to medium scale and therefore require significant reduction in capital, operating and maintenance costs in order to produce electrolytic hydrogen that is competitive with hydrogen from SMRs at the selling price that is below \$ 2.85 /kg as set by the DoE [16,46]. However, as shown in Figure 1-5, the alkaline electrolysers that are currently in the market produce hydrogen at a cost price that is above \$ 4 /kg.

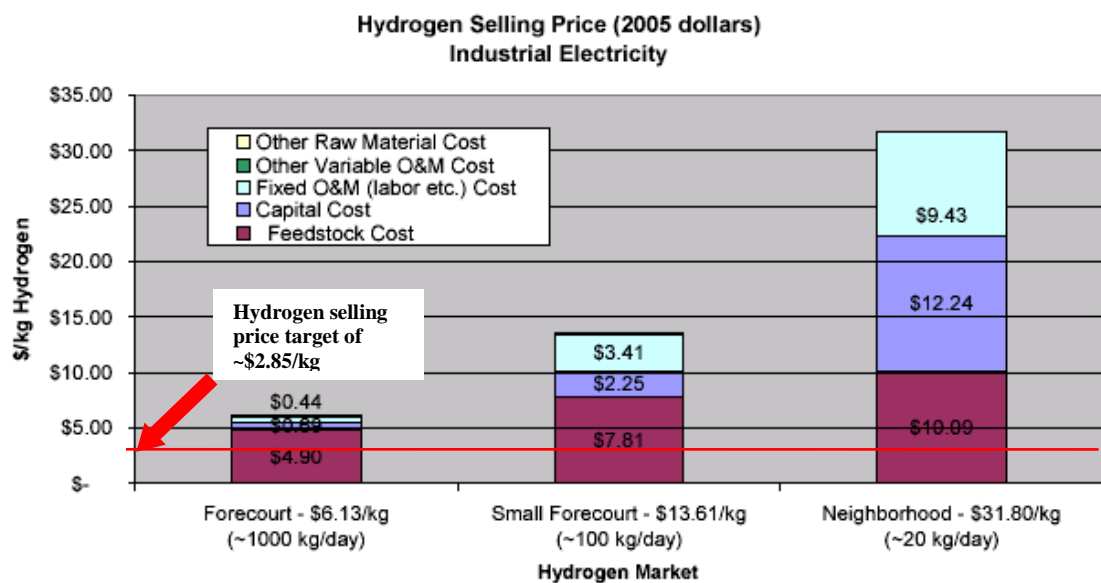


Figure 1-5 Hydrogen selling price produced by electrolysers of various capacities; Courtesy of Roy in 2006 [7]

The relatively high cost of electrolytic hydrogen has contributed to the low global market share that is currently below 4 % [7]. However, hydrogen as a fuel will be competitive with existing fossil fuels if the unit cost of electrolytic hydrogen is significantly reduced. For this reason, alkaline electrolyser manufacturers are aiming

to reduce hydrogen production cost below \$ 2.85 /kg by developing large to medium size ranges of alkaline electrolyzers which are more economical. However, as shown in Table 1-3, the typical commercial large-scale alkaline electrolyser is operated at a temperature of 80 °C (353 K) which requires auxiliary sub-units that consume additional electricity, and consequently increase the overall capital, operational and maintenance cost investments.

Table 1-3 Size and capacities of current commercial alkaline electrolyzers [46]

Manufacturer	Technology	System energy requirement including auxiliary sub-units (kWh/kg)	H ₂ production rate (kg/yr)	Power required for max H ₂ production rate (kW)	Operating temperature (°C)	Operating pressure (bar)
Avalence	Unipolar* alkaline	56.4-60.5	320-3,600	2-25	80	689.47
Teledyne	Bipolar alkaline	59.0-67.9	2,200- 33,000	17-240	80	6.89
Hydrogenics	Bipolar alkaline	53.4-54.5	2,400-71,000	15-360	80	24.82
NorskHydro	Bipolar alkaline	53.4	7,900- 47,000	48-290	80	15.99
NorskHydro	Bipolar alkaline	53.4	39,000-380,000	240-2,300	80	0.02

* In unipolar and bipolar cells the electrodes are in parallel and in series with respect to the electrical power source respectively see chapter 2 for details of unipolar and bipolar electrolyser configuration.

In contrast, however, the auxiliary sub-units are significantly minimised in an ambient alkaline electrolyser that is operated at the ambient temperature of say 23 °C (296 K), thereby potentially minimising system energy requirement as well as electricity consumption. Thus small to medium size ranges of ambient temperature alkaline electrolyser will be needed as they are economical and flexible for mass production and distributed energy generation, and are suitable for dynamic and continuous operation with renewable energy systems.

1.4 Nuclear-based Hydrogen from Alkaline Electrolyzers

Centralised methods of electrolytic hydrogen production might involve integrating alkaline electrolyzers with nuclear power plants in order to utilise nuclear heat and electricity for electrolysis. Nuclear energy offers an abundant energy source that is

clean, [47] although it could be expensive due to decommissioning costs and also environmentally damaging through the release of radioactive wastes. The technology is attractive for power generation because of the relative abundance of nuclear fuel such as Uranium-235. For example, in France where nuclear energy contributes more than 50 % of its installed generation capacity [6].

However, nuclear energy generation in the UK was only about 13 % of total electricity generated in 2008 [13]. The nuclear energy capacity has reduced due to closure of two major nuclear stations in 2007 and 2008. Figure 1-6 shows a schematic of the nuclear based hydrogen production process.

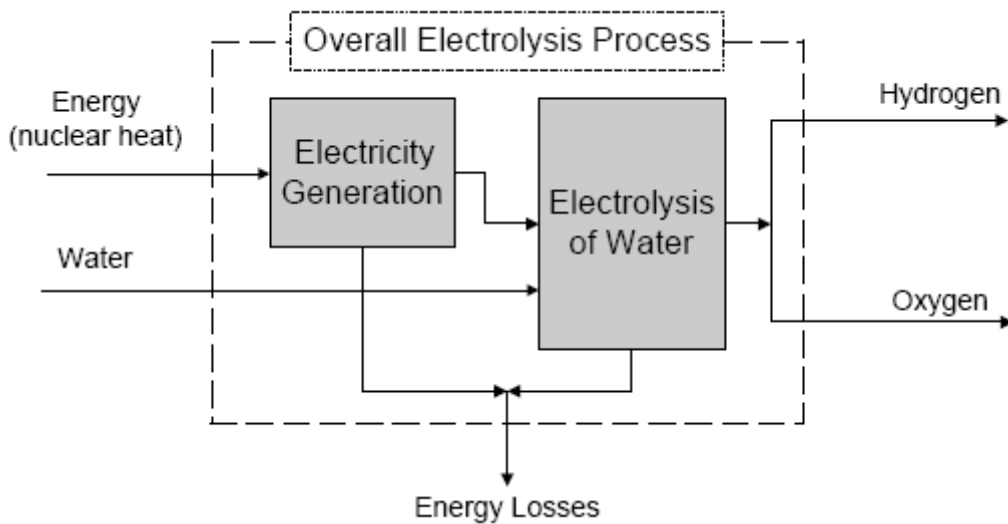


Figure 1-6 Schematic diagram of a nuclear hydrogen energy system; Courtesy of Leanne M. Crosbie [46]

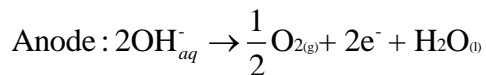
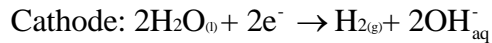
Currently, large-scale implementation of a nuclear hydrogen energy system is limited in terms safety and transport infrastructure. The thermal efficiency of nuclear plants is usually 30 % and the electrolyser has about 75 % electrical efficiency. Thus the energy efficiency of nuclear hydrogen is in the range of 22 % - 45 % [47] which can be increased further by developing newer nuclear plants that can operate at higher temperatures and have higher thermal efficiencies. However, the safety issues involved with locating the electrolyser near nuclear plants, the cost of transporting hydrogen through dedicated and distributed pipelines are inherent problems still to be tackled in this technology. Some investigations [47] have suggested operating the

electrolyser with off-peak electricity from other clean renewable resource such as wind turbines and then utilising nuclear heat from nuclear plants, but transport of heat from nuclear power stations to the electrolyser still requires significant capital cost investments. Therefore nuclear based hydrogen from conventional temperature alkaline electrolyser is not feasible in the near or medium term.

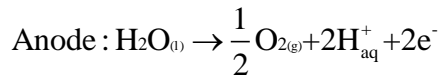
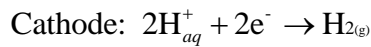
1.5 Comparison of Alkaline Electrolysers and Proton Exchange Membrane (PEM) Electrolysers for Dynamic Operation with Renewable Energy Systems

The conductive aqueous KOH in alkaline electrolysers and solid/immobilised PEM in PEM electrolysers play an important role to enhance their efficiencies as indicated in their respective half-cell reactions:

Alkaline electrolyser:



PEM (Proton exchange membrane) electrolyser:



Most commercially available alkaline electrolysers can be operated in the range of 20 % to 100 % of rated power but the commercially available PEM electrolyser can be operated in the range of 5 % to 100 % of rated power [46]. This means that PEM electrolysers have a wider operational window and thus appear better suited for dynamic operation especially at low electrical power inputs. The reason for this could be seen in Table 1-4, which indicates that the conventional alkaline electrolysers are operated at relatively higher temperatures compared with the PEM electrolysers that are operated at ambient temperatures and consequently wider electrical power range.

Table 1-4 Comparison of the commercial alkaline and PEM electrolyzers

Manufacturer /Project	Technology	Power rating for maximum hydrogen production (kW)	Part load range of rated power (%)	Efficiency (%HHV)	Operating temperature (°C)	Operating pressure (bar)	Electrode De-activation (%)
Casale Chemicals SA/Centre for Renewable Energy Systems (CRES) [40]	Alkaline electrolyser	25	20-100	65	70-80	20	2-5
Casale Chemicals/RES2H2 [40]	Alkaline electrolyser	25	20-100	Not stated	70-80	20	Not stated
Hydrogenics/HARI [3]	Alkaline electrolyser	25	20-100	75	70-80	25	Not stated
Hydrogenics [48]	PEM electrolyser	7.2	0-100	72	Ambient, +5 to +35	1.01 – 7.9	Not stated
Hydrogen Systems/Stralsund [49]	Alkaline electrolyser	20	Not stated	33-55	70-80	25	Not stated
Statoil Hydro [50]	Alkaline electrolyser	48	20-100	72-85	70-80	~15.85	Not stated
Statoil Hydro [50]	PEM electrolyser	40	5-100	81	45	~15.85	Not stated
Teledyne [50]	Alkaline electrolyser	17-240	Not stated	79-85	70-80	~4.14	Not stated
ELT GmbH or Lurgi[51]	Alkaline electrolyser	12-1392	25-100	Not stated	70-80	30	Not stated
GHW [52]	Alkaline electrolyser	2500	20-110	80-90	70-80	30	Not stated

The PEM electrolyser is capable of quick start-up (in less than 1 second) in variable electrical power mode, and hence is well suited for continuous and dynamic power of operation [35]. The PEM electrolyser is operated normally at the ambient temperature of say 5°C-45°C, thus requires relatively less auxiliary equipment compared with the conventional temperature alkaline electrolyser that is normally operated at higher temperatures of 70°C-80°C and requires significant auxiliary equipment. The PEM electrolyser has greater flexibility to variable input power because by operating at the ambient temperature it requires relatively less auxiliary systems and consumes less auxiliary electricity.

The main drawback of the PEM electrolyser however is its uncertainty in lifetime due to deterioration of the solid polymer membrane electrolyte [53]. For example the PURE⁶ project team [37] reported increased stack failure of the PEM electrolyser after operation at high electrical power. Also, the PEM electrolyser is limited due to

⁶Promoting Unst Renewable Energy

the expensive membrane-electrode assembly that consists of precious/noble metals as well as Nafion membrane. The alkaline electrolyser, on the other hand, is more matured as the lifetime duration can be up to 20 years. However, the limited operational range of conventional temperature alkaline electrolysers means that the electrolysers are not operational all the time under variable input power.

Statoil-Hydro [54] is one of the few electrolyser manufacturers that have made plans to develop an alkaline electrolyser that is capable of a wider operational range and quicker start-up under variable electrical input power. They plan to develop a high pressure (30 bar) conventional temperature alkaline electrolyser that is capable of dynamic operation at 5% -100% of its maximum electrical capacity and load change response time of less than a second. However, they have not yet demonstrated if this technology is feasible by operating at the conventional temperature. Nonetheless, this underscores the need to develop the ambient temperature alkaline electrolyser that is more compact and less costly for dynamic and flexible operation with renewable energy systems. Further, as the hydrogen and oxygen product gases from the alkaline electrolyser can be directly utilised in the alkaline fuel cells, the ambient temperature alkaline electrolyser and alkaline fuel cell system is therefore better suited for low cost energy conversion and storage, as well as distribution of renewable electricity.

1.6 The Strategy for Developing Highly Efficient Alkaline Electrolyser Cells and Objectives of PhD Research

The US DoE [24] has set a target hydrogen cost price of below \$ 2.85 /kg by the year 2015 which is adopted by some of the alkaline electrolyser manufacturers seeking to commercialise electrolytic hydrogen.

For example General Electric Global Research Centre [55] has adopted a commercial strategy to develop the alkaline electrolyser based on trade-offs between energy and capital cost requirements as shown in Figure 1-7. This Figure shows that as the operating current density is increased, production rates of hydrogen and oxygen are increased but energy cost increases due to increase in the cell voltage, and capital cost decreases due to decrease in the electrode active area. On the other hand, at lower operating current densities, production rates of hydrogen and oxygen are

reduced and energy cost is reduced but capital cost is increased. Hence, an optimum operating condition for the alkaline electrolyser would be a current density within 100 mA/cm^2 up to 200 mA/cm^2 , and a cell voltage within 1.7 V and 1.8 V.

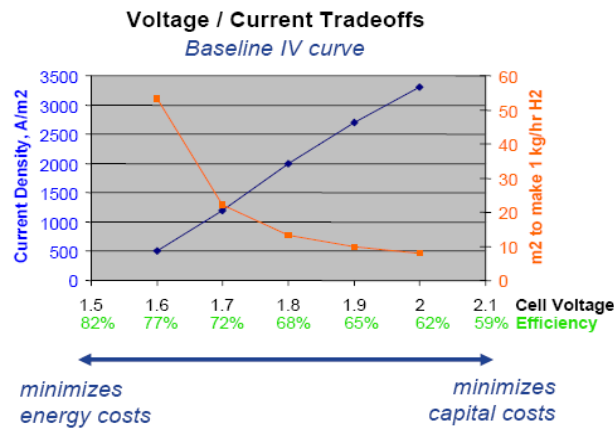


Figure 1-7 Commercial targets for low-cost hydrogen; Courtesy of GE Global Research Centre [55]

Accordingly, the current industry trend is to significantly minimise energy and capital costs of the alkaline electrolyser. The cell voltage determines electricity consumption as well as energy cost, which can be reduced by utilising low-grade heat to increase the operating temperature. Also, electricity consumption can be minimised by utilising relatively low cost electro-catalyst⁷ materials. Catalysts are usually coated on an electrode in order to increase the electrode active area and thereby reduce capital cost. Therefore electro-catalyst materials help to reduce energy and capital costs in the operation of alkaline electrolysers. The GE [55] strategy for developing low cost and highly efficient (low overpotential) electro-catalysts is shown in Figure 1-8, and Figure 1-9 shows that the cell over-voltages reduce at higher operating temperature.

⁷ Electro-catalyst is the electrode that is produced by adding a catalyst on an electrode substrate. For example the electrode that is produced by depositing a catalyst material such as nickel on an electrode substrate such as stainless steel mesh. The uncoated stainless steel mesh is the electrode and the stainless steel mesh coated with nickel is the electro-catalyst.

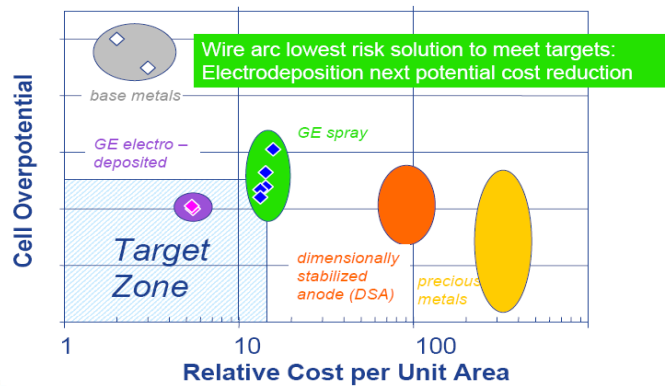


Figure 1-8 Electrode concept selection, target zone is for low cost and highly efficient electrode; Courtesy of GE global research centre [55]

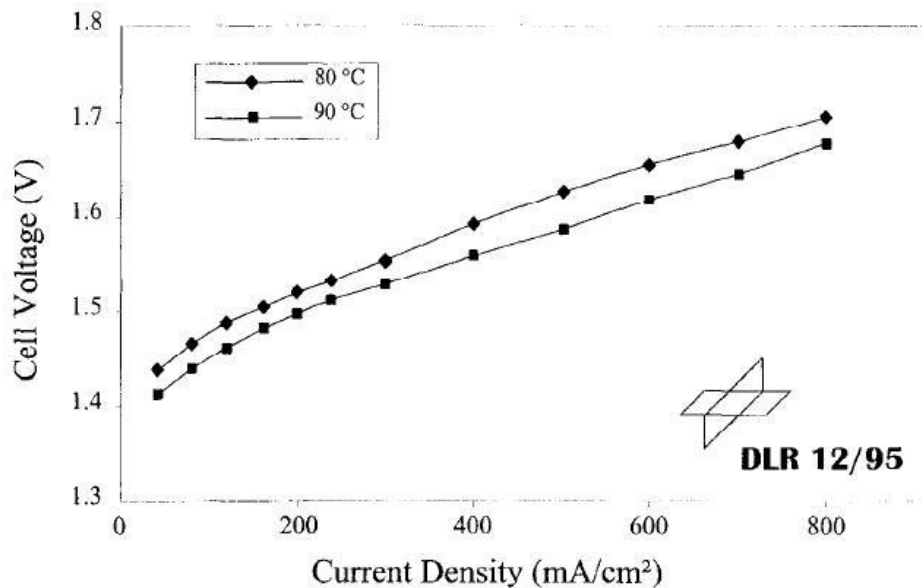


Figure 1-9 A typical effect of higher operating temperature to reduce over-voltages of the alkaline electrolyser cell; Courtesy of Vermeiren et.al [56]

It is projected that electricity prices will increase in the future [32] so it is necessary to reduce energy consumption in the alkaline electrolyser by reducing the operating cell voltage. As shown in Figure 1-10, the commercial manufacturers are developing highly active coated electrodes such as stainless steel metal that is coated with nickel and molybdenum in order to increase the electrical energy efficiency. Further examples of electrodes and electro-catalysts that increase electrical energy efficiency of the alkaline electrolyser are given in the subsequent chapter.

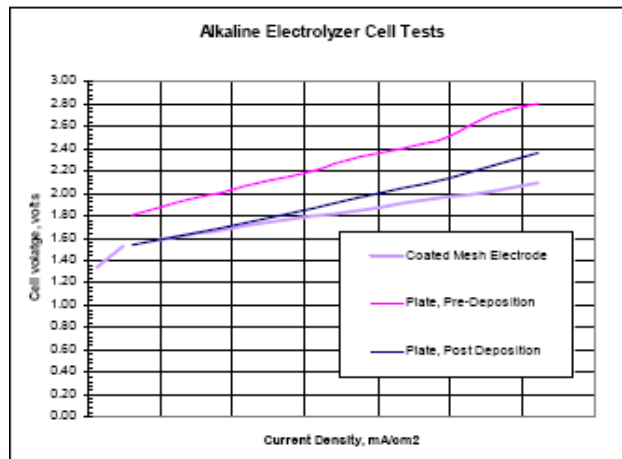


Figure 1-10 Strategy for electrode efficiency improvement. Voltage efficiency is enhanced for the coated mesh electrode; Courtesy of D. Swalla [57]

The cost of electricity consumption can be offset by increasing hydrogen and oxygen production rates in the alkaline electrolyser. Hence the industry trend is to reduce over-voltages and simultaneously increase current density in order to reduce operational and investment costs. Future plans are even aiming to operate the cells at higher temperatures of up to 100 °C [28] in order to reduce over-voltages down to 1.48 V and simultaneously increase current density.

However, a higher operating temperature accelerates electrode deactivation and degradation under variable electrical power of operation. For instance in the wind-hydrogen project that was undertaken at CRES [58] the electrode has degraded by about 2% - 5 % after intermittent operation at the conventional temperature. The manufacturers have adopted a method of preventing corrosion of the electrodes by applying ‘protective current’ in order to keep the cells working slightly and prevent mutual depolarisation of the bi-polar electrodes under open circuit. However, the ‘protective current’ could be up to 1.6 MWh annually [59] which increases operating and maintenance cost investments. The cost effective option however was to apply corrosion-resistant coatings on the electrodes by electro-deposition technique, yet the electro-catalyst coatings could not withstand the harsh alkali environment over long-term of operation.

Proposals were made to develop small to medium size range (50-250 kW) of electrolyser that can match with the AC/DC power electronics of the electrical supply and control system. In particular, Statoil-Hydro [35] suggested connecting the cells in series and/or in parallel in order to achieve the proper voltage levels close to the nominal operating voltage of the AC/DC rectifier. As much as it will be useful to model the alkaline electrolyser with respect to the AC/DC power electronics, the fundamental electrochemical processes that cause corrosion of electrodes have not been hitherto well elucidated. The suggestions made by some of the manufacturers [35, 59] and researchers [7] to apply ‘protective current or voltage’ and ‘control of AC/DC power electronics’ lack justifiable basis to tackle corrosion of electrodes in the alkaline electrolyser.

The alkaline electrolyser is a proven technology for integrating with renewable energy systems. However, the conventional temperature alkaline electrolyser is not suitable for dynamic, durable, robust and flexible operation with renewable energy systems. Any attempt to mitigate this problem has yet to be realised as long as the current industry trend for reducing hydrogen production cost is adopted. The electricity that is consumed in the ambient temperature alkaline electrolyser should no longer be considered a waste because the energy is converted and stored in the form of hydrogen and oxygen product gases that can be directly utilised in an alkaline fuel cell to generate back the electricity. Moreover, by operating at the ambient temperature corrosion rates of electrodes are likely to be minimised. The ambient temperature alkaline electrolyser is viable for dynamic, durable, robust and flexible operation with renewable energy systems. In recognition of these concepts lies the aim of this PhD thesis which is to develop an alkaline electrolyser that is highly efficient and durable under variable, constant and intermittent electrical power input for sustainable production of hydrogen and oxygen.

1.6.1 Objectives of PhD Research

- To investigate methods of producing clean and sustainable hydrogen and oxygen from renewable energy systems utilising alkaline electrolysers.

- To develop alkaline electrolyzers that can be highly responsive to variable input power from renewable energy resources.
- To develop relatively low-cost electrodes and electro-catalysts that are capable of enhancing electrical energy efficiency of the alkaline electrolyser.
- Seeking to minimise corrosion rates of the electrode that is operated under dynamic electrical power and in stand-by conditions.

Chapter 2

Recent Progress in the Research and Development of Alkaline Electrolyser Technology and Review of Literature

In this Chapter, the electrochemical, kinetic and thermodynamic governing principles are discussed for both the ambient temperature and conventional temperature alkaline electrolyzers. The ambient and conventional operating temperatures are 23°C and 80°C respectively, therefore the ambient temperature alkaline electrolyser requires no external heating of the electrolyte solution. An introduction to EIS characterisation of an alkaline electrolyser is also presented. The operational systems for ambient and conventional temperature alkaline electrolyzers are also considered, and it is shown that the ambient temperature alkaline electrolyser is capable of low-cost, highly efficient, dynamic and fast-response operation with renewable energy sources. The different types of electrolyser cell design are illustrated, with an emphasis on the filter-press type of electrolyser cell design that was developed in this study. In order to avoid duplicating research activity, it was necessary to review published works on electrodes and electro-catalysts that are utilised in conventional alkaline electrolyzers, and comparing the efficiency of these units with the commercial target for low cost hydrogen.

2.1 Basics of Alkaline Electrolyser Technology

The basic components of an alkaline electrolyser are the electrode, membrane and electrolyte which are illustrated in Figure 2-1, with the common material types shown.

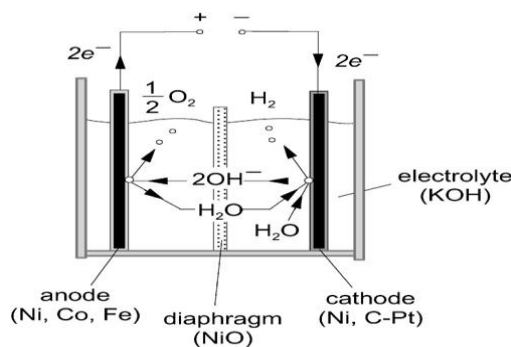
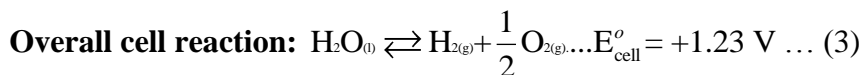
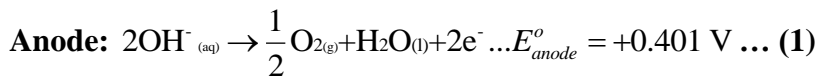


Figure 2-1 Schematic of an alkaline electrolyser cell consisting of electrode, electrolyte and membrane; Courtesy of [28, 60]

The anode and cathode are the positive and negative electrodes respectively which are connected externally to a direct current (DC) electrical source. Electrons flow into the cathode where hydrated cations or positively charged hydroxonium ions are present to gain electrons and become reduced into hydrogen and hydroxyl ions. On the other hand, at the anode, hydroxide anions are present to give away their electrons and become oxidised into oxygen and water. Therefore production of hydrogen gas is from the cathode and oxygen gas is from the anode. Catalysts are normally added to the anode and cathode electrodes to facilitate the charge transfer processes and consequently enhance the efficiencies of oxygen and hydrogen production respectively. As water is not a very good electrical conductor; the conductivity of deionised water is about 5.5 $\mu\text{S/m}$, potassium hydroxide is added as an electrolyte to enhance the ionic conductivity of water hence, the 30 % aqueous solution of potassium hydroxide has conductivity of about 40 S/m below 100 $^{\circ}\text{C}$. Other methods to enhance ionic conductivity of the electrolyte involves: increasing the operating temperature, reducing the separation distance between the electrodes, stirring/agitation of the electrolyte solution and use of appropriate membrane between the electrodes. The generated hydrogen and oxygen gas-bubbles during electrolysis could subsequently hinder the electrolysis process by increasing the internal cell resistance. Therefore, increasing the electrolyte temperature, reducing separation distance between the electrodes and stirring/agitation of the electrolyte solution facilitates removal of the gas-bubbles from the electrolyser and thereby reduce internal cell resistance. The membrane or diaphragm ensures separation of the hydrogen and oxygen gases as well as selective transport of hydroxide ions and water across the electrodes. The electrochemical reactions taking place in the alkaline electrolyser can be written as [61]:



As can be seen from the overall reaction (3), equilibrium is established for water and its constituent hydrogen and oxygen molecules. The forward process i.e. electrolyser operation requires energy input whereas the backward process i.e. fuel cell operation is favoured under standard temperature and pressure conditions. In other words, energy is required to drive the forward process of water splitting, and energy is generated in the spontaneous backward process of water formation. This reversible property of water splitting and formation can be utilised for energy storage applications, provided the hydrogen and oxygen product gases are captured from the alkaline electrolyser and are subsequently utilised in the alkaline fuel cell to generate back electricity. The equilibrium cell potential of $E_{cell}^o = +1.23$ V is the potential difference between the anode and cathode [60] as expressed in equation 4:

$$E_{cell}^o = E_{anode}^o - E_{cathode}^o \quad (4)$$

The equilibrium cell potential is also regarded as the reversible cell voltage or open-circuit voltage (OCV) under zero net electrical current load of the alkaline electrolyser.

2.2 Comparison of Efficiency of the Ambient and Conventional Temperature Alkaline Electrolyser

The equilibrium cell voltage is related to the Gibbs free energy as expressed in equation 5:

$$\Delta G^o = nFE_{cell}^o \quad (5) \quad (\Delta G^o = +237.2 \text{ kJmol}^{-1}) \quad [61]$$

The *reversible cell voltage* is the minimum electrical energy requirement for electrolysis to take place. For an isolated cell, the *thermoneutral voltage* ($E_{therm}^o = +1.48$ V) [6, 61] accounts for the energy balance between electrical and thermal energy requirement based on the relation:

$$\Delta H^o = \Delta G^o + T\Delta S^o \quad (6)$$

The *thermoneutral voltage* is almost independent of the operating temperature, but the *reversible voltage* is slightly reduced by about 5% as the operating temperature is increased by 57°C as shown in Table 2-1.

Table 2-1 Comparison of thermodynamic voltages of the ambient and conventional temperature alkaline electrolyzers [6]

Temperature dependence of the thermodynamic voltage at atmospheric pressure	Voltage (V) of ambient alkaline electrolyser at 23°C	Voltage (V) of conventional alkaline electrolyser at 80°C
$E_{rev} = 1.5184 - (1.5421 \times 10^{-3} \times T_K) + (9.523 \times 10^{-5} \times T_K \times \ln T_K) + (9.84 \times 10^{-8} \times T_K^2)$	1.23	1.18
$E_{therm} = 1.5187 - (9.763 \times 10^{-5} \times T_K) - (9.50 \times 10^{-8} \times T_K^2)$	1.48	1.47

The voltage efficiency⁸ is based on the cell voltage as expressed in equation 7 [61].

$$\eta_{ELEC} = \frac{1.48}{E_{cell}} \quad (7)$$

Where

$$E_{cell} = (E_{anode}^o - E_{cathode}^o) + \sum \eta_{electrode} + JR_{\Omega} \quad (8)$$

From thermodynamic stand-point, the efficiency of conventional temperature alkaline electrolyser is increased by applying external heat to raise the operating temperature and as a result reduce the electrical energy demand. This is illustrated in the temperature –voltage plane that is shown in Figure 2-2:

⁸The electrolyser efficiency is estimated based on two main methods which are voltage efficiency and hydrogen production efficiency. The voltage efficiency in particular is a comparison between total cell voltage and thermodynamic cell voltage.

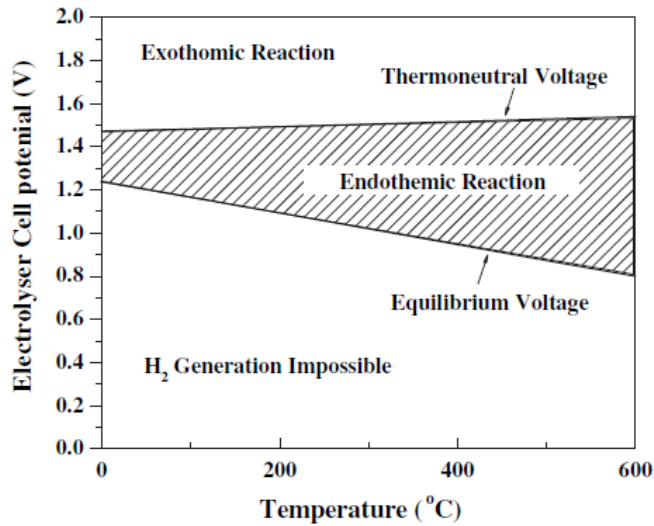


Figure 2-2: Cell potential for hydrogen production by water electrolysis as a function of temperature; Courtesy of Zeng *et.al* [61].

Figure 2-2 shows that water electrolysis does not take place below the equilibrium voltage that is related to the electrical energy demand and which reduces as the operating temperature is increased. The thermoneutral voltage is the actual electrical energy demand that also accounts for the heat energy demand for water electrolysis to take place. Hence, water electrolysis is endothermic and exothermic below and above the thermoneutral voltage respectively. In the operation of conventional temperature alkaline electrolyser, external heat is applied in addition with internal heat that is generated due to electrolysis (resistance losses). As a result, most conventional alkaline electrolysers operate above the thermoneutral voltage i.e. in the exothermic mode and thus heat removal from the stack or electrolyte cooling becomes necessary in order to maintain the operating temperature around 80-90°C which is below the boiling point of the reactant water. The advantage however, for operating at a higher temperature is to reduce operating cost and enhance efficiency especially by utilising low-grade or waste heat to raise the electrolyte temperature.

The voltage efficiency is relatively higher at the conventional temperature because the total cell voltage (E_{cell}) is reduced. The reversible voltage is slightly reduced by about 5 % while the over-voltages due to resistance from the electrodes, transport resistance of the electrolyte solution, membrane resistance and resistance of the electrical circuit are significantly reduced by more than 10 % at the conventional

operating temperature. This means the thermodynamic and kinetic efficiency is influenced by temperature. However, higher operating temperature can lead to increased corrosion rates of the electrode and cell components. The kinetic efficiency, however, can be increased at an ambient operating temperature by electro-catalysis i.e. addition of catalyst to the electrode and by good electrochemical engineering of the cell involving optimising the cell configuration, management of ionic transport and mass transport of the gas-bubbles.

The kinetic efficiency can be increased by reducing the total cell voltage and simultaneously increasing the current density for hydrogen and oxygen production. This can be achieved by electro-catalysis and appropriate cell design, which is demonstrated in this research from Chapter 3 up to 7. The efficiency of electrodes also depends on the electrical power profile of operation. Thus, at low electrical power of operation, over-potential due to electrode reactions becomes predominant while at high electrical power of operation, over-potential due to electrolyte conductivity and gas-bubbles become predominant. Therefore, under variable electrical power of operation the cell voltage should account for electrode overpotential and Ohmic overpotential. The electrode overpotential accounts for activation and concentration polarisation losses as expressed in equation 9, whereas the Ohmic overvoltage is accounted by the JR_{Ω} term that is expressed in equation 8. The activation overvoltage is the extra potential due to charge transfer processes taking place on the electrode. The Ohmic overvoltage is the extra potential due to ionic transfer, gas-bubble void fraction, and nature of membrane, while the concentration overpotential is the extra potential due to electrolyte concentration difference/gradient near the electrode surface.

$$\Sigma \eta_{electrode} = \eta_{act} + \eta_c \quad (9)$$

The key objective is to develop the electrode and electro-catalysts that have low activation overpotential, and to design the cell that minimises Ohmic and concentration over potentials. This will no doubt increase efficiency of the alkaline electrolyser under variable electrical power of operation.

The resistances that cause inefficiency in the alkaline electrolyser are: electrical resistance, reaction resistance and transport resistance [61] which are illustrated in Figure 2-3.

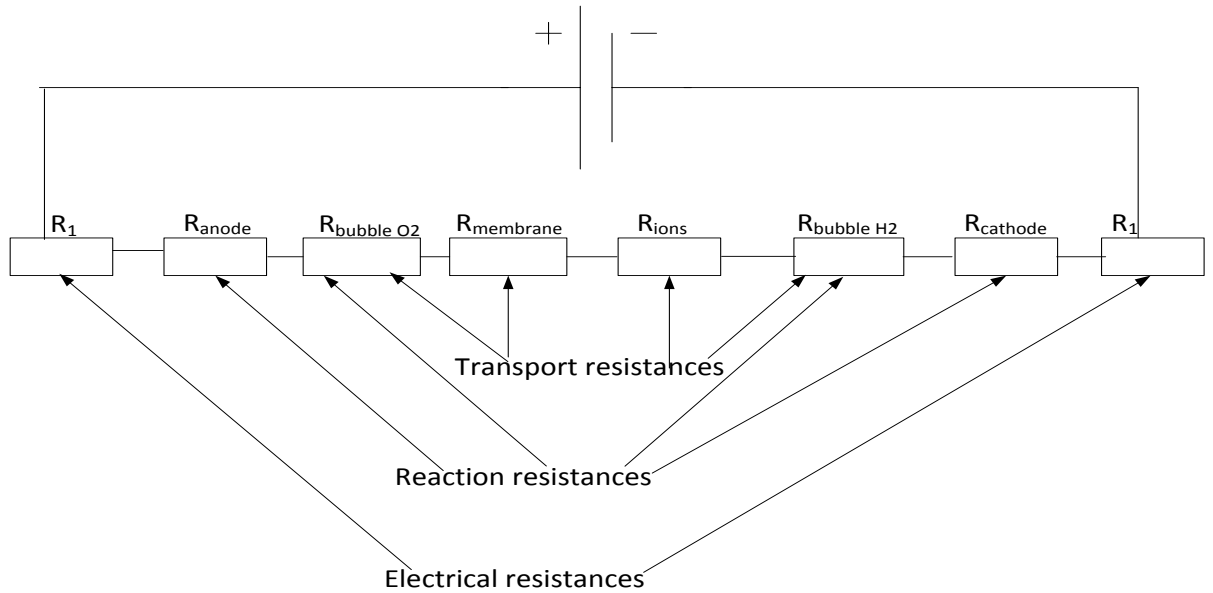


Figure 2-3 Schematic illustration of the cell resistances⁹ [61]

The resistances cause heat to be generated in the alkaline electrolyser according to the Joules law [61-63] and transport phenomena [62-63]. The ‘leakage’ current is a parasitic current that also generates heat in the cell. The parasitic current does not take part in electrolysis and contributes to cell voltage inefficiency. Equation 10 describes the temperature rise due to internal heat generation in the alkaline electrolyser. For example assuming that; total cell voltage (E_{cell}) is 2.12 V at 200 mA/cm² and at 23°C, standard cell voltage (E_{cell}^o) is 1.48V, specific heat capacity of water (C_p) is 4.18 J/gK, number of moles of electrons (n) is 2 moles, and Faraday’s constant (F) is 96,500 C/mol; it is estimated based on equation 10 that the electrolyte temperature will rise by 30°C for electrolysis of 1 kg of aqueous potassium hydroxide electrolyte at the ambient temperature.

⁹ The reaction resistance is the same as activation resistance or polarisation resistance; The transport resistance is the same as Ohmic resistance.

$$\Delta T = \frac{nF(E_{cell} - E_{cell}^o)}{C_p m} \quad (10)$$

The amount of oxygen and hydrogen that is generated from the alkaline electrolyser can be determined based on the amount of charge that is conducted by the electrode. Thus for a given cell voltage the electrode conducts charges that are proportional to hydrogen and oxygen production rates. Based on the stoichiometry of equations 1 and 2, hydroxyl ions (OH^-) are the electro-active ions at the anode that generates oxygen and water, while reactant water or hydroxonium ions (H_3O^+) are the electro-active ions at the cathode that generates hydrogen and hydroxyl ions. The amount of charge which is product of current and time is proportional to the number of moles of electro-active ions as described in equation 11.

$$N = \frac{Jt}{nF} \quad (11)$$

The current density rather than current is proportional to the corrosion rate of the electrode because the same current that is concentrated in a smaller area results in a larger corrosion rate. In other words, besides hydrogen and oxygen production rates, the current density also accounts for corrosion rate per unit of active area of the electrode. The Faraday's relation given in equation 12 can be used to determine production rates of hydrogen and oxygen gases as well as mass loss of electrode due to corrosion.

$$m = \frac{Jta}{nF} \quad (12)$$

Where: J can also be equal to J_{corr} that accounts for current density of production as well as corrosion rate per unit of electrode active area.

2.3 Electrical Double-Layer Capacitance and Electrode Kinetics

The ionic composition in the electrolyte solution forms a *double-layer* that is illustrated in Figure 2-4. The phenomenon of *double-layer* formation also leads to capacitance of the alkaline electrolyser, which is due to electric and ionic charges at the electrode/electrolyte interface. The capacitance therefore is a measure of the amount of charges that are stored per unit of potential difference between the electrodes. The capacitance depends on the electrode potential, electrolyte conductivity, liquid-gas or gas-bubbles concentration near the electrode surface, separation distance between the electrodes and geometry of the electrode/electrolyte interface. At high current density, of say $>0.5 \text{ A/cm}^2$, mass transport limitation of ions in the electrolyte solution can lead to a concentration gradient near the electrode surface and consequently concentration polarisation [63].

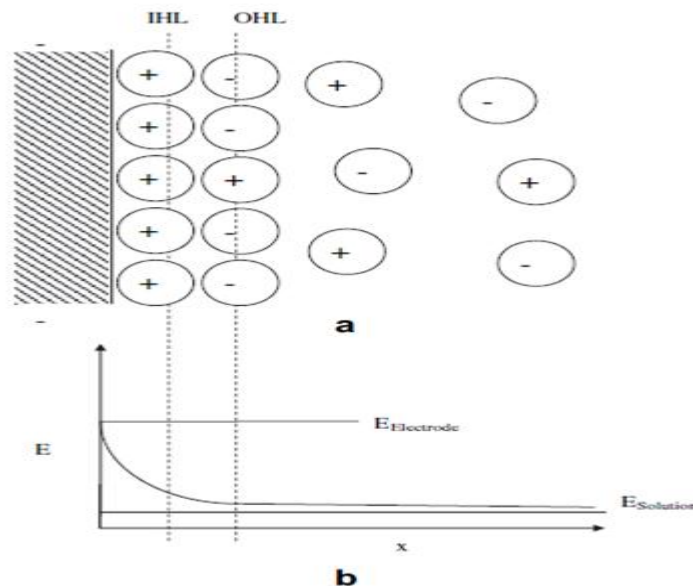


Figure 2-4 Schematic of the electrolytic double-layer in the alkaline electrolyser, potential of the electrode is stable but potential due to the solution varies with distance; Courtesy of Zeng *et al* [61].

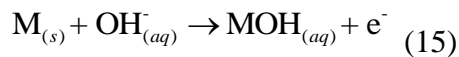
The two layers that are formed, the inner Helmholtz layer (IHL) and outer Helmholtz layers (OHL) [7], are distorted as the current density varies. Concentration polarisation takes place due to an interfacial potential difference between the electrode surface and electrolyte solution; in particular between the anode surface and the adjacent electrolyte solution. The electrode polarisation due to limited

depletion of hydroxyl ions near the anode surface can be determined based on the Nernst equation 13, and the concentration polarisation is expressed in equation 14 [64].

$$E_{electrode} = E_{electrode}^o + 0.0592 \log_{10} C_{OH} \quad (13) [64]$$

$$\eta_c = 2.3 \frac{RT_K}{nF} \log \left(1 - \frac{i_a}{i_L} \right) \quad (14) [64]$$

The OCV depends on capacitance which varies due to charge and gas-bubble migration. Thus a rapid drop in current i.e. instantaneous cell shut-down does not always result in a rapid drop in the cell voltage as only the Ohmic voltage drops rapidly but the activation voltage drops fairly slowly to its equilibrium value. The OCV is critical as it determines the minimum electrical energy that is required for electrolysis and also indicates internal energy in the alkaline electrolyser. The migration of ions and transport of gas-bubbles near the electrode surface influence the OCV. The electrochemical process taking place on the electrode and in the electrolyte that is on open-circuit can be illustrated in equation 15, and Figure 2-5 shows that the double-layer capacitance is in series with the Ohmic resistance under open-circuit. A quantitative model of the OCV should be carried-out in order to better predict the conditions influencing OCV but that is slightly beyond the scope of this thesis. Nonetheless, in Chapter 7, qualitative conditions affecting the OCV are presented and discussed.



Where M is the electrode metal

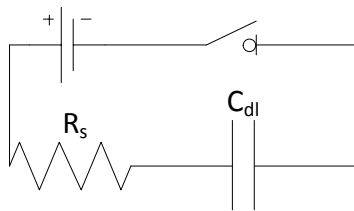


Figure 2-5 Electrochemical circuit of the alkaline electrolyser under open-circuit

2.3.1 Hydrogen Evolution Reaction (HER) and Oxygen Evolution Reaction (OER) Mechanisms on the Electrode

The kinetic mechanism for the hydrogen evolution reaction is widely accepted to be a series of steps as described below [65]:

$\text{H}_2\text{O} + \text{M} + \text{e}^- \rightarrow \text{MH}_{\text{ads}} + \text{OH}^-$ (16); which is the Volmer mechanism involving water dissociation through a reduction process that leads to metal hydride formation.

This is followed by either the electrochemical desorption:

$\text{H}_2\text{O} + \text{MH}_{\text{ads}} + \text{e}^- \rightarrow \text{H}_2 + \text{OH}^- + \text{M}$ (17); which is the Heyrovsky mechanism involving water dissociation through a reduction process that leads to hydrogen evolution.

Or by chemical desorption:

$\text{MH}_{\text{ads}} + \text{MH}_{\text{ads}} \rightarrow \text{H}_2 + 2\text{M}$ (18); which is the Tafel mechanism involving combination of atomic hydrides to form hydrogen molecules.

The overpotential for hydrogen formation is generally given by the Tafel equation 19 [24]:

$$\eta_{\text{cathode}} = 2.3 \frac{RT_K}{\alpha F} \log \frac{i_c}{i_o} \quad (19);$$

Where the cathodic Tafel constant is $\beta_c = 2.3 \frac{RT_K}{\alpha F}$ (20)

Likewise, the oxygen evolution reaction [61] is known to be a stepwise process:

$\text{OH}^- \rightarrow \text{OH}_{\text{ads}} + \text{e}^-$ (21); which involves adsorption of hydroxides followed by:

$\text{OH}_{\text{ads}} + \text{OH}^- \rightarrow \text{O}_{\text{ads}} + \text{H}_2\text{O} + \text{e}^-$ (22); which involves oxidation to higher oxides, and

$O_{ads} + O_{ads} \rightarrow O_2$ (23); which involves combination of atomic oxides to form oxygen molecules.

The overpotential for oxygen formation is generally given by the Tafel equation 24:

$$\eta_{anode} = 2.3 \frac{RT_K}{(1-\alpha)F} \log \frac{i_a}{i_o} \quad (24);$$

Where the anodic Tafel constant is $\beta_a = 2.3 \frac{RT_K}{(1-\alpha)F}$ (25)

The overall activation overpotential is expressed in equation 26:

$$\eta_{act} = 2.3 \frac{RT_K}{\alpha F} \left(\log \frac{i_c}{i_o} \right) + 2.3 \frac{RT_K}{(1-\alpha)F} \left(\log \frac{i_a}{i_o} \right) \quad (26)$$

The total electrode overpotential is expressed in equation 27 which accounts for activation and concentration polarisations.

$$\sum \eta_{electrode} = 2.3 \frac{RT_K}{\alpha F} \left(\log \frac{i_c}{i_o} \right) + 2.3 \frac{RT_K}{(1-\alpha)F} \left(\log \frac{i_a}{i_o} \right) + 2.3 \frac{RT_K}{nF} \log \left(1 - \frac{i_a}{i_L} \right) \quad (27)$$

The activation overpotential is related to the activation energy which depends on several factors including: temperature, current density, and exchange current density of the electrode. Considering equation 26, it looks like activation overpotential increases as temperature increases, but in practise activation overpotential is significantly reduced as exchange current density is increased [66-68]. The exchange current density is the equilibrium rate constant of the electrode reaction. It is that current in the absence of net electrolysis that is a balance of partial anodic and cathodic current at the electrode/solution interface. Hence, it accounts for electrode activity in the alkaline electrolyser. A good electrode will exhibit a high exchange current density and a low Tafel slope, which can be achieved with a high surface area

electro-catalyst that has favourable microstructure and good electronic conductivity. In the subsequent chapter, method of determining the Tafel slope and exchange current density from empirical data is demonstrated.

The Tafel slope is widely reported in the literature [61] for comparing different electrodes and also for determining reaction mechanisms. For example in the *HER* mechanism, if the Volmer reaction step i.e. adsorption of hydrogen is the rate determining step, the resulting Tafel curve should yield a slope of around 120 mV at 25 °C [69]. On the other hand, if the Heyrovsky step i.e. hydrogen desorption is rate determining, the measured Tafel slope should yield a value of about 40 mV or 50 mV at 25 °C. The Tafel slope and exchange current density are determined from the current-overvoltage polarisation plot that is generally known as the Tafel curve. However, the general method to determine exchange current density from the Tafel curve based on the current density at zero overpotential is not reproducible for comparing activity of different electrodes. Hence researchers have presented data which vary by almost ten orders of magnitude even for the same electrode material [70]. In the subsequent chapter, however, a reliable method to determine the exchange current density is demonstrated based on EIS measurement of polarisation resistance.

Concentration polarisation takes place more readily at the anode in the alkaline electrolyser. This partly explains why anodic overpotential is generally higher than cathodic overpotential [61]. Although there are other factors responsible for higher anodic overpotential such as: (a) formation of oxides on the anode surface (b) increase in corrosion rates of electro-catalyst and catalyst support (c) complex mechanism of oxygen evolution and reduction, which involves electron and proton transfers and (c) relatively slow kinetics of oxygen evolution [70]. During electrolysis, negative charged hydroxyl ions (anions) migrate to the positive electrode (anode) where they are converted into oxygen and water by the loss of electrons. However, transport resistance of hydroxyl ions takes place due to the nature of the membrane, the separation distance between the electrodes and conductivity of the electrolyte thereby resulting in a concentration gradient and

ultimately leading to a concentration polarisation at the anode. In contrast, concentration polarisation is less likely to take place at the cathode as there is availability of reactant water near the cathode surface. Water molecules are always present at the negative electrode (cathode) where they are converted into hydrogen and hydroxyl ions by the addition of electrons.

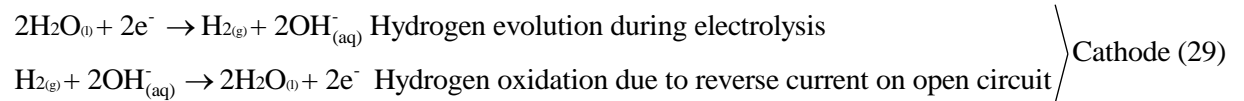
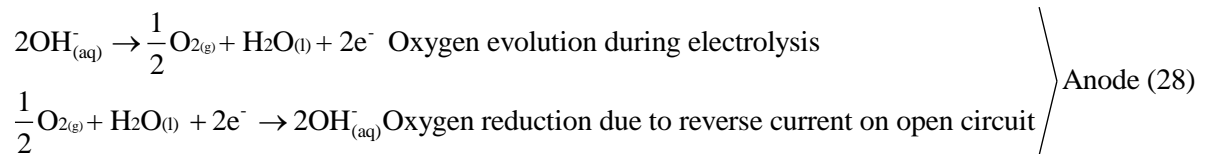
The predominant reaction step for electrode kinetic mechanisms is dependent on the surface structure of the electrode as reported by Zeng and co-workers [61]. They have proposed that edges and cavities of the electrode surface influence the rate of hydrogen adsorption, and that the degree of surface roughness or perforation on the electrode surface determines the rate of hydrogen desorption. Therefore the electrode surface must provide adequate sites for nucleation of gas bubbles and facilitate the escape of gas bubbles in order to prevent gas trapping or gas bubble coverage. Typical diameters for electrode perforation are 0.1 mm for the cathode and 0.7 mm for the anode [6, 71]. The commercially available stainless steel metal meshes (type-304) which has an aperture size of 0.15 mm was investigated predominantly in this research as described in the subsequent chapters.

Passivation of the electrode due to oxide formation could result to higher anodic overpotential compared to cathodic overpotential that is due to hydride formation. Oxide or hydride products that are formed on the electrode surface can be removed by neutralisation reaction that takes place by reversing the electrode polarity after some time of electrolysis. This method is recognised in the literature as Reverse Potential Cycling (RPC) [72]. For example after some time of electrolysis, reversing anode to cathode would generate hydrogen on the same electrode thereby removing oxide products by neutralisation reaction. Similarly, after some time of electrolysis, reversing cathode to anode would generate oxygen on the same electrode thereby removing hydride products by neutralisation reaction. For this reason, *HER* and *OER* electrolysis were carried-out reversibly on the electrodes as evident in the subsequent Chapters.

2.3.2 Corrosion of the Electrode during Electrolysis and Open Circuit

Conditions

Corrosion takes place on the electrode due to reversible electrochemical reactions that take place during electrolysis and under open circuit as described in equations 28 and 29. During intermittent operation and under open circuit, commercial alkaline electrolysers are prone to mutual depolarisation/ discharge of the bi-polar electrodes due to reverse current [6]. Thus reversible reactions of oxidation and reduction take place on the same electrode and result in corrosion. For example at the anode, oxygen evolution takes place during electrolysis and oxygen reduction takes place due to reverse current under open circuit. On the other hand, at the cathode, hydrogen evolution takes place during electrolysis and hydrogen oxidation takes place due to reverse current under open circuit. This is illustrated in equations 28 and 29 respectively.



2.4 Introduction to Electrochemical Impedance Spectroscopy (EIS) of Alkaline Electrolysers

The electrochemical processes taking place in the alkaline electrolyser can be electrically modelled by resistors and capacitors. The electrical resistance is a measure of opposition to the flow of electric current. However, the magnitude of resistance or opposition to current can be dependent on frequency due to capacitance. Therefore the impedance is a measure of opposition to flow of electrical current at an applied voltage over a broad range of frequencies. The EIS provides qualitative and

quantitative information on reaction rates, reaction mechanisms and corrosion rates of electrodes in the alkaline electrolyser.

During impedance measurement, a frequency response analyser (FRA) supplies a small sinusoidal AC voltage that is added to a DC bias voltage that is then supplied to the electrolyser as illustrated in Figure 2-6. The AC current response is recorded and the impedance is then determined over a given frequency range.

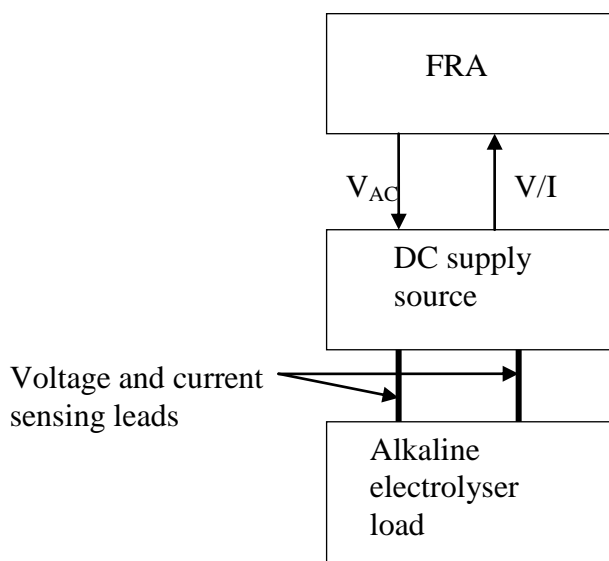


Figure 2-6 Schematic of EIS measurement

The sinusoidal AC voltage is expressed in equation 30 [73-74]:

$$V_{AC} = |V_o| \sin(\omega t) \quad (30)$$

The current response is shifted in phase by an angle due to capacitance as expressed in equation 31:

$$I_{AC} = |I_o| \sin(\omega t + \phi) \quad (31)$$

The German physicist Georg Ohm defined ‘Ohms Law’ in 1827 that electrical resistance is the ratio of potential difference to the current flowing through the conductor. The impedance is determined based on Ohms law provided the applied AC signal is small enough not to interfere with the linear relation between DC

voltage and DC current. Hence the impedance is determined as described in equation 32:

$$Z(\omega) = \frac{V(t)}{I(t)} = \frac{|V_o| e^{j\omega t}}{|I_o| e^{j(\omega t + \phi)}} \quad (32)$$

The impedance is resolved into its ‘real’ and ‘imaginary’ components [73] by vector representation, complex analysis and trigonometry. The real component accounts for the resistance that is independent on frequency while the imaginary component accounts for the capacitance that is dependent on frequency. The real and imaginary components are expressed in equations 33 and 34 respectively.

$$Z' = \frac{|V_o| \cos(\omega t)}{|I_o| \cos(\omega t + \phi)} \quad (33)$$

$$Z'' = \frac{|V_o| \sin(\omega t)}{|I_o| \sin(\omega t + \phi)} \quad (34)$$

The real and imaginary impedance, phase angle and the magnitude of impedance are the four basic experimental data that are determined by EIS measurement, and are expressed from equations 35 to 37.

$$Z(\omega) = Z' + jZ'' \quad (35)$$

$$\tan \phi = \frac{Z''}{Z'} \quad (36)$$

$$|Z|^2 = |Z'|^2 + |Z''|^2 \quad (37)$$

The various physicochemical processes such as electron and ion transport, liquid-gas transport occur at different rates within the alkaline electrolyser and therefore take

place at different characteristic time constants and AC frequencies. The overall equivalent circuit model of the EIS data is used to extract information about physicochemical properties of the electrode. For example as shown in Figure 2-7, the simple equivalent circuit model describes the transport resistance of the electrolyte solution (R_s) that is in series with a parallel combination of polarisation resistance (R_p) and double-layer capacitance (C_{dl}) of the electrode.

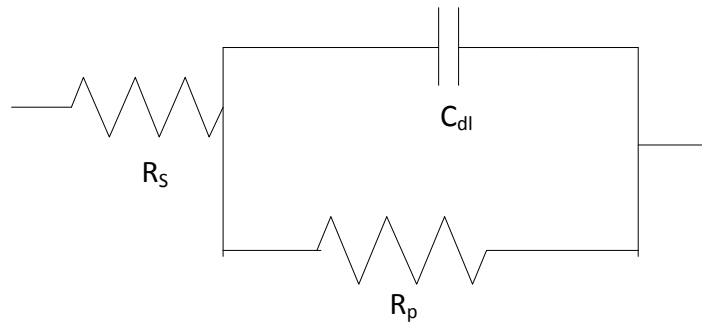


Figure 2-7 Equivalent circuit model for an ideal alkaline electrolyser

For example if a 10Ω precision resistor ($R_s = 10 \Omega$) is in series with a parallel arrangement of 100Ω precision resistor ($R_p = 100 \Omega$) and $100\mu\text{F}$ precision capacitor ($C_{dl} = 100 \mu\text{F}$), the resulting Nyquist and Bode plots are shown in Figure 2-8.

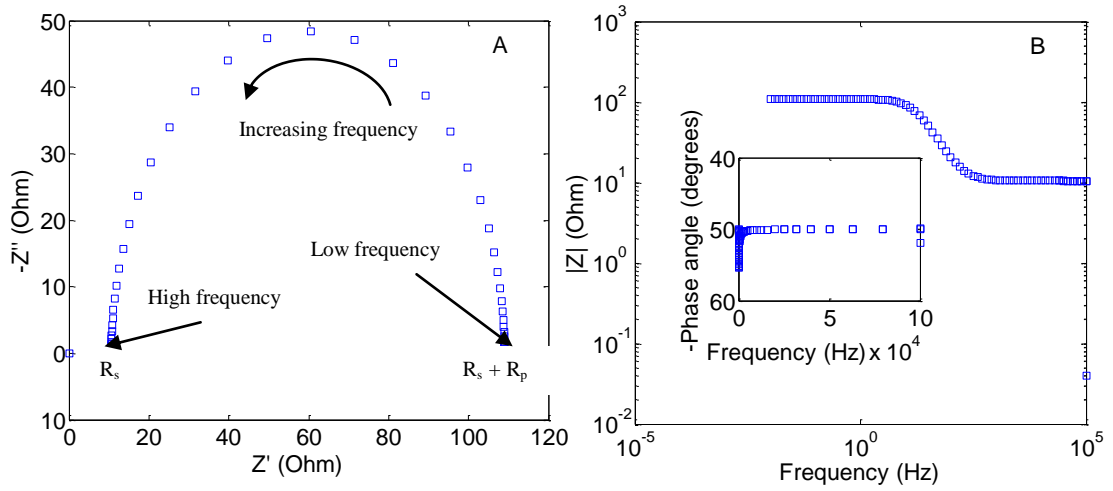


Figure 2-8 (A) Nyquist plot showing real and imaginary impedance, (B) Bode plot showing phase angle, frequency and magnitude of impedance

As indicated in Figure 2-8(A) the resistance is determined from the Nyquist plot. The Ohmic resistance is determined at the high frequency region and the total resistance which is sum of polarisation and Ohmic resistances is determined at the low frequency region. Thus on the real impedance axis the distance from origin is the Ohmic resistance and the diameter of the semi-circle is the polarisation resistance. The double-layer capacitance is determined based on the imaginary impedance at a specific frequency as expressed in equation 38.

$$Z'' = \frac{-1}{\omega C_{dl} j} \quad (38)$$

The exchange current density of the electrode can be determined reliably from EIS measurement of polarisation resistance. As expressed in equation 39, [64] the polarisation resistance is inversely proportional to the exchange current density.

$$R_p = \left[\frac{RT_K}{nFi_o} \right] \quad (39)$$

The main advantage of EIS measurements is to accurately determine the Ohmic resistance. Under DC measurements, the Ohmic resistance cannot be completely isolated because the cell resistance is sum of activation and Ohmic resistances due to gas blanketing of the electrode at relatively low or zero frequency. The Ohmic resistance however can be determined by EIS measurement at high frequency. The Ohmic overvoltage can then be determined based on equation 40. Further, IR compensation can be carried-out by subtracting Ohmic overvoltage from the total cell voltage as expressed in equation 41, thereby determining the activation overvoltage that takes place under relatively low to medium current density of operation.

$$E_{Ohmic} = JR_\Omega \quad (40)$$

$$E_{act} = E_{cell} - E_{Ohmic} \quad (41)$$

2.5 Comparison of Operational Costs for the Ambient and Conventional Temperature Alkaline Electrolysers

The conventional temperature alkaline electrolyser mainly produces hydrogen as an energy carrier in the hydrogen energy system. Auxiliary sub-units are required to operate the conventional temperature alkaline electrolyser. These units include: heaters, heat exchangers, separators, deoxidisers, and driers, which are needed for heating and cooling of the electrolyte and to effectively separate the hydrogen gas from the liquid-gas or product gas mixtures. However, the auxiliary sub-units incur additional investment cost [6, 35]. In particular, the heaters, and heat exchangers consume electricity and consequently increase operational costs for hydrogen production, in addition with capital and maintenance costs of the equipment. For example, Figure 2-9 illustrates an operational system that optimises heating and cooling requirement of the conventional temperature alkaline electrolyser.

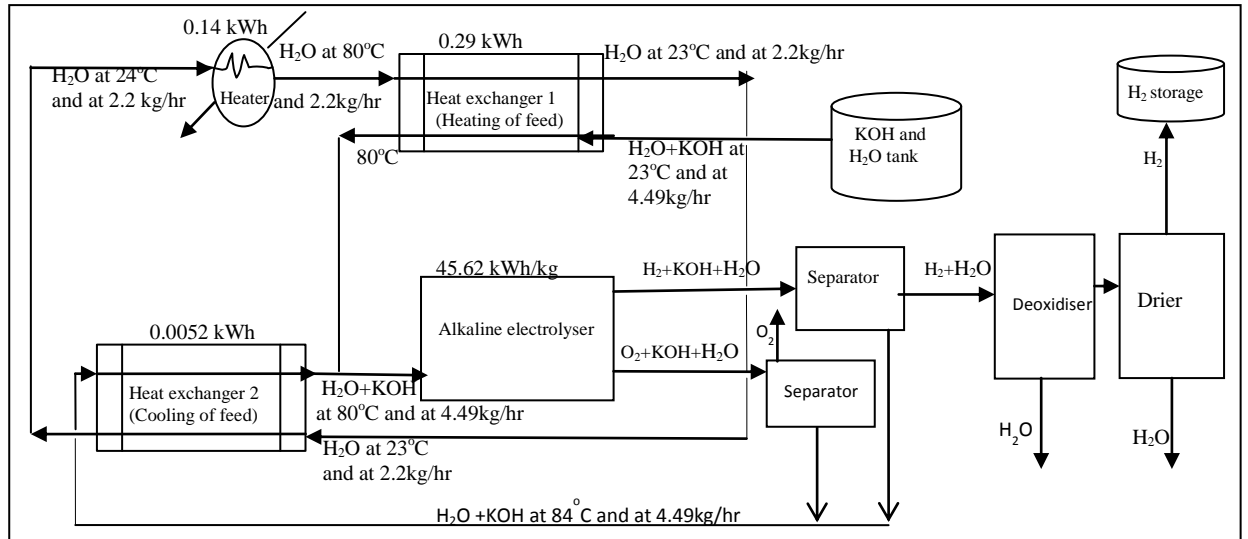


Figure 2-9 Optimised system operation for hydrogen production from the conventional temperature alkaline electrolyser

The hydrogen production cost is the ratio of total operational costs to hydrogen production rates. Table 2-2 presents commercial data for a conventional temperature single-cell alkaline electrolyser, assuming that the efficiency is 86 % (HHV) [28], and in Table 2-3 shows the feedstock and utility cost, assuming 70 % efficiency for the heater and heat exchanger [28]. The hydrogen production cost is estimated based on equations 42 to 52 and presented in Table 2-4.

Table 2-2 Commercial data for the conventional temperature single-cell alkaline electrolysers [28]

Cell energy requirement (KWh/Kg) [28]	Hydrogen production rate (Kg/hr)	Outlet pressure (bar)	Operating temperature (°C)	Maximum power (kW)
45.62	4.49	1	80	6.6

Table 2-3 Assumptions for feedstock and utility requirement for the conventional temperature single-cell alkaline electrolyzers [1, 11]*

$X_{H_2O/KOH}$ (kg/hr)	X_{H_2O} (Kg/hr)	U_{heater} (kWh)	$U_{heat\ exchanger\ 1}$ (kWh)	$U_{heat\ exchanger\ 2}$ (kWh)	Industrial electricity price (\$/kWh)	Industrial heating price (\$/kWh)	Demineralised water price (\$/kg)
4.49	2.2	0.14	0.29	0.0052	0.21	0.09	1.61

*GBP £1= US \$1.61 as at the time of writing this report

$$Y_{electricity} = \text{Cell energy requirement} \times \text{Hydrogen production rate} \times \text{Electricity price} \quad (42)$$

$$U_{heater} = \left(\Delta H_{H_2O}(T_{353}) - \Delta H_{H_2O}(T_{297}) \right) \times X_{H_2O} \quad (43)$$

$$Y_{heater} = U_{heater} \times \text{Heat price} \times \text{Efficiency} \quad (44)$$

$$Y_{heat\ exchanger} = \left(Q_{heat\ exchanger\ 1} + Q_{heat\ exchanger\ 2} \right) \times \text{Electricity price} \quad (45)$$

Where

$$Q_{heat\ exchanger\ 1} = U_{heat\ exchanger\ 1} \times \text{Efficiency} \quad (46)$$

$$U_{heat\ exchanger\ 1} = \left(\Delta H_{H_2O}(T_{353}) - \Delta H_{H_2O}(T_{296}) \right) \times X_{H_2O/KOH} \quad (47)$$

$$Q_{heat\ exchanger\ 2} = U_{heat\ exchanger\ 2} \times \text{Efficiency} \quad (48)$$

$$U_{heat\ exchanger\ 2} = \left(\Delta H_{H_2O}(T_{357}) - \Delta H_{H_2O}(T_{353}) \right) \times X_{H_2O/KOH} \quad (49);$$

$$Y_{demineralised\ water} = X_{H_2O} \times \text{Demineralised water cost} \quad (50)$$

$$Y_{Total} = Y_{electricity} + Y_{heater} + Y_{heat\ exchanger} + Y_{demineralised\ water} \quad (51)$$

$$H_2\ \text{production cost} = \frac{Y_{Total}}{H_2\ \text{production rate}} \quad (52)$$

Table 2-4 Operational and hydrogen production costs for the conventional temperature single-cell alkaline electrolyser

$Y_{electricity}$ (\$/hr)	Y_{heater} (\$/hr)	$Y_{heat\ exchanger}$ (\$/hr)	$Y_{demineralised\ water}$ (\$/hr)	Y_{Total} (\$/hr)	H_2 production cost (\$/kg)
43.02	0.0090	0.081	3.54	46.65	10.39

As can be seen from Table 2-4, heating cost is insignificant compared with electricity cost which contributes to about 85 % cost of hydrogen. This means electricity cost contributes greatly to hydrogen cost. Therefore the industrial practice is to reduce electricity consumption by increasing heat consumption as described based on Figure 2-2. This is economical as long as low-cost heat can be sourced as waste by-products from industrial plants. However, this is only profitable for the people in the business of producing hydrogen that can also be sold as chemical feedstock raw material for other industrial applications. In the case of producing hydrogen for energy storage applications, electrical heating of electrolyte is the only option especially in remote communities where heat sources are not readily available, and since the heaters and heat exchangers consume additional electricity, the overall operational cost is increased and the alkaline electrolyser is limited for dynamic and continuous operation with the electrical grid or wind energy sources.

The remedy to this problem is to develop a hydrogen and oxygen energy system that utilises the ambient temperature alkaline electrolyser in order to reduce auxiliary utilities. The cost of hydrogen can be reduced in the ambient temperature alkaline electrolyser by reducing auxiliary subunits thereby reducing operational, maintenance and capital cost investments. Since the alkaline electrolyser is operated at the ambient temperature of say 23°C, there is minimal or no use of external heaters and heat exchangers. Further, as there is internal heat generation, the hot aqueous electrolyte can be recycled to the alkaline electrolyser in order to enhance the efficiency as illustrated in Figure 2-10.

Electrolytic Hydrogen and Oxygen Production

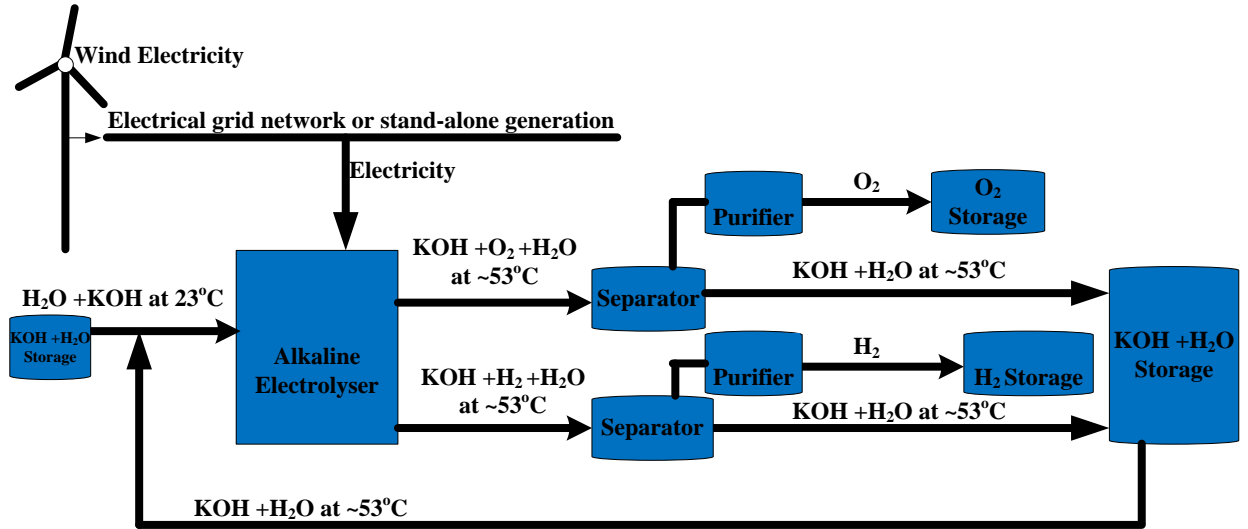


Figure 2-10: Electrolytic production of hydrogen and oxygen from the ambient temperature alkaline electrolyser

It should be noted that based on the model of equation 10, the electrolyte temperature is increased to about 53°C and as illustrated in Figure 2-10, heat removal from the electrolyte is no more necessary thereby eliminating external coolers or heat exchangers. It should be noted also that in the conventional temperature alkaline electrolyser, as a result of internal heat generation the electrolyte temperature could rise up to 100°C where there is evaporation of water that can result in increase in electrolyte concentration and consequent increase in corrosion rates of the cell components. For this reason, external heat exchangers or coolers are required in the operation of conventional temperature alkaline electrolysers in order to cool and

maintain the electrolyte temperature below the boiling point of water at about 70°C -90°C. In the ambient temperature alkaline electrolyser however, as a result of internal heat generation the electrolyte temperature could rise up to 53°C (see Figure 2-10) which is below the boiling point of water, and since there is no evaporation of water, external heat exchangers or coolers and driers are eliminated in the operation of ambient temperature alkaline electrolysers.

In Figure 2-11, it is illustrated that the hydrogen and oxygen product gases from the alkaline electrolyser can be directly utilised as energy source for the operation of alkaline fuel cell to essentially generate back electricity. This type of arrangement of an alkaline electrolyser and an alkaline fuel cell is a regenerative alkaline fuel cell, and it is evident that auxiliary sub-units such as separators, gas driers, and deoxidisers are eliminated in the operation of a regenerative alkaline fuel cell.

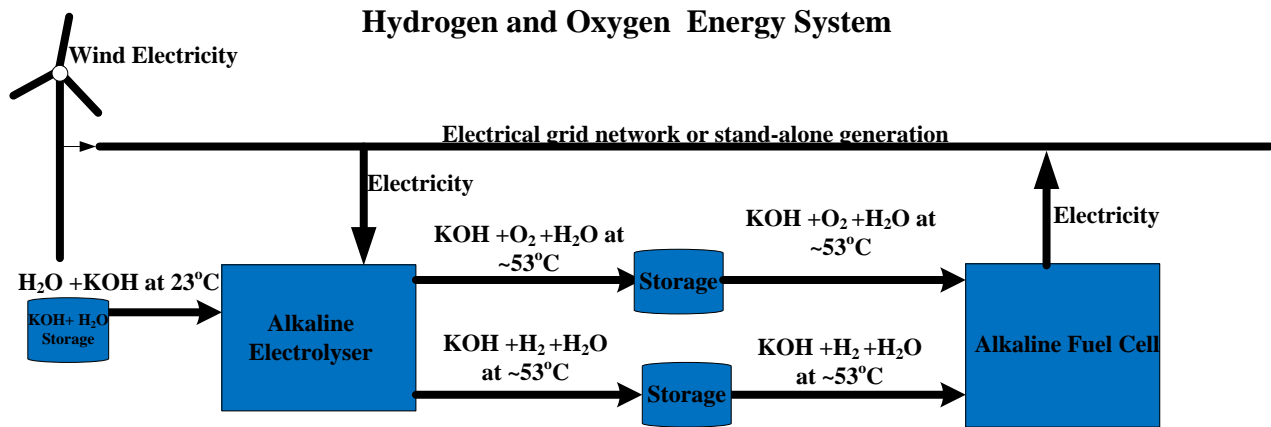


Figure 2-11: Hydrogen and Oxygen Energy System utilising the ambient temperature alkaline electrolyser

Further, in Figure 2-12, it is illustrated that the ambient temperature regenerative alkaline fuel cell is potentially suitable as a flexible and portable technology for micro-generation applications such as in stationary, portable and transport systems. Example of these applications include: CHP generation for residential and/or commercial buildings, portable electronics such as laptop and mobile phone devices, and ‘true’ hybrid fuel cell electric vehicles.

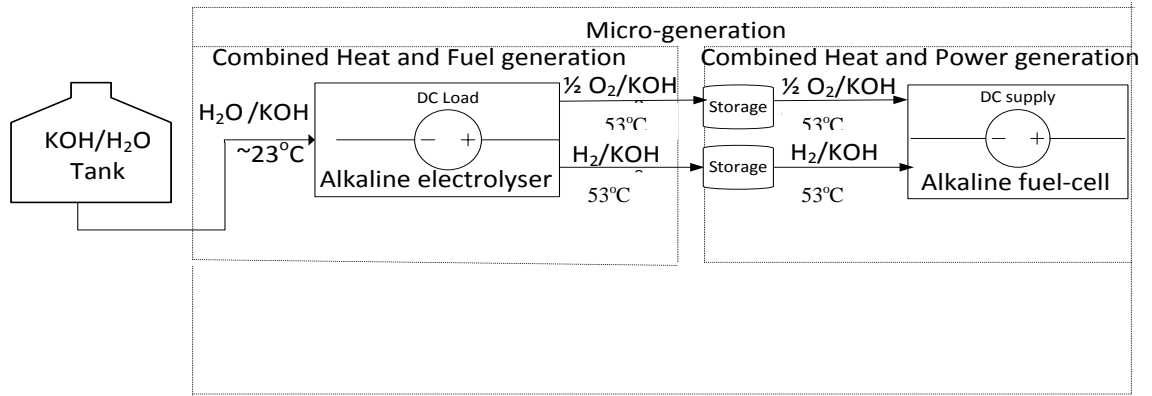


Figure 2-12 Micro-generation application of the ambient temperature alkaline electrolyser

As the auxiliary units as well as auxiliary electricity consumption are significantly minimised in the ambient hydrogen and oxygen energy system, the ambient temperature alkaline electrolyser can be operated continuously under dynamic wind electricity input. This implies that the ambient temperature alkaline electrolyser is potentially capable of wider operational range of 5%-100% of the rated electrical power capacity and faster response time less than a second compared to the conventional temperature alkaline electrolyser.

The hydrogen and oxygen that is produced from the alkaline electrolyser is in the ratio of 2:1 respectively, thus the product gases can be directly utilised in the alkaline fuel cell for energy conversion and for distributed electricity generation. By increasing rates of hydrogen and oxygen production from the alkaline electrolyser-which can be achieved by electro catalysis and good electrochemical engineering of the cell, it is anticipated that round trip-energy efficiency can be increased. Hence, the regenerative alkaline fuel cell can be utilised for micro-generation applications, as one unit serves for combined heat and fuel (CHF) generation while the other unit serves for combined heat and power (CHP) generation. Although considering the model of equation 10, internal heat generation will be relatively higher in the ambient temperature alkaline electrolyser due to relatively higher overpotential. Nonetheless, as the electrolyte temperature is not up to the boiling point of water, the electrolyte can be directly recycled to enhance the efficiencies for hydrogen and

oxygen production thereby eliminating any need for heat removal or electrolyte cooling.

The hydrogen and oxygen production costs are estimated as the ratio of the total operational cost to their respective production rates. For example assuming 80% efficiency for the ambient temperature alkaline electrolyser, Tables 2-5 and 2-6 present preliminary operational data for the electrolyser and based on equations 53 to 59 the operational costs as well as hydrogen and oxygen production costs are estimated and presented in Tables 2-7 and 2-8 respectively. It is reasonable to assume 80 % efficiency for the ambient temperature alkaline electrolyser considering that- as demonstrated in this research from Chapters 3 to 8, the efficiency can be increased by electro-catalysis, and good electrochemical engineering of the cell involving ‘zero-gap’ cell configuration, forced or natural circulation of the electrolyte and product gases in order to enhance ionic conductivity and facilitate gas-bubble removal from the electrode surface.

Table 2-5 Assumed data for the ambient temperature alkaline electrolyser

Cell energy requirement (KWh/Kg)	Hydrogen production rate (Kg/hr)	Oxygen production rate (Kg/hr)	Outlet pressure (bar)	Operating temperature (°C)
49.26	4.49	2.24	1	23

Table 2-6 Assumptions for feedstock and utility for the ambient temperature alkaline electrolyser

$X_{H_2O/KOH}$ (kg/hr)	X_{H_2O} (Kg/hr)	Industrial electricity price (\$/kWh)	Demineralised water/KOH price (\$/kg)
4.49	2.2	0.21	1.61

$$Y_{\text{electricity for H}_2 \text{ production}} = \text{Cell energy requirement} \times \text{Hydrogen production rate} \times \text{Electricity price} \quad (53)$$

$$Y_{\text{electricity for O}_2 \text{ production}} = \text{Cell energy requirement} \times \text{Oxygen production rate} \times \text{Electricity price} \quad (54)$$

$$Y_{\text{demineralised water}} = X_{H_2O} \times \text{Demineralised water price} \quad (55)$$

$$Y_{\text{cost for H}_2 \text{ production}} = Y_{\text{electricity for hydrogen production}} + Y_{\text{demineralised water}} \quad (56)$$

$$Y_{\text{cost for O}_2 \text{ production}} = Y_{\text{electricity for oxygen production}} + Y_{\text{demineralised water}} \quad (57)$$

$$H_2 \text{ production cost} = \frac{Y_{\text{cost for H}_2 \text{ production}}}{H_2 \text{ production rate}} \quad (58)$$

$$O_2 \text{ production cost} = \frac{Y_{\text{cost for O}_2 \text{ production}}}{O_2 \text{ production rate}} \quad (59)$$

Table 2-7: Operational costs for the ambient temperature alkaline electrolyser

$Y_{\text{electricity for H}_2 \text{ production}}$ (\$/hr)	$Y_{\text{electricity for O}_2 \text{ production}}$ (\$/hr)	$Y_{\text{demineralised water/KOH}}$ (\$/hr)	$Y_{\text{cost for H}_2 \text{ production}}$ (\$/hr)	$Y_{\text{cost for O}_2 \text{ production}}$ (\$/hr)
46.45	23.17	3.54	49.99	26.71

Table 2-8: Production costs for the ambient temperature alkaline electrolyser

H_2 production cost (\$/kg)	O_2 production cost (\$/kg)
11.13	11.92

It should be noted that based on Table 2-5, the hydrogen production rate is 107.7 kg/day which is in the category of small forecourt size conventional electrolysers [46]. By comparing Table 2-8 and Figure 1-5, it is estimated that the cost of hydrogen production from the ambient temperature alkaline electrolyser is lower by about \$2.48 /kg compared with the selling cost of hydrogen from small forecourt size conventional electrolysers. However, the hydrogen production cost from the ambient temperature alkaline electrolyser is higher by about \$8.28 /kg compared with the US DoE target of \$2.85 /kg for hydrogen selling price by the year 2015. It is still unclear whether the US DoE target for hydrogen selling price is relevant to compare with production costs from the alkaline electrolyser. This is because the hydrogen selling price only takes account of the production of hydrogen, whereas the alkaline electrolyser produces both hydrogen and oxygen. The hydrogen and oxygen gases can be directly utilised in the alkaline fuel cell to essentially generate back electricity, therefore the hydrogen and oxygen production costs should be accounted as shown in Table 2-8 which indicates that there is an added value for

producing and storing oxygen thereby ultimately reducing the overall cost of production.

The energy that is stored in the hydrogen and oxygen product gases can be converted back into electricity, and based on 70% efficiency for each of the alkaline electrolyser and alkaline fuel cell, the overall efficiency can be up to 49 %. This means that at least 49 % of electricity that is consumed in the ambient temperature alkaline electrolyser can be recovered. The remaining 51% is converted into heat that can be inherently utilised by recycling the electrolyte in order to enhance efficiency of the cell. The overall efficiency can be increased further by increasing rates of hydrogen and oxygen production from the ambient temperature alkaline electrolyser, which can be achieved by electro-catalysis and good electrochemical engineering of the cell.

The overall efficiency can be increased further by increasing the kinetic efficiency of the electrodes and electro-catalysts at the ambient temperature. The kinetic efficiency can be increased by minimising reaction resistances, transport resistances due to gas-bubble coverage on the electrode surface and concentration polarisation at the high current density of operation. In general, efficiency improvement and heat management should be considered in order to improve performance and reduce the cost of the ambient temperature alkaline electrolyser.

Gas losses can be reduced by eliminating the gas drier in the hydrogen and oxygen energy system that utilises the ambient temperature alkaline electrolyser. About 4 % of gas losses from the drier regeneration unit have been reported [7] for a conventional alkaline electrolyser system. The drier unit is no longer required in the ambient hydrogen and oxygen energy systems that are illustrated in Figures 2-10 and 2-11. This is because at the ambient operating temperature, although there might be internal heat generation, the electrolyte temperature would not rise up to the boiling point of water so that the product gases are not mixed with water vapour. Moreover, the alkaline electrolyser produces hydrogen and oxygen product gases that can be directly utilised in the alkaline fuel cell as shown in Figures 2-11 and 2-12. Since gas

losses are reduced, the hydrogen and oxygen production rates will be higher in the ambient hydrogen and oxygen energy system compared to the conventional hydrogen energy system. Table 2-9 summarises the comparison between the ambient and conventional temperatures alkaline electrolyzers.

Table 2-9: Comparison of the ambient and conventional temperatures alkaline electrolyzers

Conventional temperature alkaline electrolyzers	Ambient temperature alkaline electrolyzers
Requires external heating of the electrolyte solution	No need for external heating of the electrolyte solution
Requires cooling of the unreacted electrolyte solution	No need for cooling of the unreacted electrolyte solution.
Requires 'auxiliary' electricity consumption in heaters, heat exchangers and driers.	'Auxiliary' electricity consumption is significantly reduced by eliminating or reducing auxiliary equipment such as heaters, heat exchangers and driers.
Requires dryers to remove water vapour or moisture from the product gases.	No need for dryers as there might not be water vapour in the product gases.
Relatively higher capital, operating and maintenance costs.	Relatively lower capital, operating and maintenance costs.
Relatively higher efficiency for production of hydrogen and oxygen.	Relatively lower efficiency for production of hydrogen and oxygen
Relatively higher rates of corrosion or degradation of the cell components	Relatively lower rates of corrosion or degradation of the cell components.
Limited to operational range within 20% and 100% of the rated electrical power capacity.	Wider operational range potentially within 5% and 100% of the electrical power capacity.
Slower response time for optimum performance at start-up.	Faster response time for optimum performance at start-up
Too complex for flexible applications	More compact for portable, stationary and transport applications.

2.6 Cell Design, Configuration and Geometry

The two main types of cell designs are monopolar or tank type and bi-polar filter press. Hydrogenics are recognised to be leaders in monopolar cell design [6, 28]. However, the cell design based on the bi-polar principle is common with the commercial alkaline electrolyser manufacturers as shown in Table 2-10.

Table 2-10 Data for the industrial alkaline electrolysers [6, 75 - 77]

Manufacturer	Cell type	Operating temperature (°C)	Operating pressure (bar)	Electrolyte (% wt)	Current density ($kA m^{-2}$)	Cell voltage (V)	Cell efficiency	Electrode surface structure and composition
Hydrogenics	Monopolar tank	70	1	28	1.34	1.90	64.70	Nickel-plated steel
Norsk Hydro	Bi-polar filter press	80	1	25	1.75	1.75	70.28	Perforated sheet metal activated by NiS coating
DE Nora S.P.A	Bi-polar filter press	80	1	29	1.5	1.85	66.49	Expanded metal made of nickel-plated mild steel and sulphide-activated
LURGI, GmbH	Bi-polar filter press	90	30	25	2	1.86	66.13	Honey comb nickel-plated steel

In the monopolar cell design, each individual electrode and its feed line is either an anode or a cathode having only one polarity such that a number of single separate cells are electrically connected in parallel to one another as shown in Figure 2-13. The electrical connection however involves relatively long electrical cables which increases the electrical resistance.

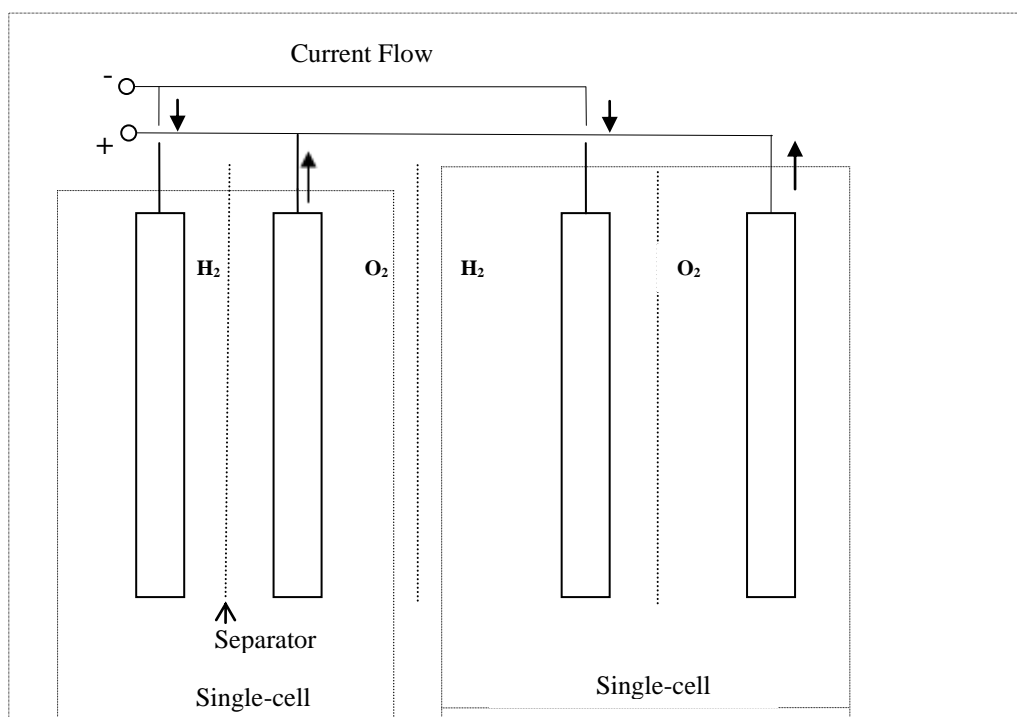


Figure 2-13 Schematic diagram of the monopolar cell design

In the bi-polar cell design, each individual metallic electrode serves as a current-carrying element supplying on one side the cathode and on other side the anode and as a partition wall separating one cell from the next. Each electrode is electrically in series with its neighbour. Thus the cathode and anode are integrated in one single metallic part which simultaneously separates the anode and cathode chamber of two adjacent cells that are all connected in series via the electrolyte solution [28]. The bi-polar cell has the advantage of increasing the number of electrodes as shown in Figure 2-14 but the electrical cables for current collection are long, which can increase the electrical resistance [6]. However, the electrical cables in the bi-polar cells are relatively shorter than in the monopolar cells as also indicated in Table 2-11.

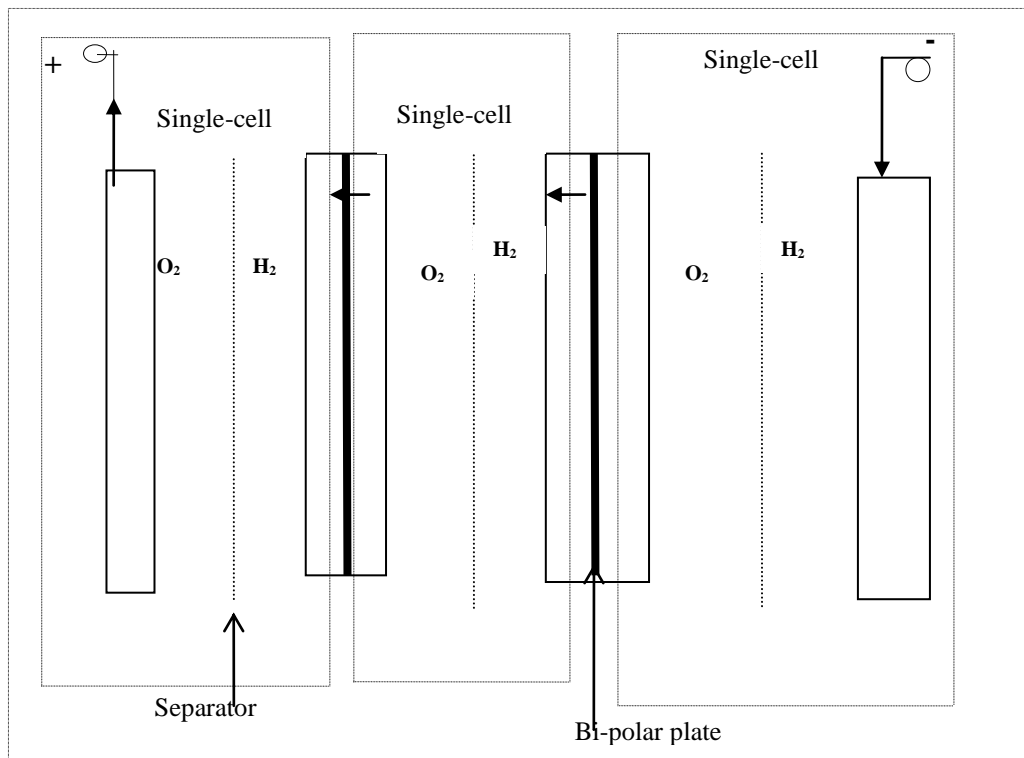


Figure 2-14 Schematic illustration of the bi-polar cell design

Table 2-11 Comparison of monopolar and bi-polar cell designs

Monopolar cell design	Bi-polar cell design
Simple design structure	Requires precise method of fabrication
Common for atmospheric electrolyzers that are designed as tank-type and immobilised aqueous electrolyte solution.	Common for pressurised electrolyzers that are designed as flow-type for circulation of the aqueous electrolyte solution.
Not easily adaptable for compact systems	Easily adaptable for compact systems
Higher electrical resistance due to relatively longer current path length of electrical wiring.	Lower electrical resistance due to relatively shorter current path length of electrical wiring.
Relatively safe by natural circulation of the electrolyte.	Pressure operation can result in electrolyte and gas leakage between the cells.
Complete cell shut-down can be carried-out by disconnecting adjacent cells from the electrical power source.	Cell shut-down is partial due to parasitic or residual currents that can cause mutual depolarisation of electrodes [6, 28].
Typical operating voltage is 2.2 V for a single-cell [28].	Typical operating voltage is $2.2(n-1)V$, where n is the number of electrodes [28].

The bi-polar filter press is an advanced electrolyser cell design that is a hybrid of the monopolar and bi-polar cell designs. It has the main advantage of relatively short current path length of the electrical input terminals. In other words, the electrical resistance is reduced by reducing the length of electrical wiring for current collection. The electrical source is connected ‘point-wise’ in order to reduce the current path length. The direction of the current is from one end of the ‘cell pack’ to the other. This means only the two end monopolar electrodes are connected to the electrical power source. The bi-polar filter press permits use of electrodes that have a high surface area. The electrode chamber may consist of a single massive assembly of relatively large number of monopolar or bi-polar electrodes that are held together by heavy longitudinal tie rods. The assembly of cells has superficial resemblance to a filter press because the electrolyte is manifolded to flow through each cell as well as the hydrogen and oxygen exit lines. Figure 2-15 illustrates the filter-press cell construction that was developed in this study for characterising the electrode.

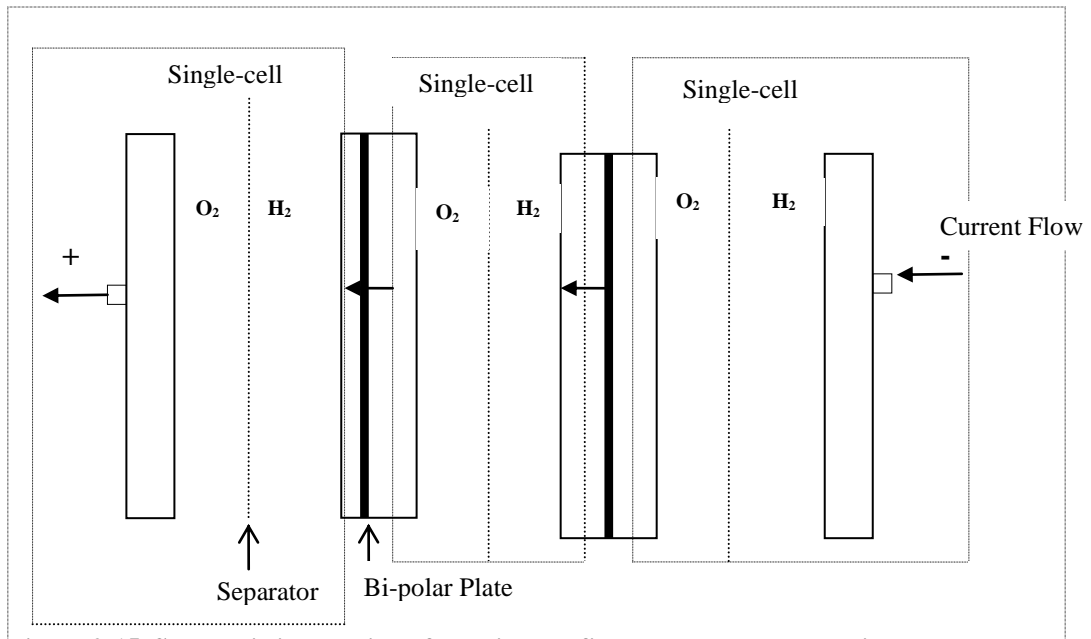


Figure 2-15 Schematic illustration of the bi-polar filter-press cell construction

The cell design permits use of high surface area electrodes in order to uniformly distribute the current and minimise overvoltage losses. For example based on equation 58 [6], the voltage drop can be minimised for the electrode mesh that has three dimensional surface area and reduced distance of separation between adjacent wires.

$$\Delta E_{electrode} = \frac{\rho L^2 J}{tE} \quad (58)$$

2.6.1 Cell Geometry

The method of constructing the ‘zero-gap’ cell geometry involves sandwiching of anode and cathode together with the membrane separator as shown in Figure 2-16 [6, 78].

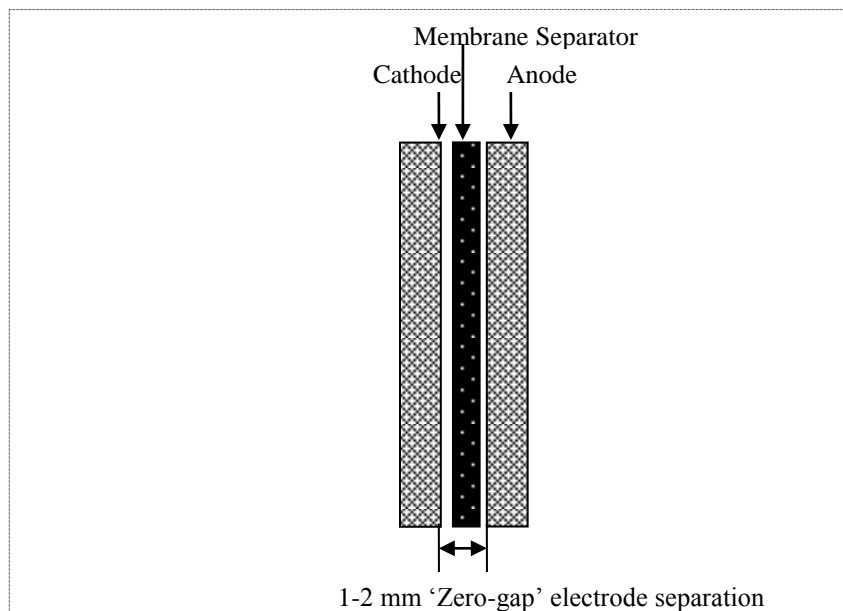


Figure 2-16 Schematic illustration of ‘zero-gap’ cell construction

The gap between the electrodes or adjacent cells of the electrolyser is important because it determines the travel distance of electro-active ions in the electrolyte, and mass transport of gas-bubbles which influence on transport resistance [79]. A smaller gap would reduce internal resistance for ionic transport, minimise concentration polarisation of electro-active ions and facilitate mass transport of produced gas-bubbles from the electrode surface. However, the gap needs to be not too small in order to allow space for gas bubble movements [61].

Nagai *et.al* [80] has reported an optimum gap of 1-2 mm between the electrodes at an operational current density of over 0.5 A/cm². This has been recognised as the ‘zero-gap’ cell configuration. They have observed that separation distance between the electrodes do not only influence ionic transport but also the rate of bubble formation especially at a high current density of operation. Their results indicate that cell voltage efficiency increases with reduced space between the electrodes and reduced height of each electrode. By reducing the height of the electrodes the current path length is minimised thereby improving uniform current density distribution in accordance with equation 59 that also permits the use of thin membranes in order to minimise internal cell resistance.

$$J = \frac{E_{anode} - E_{cathode}}{h\rho_{membrane}} \quad (59)$$

The micro-porous polypropylene membrane that is manufactured by Celgard® [81] was used for this research. A comparison of this membrane with other types of diaphragm material is given in Table 2-12.

Table 2-12 Comparison of membranes in the alkaline electrolyser [6, 75, 81]

Material	*Gas breakthrough pressure/bar	Surface-specific electrical resistance (Ohm-m²)	Remarks
Polypropylene (Celgard [®] 5550)	0.012	$\sim 1 \times 10^{-5}$	Stable in KOH up to 80°C
Asbestos polymer reinforced	0.03	$3 \times 10^{-5} - 4 \times 10^{-5}$	Not stable in concentrated KOH above 90°C
Polysulphone	0.10	$2 \times 10^{-5} - 3 \times 10^{-5}$	Stable in KOH up to 120°C
NiO ceramic supported on nickel metal net	0.25	$1 \times 10^{-5} - 2 \times 10^{-5}$	Manufactured by oxidative sintering process
Ba(Ca)TiO ₃ ceramic supported on nickel net	0.30	$1 \times 10^{-5} - 2 \times 10^{-5}$	Manufactured by reductive sintering process
Polyphenylene sulphide (Ryton)/Polytetrafluoroethylene	0.02	$1 \times 10^{-5} - 2 \times 10^{-5}$	Stable in KOH up to 160°C

* The minimum differential pressure across the membrane for gas to pass through; it depends on pore size and porosity of the membrane.

The pore size, porosity, surface-specific resistance, thickness, mechanical strength and chemical stability of the membrane are important for application in the alkaline electrolyser. The pressurised operating environment increases supersaturation of the electrolyte with gases which can occlude in the pores of the membrane, and consequently increase internal Ohmic resistance [6]. The membrane should therefore be hydrophilic, possess appropriate pore size, and porosity that allow ionic transport of hydroxyl ions, and prevent mixing of hydrogen and oxygen gas molecules or clogging of the pores by gas bubbles. It should also be chemically and structurally stable in the corrosive environment and filter-press system. Thus a pore size lower than 10 µm and porosity of at least 50 % is recommended [6] for the membrane in an alkaline electrolyser. The Celgard[®]5550 membrane [81] meets these requirements as it possess pore size of 0.064 µm, porosity of about 55 %, thickness of 110 µm and a tensile strength of 1600 kg/cm². Moreover, the Celgard[®]5550 membrane has a surface-specific resistance that is lower by 0.1 Ω-cm² compared to the allowable maximum surface-specific resistance of membrane [6] in the electrolyser. Also, the

membrane is structurally and chemically stable in KOH electrolyte at the ambient and conventional operating temperature of alkaline electrolyzers. The conductivity of KOH electrolyte solution increases with temperature by about 2 % -3 % per degree Celsius [6], however, corrosion rate due to the KOH electrolyte solution also increase with temperature at the same rate. A good membrane however, should withstand corrosion as the electrolyte temperature changes.

2.7 Efficiency and Corrosion Rates of Electrode Materials in the Conventional Temperature and Ambient Temperature Alkaline Electrolyzers

Electrolyser efficiency gains must be balanced against any additional capital cost incurred for the electrode [82]. For this reason, nickel plated steel [83] and nickel alloys [84-85] are widely used as electrode materials to minimise *HER* overpotentials and to increase the efficiency of the alkaline electrolyser. Nickel (Ni) metal is not used in its pure metallic form because of its higher cost compared to stainless steel (SS) metal [28] as shown in Figure 2-17, therefore stainless steel that is relatively lowest-cost is the choice electrode substrate for nickel based electro-catalyst.

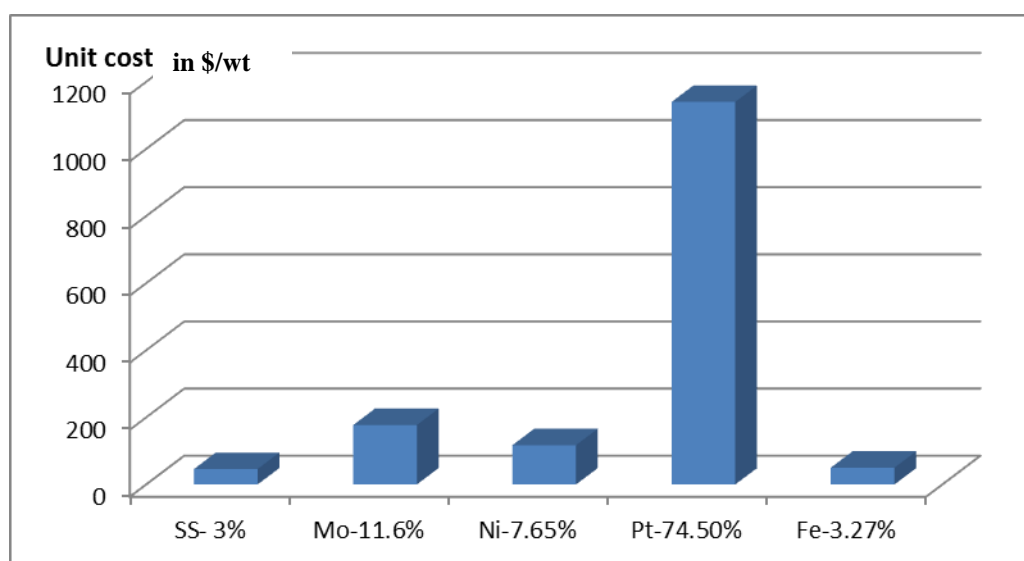


Figure 2-17 Comparison of electrode material cost [86]

However, hydrogen embrittlement is accelerated in steel electrodes under cathodic polarisation in hot KOH electrolyte [6]. As a consequence, steel electrodes are not stable at the higher operating temperature of alkaline electrolyzers. Steel is more

susceptible to corrosion at the higher temperature of 100°C than at the ambient temperature of 25°C as shown in the Pourbaix diagram⁹ in Figure 2-18 [87]. Nickel however has better resistance to cathodic corrosion than steel [6], thus a nickel-plated steel cathode and a nickel alloy anode are common electrodes in commercial alkaline electrolyzers.

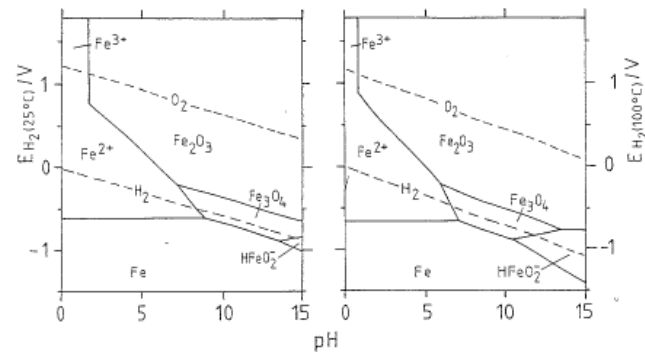


Figure 2-18 Potential-pH (Pourbaix¹⁰) diagrams for steel. Corrosion of steel takes place due to hydride formation (HFeO_2^-), which increases at higher operating temperature up to 100°C; Source [6].

The voltage efficiency is increased by increasing the conductivity of the KOH electrolyte at relatively higher operating temperature. The conductivity of 30 % (by weight) of the KOH electrolyte is increased by up to 3 % per degree Celsius [83] as shown in Figure 2-19. As can be seen, the conductivities of caustic potash (KOH) and caustic soda (NaOH), which are commonly used as electrolytes in commercial electrolyzers, increase with temperature as well as concentration and reach optimum values at around 150°C and then the conductivities begin to decrease. This implies that 150°C is the operational limit for higher temperature alkaline electrolyzers.

¹⁰ A Pourbaix diagram is a potential-pH plot that describes the regions of thermodynamic stability and corrosion of an electrode in contact with the electrolyte solution.

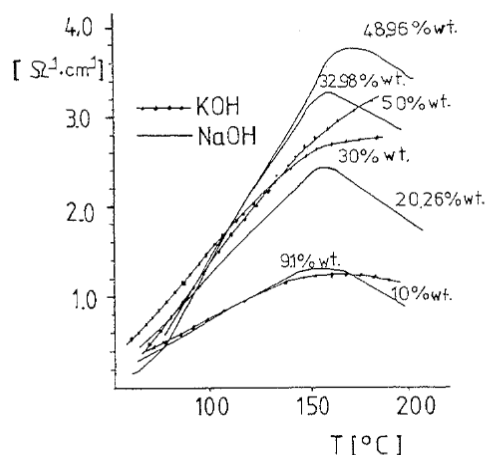


Figure 2-19 Temperature dependence of the electrical conductivity of aqueous solution of KOH and NaOH; Source [6]

The energy losses due to overpotential are minimised by raising the operating temperature of the alkaline electrolyser. However, the electrode and electro-catalyst materials are less stable at the higher operating temperature [28]. As such, researchers [88-90] are aiming to develop electrodes and electro-catalysts that exhibit maximum electrical conductance, minimum overvoltage and long-term durability. For example, Martin *et al* [91] have reported that Raney nickel (an alloy of nickel and aluminium or zinc) impregnated with cobalt oxides has a better performance due to a reduction of anodic overpotential by more than 130 mV after 24 hr of electrolysis at 80 °C and at a current density of 1000 mA/cm².

2.7.1 Research Trends on Electrode and Electro-catalyst Materials

In general, it is desirable to make the electrode surface area as large as possible in order to maximise the reaction area and minimise the overpotential losses. Large surface areas can be achieved by fabricating the metal electrode in the form of perforated flat plates, large-area sheets, strips or mesh. For example in Figure 2-20, it can be seen that the electrode activity is influenced by the electrode surface structure, hence the nickel split sheet type 2 shows the highest activity because its overvoltage is lowest. Bailleux [92] reported these results on the effect of surface structure of nickel electrodes in 40% KOH at 120°C-160°C and 20 bar. The best result was obtained on a split sheet nickel metal that has a reticulated surface structure in the

form of a mesh. The anodic overpotential was reduced by 0.1 V in 2000 hr of electrolysis.

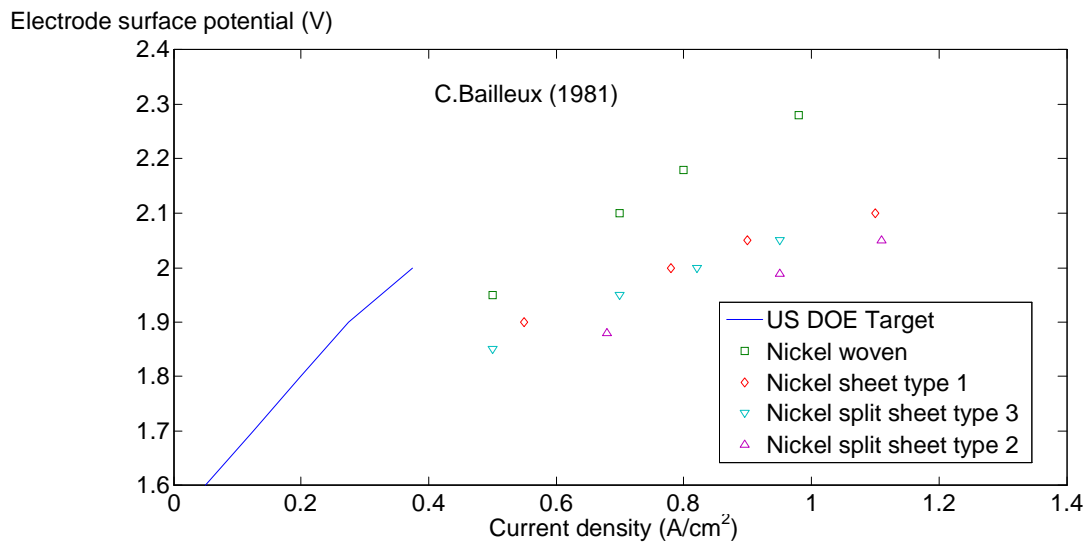


Figure 2-20 Electrode efficiency by Bailleux and comparison with commercial target;
Source [92]

Catalytic active materials such as nickel alloys and molybdenum are applied to the electrode in order to reduce energy consumption and increase effective current density. Nickel based alloys are widely employed not only due to relatively low cost but the increased surface area of nickel oxides and ability of nickel to form complex compounds with other transition metals such as cobalt and molybdenum thereby enhancing the catalytic active sites [93-94].

The method of manufacturing nickel electro-catalyst by thermal spraying or sintering at extremely high temperatures >800 °C requires significant energy expenditure, although these electro-catalysts developed by thermal methods are reported to be highly efficient. For example Balej [95] has achieved up to 1 A/cm^2 at 2 V on a nickel flame-sprayed electrode in 40 % KOH at 100 °C as shown in Figure 2-21.

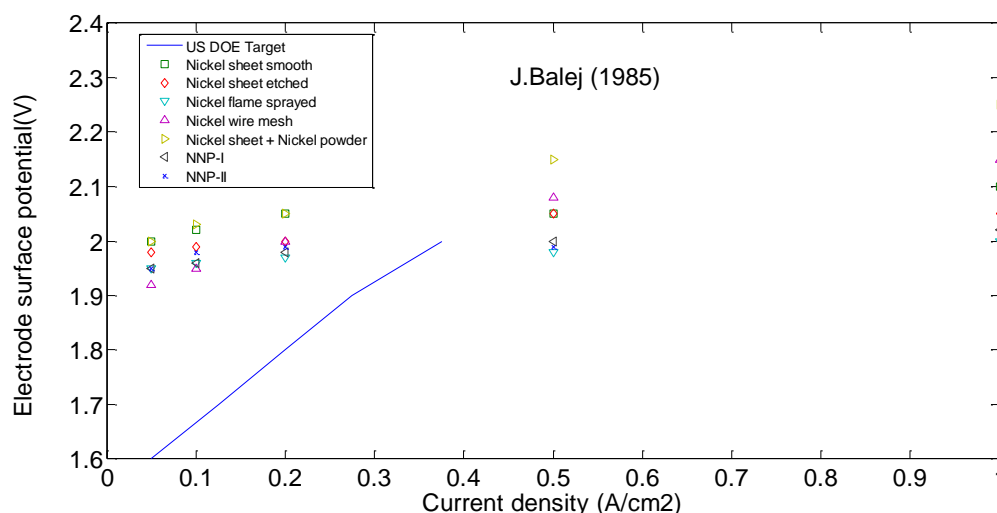


Figure 2-21 Electrode efficiency by Balej and comparison with commercial target; Source [95]

The electrodes that were made by sintering are particularly suitable for high pressure electrolysis up to 30 atm [28]. This was partly due to porosity of the electrode. The oxygen overpotential for sintered porous nickel anodes was about 100 mV lower compared to smooth nickel anodes at current densities of 500-1500 mA/cm² in 35 % KOH electrolyte [28]. The morphology of the nickel coatings is dependent on the sintering temperature and, to a lesser extent the sintering time [96]. For example a nickel electrode sintered by thermal cycling at 980°C-760°C for 30-35 min resulted in anodic overpotential being reduced by about 70 mV under electrolysis at 200 mA/cm² in 30 % KOH electrolyte at 80°C.

The activity of a coated nickel-foam anode has been reported [97]. The anodes were operated at 500 mA/cm² in 40 % KOH electrolyte at 90 °C and the overpotential was reduced by 50-100 mV compared with the uncoated foamed nickel electrodes.

Raney nickel that was made by electrodeposition from chloride electrolyte [98] has a high electrochemical activity due to a high surface area structure that was obtained by leaching of the alloying metals in an alkaline solution. The BET¹¹ specific surface

¹¹ Brunauer-Emmett-Teller method for determining specific surface area of a material

area was greater than 25 m²/g for the leached anode at a deposition potential of 1.07 V/SCE¹² [97].

The Raney nickel electrodes were further improved by doping with either lithium or cobalt. The best results were obtained by impregnating Raney nickel with cobalt oxides in order to reduce overpotentials by more than 130 mV after 24 hr of electrolysis at 80 °C and current density of 1000 mA/cm² [92].

Similar result was reported by Ganley [99] for a cell that was operated at 400 °C and 8.7 MPa. However, Ganley has observed limitations of the cell performance at higher temperatures due to electrode oxidation which results in deactivation. At a higher temperature, the electrolyte becomes more corrosive as water is evaporated and lost. It was observed [100] that at 200 °C the electrolyte is dehydrated to the point at which co-deposition of sodium, potassium and hydrogen atoms result in corrosion of the cathode electrode.

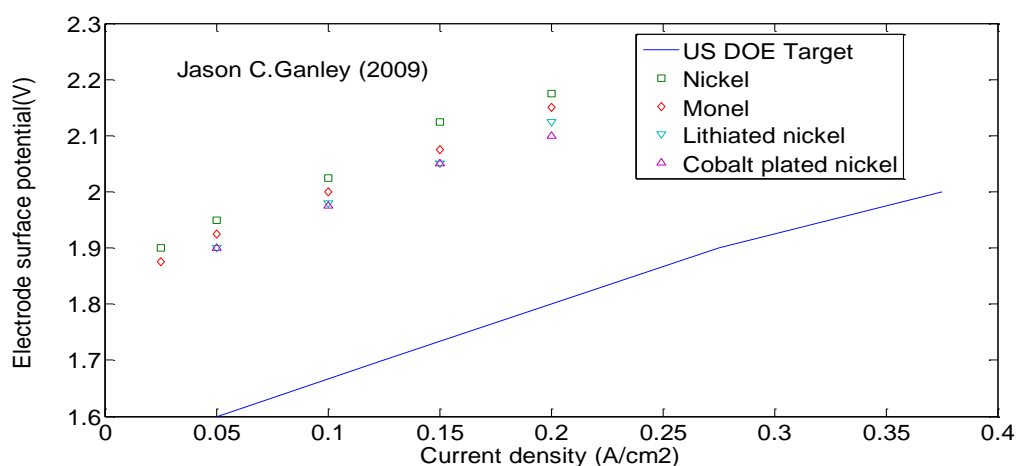


Figure 2-22 Electrode efficiency by Ganley and comparison with commercial target;
Source [100]

The corrosion rate for high purity nickel in oxygenated KOH electrolyte has been reported [101] to be 10-15 μm/yr at 180°C, and for nickel mesh it is 30-45 μm/yr at 130 °C. The corrosion products at 180 °C and 130 °C were NiO and Ni(OH)₂ respectively. Ni(OH)₂ is the electro-catalyst precursor [102] and has optimum loading of about 1-4 mg/cm² on the apparent anode surface area. As a result, the

¹²Standard Calomel Electrode is a reference electrode that consists of mercury chloride.

oxygen evolution overpotential was 45-60 mV lower in Ni(OH)₂-impregnated anodes compared to un-catalysed anodes at 200 mA/cm² in 30 % KOH electrolyte and 80 °C. At higher loadings, however, overpotentials rose as the outer pores of nickel coatings became plugged with Ni(OH)₂ resulting in the loss of effective anode surface area.

Lithiated NiO electro-catalyst was prepared by vacuum decomposition of a mixed slurry of Ni(OH)₂ and LiOH [103-108] followed by mixing the catalyst with tetrafluoroethylene (TFE) binder and sintering onto nickel mesh. The BET specific surface area of the finished catalyst was 100 m²/g and the electronic resistivity reduced from >10⁸ Ω-cm to 100 Ω-cm.

NiCO₂O₄ is a type of anode catalyst that was prepared by freeze-drying mixed Ni and Co nitrates, followed by vacuum decomposition at 250°C and final heat-treatment for 10 hr at 400 °C in air. The resulting catalyst had a BET specific surface area of 70 m²/g and an electrical resistivity of 10 Ω-cm [103].

Chemical vapour deposition (CVD) of Ni(CO)₄ gas followed by sintering at 800 °C-1000 °C was the method used to prepare nickel whisker anodes [28,104-105]. The whisker anodes have a porosity of 90 % with a specific surface area of up to 0.5 m²/g. The anodes were tested in 30 % KOH electrolyte at current densities of 100 mA/cm² to 1000 mA/cm². The oxygen evolution overpotential was about 100mV lower on whisker anodes compared to multilayer nickel screens and there was no loss of structural integrity for up to 48 hr of electrolysis at 1000 mA/cm².

Appleby *et al* [106] have investigated oxygen evolution on smooth platinum and iridium electrodes compared to oxygen evolution on pure nickel. In 25 % KOH electrolyte, Ir was markedly superior to Pt in the temperature range of 25°C-90°C. However, neither Ir nor Pt was more effective than pure nickel as electro-catalysts.

Pt, Pd, Rh and Ni coatings were electrodeposited onto foamed Ni anode supports and tested at a current density of 200 mA/cm² in 30 % KOH electrolyte at 90 °C [99].

The rhodium coating performed best providing a cell voltage of 1.72V, followed by Pd (1.74 V), Ni (1.75 V), and Pt (1.80 V).

The work of Rosalbino *et al* [107] has demonstrated the unique synergy on electro-activity of the transition metal alloys. On the basis of the Brewer-Engel valence bond theory [108 -109], the *HER* is enhanced over a wide range of current densities by alloying appropriate combinations of the transition metals. The *HER* takes place on the electrode surface and free electrons facilitate the electron transfer mechanism for adsorption of reactant water (i.e. the Volmer step). Also, empty orbitals facilitate the electron transfer mechanism for hydrogen desorption (i.e. the Heyrovsky step). This synergy of electron transfer process for the *HER* can be achieved by alloying different *d*-series of the transition metals. Thus the *HER* can be enhanced by alloying metals of filled *d*-orbitals that are on the right-half of the transition metal series with metals of empty *d*-orbitals that are on the left-half of the transition metal series. For example, alloying of metals such as Fe, Co or Ni with metals such as W, Mo, La, Hf and Zr. The lattice energy of the alloy determines its stability and depends on the electrostatic forces and inter-atomic distance between the alloying elements. By alloying metals from the left and right half-sides of the transition series, the electrostatic forces of attraction might increase and inter-atomic distance might reduce due to overlap of the electron orbitals of neighbouring atoms, and thereby increase the lattice energy as well as stability of the alloy. The extent of overlap of electron orbitals however can influence on catalytic activity of the individual hyperelectronic (i.e. the metal with high electron density e.g. Ni) and hypoelectronic (i.e. the metal with low electron density e.g. Mo) and ultimately influence electro-activity of the alloy.

The transition metals have the unique property to form complex metal oxides that have high surface area and high electrochemical activity. For example nickel metal has electronic configuration of $[\text{Ar}] 4s^2 3d^8$ that can form stable Ni^{2+} complexes such as $\text{Ni}(\text{OH})_2$ and NiO thereby increasing the electrode surface area. For this reason, nickel can be suitable as an anode and cathode electro-catalyst in the alkaline electrolyser. By alloying of nickel and molybdenum that has electronic configuration

of [Kr] 5s¹ 4d⁵, the electro-activity of Ni-Mo alloy is enhanced due to synergy. Nickel metal has free electrons to facilitate adsorption of reactant water on the electrode surface and molybdenum has vacant orbitals to facilitate desorption of hydrogen from the electrode surface. Moreover, Ni-Mo is relatively low-cost material that is suitable for large-scale applications.

The method of electro-depositing Ni-Mo on the electrode substrate was described by Luciana *et al* [110]. Ni-Mo was electroplated on platinum electrode substrate at 30mA/cm² for 1-2 hours under continued stirring of the plating solution at 25 °C. The plating bath composition is shown in Table 2-13, and it consisted of sodium citrate and citric acid. Citric acid was added to control the solution pH at 4.0, and sodium citrate was added to form complex compounds with nickel and molybdenum in the form of [Ni(II) LMoO₂]_{ads} intermediate where L is the ligand that is the organic compound [111-113]. The NiSO₄ that is present in the plating bath induce co-deposition of molybdenum as an intermediate of Mo(IV) [114-116]. The co-deposition mechanism involves soluble nickel as catalyst and molybdenum as a co-catalyst that are deposited through an absorbed intermediate species on the electrode surface [114]. According to the authors [110, 116], the solution pH was maintained in acidic conditions in order to induce homogenous deposition of Ni-Mo on the electrode substrate. They observed that an increase in Ni (II) concentration facilitates the deposition process leading to films with greater thickness. Hence the composition of bath 2 (10:1 mixture of nickel sulphate and disodium molybdate respectively) was recommended for optimum electrodeposition of Ni-Mo catalyst.

Table 2-13 Composition of plating solution for Ni-Mo catalyst prepared by Luciana *et al*

Bath number	[Ni (II)] (mol L⁻¹)	[Mo (VI)] (mol L⁻¹)	[Ni(II)/Mo(VI)]	Sodium Citrate (mol L⁻¹)	pH
1	0.01	0.01	1:1	0.02	4.0
2	0.1	0.01	10:1	0.02	4.0
3	0.01	0.1	1:10	0.02	4.0

However, Weikang observed [117] that the Ni-Mo electro-catalyst is not highly stable under anodic oxidation due to leaching of it in a strong alkali solution. They observed that the nickel and molybdenum content in Ni-Mo have reduced by up to

15 % and 17 % respectively after oxidation treatments in KOH electrolyte at 70 °C. The work of Divisek and co-workers [118-119] have also reported loss in the activity of Raney nickel and Ni-Mo electrodes after long periods of continuous electrolysis due to oxidative dissolution of Al and Mo from the alloys respectively. As a result, there was visible destruction on the electrode surface after electrolysis.

Weikang has developed the Ni-Mo electro-catalyst that consists of hydrogen storage intermetallic alloys which impart the properties of hydrogen adsorption to form hydrides and hydrogen desorption to form hydrogen molecules. This electro-catalyst significantly improves the voltage efficiency >100%, as the cell voltage is significantly reduced below the thermoneutral equilibrium cell voltage, and also lower than the commercial target for low cost hydrogen as shown in Figure 2-23. The hydrogen storage alloy electro-catalyst also imparted better time stability under intermittent and continuous operation in the conventional temperature alkaline electrolyser. It is believed that the hydrogen storage alloys prevent corrosion through a series of electrochemical steps involving adsorption of hydrogen during electrolysis to form metal hydrides and release of hydrogen during stand-by conditions to form water. However, the hydrogen storage alloys are made of *rare-earth metals* that are relatively high cost materials and therefore are not economical for large-scale commercial applications.

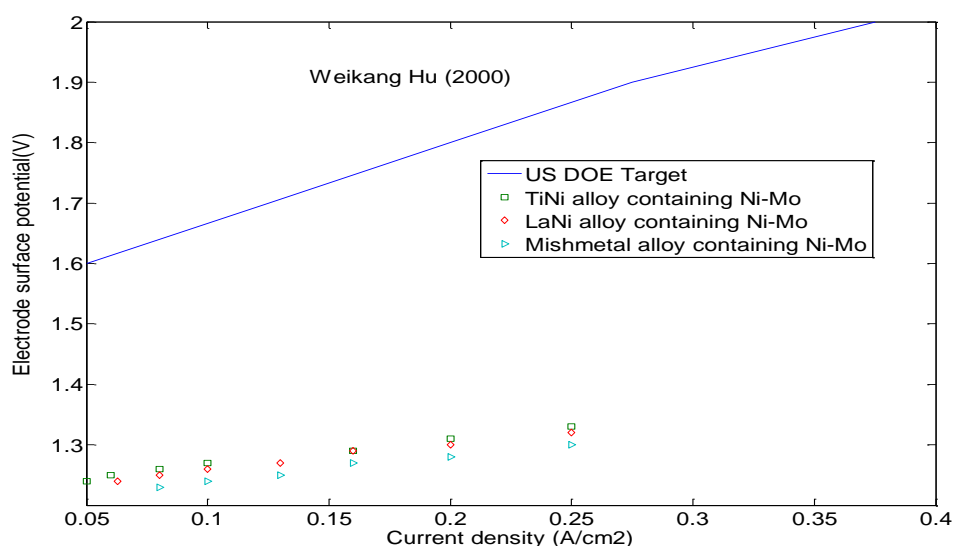


Figure 2-23 Electrode efficiency by Weikang and comparison with commercial target; Source [117]

Kaninski *et al* [120] have reported the method of depositing a Ni-Mo catalyst on the electrode by *in-situ*¹³ electrodeposition. The authors claim that by this method the electro-catalyst increase *HER* efficiency by about 20 %, and the activity is stable at the conventional temperature. A nickel complex salt; tris(ethylenediamine) Ni (II) chloride (Ni (en) Cl₂) and molybdenum salt; sodium molybdate (Na₂MoO₄) were mixed in a proportion of 10:1 respectively as optimum combination of the *d*-metal electro-catalysts.

The alkaline electrolyser that was used in the HARI project consisted of nickel electrodes. It was reported that the efficiency increased by operating at the conventional temperature and high pressure, and the efficiency is lower than the DoE target for low cost hydrogen production as shown in Figure 2-24 [7]. However, the authors reported corrosion of the electrode due to hydrogen embrittlement [121].

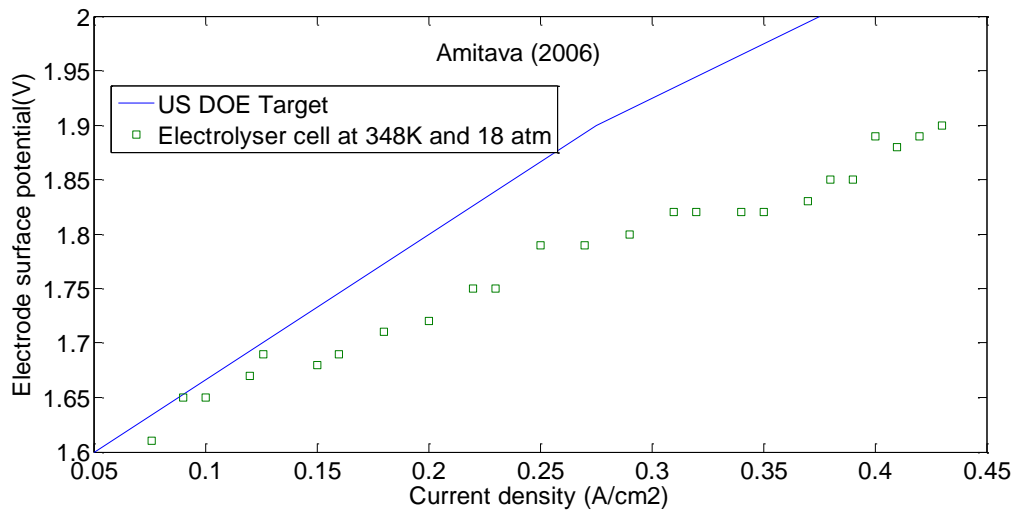


Figure 2-24 Electrode efficiency by Amitava and comparison with commercial target; Source [7]

¹³ In-situ electrodeposition is addition of catalyst in the electrolyte solution during electrolysis at a certain electrode potential or current density for depositing the catalyst on the electrode.

2.8 Conclusion of Chapter

The primary focus is not only to increase efficiency but to increase stability of the electrode and electro-catalyst in the alkaline electrolyser. The longevity of electrolysers is important in order to minimise operational and maintenance costs as well as to increase the return on investments. However, the operational conditions of conventional temperature alkaline electrolysers accelerate corrosion of the electrode; particularly on stainless steel metal that is prone to hydrogen embrittlement, and thereby reduce the lifetime of the electrolyser. The stability of stainless steel metal is relatively enhanced in the ambient temperature alkaline electrolyser, as the rate of hydrogen embrittlement is minimised. Moreover, the ambient temperature alkaline electrolyser is capable of dynamic and fast response of operation, as well as efficient and low cost production of hydrogen and oxygen.

Ni-Mo is the alloy catalyst of choice due to its superior electroactivity, high active area and relatively low cost. For this reason, extensive studies have been carried-out on the Ni-Mo catalyst, which are mostly in the conventional temperature alkaline electrolysers. However, in the next chapter the activity of this catalyst is investigated at both ambient and conventional operating temperatures, in order to provide evidence to support the case for utilising this catalyst in the ambient temperature alkaline electrolyser.

Chapter 3

Comparative Thermal Investigation of the Electrode and Catalyst in a Conventional Alkaline Electrolyser

3.1 Background and Theory

As discussed in section 2.7.1, several of the research papers [107,117,122-125] are investigating trying to increase the *HER* activity of the cathode electrode in order to increase the rate of hydrogen production and improve the electrolyser energy efficiency. Table 3-1 summarises the *HER* activity of the cathode electrode by some of the authors:

Table 3-1: Summary of *HER* activity of investigated cathode electrodes in the conventional temperature alkaline electrolyser

Reference source	Type of electro-catalyst	<i>HER</i> voltage (V) at 200 mA/cm ²	Efficiency (%)
[95]	Nickel flame sprayed	1.95	76
[100]	Cobalt plated nickel	2.1	70
[117]	Mishmetal alloy containing Ni-Mo	1.28	116

A few authors [95,126] have claimed to develop electrodes that are highly stable under *OER* in an alkaline electrolyser. In the literature, activity of the electrode for *HER* and *OER* are treated separately, however in this chapter and subsequent ones the electrodes are characterised under *HER* and *OER* in view of enhancing the efficiencies for both hydrogen and oxygen production. The author's flow-cell alkaline electrolyser was constructed to be able to capture the product gases that can be reused for fuel-cell operation.

The exchange current density is commonly reported in the literature for evaluating and comparing activities of different types of electrode and electro-catalyst material.

But the Tafel method for determining exchange current density is unreliable as different researchers are obtaining wide varying results in the orders of tens of magnitude [70]. However, in this study the exchange current density is determined by EIS measurement of polarisation resistance as described by equation 39 under section 2.4. The exchange current density is the equal anodic and cathodic partial current densities under open-circuit. The exchange current density depends on the nature of electrode, and is determined to assess a suitable electrode for operation in the alkaline electrolyser.

The reversible potential and ohmic overpotential can both be reduced by operating at the conventional electrolyser temperatures of 70-80°C. However, the activation overpotential is weakly dependent on temperature compared with the effect of exchange current density. In other words, the exchange current density significantly influence on the electrode kinetics and consequently enhance the rate of reaction. For example, although the overpotential is reduced by about 200 mV by increasing the operating temperature from 23°C to 80 °C, the overpotential however is reduced by more than 200mV by employing an electro-catalyst that increase the exchange current density [66-68,70]. Therefore energy efficiency can be improved thermodynamically in the conventional temperature alkaline electrolyser, and kinetically by employing electro-catalysts in the ambient temperature alkaline electrolyser. This chapter provides an overview of a general approach to characterise the electrode in the ambient and conventional temperatures, with a view to enhance efficiency as well as lifetime viability of the alkaline electrolyser. It also provides a brief insight on the open-circuit voltage (OCV) of alkaline electrolyser. Further details about activity of electrodes and electro-catalyst materials in an ambient temperature alkaline electrolyser are discussed in subsequent Chapters.

The charge transfer resistance or reaction resistance (R_p) (see Figure 2-2) is the inherent resistance to the *HER* and *OER* that take place on the electrode [61]. The basic electrical circuit elements of resistances and capacitance are determined by DC polarisation and EIS analysis. The reaction and ohmic resistances result in lost energy (i.e. heat generation) in the alkaline electrolyser, and both the ohmic and reaction resistances can be determined directly from the Nyquist impedance plots. At

low frequency (DC conditions) the double-layer capacitance (C_{dl}) is open circuit, however, at intermediate or high frequency the impedance due to capacitance is purely reactive thus the capacitance is determined based on the imaginary impedance as expressed in equation 38 in section 2.4.

The corrosion rates of electrodes are critical in assessing continuous operation and lifetime viability of the alkaline electrolyser. Therefore corrosion current density of the electrodes is determined by the resistance polarisation method [127] which involves substituting the Tafel parameters and polarisation resistance into equation 60.

$$R_p = \left[\frac{\Delta \varepsilon}{\Delta J_{app}} \right] \varepsilon \rightarrow 0 = \frac{\beta}{J_{corr}} \quad (60)$$

Where

$$\beta = \frac{\beta_a \beta_c}{2.3(\beta_a + \beta_c)} \quad (61)$$

3.2 Experimental Measurements

DC polarisation and EIS measurements were carried out using the electrolyser cell arrangement that is shown in Figures 3-1 and 3-2. The Solartron 1287 (potentiostat/galvanostat) and 1255B frequency response analyser (FRA) have been used to carry-out these measurements. For DC measurement, the potentiostat/galvanostat supplies a voltage/current respectively, the signal gain is adjusted through a differential amplifier and then supplied to the cell. The sensed current/voltage response from the cell is then input through another differential amplifier and received back to the potentiostat/galvanostat. These differential amplifiers adjust the signal outputs so that the potentiostat/galvanostat receives signals that are in its rated capacity range of 0-2 A. For EIS measurement, the FRA generates an AC voltage signal that is superimposed on a DC voltage from the potentiostat/galvanostat, which is then supplied to the cell through a differential amplifier. The corresponding voltage and current response is received back at the FRA where the data is translated in the frequency domain.

A personal computer that runs the applications (CorrWare , Zplot and Zview) for windows is used to communicate with the Solartron instruments through a GPIB interface board and to perform DC and EIS measurements as well as recording of the data. The algorithm and equipment have been verified to conform with the ASTM international standard practice: G106-89 [128]. Therefore the results are comparable with other laboratories.

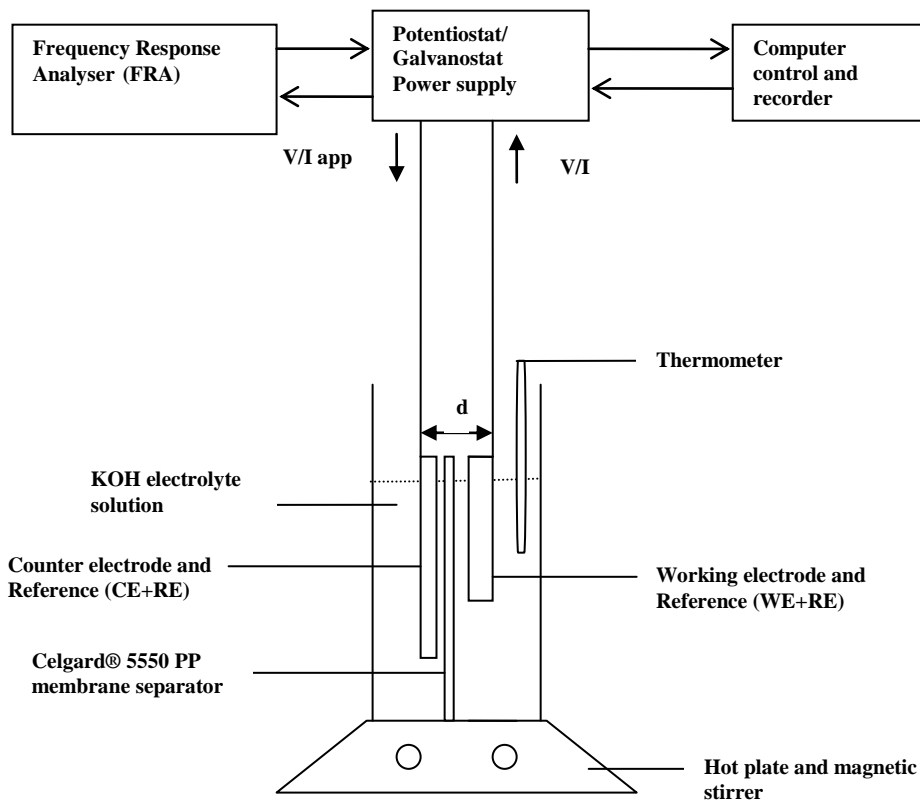


Figure 3-1 Schematic representation for DC and EIS measurements of the alkaline electrolyser cell¹⁴

¹⁴ The reference electrode is a SHE (0.00V) and it is pseudo-reference.

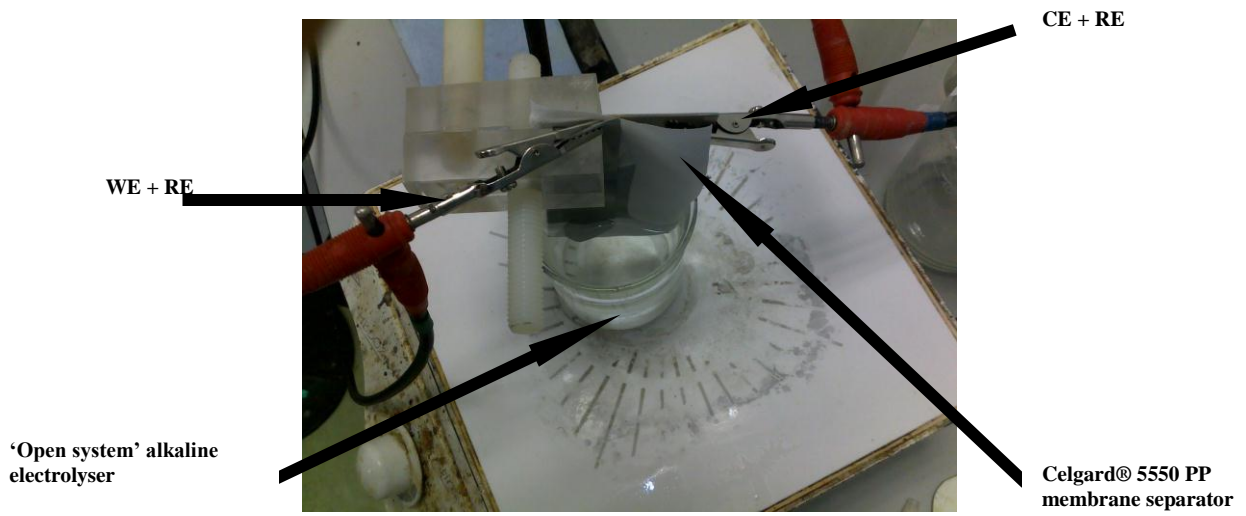
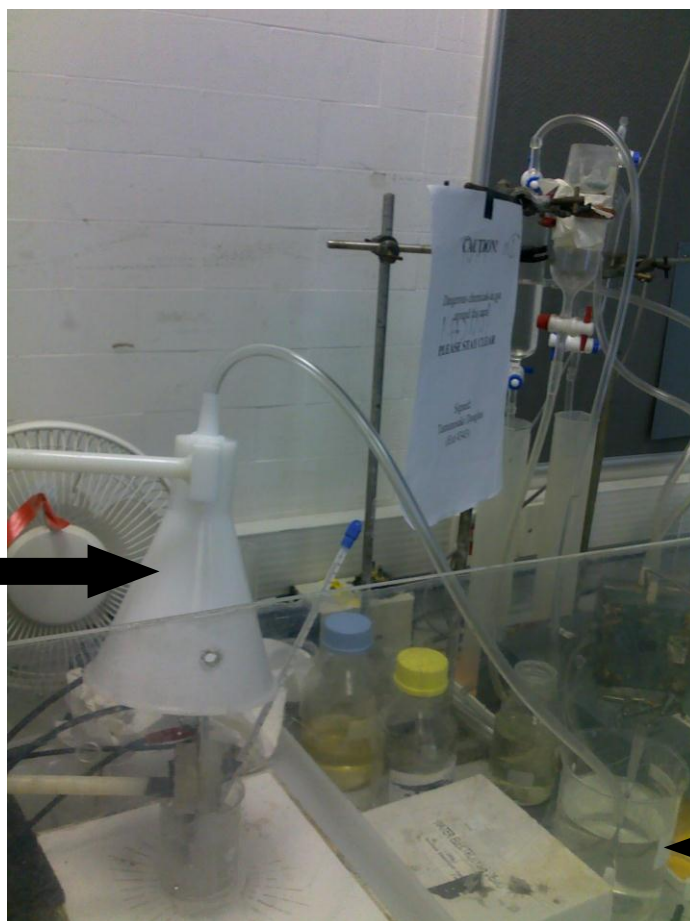


Figure 3-2 Image of the ‘open-system’ alkaline electrolyser cell

Fume hood as a safety measure to minimise discharge of gases directly to the atmosphere



Evolved hydrogen and oxygen gases are mixed in water

Figure 3-3 Image of the ‘open-system’ alkaline electrolyser cell under a fume hood

The working electrodes (WE) were nickel and stainless steel meshes. The geometric active area of the nickel and stainless steel meshes were 2.52 cm^2 and 2.46 cm^2 respectively, and the applied current density was estimated based on this geometric active area. The counter electrode (CE) was a stainless steel sheet that had a geometric area of about 15 cm^2 . Polarisation of the working electrode was carried-out for *HER* (cathodic) and for *OER* (anodic) operations at a scan rate of 5 mA/sec . The data were collected in triplicate measurements and the steady-state potentials were recorded as average of the triplicate measurements. The EIS measurements were carried out at steady-state DC potential of 2 V and at constant AC amplitude of 10 mV . The frequency was in the range of 100 kHz to 0.1 Hz . The electrolyte was 30% (vol/vol) aqueous KOH and a separation distance of about 1 mm was maintained between the WE and CE. After the experiments, the cell was emptied and washed. The catalyst (Ni-Mo) was obtained from nickel sulphate heptahydrate ($\text{NiSO}_4 \cdot 7\text{H}_2\text{O}$) and sodium molybdate dihydrate ($\text{Na}_2\text{MoO}_4 \cdot 2\text{H}_2\text{O}$) in a composition

ratio of 10:1 respectively, which was added to the electrolyte solution during electrolysis with continued stirring. All the chemicals were of analytical grade and were supplied by Sigma-Aldrich [129]. The electrodes were supplied by Advent Research Material [86].

3.3 Discussion of the Results: Investigation of the Electrodes and Catalyst under Variable Electrical Power of Operation

The *HER* and *OER* polarisation on the electrodes is shown in Figure 3-4a in comparison with the commercial targets for low cost hydrogen production and it is obvious that the overvoltages are reduced at the conventional operating temperature.

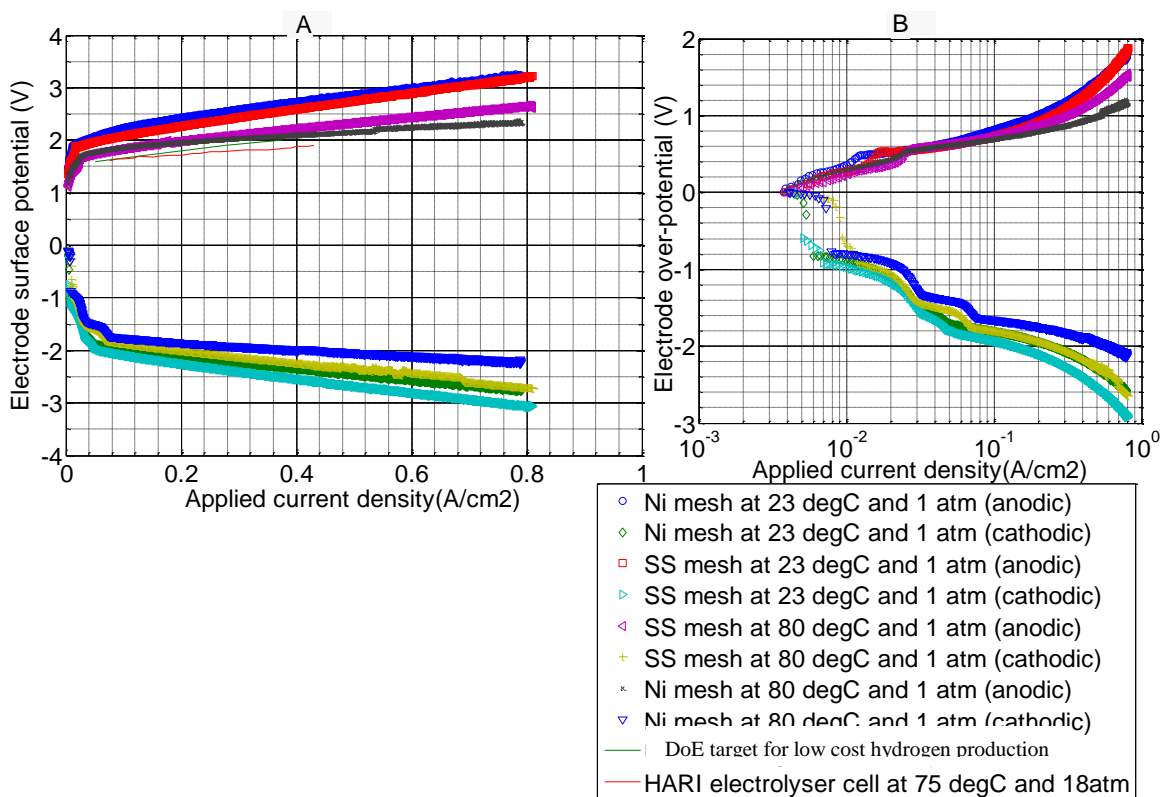


Figure 3-4 (A) *HER* and *OER* polarisation on the electrodes in the ambient and conventional temperatures alkaline electrolyzers. The electrode surface potential is the half-cell voltage of the working electrode; (B) Tafel relation. The electrode over-potential was obtained by subtracting the reversible voltage from the electrode surface potential.

The Tafel parameters (β_a and β_c) that are shown in Table 3-2 were obtained from Figure 3-4b. The Tafel constants are reduced at high temperature which indicates increase in the rate of reaction. At the conventional temperature, the total cell voltage

or energy consumption is slightly reduced at a specific current density to produce a given amount of oxygen and hydrogen. Therefore it is obvious that efficiency is slightly enhanced at the conventional operating temperature of alkaline electrolyzers.

Table 3-2 Summary of kinetic parameters for the electrodes in the ambient and conventional temperatures alkaline electrolyzers

Electrode	β_a (mV)	β_c (-mV)	E_{200}^* (V)	E_{-200}^{**} (-V)
SS mesh at 23°C	218.23	162.80	2.3	2.3
SS mesh at 80°C	177.78	102.65	2.0	2.0
Ni mesh at 23°C	266.59	292.73	2.4	2.1
Ni mesh at 80°C	267.17	107.18	2.0	1.9

*Half-cell voltage for oxygen production at 200 mA/cm², **Half-cell voltage for hydrogen production at -200 mA/cm²

The corresponding Nyquist impedance plot is shown in Figure 3-5. The semi-circle is depressed at the conventional temperature thereby indicating increased reaction rates on the electrode surface. As a consequence, the Ohmic and polarisation resistances are significantly reduced at higher operating temperature. The existence of a capacitance indicates that the electrode reactions are controlled by charge transfer mechanisms. Hence, the polarisation resistance is generally lower especially for the cathodic reactions that take place through the characteristic step-wise electron transfer mechanism (Volmer-Heyrovsky) that was described in section 2.3.1. The capacitance was estimated at intermediate frequencies (10 kHz to 50 kHz), and has generally increased at the conventional temperatures possibly due to an increase in conductivity of the double-layer interface and consequently increase in the electrochemical accessible surface area.

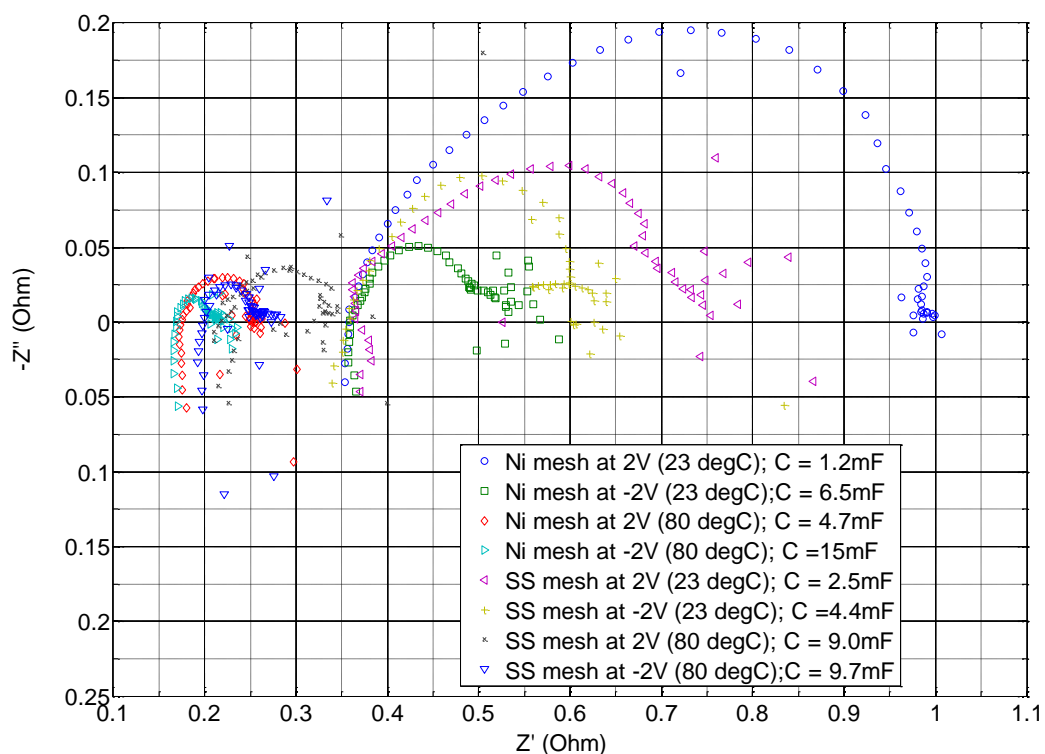


Figure 3-5 Nyquist impedance plot for electrodes in the ambient and conventional temperatures alkaline electrolyzers

As shown in Table 3-3, the exchange current density is generally increased at the conventional temperature. Nickel and SS metals exhibit similar kinetic properties in all the investigated conditions, although the geometric active area of nickel metal is 2 % higher (see section 3.2), and because of the favourable electronic property of nickel metal, it is able to reduce the polarisation resistance and enhance the *HER* activity. The polarisation resistance is reduced at the higher temperature due to an increase in electrolyte conductivity and gas-bubble migration from the electrode surface. The polarisation resistance differs for both *OER* and *HER* as these reactions take place through different mechanisms (see section 2.3.1).

Table 3-3 also indicates that corrosion current density is generally increased at the conventional temperature. In particular, the corrosion current density is increased by up to 60 % on SS mesh under cathodic polarisation at the conventional temperature compared with the ambient temperature. This could be due to hydrogen embrittlement of steel, which is accelerated at high temperature and consequently extending the

corrosion area to the active-passive transition region as described in Figure 2-15 [6] which is the Pourbaix diagram for steel in KOH electrolyte.

Table 3-3 Resistance, exchange current density and corrosion rates of electrodes in the ambient and conventional temperatures alkaline electrolyzers

Electrode	R_{Ohm} (Ω) At 2V	R_P (Ω) At 2V	i_o (A/cm ²) At 2V	$*J_{corr}$ (A/cm ²) At 2V	R_{Ohm} (Ω) At -2V	R_P (Ω) At -2V	i_o (A/cm ²) At -2V	$*J_{corr}$ (A/cm ²) At -2V
SS mesh at 23 °C	0.37	0.31	0.04	0.13	0.34	0.26	0.05	0.15
SS mesh at 80 °C	0.22	0.11	0.14	0.17	0.19	0.05	0.30	0.38
Ni mesh at 23 °C	0.35	0.64	0.02	0.06	0.37	0.16	0.08	0.23
Ni mesh at 80 °C	0.18	0.08	0.19	0.38	0.17	0.05	0.30	0.60

* The corrosion current density was determined based on equations 60 and 61 in section 3.1.

Similarly, the *HER* and *OER* polarisation on the electrodes with a Ni-Mo catalyst is shown in Figure 3-6. At the conventional operating temperature, the polarisation behaviour of Ni-Mo catalysed SS mesh is similar to the DoE commercial targets for low cost hydrogen production, therefore there is significant increase in efficiency on Ni-Mo catalysed SS mesh at the conventional temperature.

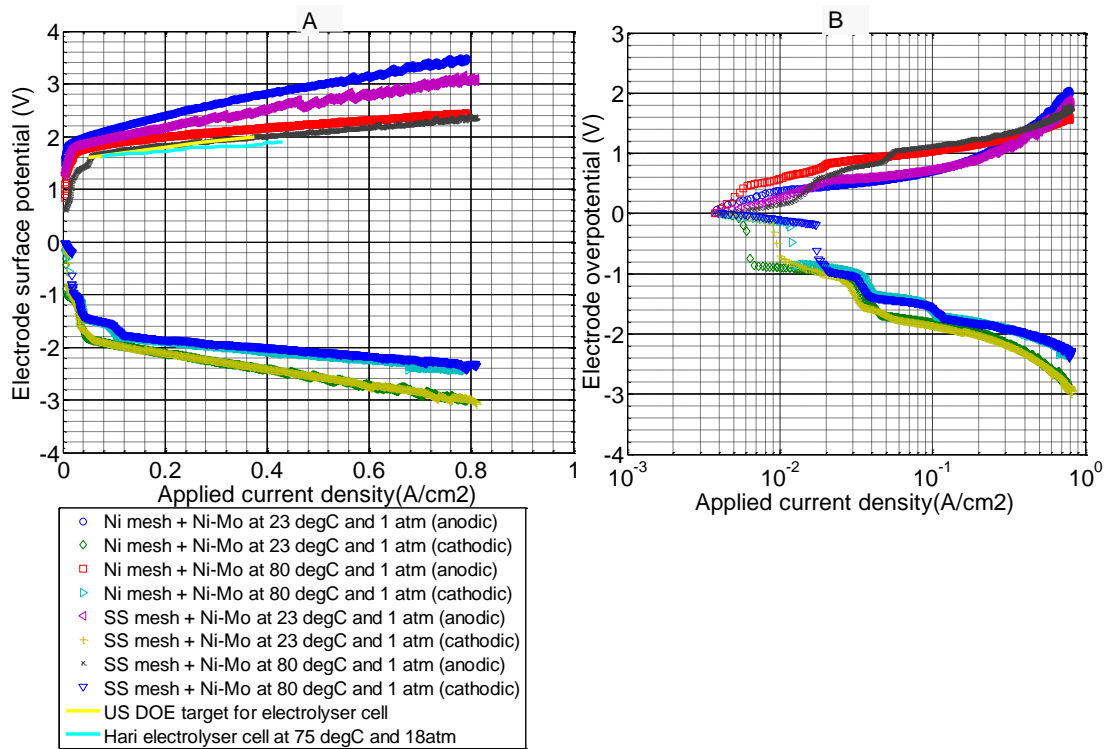


Figure 3-6 (A) HER and OER polarisation on the electrode and catalyst in the ambient and conventional temperatures alkaline electrolyzers; (B) Tafel relation

By comparing Tables 3-2 and 3-4 for the SS mesh, it is clear that energy consumption is reduced for a fixed amount of hydrogen and oxygen production on Ni-Mo catalysed SS mesh. For example at 200mA/cm² and at the ambient temperature, the voltage efficiency is increased by 4 % and 9 % for oxygen and hydrogen production respectively on Ni-Mo catalysed SS mesh. Likewise, at 200mA/cm² and at the conventional temperature, the voltage efficiency is increased by 10 % and 5 % for oxygen and hydrogen production respectively on Ni-Mo catalysed SS mesh. Hence, efficiency is increased on Ni-Mo catalysed SS mesh at both the ambient and conventional operating temperatures. This is attributed to the presence of the catalyst in the alkaline electrolyser. The Tafel constants in Table 3-4 are not consistent with temperature thereby suggesting that the increase in efficiency at high temperature is mainly due to an increase in reaction rates based on exchange current density.

Table 3-4 Summary of kinetic parameters for the electrodes and catalyst in the both ambient and conventional temperatures alkaline electrolyzers

Electrode metal and catalyst	β_a (mV)	β_c (-mV)	E_{200}^* (V)	E_{-200}^{**} (-V)
Ni mesh + Ni-Mo at 23 °C	359.02	295.74	2.4	2.1
Ni mesh + Ni-Mo at 80 °C	486.92	164.63	2.0	1.9
SS mesh + Ni-Mo at 23 °C	338.27	150.19	2.2	2.1
SS mesh + Ni-Mo at 80 °C	161.99	187.20	1.8	1.9

*Half-cell voltage for oxygen production at 200 mA/cm², **Half-cell voltage for hydrogen production at -200 mA/cm²

The corresponding Nyquist impedance plot is shown in Figure 3-7 for the catalysed electrodes, and by referring to Table 3-5 it is clear that polarisation resistance is significantly reduced and exchange current density is significantly increased on Ni-Mo catalysed SS mesh at the conventional temperature. This indicates that efficiency is increased for hydrogen and oxygen production due to an increase in the reaction rates of Ni-Mo catalysed SS mesh. It is likely that the exchange current density plays a significant role to enhance the kinetics for *HER* and *OER*. In particular, the *HER* activity is enhanced on the Ni-Mo catalysed SS mesh due to synergy of the metal and catalyst material, favourable electronic property of the alloying metals and an increase in ionic conductivity of the electrolyte solution. It is also possible that a higher concentration of the catalyst might have resulted in higher activity of the Ni-Mo catalysed SS mesh. Nevertheless, the result indicates the effect of utilising catalyst materials to enhance the efficiency of electrolysis. The corrosion current density, however, is significantly increased on Ni-Mo catalysed SS mesh at the conventional temperature as was observed previously for the uncatalysed SS mesh. It is evident that SS mesh degrades relatively faster due to hydrogen embrittlement which takes place rapidly in hot KOH electrolyte [6] (see also Figure 2-15 in section 2.7).

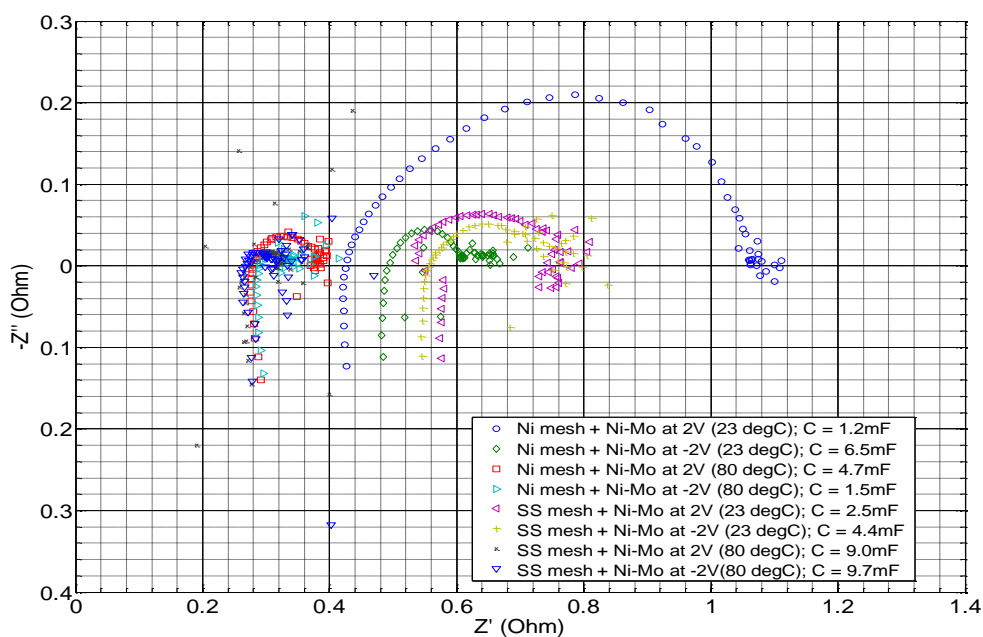


Figure 3-7 Nyquist impedance for the electrode and catalyst in the ambient and conventional temperatures alkaline electrolyzers

Table 3-5 Resistance, exchange current density and corrosion rates of the electrode and catalyst in the ambient and conventional temperatures alkaline electrolyzers

Electrode	R_{Ohm}	R_p	i_o	$*J_{corr}$	R_{Ohm}	R_p	i_o	$*J_{corr}$
	(Ω)	(Ω)	(A/cm ²)	(A/cm ²)	(Ω)	(Ω)	(A/cm ²)	(A/cm ²)
	At 2V	At 2V	At 2V	At 2V	At -2V	At -2V	At -2V	At -2V
Ni mesh + Ni-Mo at 23°C	0.43	0.58	0.02	0.074	0.48	0.13	0.10	0.33
Ni mesh + Ni-Mo at 80°C	0.29	0.09	0.17	0.37	0.29	0.06	0.25	0.56
SS mesh + Ni-Mo at 23°C	0.57	0.18	0.07	0.21	0.55	0.22	0.06	0.18
SS mesh + Ni-Mo at 80°C	0.28	0.04	0.38	0.70	0.28	0.03	0.51	0.93

* The corrosion current density was determined based on equations 60 and 61 in section 3.1.

3.4 Investigation of the Electrodes under Intermittent Electrical Power of Operation

The on/off switching cycle was investigated for the electrodes at both ambient and conventional temperatures. A constant current load of 200 mA/cm^2 was applied for 5 minutes; the current was switched off for about 10 minutes and then re-applied for another 5 minutes. This test was repeated several times and all the data points were plotted as shown in Figures 3-8 and 3-9. It is evident that the cell voltages are relatively more stable at the ambient temperature. The cell voltages are not stable at high temperature, and this is attributed to fluctuating temperature of the hot plate. The overvoltage however is reduced by about 13 % and 11 % on Ni and SS mesh respectively at the conventional temperature. However, the OCV is reduced by about 47 % and 38 % on Ni and SS mesh respectively at the conventional temperature. A reduction in OCV indicates that free energy is reduced in the alkaline electrolyser that is operated at the conventional temperature. This free energy can be useful under fuel-cell operation, and is higher at the ambient temperature thereby suggesting that round-trip or overall efficiency will be increased for the ambient temperature regenerative or unitised regenerative alkaline fuel-cell.

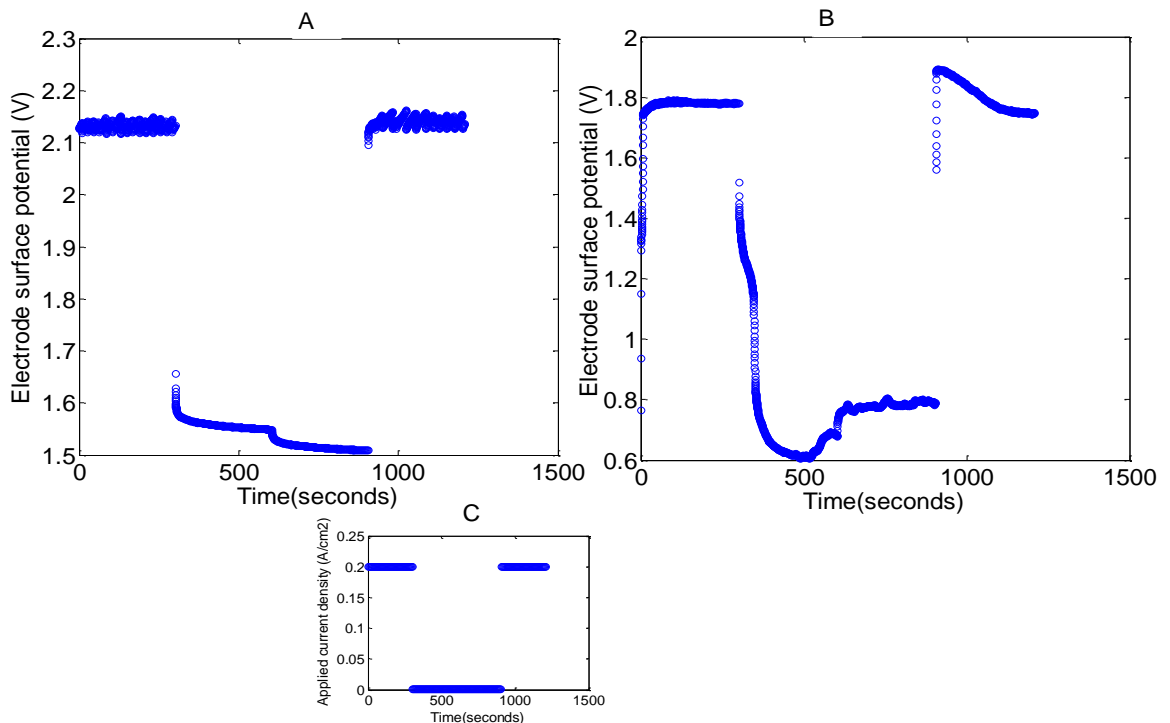


Figure 3-8 Stability of Ni mesh under intermittent electrical power supply: (A) at 23 °C, (B) at 80 °C and (C) Applied current load profile

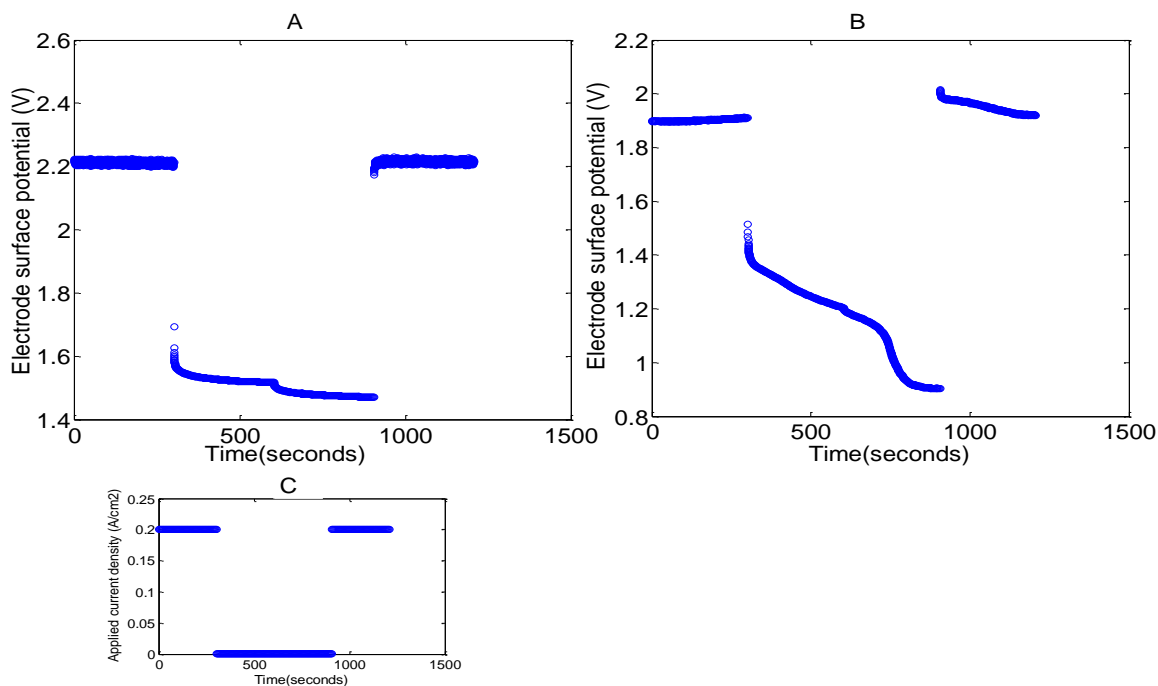


Figure 3-9 Stability of SS mesh under intermittent electrical power supply: (A) at 23 °C, (B) at 80 °C. (C) Applied current load profile

3.5 Investigation of the Electrode and Catalyst in a Flow-Cell Alkaline Electrolyser

Figure 3-10 shows the flow-cell alkaline electrolyser that is operated at the ambient temperature and consisted of SS mesh electrode and Ni-Mo catalyst. The Ni-Mo catalyst was added into the electrolyte solution in a proportion of 10:1 respectively to induce *in-situ* electrodeposition that is similar with [120]. The separation distance between the electrodes was about 3cm, and the electrolyte was 30% (vol/vol) aqueous KOH. Basically, the cell was designed to collect and capture the hydrogen and oxygen product gases that can be subsequently utilised in the alkaline fuel-cell to generate back electricity. By comparison and referring to section 2.6, the flow-cell in Figure 3-10 was constructed similar with the bipolar cell configuration, whereas the ‘open-system’ alkaline electrolyser cell in Figure 3-2 was constructed similar with the monopolar cell configuration.

The flow-cell was constructed by assembling end plates, electrode and electrolyte compartments with gaskets and longitudinal tie rods. Further details about the cell construction and its performance are given in Chapter 7. It should be noted that due to the relatively large separation distance between the electrodes, the performance of this flow-cell was not compared with the ‘open-system’ alkaline electrolyser. Nonetheless, the main purpose of this experiment was to investigate the electrode performance in a flow-cell alkaline electrolyser that is operated by circulation of electrolyte in order to capture the product gases.

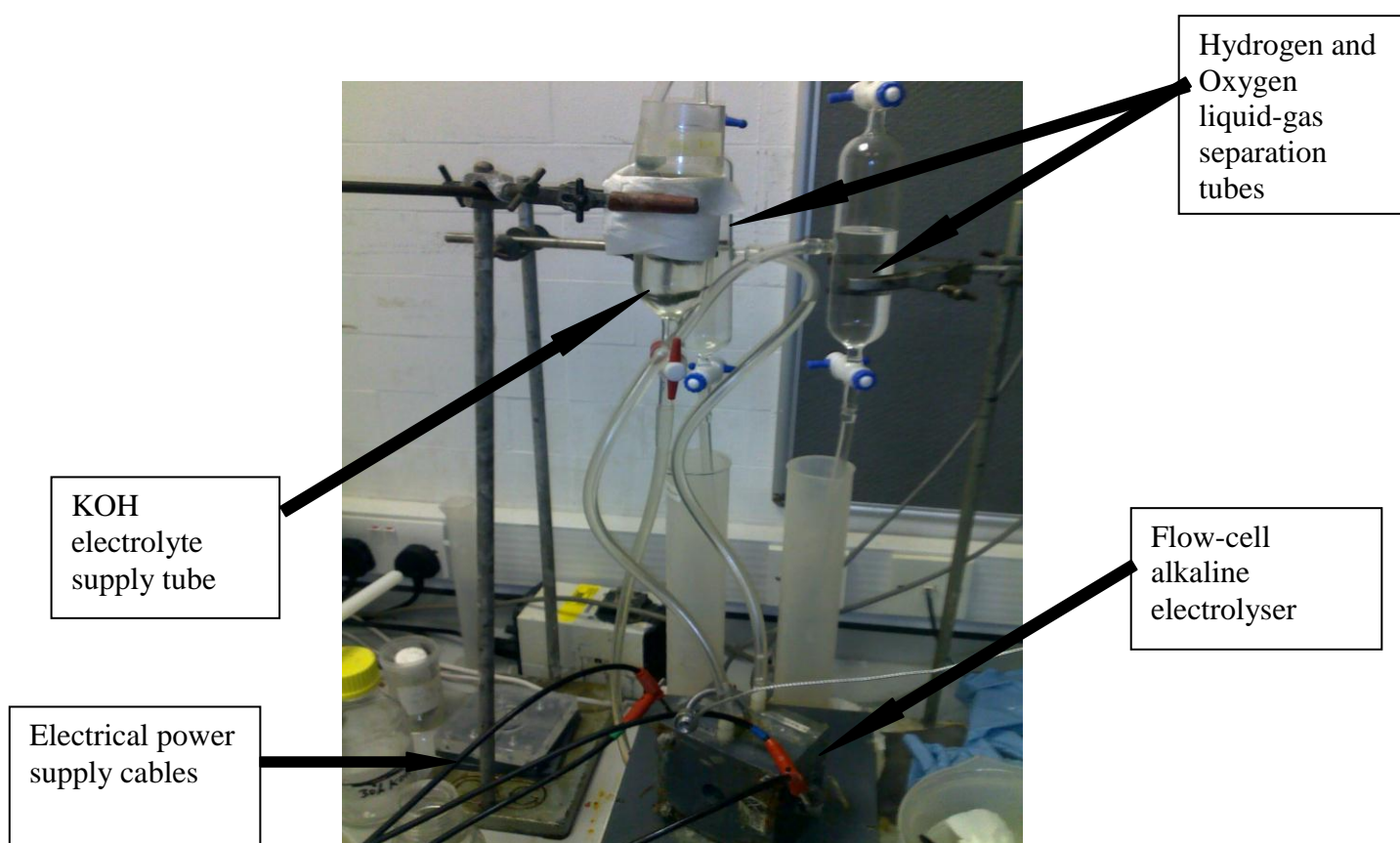


Figure 3-10 Image of the flow-cell ambient temperature alkaline electrolyser which consists of SS mesh, and Ni-Mo catalyst added to the electrolyte solution

The polarisation and EIS results on SS mesh and Ni-Mo catalyst in the flow-cell ambient temperature alkaline electrolyser are shown in Figures 3-11 and 3-12 respectively. Obviously, energy consumption is significantly higher in this alkaline electrolyser cell compared with the commercial targets for low-cost hydrogen production. The internal cell resistance is relatively high, which has

resulted in a sudden increase in the overvoltages at high current densities (at about 400 mA/cm²). This is also evident in the Nyquist plot of Figure 3-12, which indicates relatively high Ohmic and polarisation resistances. The increase in internal cell resistance could be due to several factors including: the physical set-up of the cell, electrode surface that is partially covered by gas-bubbles, and overpolarisation on the electrode due to relatively low surface area. Therefore, the internal cell resistance can be minimised by increasing the electrode active area, reducing the separation distance between the electrodes, use of appropriate membranes, and modification of the flow-channels in order to promote mass transport of electrolyte and to facilitate removal of gas bubbles from the electrode surface.

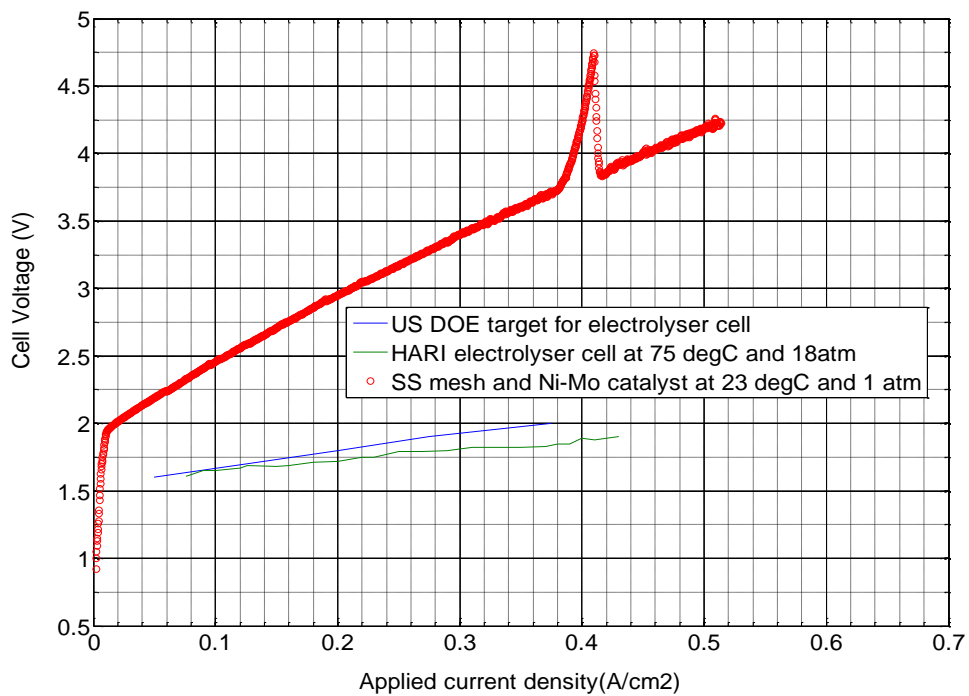


Figure 3-11 Polarisation of SS mesh and Ni-Mo catalyst in the flow-cell ambient temperature alkaline electrolyser

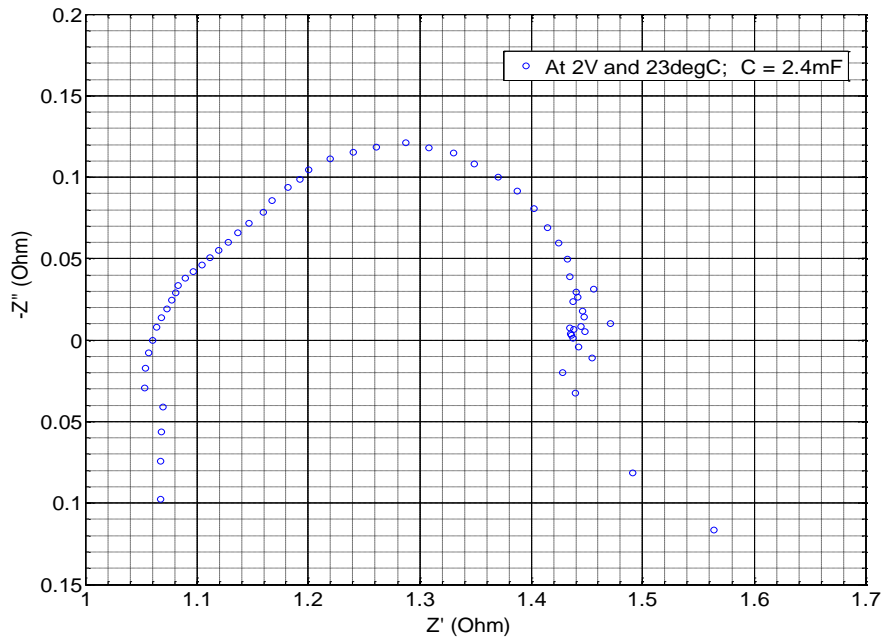


Figure 3-12 Nyquist impedance plot for SS mesh and Ni-Mo catalyst in the flow-cell ambient temperature alkaline electrolyser

From analysis of Figure 3-6, it is clear that higher operating temperature improves the cell performance. The cell voltage is reduced by 0.3 V at the conventional operating temperature for Ni-Mo catalysed SS mesh in the monopolar alkaline electrolyser cell. If the effect of temperature is taken into account, it is likely that the cell voltage will be 2.2 V at 200 mA/cm² for Ni-Mo catalysed SS mesh in the flow-cell conventional temperature alkaline electrolyser. This will be a significant reduction of the cell voltage by about 0.7 V at the conventional operating temperature compared with the ambient temperature. However, based on Table 3-5, the corrosion rate is increased by 70 % and 80 % at the anode and cathode respectively for Ni-Mo catalysed SS mesh. This means that for the flow-cell alkaline electrolyser, although efficiency will be increased at the conventional operating temperature, there will be a significant reduction in lifetime durability of the electrodes and catalyst material at the conventional operating temperature.

3.6 Conclusion of Chapter

The overvoltages are significantly minimised by operating the alkaline electrolyser at the conventional temperature of 80°C. The efficiencies for hydrogen and oxygen production are increased at the conventional operating temperature. This is mainly due to an increase in exchange current density which increases the kinetics for *HER* and *OER*. However, the corrosion rate is significantly increased especially on the stainless steel electrode at the conventional temperature. Hydrogen embrittlement is accelerated on stainless steel electrode at the conventional operating temperature for hydrogen production. Conversely, efficiency can be increased and corrosion rate can be minimised by the addition of a catalyst to the electrode at the ambient temperature. The catalyst has the advantage of increasing the exchange current density and enhancing efficiency particularly for hydrogen production. Moreover, the catalyst is more stable at the ambient temperature.

Chapter 4

Fabrication and Characterisation of the Electrode

In this chapter, the kinetic efficiency and time stability of commercially available SS alloys were investigated in the ambient temperature alkaline electrolyser. The surface structure of the electrode is modified by etching in order to increase the surface area or active sites, and to enhance the rates of *HER* and *OER*. It is expected through this analysis to identify the most efficient form of the SS alloy that can be subsequently developed into an electro-catalyst material.

4.1 Background

Stainless steel (SS) is an alloy of iron and consists of a minimum of 10 % chromium which makes it corrosion resistant. In particular, SS-304 consists of: Cr (17-20 %), Ni (8-11 %), and Fe (balance), and in contrast, SS-316 consists of: Cr (16-18 %), Ni (10-14 %), Mo (2-3%), and Fe (balance) [86]. The commercially available SS alloys are supplied in various physical forms and dimensions [86] that influence on kinetic efficiency of the electrolyser under variable and intermittent electrical power of operation. SS has the unique property of exhibiting passivation in an oxygen environment which can influence the kinetic efficiency of the electrolyser, and the degree of passivation and time stability depend on the electrode surface structure [117-118]. For this reason, the *OER* and *HER* processes were investigated on the commercially available types of SS electrodes. The most suitable electrode substrate is identified based on efficiency, stability, cost and manufacturing scale-up.

4.1.1 Physical Dimensions and Electrical Resistance of Stainless Steel

The electrical resistance is directly proportional to the length and resistivity of the metallic conductor and inversely proportional to its cross-sectional area. It is expressed in equation 62.

$$R = \frac{\rho L}{A} \quad (62)$$

The electrodes that are investigated have a circular shape of 2 cm diameter. The electrical resistivity of stainless steel grades: SS-304 and SS-316 are $6.897 \times 10^{-7} \Omega\text{-m}$ and $7.496 \times 10^{-7} \Omega\text{-m}$ respectively [130]. The geometric active area for the SS mesh 304 is increased by 19 % compared to the SS smooth sheet 304 as shown in Table 4-1.

Table 4-1 Physical dimensions and electrical properties of the commercial SS electrodes

Electrode	Surface structure	*Geometric surface area (cm ²)	Thickness (mm)	Electrical resistance (Ω)	Aperture size (mm)
SS mesh type-304	Plain weave	3.88	0.1	3.55×10^{-5}	0.15
SS mesh type-316	Twill weave	4.86	0.025	3.08×10^{-5}	0.026
SS sheet type-304	Smooth sheet	3.143	1.0	4.38×10^{-5}	N/A

* See Appendix B for the method of calculating geometric surface area and electrical resistance of the mesh electrode

4.2 Experimental Measurements

The ‘open-system’ monopolar cell that is shown in Figure 3-2 was used for this experiment. DC polarisation and EIS were recorded on the SS working electrode (WE) in 30% KOH electrolyte at an ambient temperature of 23°C. The current densities were estimated based on the geometric surface area of the electrodes as stated in Table 4-1.

The counter electrode (CE) was a SS sheet that has a geometric area of 13.5cm². A separation distance of 1mm was maintained between the WE and CE in all of the experiments and a Celgard[®]5550 micro-porous polypropylene (PP) membrane was used to separate the electrodes. Celgard[®] supplied three (3) types of membrane: 3401, 3501 and 5550 but the 5550 membrane was used because Celgard[®] [81] claims that it has good surface wettability; i.e. it is hydrophilic to allow ionic transport, and has porosity of 50%-55% and pore size of 0.064µm. Moreover, the 5550 type of

membrane is laminated and woven which makes it structurally stable to withstand compression in the filter-press cell design.

The test methods are essentially aimed to determine electrochemical efficiency of the electrode under variable electrical power input, stability of the electrode under intermittent and constant electrical power input. These test methods were undertaken in order to simulate the alkaline electrolyser that is powered by: (a) variable and/or intermittent electrical power from the wind turbine, and (b) constant electrical power from the electrical grid. The open-circuit stability of the electrode was measured by repeated on/off switching cycle under a constant current load of about 200 mA/cm². The oxygen and hydrogen evolution rates were determined based on the electrode current density in relation with the Faraday's equation 12 under potentiostatic (constant voltage) mode of operation.

4.3 Discussion of the Results

4.3.1 Kinetic Efficiency under Variable Electrical Power of Operation

Figure 4-1 shows the polarisation comparison of SS mesh (304) and SS sheet (304) types of electrode. There is no significant difference in kinetic efficiency of the electrodes. However, the Tafel relation does indicate relatively lower activation overpotential (Tafel slope) on SS mesh cathode and SS smooth sheet anode. This means that rate of hydrogen evolution is enhanced on SS mesh, which could be attributed to its porosity or aperture size that increase the surface area and facilitates detachment of the hydrogen gas-bubbles.

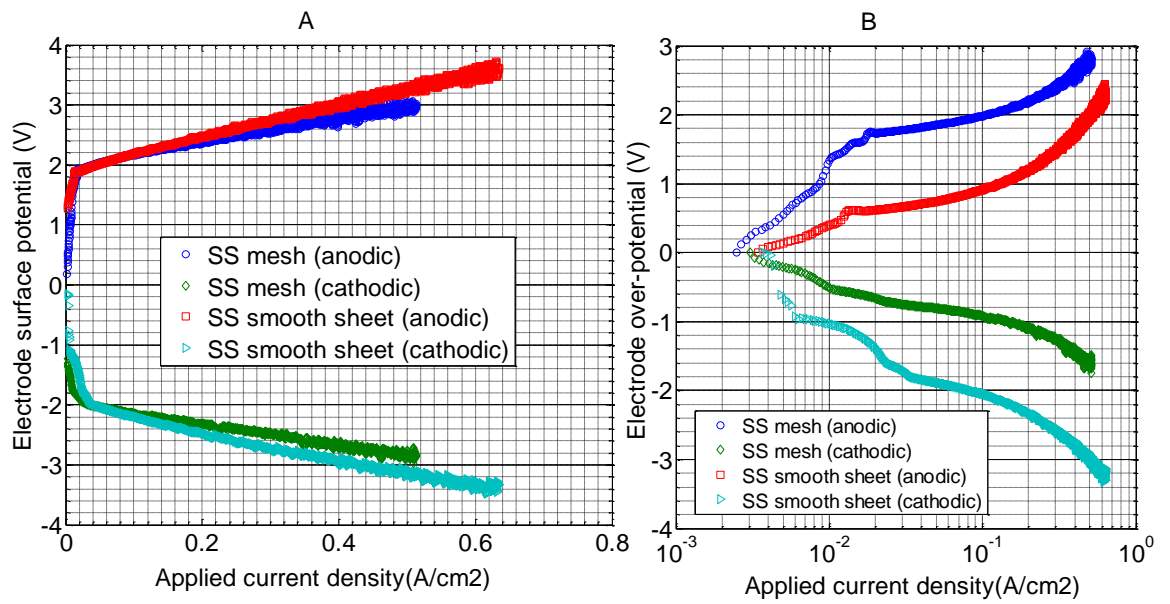


Figure 4-1 Comparison of kinetic efficiency of SS mesh type-304 and SS sheet type-304 electrodes in 30% KOH at 23°C: (A) DC polarisation, (B) Tafel relation

The corresponding complex plane impedance is shown in Figure 4-2 which indicates a reduction in Ohmic resistance on SS mesh.

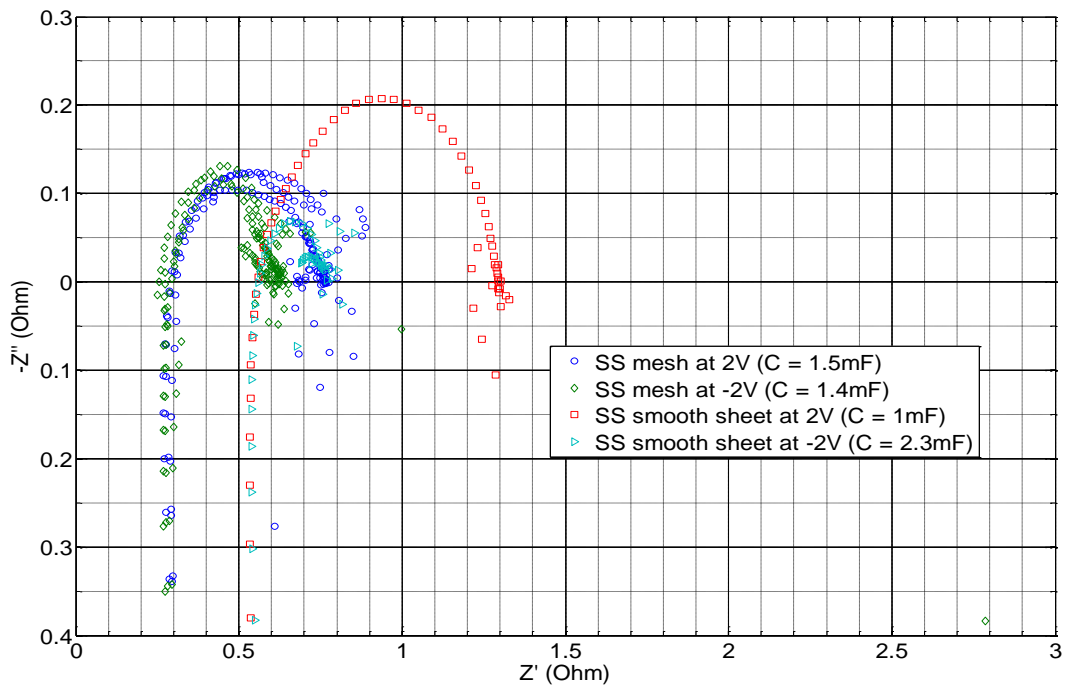


Figure 4-2 Nyquist impedance comparison of SS mesh type-304 and SS smooth sheet type-304

In particular, polarisation resistance is reduced for the cathodic reaction on SS mesh. The surface structure and relatively higher surface area of SS mesh type-304 (see Table 4-1) favour nucleation and detachment of the hydrogen gas-bubbles. The existence of capacitance is evidence that the electrode reactions are controlled by charge transfer mechanisms as described in section 2.3.1.

The polarisation behaviour of SS mesh type-304 was carried-out as shown in Figure 4-3 in order to determine the resistance under variable electrical power input.

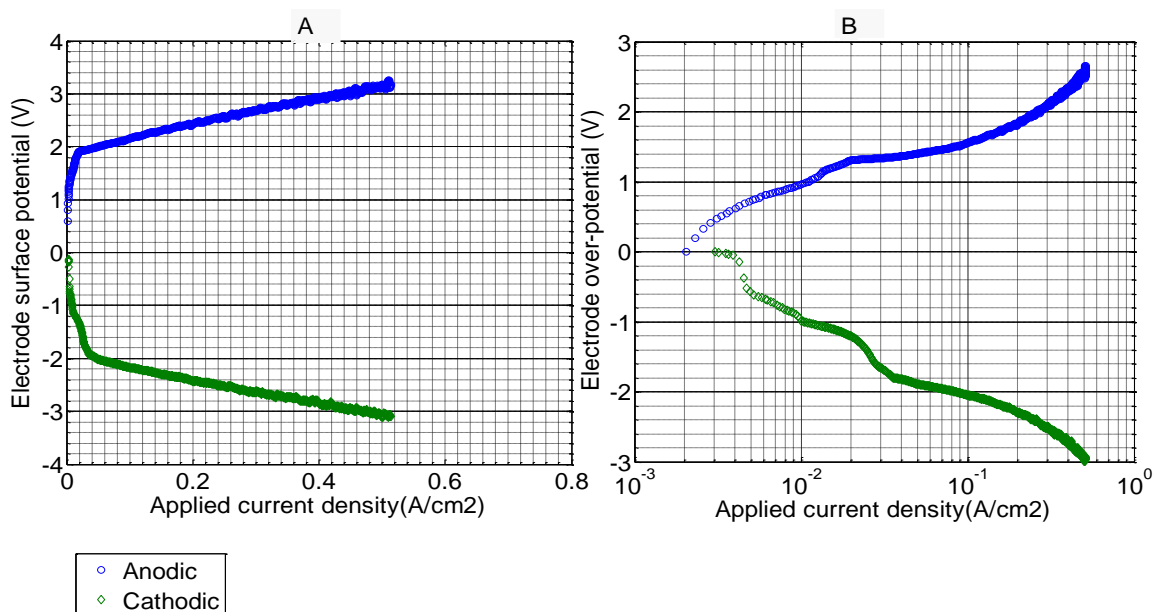


Figure 4-3 Kinetic efficiency of SS mesh in 30% KOH at 23°C: A. DC polarisation, B. Tafel relation

Figures 4-4 and 4-5 show the corresponding impedances for *OER* and *HER* respectively. The polarisation resistance increases at relatively lower potentials under *OER* and *HER* due to oxygen and hydrogen gas-bubble coverage on the SS mesh respectively. The polarisation resistance, however, is reduced at relatively higher potentials under *OER* and *HER* because sufficient energy is supplied to drive the electrochemical processes and thereby facilitate detachment of oxygen and hydrogen gas-bubbles from the surface of the SS mesh. In other words, at low to medium

electrical power of operation, the cell performance is dominated by activation and Ohmic resistances respectively. The Nyquist impedance for *HER* shows double capacitive arcs at relatively low potentials. The smaller capacitive arc can be attributed to adsorbed hydrogen gas-bubbles on the SS mesh [66]. At higher cathodic potentials however, there is a single capacitive arc because the reaction rate is increased and the hydrogen gas-bubbles migrate faster. In general, as the potential is increased the capacitance as well as the electrochemical active area is increased [66].

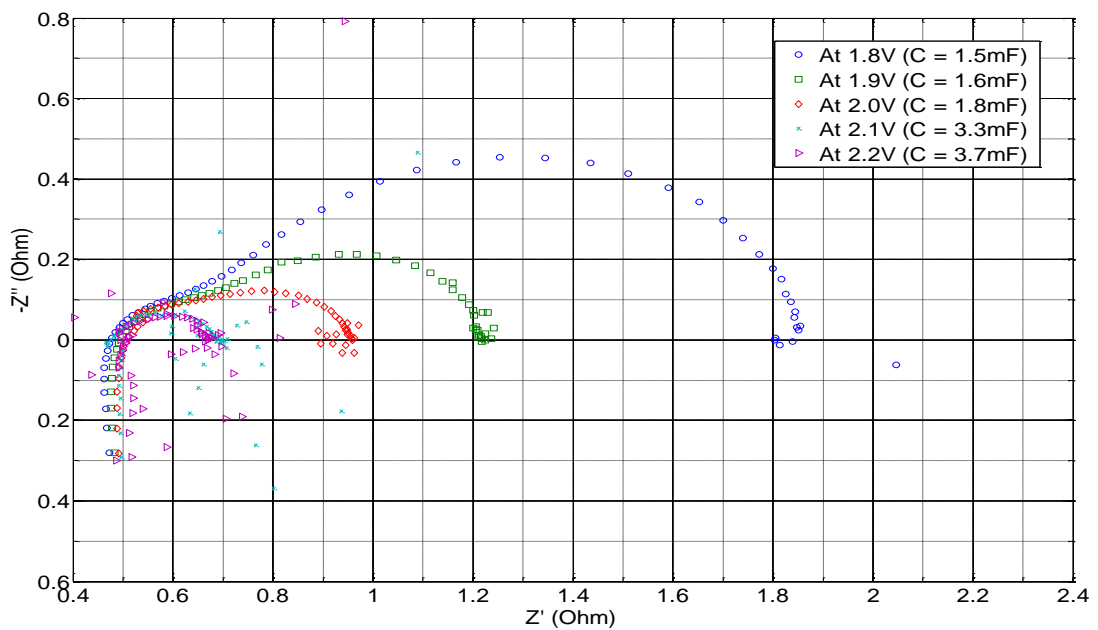


Figure 4-4 Nyquist impedance for *OER* on SS mesh

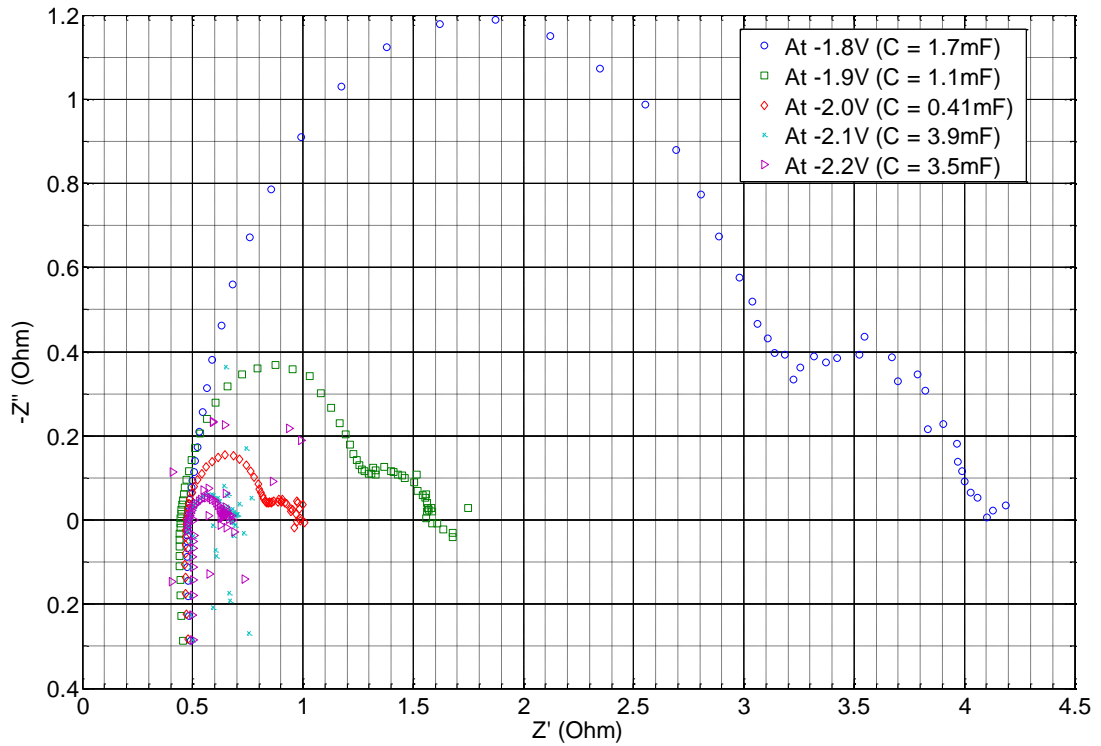


Figure 4-5 Nyquist impedance for *HER* on SS mesh.

Figure 4-6 shows DC polarisation on the two common commercial types of SS mesh (types 304 and 316). The kinetic efficiency is slightly increased on SS mesh-304 at higher current density and the Tafel relation also indicates better kinetic property of this type of electrode. The corresponding impedance is shown in Figure 4-7 which indicates reduction of Ohmic resistance on the SS mesh-304.

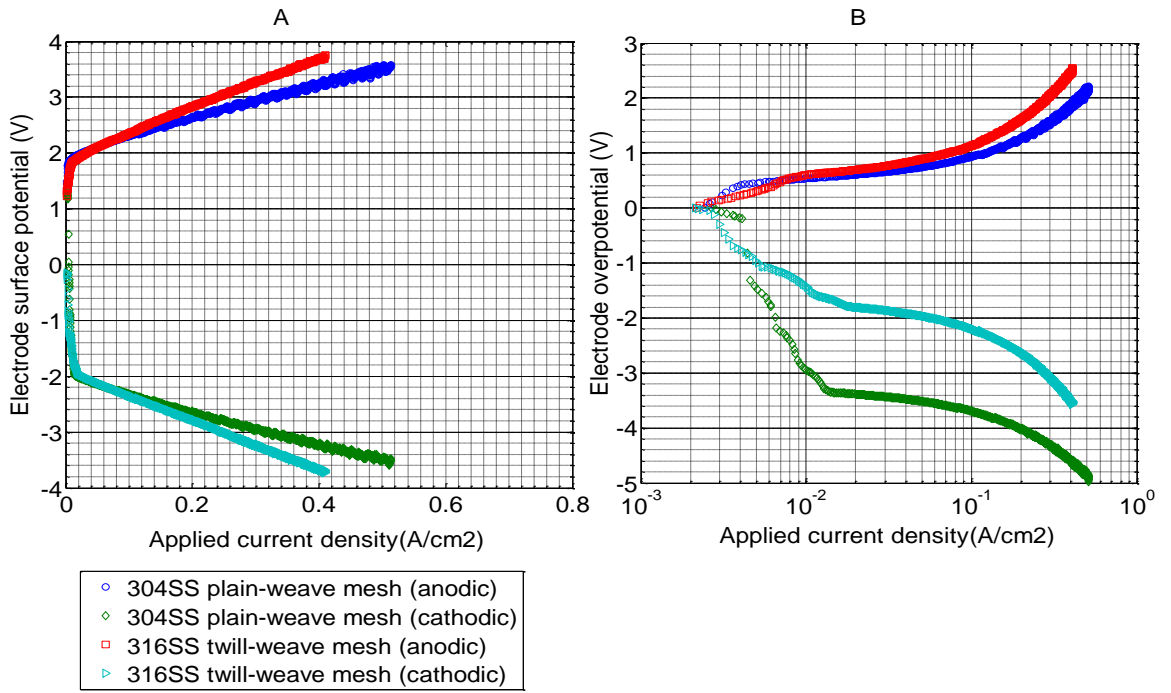


Figure 4-6 Comparison of kinetic efficiency of SS mesh (types 304 and 316) in 30% KOH at 23°C: A. DC polarisation, B. Tafel relation

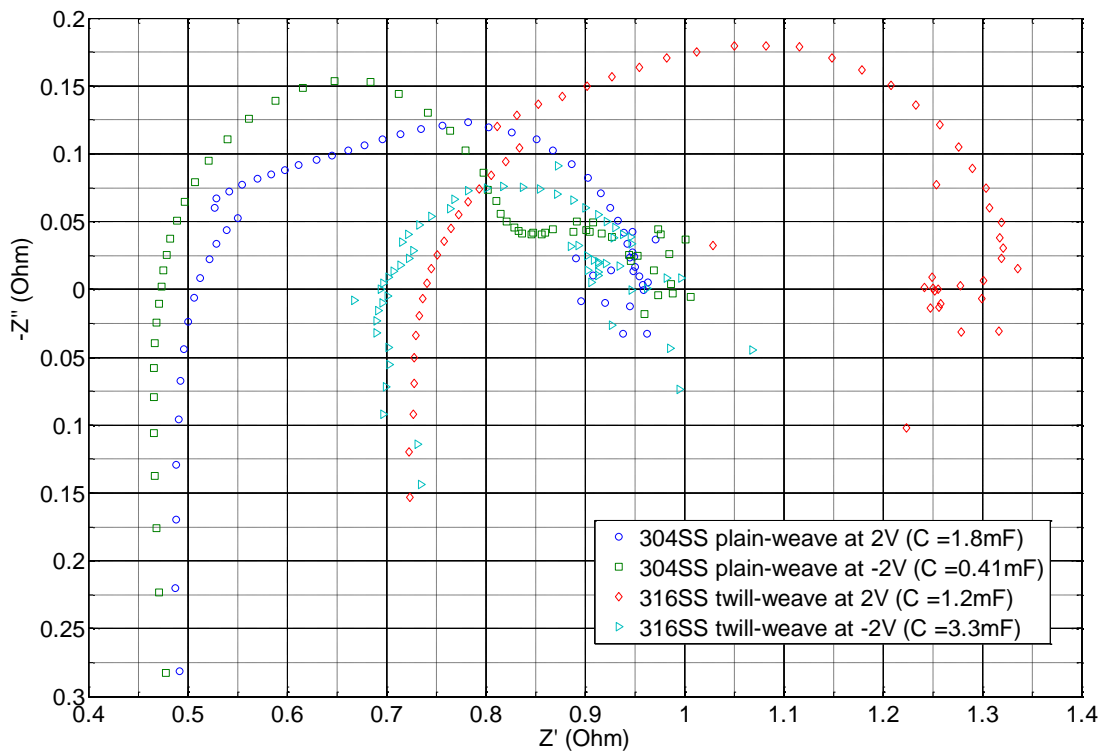


Figure 4-7 Comparison of Nyquist impedance on SS mesh (types 304 and 316)

The Ohmic resistance is increased on SS mesh-316. This was not expected considering that in Table 4-1 SS-mesh 316 has a higher geometric area and lower electrical resistance compared with SS mesh-304. However, the SS mesh-316 readily passivates which increases the resistance. Ordinarily the chromium component (see section 4.1) prevents passivation of iron component in steel, but the SS mesh-316 was highly passivated which could be due to impurities or passive oxide films on its surface.

It is apparent that the SS mesh type-304 has better kinetic efficiency under variable electrical power input compared with SS mesh type-316 and SS smooth sheet type-304. This could be attributed to the higher electrochemical surface area of the electrode, and favourable micro-structure that facilitates gas-bubble migration thereby preventing gas-bubble coverage on the electrode. Nevertheless, it was necessary to carry-out pre-treatment of the electrodes in order to reduce passivation and increase the electrochemical active area. This was carried-out by etching the electrodes followed by characterisation as described in the following section 4.3.2.

4.3.2 Etching of the Electrode and Kinetic Efficiency under Variable Electrical Power of Operation

The SS electrodes were immersed in 95 % sulphuric acid for 24 hours and the cathodic current density of 5 mA/cm^2 was applied for 5 minutes at 23°C . As shown in Figure 4-8, the kinetic efficiency is slightly increased on the etched-SS mesh (type 304) at high current density compared with ordinary SS mesh (type 304).

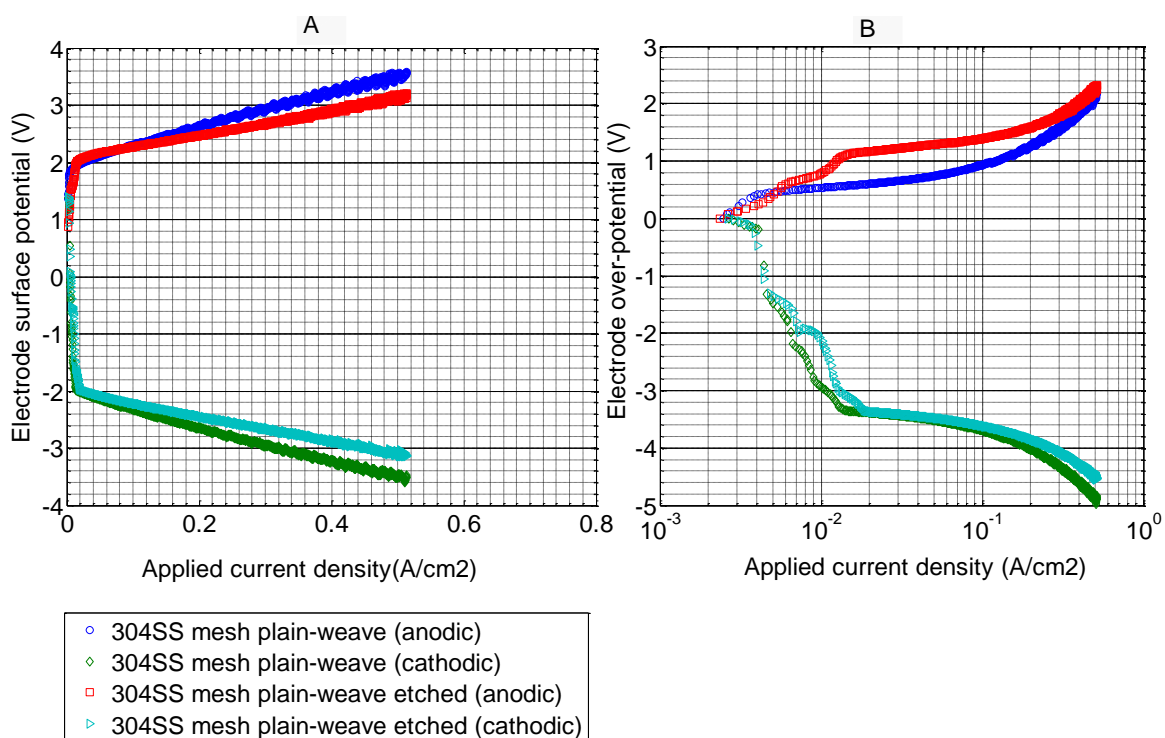


Figure 4-8 Comparison of kinetic efficiency of etched-SS mesh (type 304) and ordinary SS mesh (type 304) in 30 % KOH at 23 °C: (A). DC polarisation, (B). Tafel relation

The corresponding impedance is shown in Figure 4-9 which indicates that Ohmic resistance is reduced and capacitance is slightly increased on etched-SS mesh (type 304).

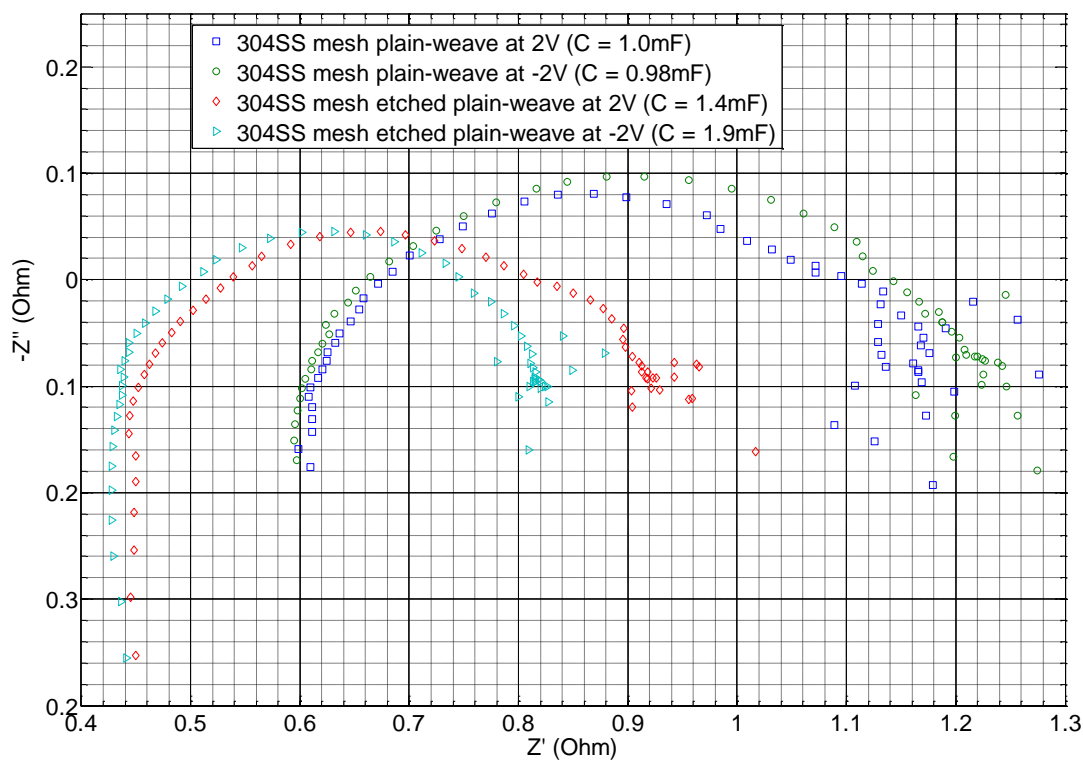


Figure 4-9 Comparison of Nyquist impedance on etched SS mesh (type 304) and ordinary SS mesh (type 304)

Etching the electrode is a form of chemical roughening of the electrode in order to increase the active sites or electrochemical surface area. Acidic treatment of the electrode is a pre-treatment method that is commonly adopted [66, 68,120,122,123,133] to roughen the surface prior to electrodeposition, and thereby increase electrochemical active sites. This facilitates the charge transfer process. Thus, the polarisation resistance is reduced by increasing surface roughness of the electrode.

As shown in Figure 4-10, kinetic efficiency is slightly improved due to etching of SS mesh (type 316). In particular, kinetic efficiency is enhanced for hydrogen production on etched-SS mesh (type 316).

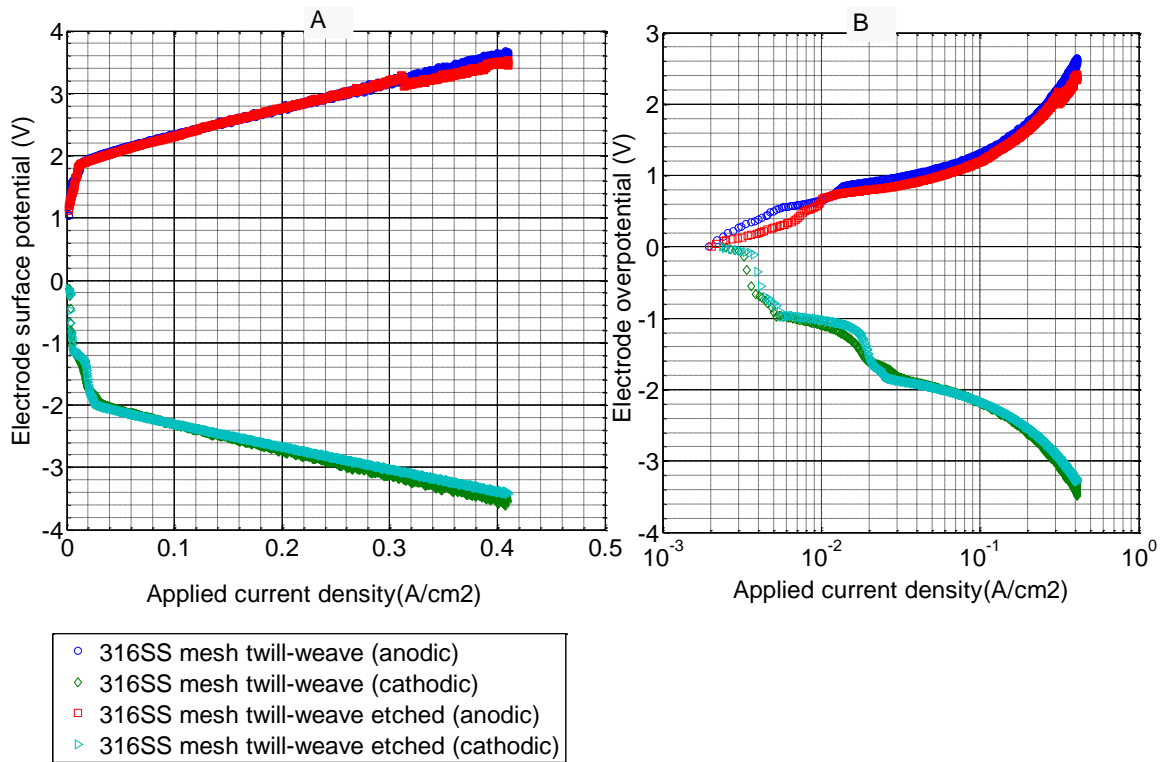


Figure 4-10 Comparison of kinetic efficiency of etched SS mesh-type 316 and ordinary SS mesh-type 316 in 30% KOH at 23°C: A. DC polarisation, B. Tafel relation

The corresponding Nyquist impedance is shown in Figure 4-11, which indicates that the improvement in kinetic efficiency is due to a reduction in Ohmic and polarisation resistances by about 8 % and 50 % respectively.

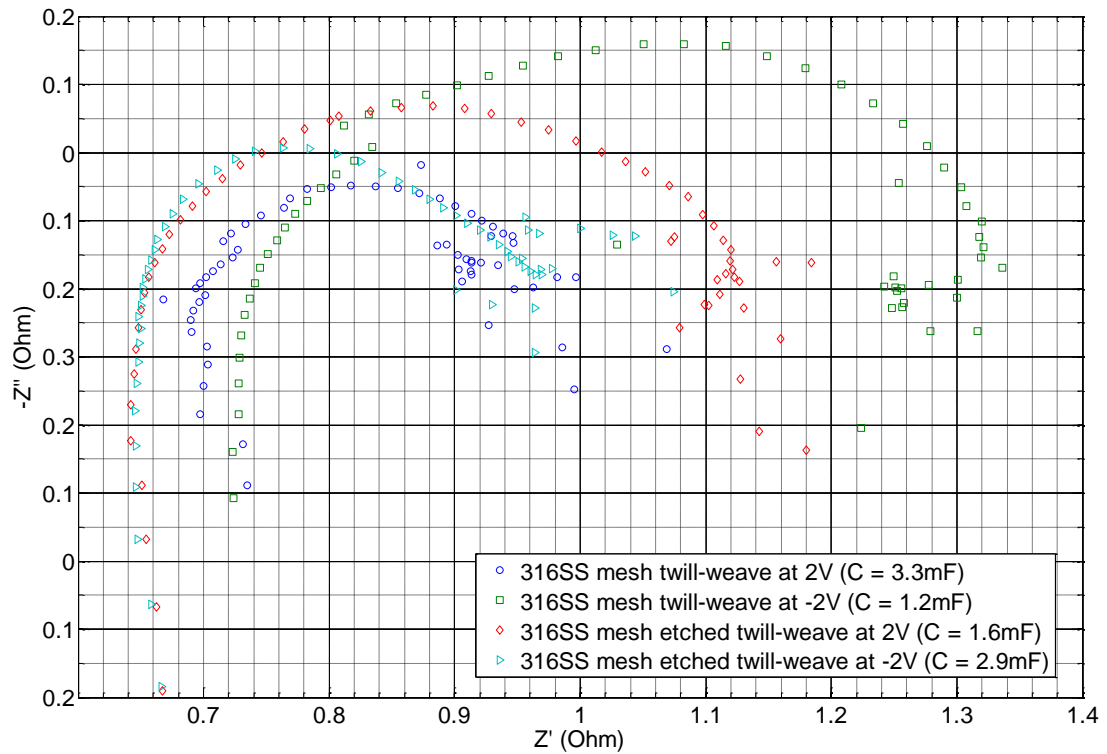


Figure 4-11 Comparison of Nyquist impedance on etched SS mesh-type 316 and ordinary SS mesh-type 316

The Ohmic resistance is reduced for oxygen and hydrogen production on etched-SS mesh (type 316), and this could be attributed to an increase in the electrochemical active area. The polarisation resistance is reduced as the electrode surface is modified to increase active sites.

Similar investigations were made on etched-SS sheet electrodes. As shown in Figure 4-12, the kinetic efficiency is slightly improved for anodic and cathodic processes on etched-SS sheet.

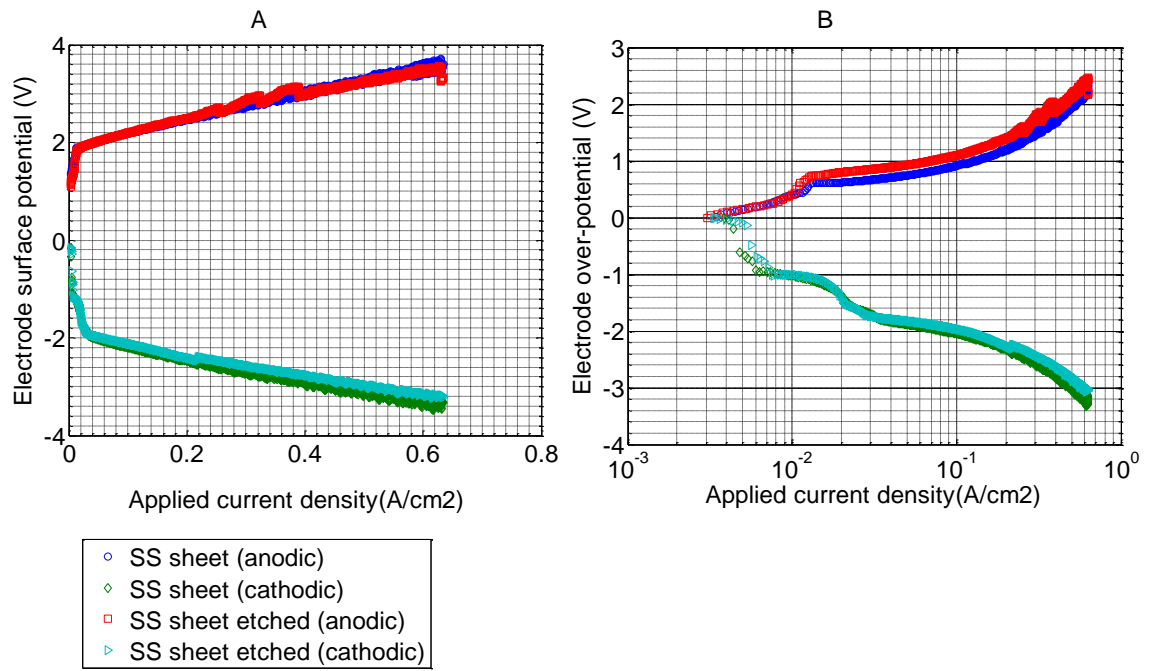


Figure 4-12 Comparison of kinetic efficiency of etched SS sheet and ordinary SS sheet in 30 % KOH at 23 °C: A. DC polarisation, B. Tafel relation

The corresponding Nyquist impedance is shown in Figure 4-13 which indicates that the improvement in kinetic efficiency is mainly due to reduction in polarisation resistance by about 37 % and 9 % for the anodic and cathodic processes respectively.

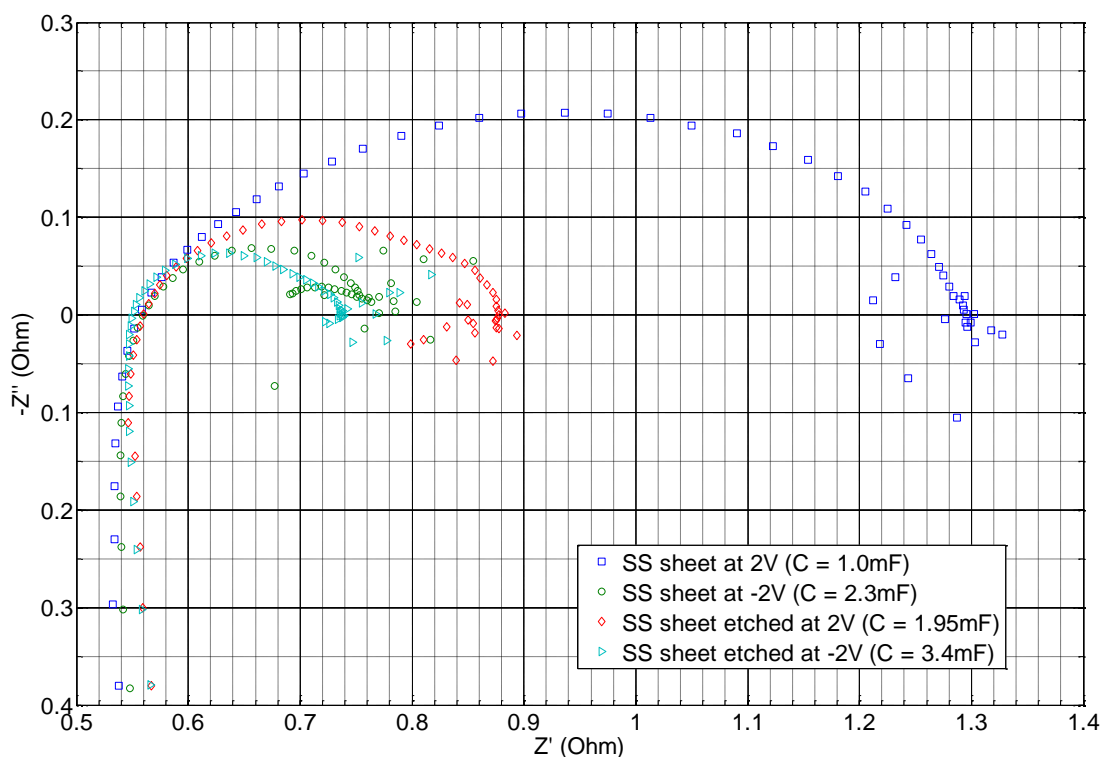


Figure 4-13 Comparison of Nyquist impedance on etched SS sheet and ordinary SS sheet

At the start of electrolysis, polarisation resistance was significantly high on ordinary SS sheet that is passivated and non-activated. In contrast, the polarisation resistance is significantly reduced on etched SS sheet due to increased surface roughness. The electrode surface structure determines the electrode active area which plays a more important role in influencing its activity. This is also evident as shown in Figure 4-1 (A) which compares between the SS smooth sheet (type 304) and SS mesh (type 304) whereby the activity is increased on the latter for both hydrogen and oxygen production due to its higher surface roughness and porosity.

4.3.3 Stability under Intermittent Electrical Power of Operation

The open-circuit time stability of the electrodes was investigated by on/off switching of the electrolyser at a constant current load of 200 mA/cm² for 15 minutes; the power was switched off for about 30 minutes, and supplied again for 15 minutes. This was repeated for up to 5 cycles. As shown in Figure 4-14, for SS sheet and SS mesh the over-voltages are unchanged after open-circuit thereby indicating that the electrodes are essentially stable under intermittent electrical power of operation.

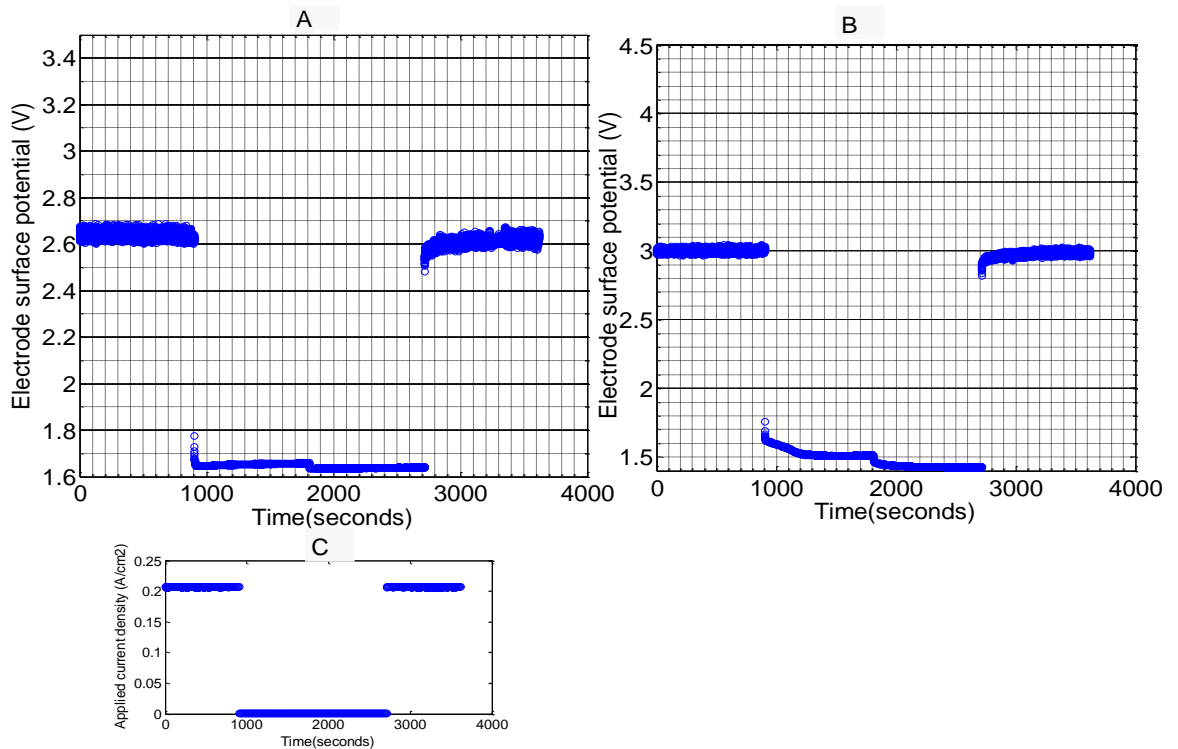


Figure 4-14 Comparison of open-circuit test on the electrodes in 30% KOH at 23°C; A. SS mesh, B. SS sheet, C. applied current load

The over-voltage, however, is 0.4 V lower on SS mesh compared with SS sheet. SS sheet has higher overvoltage possibly due to the passive oxide film that forms on its smooth surface during electrolysis and consequently increases the reaction or polarisation resistance. It should be noted, however, that this test shows that the electrodes in the alkaline electrolyser have considerable OCV which indicates that considerable energy (free energy) is stored in the cell under open-circuit.

The open-circuit stability test indicates that the electrodes are stable over a relatively short period of time under intermittent electrical power input that is characteristic of a wind turbine operation. Further tests on the electrodes over relatively longer periods are necessary in order to investigate the degradation effects due to reversible reactions as well as reaction products on the electrode surface. Nonetheless, this test indicates that considerable internal energy is present in the alkaline electrolyser under open-circuit. The OCV indicates the potential of this cell for reversible fuel cell operations which will be further investigated as part of future work by the author of this thesis.

4.3.4 Stability under Constant Electrical Power of Operation

Continuous electrolysis was carried out on SS mesh at about 206 mA/cm^2 for 4 hours, thereafter the power was switched off for about 1 hour and repeated at the same current load for 3 hours. As shown in Figure 4-15, the blue data points were obtained from the first experiment and the red data points were obtained from the second experiment.

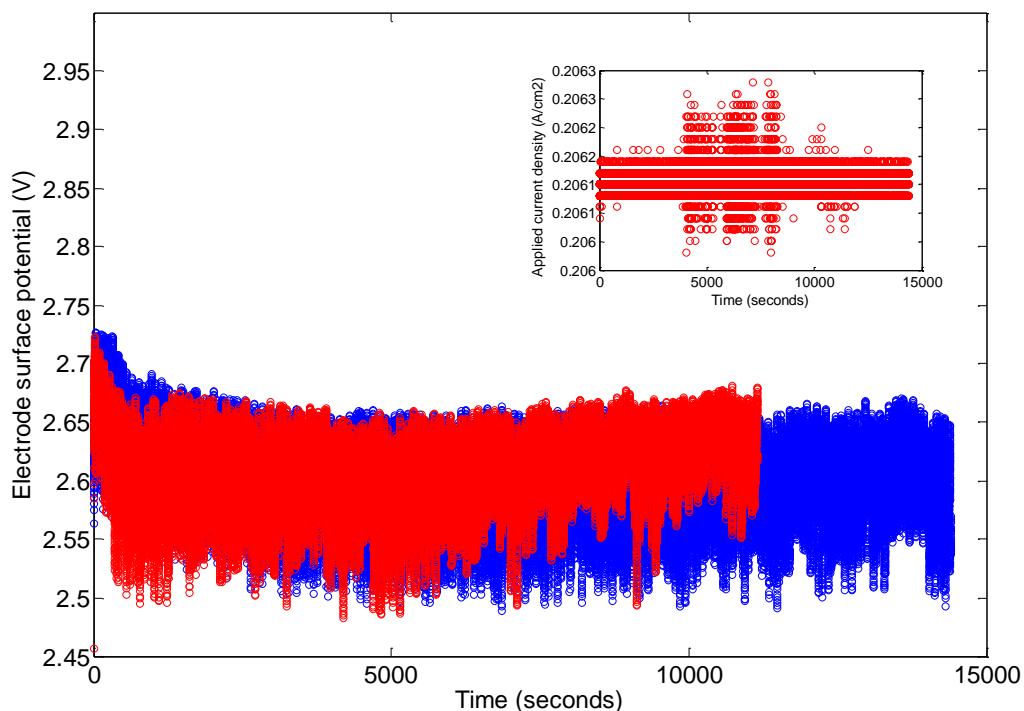


Figure 4-15 Continuous electrolysis at 206 mA/cm^2 on the SS mesh in 30 % KOH at $23 \text{ }^\circ\text{C}$; inset shows applied current load

It can be seen that activity of SS mesh is stable for up to 4 hours under continuous electrolysis. The average electrode potential was 2.6 V, although the current and voltage have fluctuated very rapidly which is due to energy that is exerted on the electrode surface by the movement of gas-bubbles. This fluctuation in current and voltage is particularly observed in the ‘zero-gap’ cell configuration due to gas-bubbles imparting energy on the electrode surface.

The polarisation of SS mesh was measured before and after the period of continuous electrolysis. As shown in Figure 4-16, the electrode over-voltage has increased

significantly after the period of continuous electrolysis. This could be attributed to an increase in Ohmic resistance that is caused by gas-bubble coverage on the electrode surface and gas-bubbles dissolving into the electrolyte.

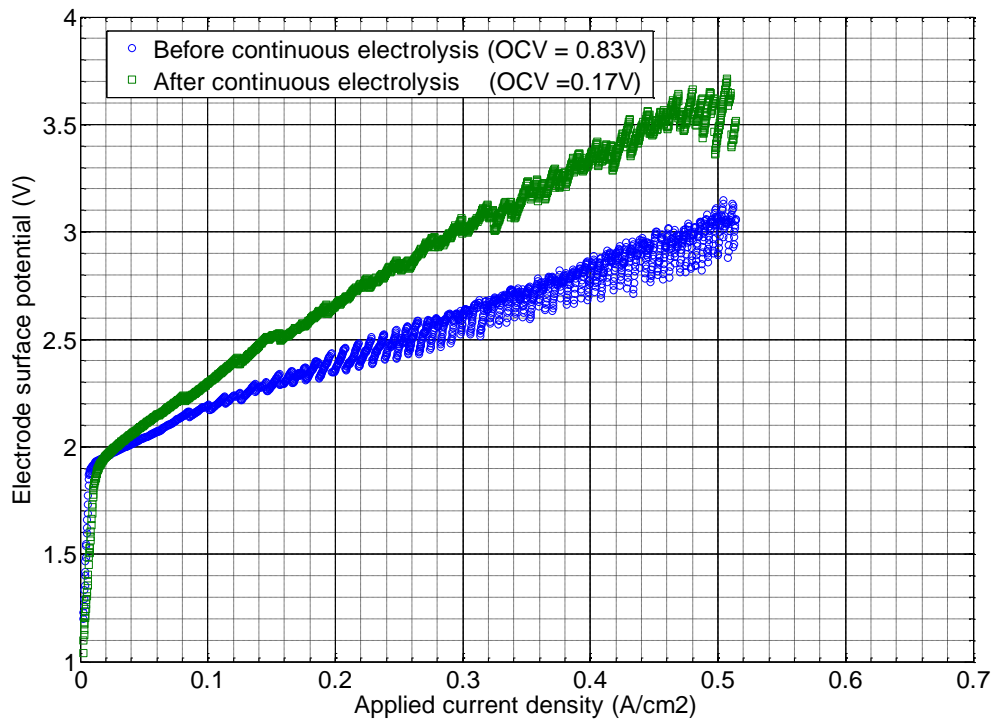


Figure 4-16 Comparison of polarisation on SS mesh before and after continuous electrolysis in 30% KOH at 23°C.

The corresponding Nyquist impedance is shown in Figure 4-17 which indicates that Ohmic resistance has increased by 0.4 Ohm and double-layer capacitance has also increased by 1.2 mF after the period of continuous electrolysis.

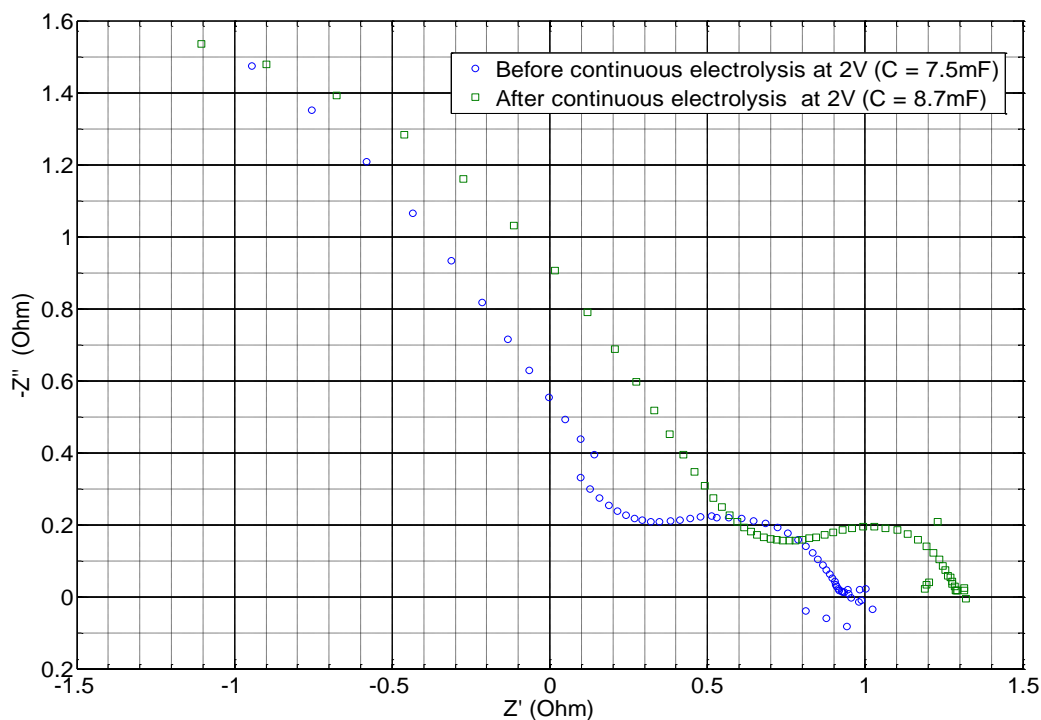


Figure 4-17 Comparison of Nyquist impedance on SS mesh before and after continuous electrolysis.

The electrode surface becomes covered in evolved gas bubbles after some time of electrolysis, which result in passivation and consequently an increase in transport or Ohmic resistance. However, the reaction resistance is almost unchanged thereby indicating that activity of SS mesh is stable under continuous electrolysis. During continuous electrolysis the porous surface structure of SS mesh facilitates gas-bubble detachment and prevents further passivation as indicated by an increase in the capacitance as well as electrochemical surface area.

Continuous electrolysis was carried-out on the SS sheet and as shown in Figure 4-18 a constant current load of about 190 mA/cm^2 was supplied for 4 hours, the power was switched off for about 1 hour and repeated for about 4 hours. The blue data points were obtained from the first experiment and the red data points were obtained from the second experiment.

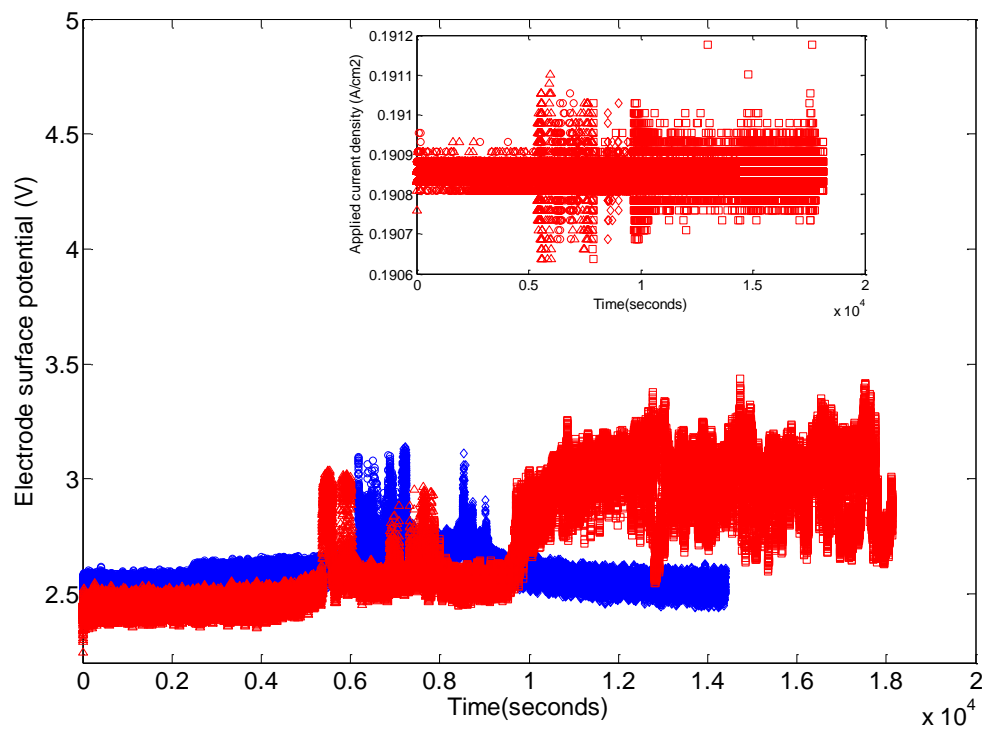


Figure 4-18 Continuous electrolysis at 190 mA/cm² on SS sheet in 30 % KOH at 23 °C; inset shows applied current load

The current and voltage have fluctuated very rapidly due to the impact of generated gas-bubbles on the electrode surface in the ‘zero-gap’ (1mm separation distance) cell configuration. The over-voltage has only slightly reduced after about 33 minutes because the SS sheet becomes activated after some time of electrolysis. However, the over-voltage is suddenly increased by about 0.3V after about 6 hours of continuous electrolysis due to the formation of a passive oxide layer which reduces the apparent active area of SS sheet and consequently increases the transport resistance.

Monitoring of polarisation behaviour of SS sheet was carried-out over the period of continuous electrolysis. As shown in Figure 4-19, the overvoltage is reduced after the first 4 hours of electrolysis as the SS sheet becomes activated. However, the over-voltage is increased after 8 hours of electrolysis due to passivation on the SS sheet and consequent increases in the reaction and Ohmic resistances. It should be noted from Figure 4-19 that at relatively high current densities, the gas bubbles exert more energy on the electrodes in the ‘zero-gap’ cell configuration. This has resulted in massive variability of the polarisation at relatively higher current densities.

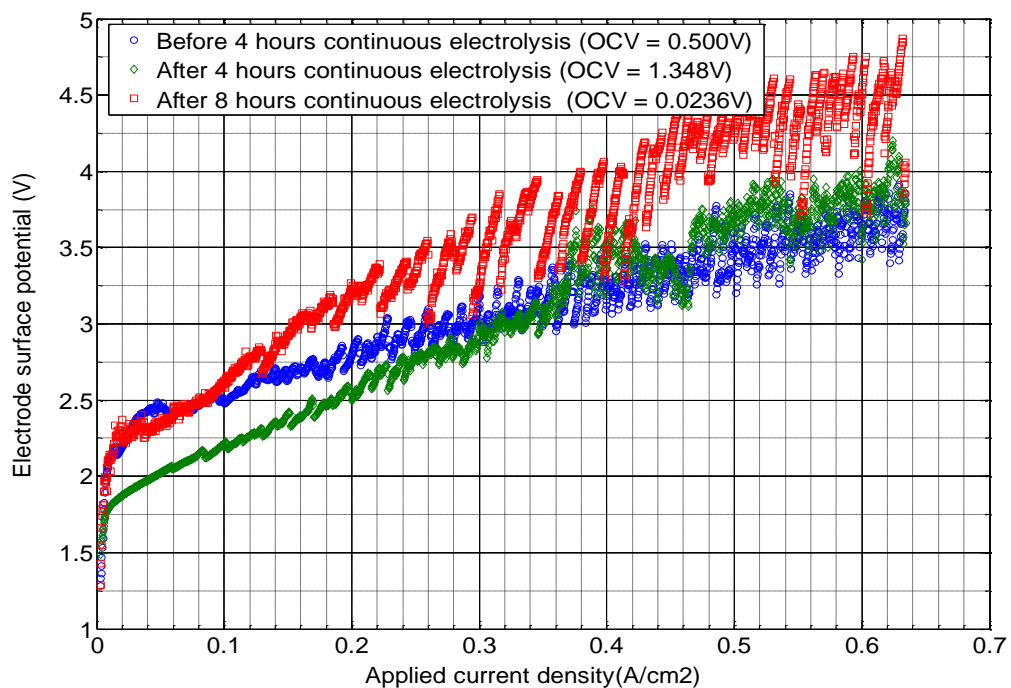


Figure 4-19 Comparison of polarisation on the SS sheet before and after continuous electrolysis in 30% KOH at 23°C

The corresponding impedance is shown in Figure 4-20 which indicates an increase in the Ohmic and reaction resistances by about 0.3Ω and 0.1Ω respectively after 8 hours of continuous electrolysis. This indicates that SS sheet exhibits poor time stability under continuous electrolysis. The 45° impedance line that is observed before electrolysis could be attributed to diffusion-limited processes due to gas-bubble evolution and migration on the electrode surface. The apparent semi-circle that is observed after electrolysis indicates that although sufficient energy has been supplied to facilitate gas-bubble migration, the Ohmic and reaction resistances are increased due to passivation on the surface of SS sheet.

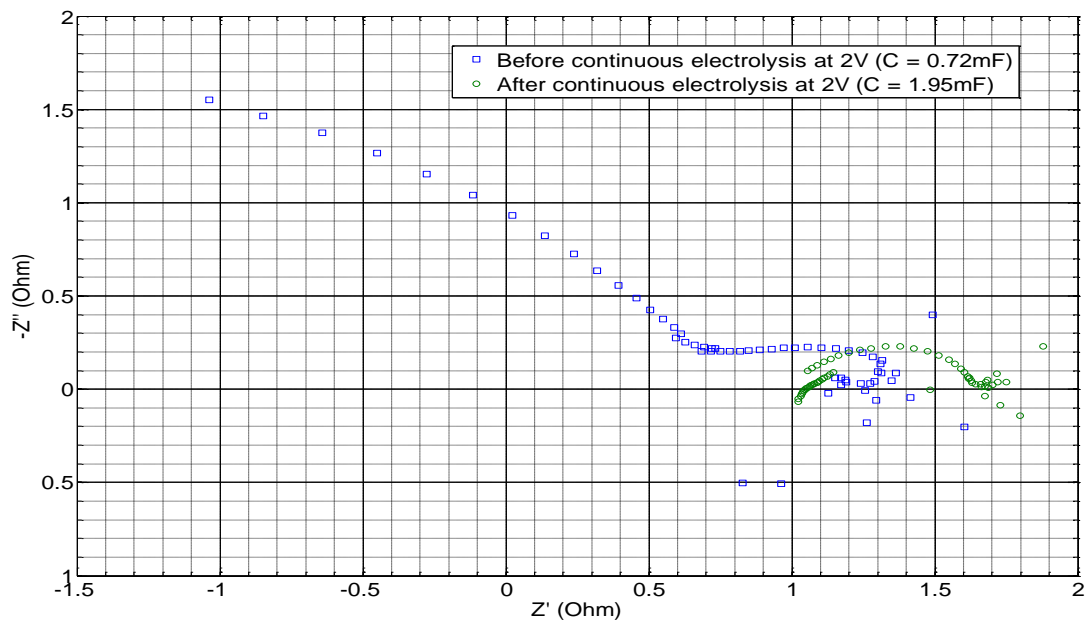


Figure 4-20 Comparison of Nyquist impedance on the SS sheet before and after continuous electrolysis.

A comparison of the SS mesh and SS sheet electrodes indicate that the former is more stable and active than the latter over relatively longer period of operation in the alkaline electrolyser. This is mainly attributed to the increased electrode active area and surface structure. The SS mesh has a relatively higher surface area which reduces the overvoltage, and its porous surface structure facilitates gas bubble removal thereby minimising passivation during electrolysis.

4.3.4.1 OER and HER Production Rates on the Electrode

As shown in Figure 4-21, the activity of SS mesh increases with time under OER for up to 4 hours of continuous electrolysis. At the electrode potential of ~ 2 V the average electrode current density was about 0.07 A/cm^2 which accounts for about 0.16 g of oxygen production and electrical power consumption of about 0.54 W .

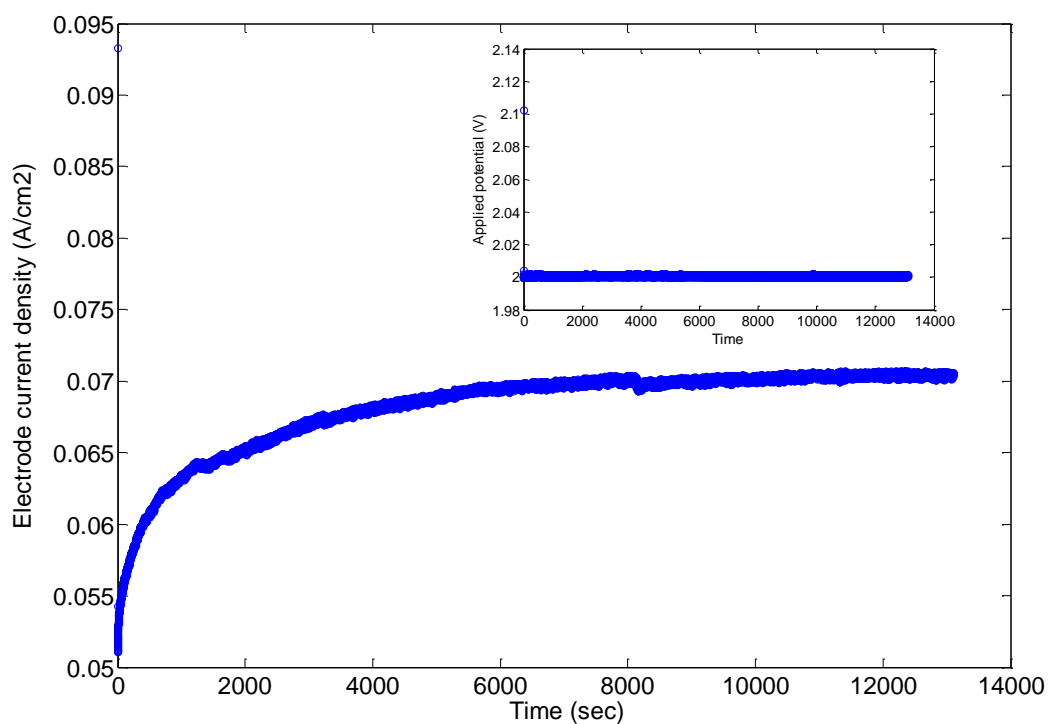


Figure 4-21 OER at 2 V for 4 hours on SS mesh in 30 % KOH at 23 °C; inset shows applied voltage

The reaction and Ohmic resistances on SS mesh were investigated over longer period of electrolysis for up to 12 hours. As shown in Figure 4-22, the reaction and Ohmic resistances are increased by about 0.3Ω and 1.2Ω respectively after this period of continuous electrolysis. This could be attributed to passivation of SS mesh after the relatively longer period of continuous electrolysis.

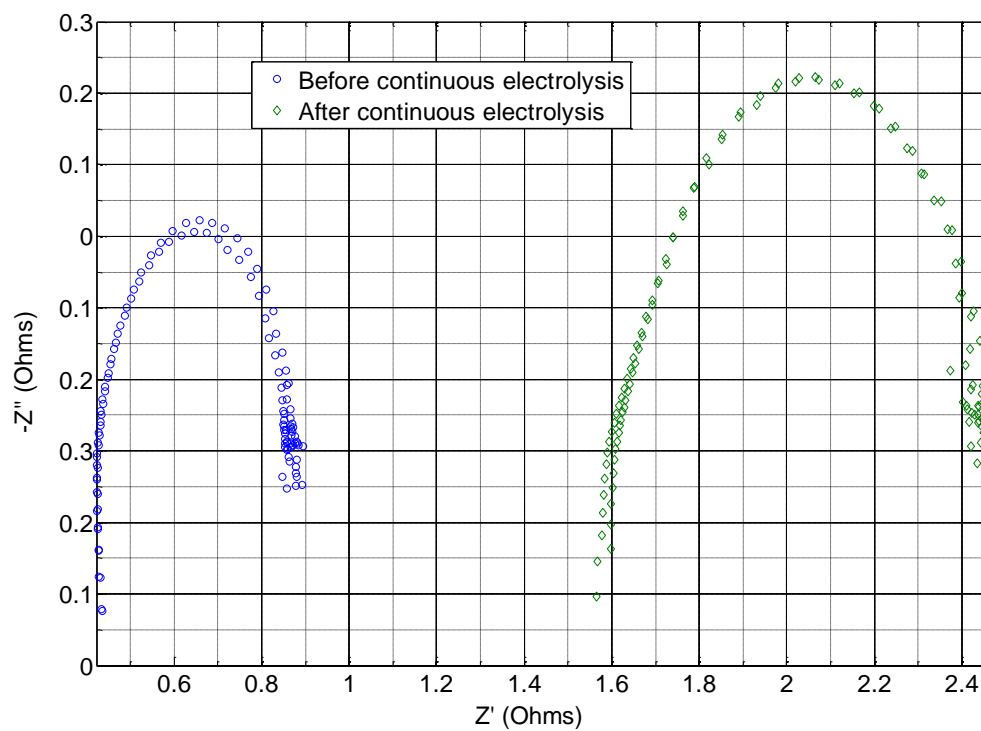


Figure 4-22 Nyquist impedance before and after *OER* at 2 V for 12 hours on SS mesh

The *OER* was investigated on SS mesh for 2 hours of continuous electrolysis. As shown in Figure 4-23, the electrode current density has risen steadily to around 0.061 A/cm^2 at $\sim 2 \text{ V}$.

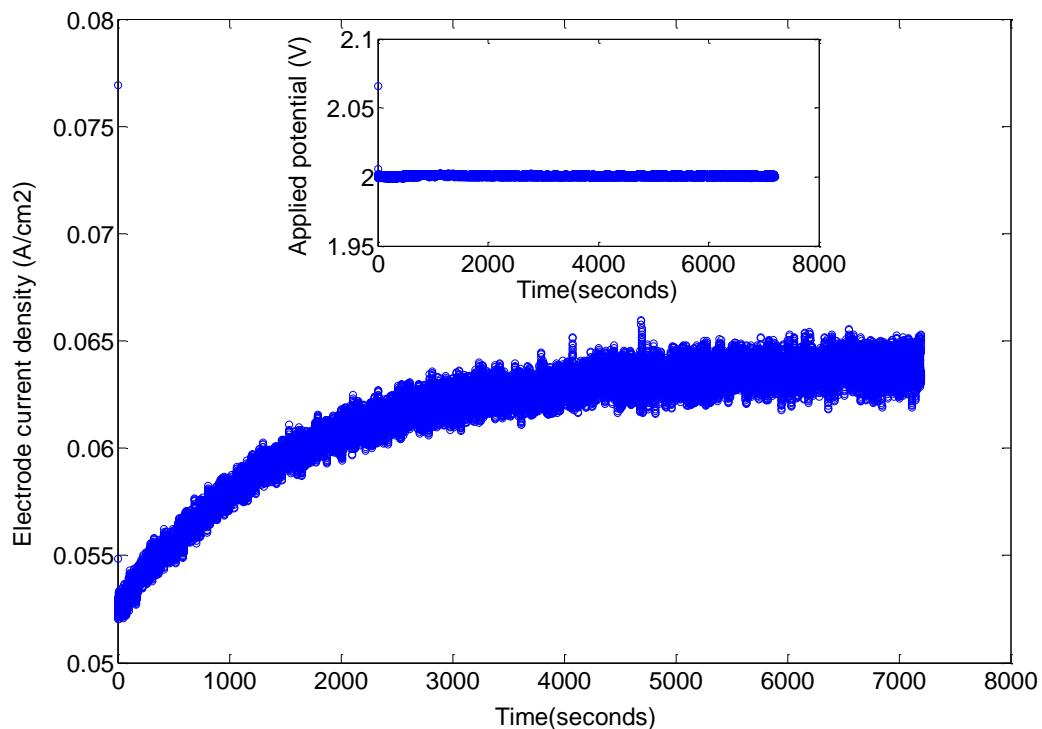


Figure 4-23 *OER* at 2 V for 2 hours on SS mesh in 30 % KOH at 23 °C; inset shows applied voltage

The corresponding impedance in Figure 4-24 indicates no significant change in the reaction resistance after *OER*; however Ohmic resistance is slightly increased by about 0.08 Ω after *OER*. This could be attributed to dissolved oxygen gas-bubbles in the electrolyte solution. The double-layer capacitance is slightly increased after some time of electrolysis due to activation of the electrode, which for a non-passivating surface indicates an increase in electrochemical surface area.

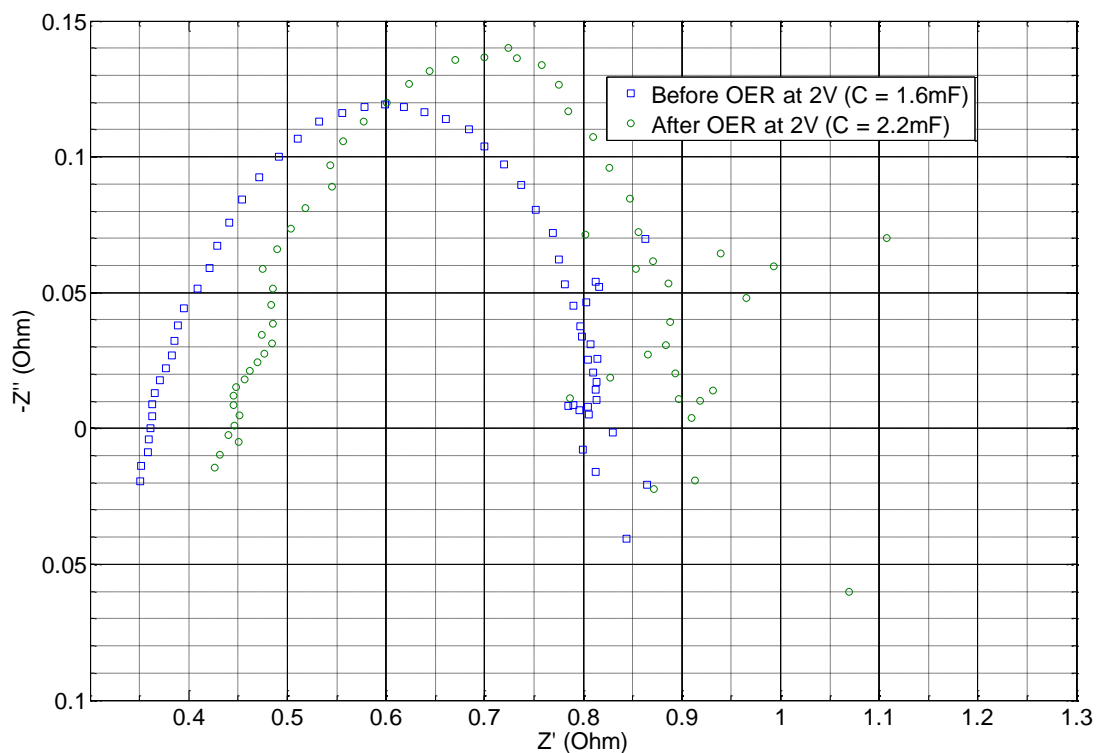


Figure 4-24 Nyquist impedance before and after *OER* at 2 V for 2 hours on SS mesh

The average electrode current density for the *HER* on SS mesh was $\sim 0.051 \text{ A/cm}^2$ at $\sim 2 \text{ V}$ as shown in Figure 4-25. The current has fluctuated very rapidly due to energy that is exerted on the electrode surface by the evolved gas-bubbles.

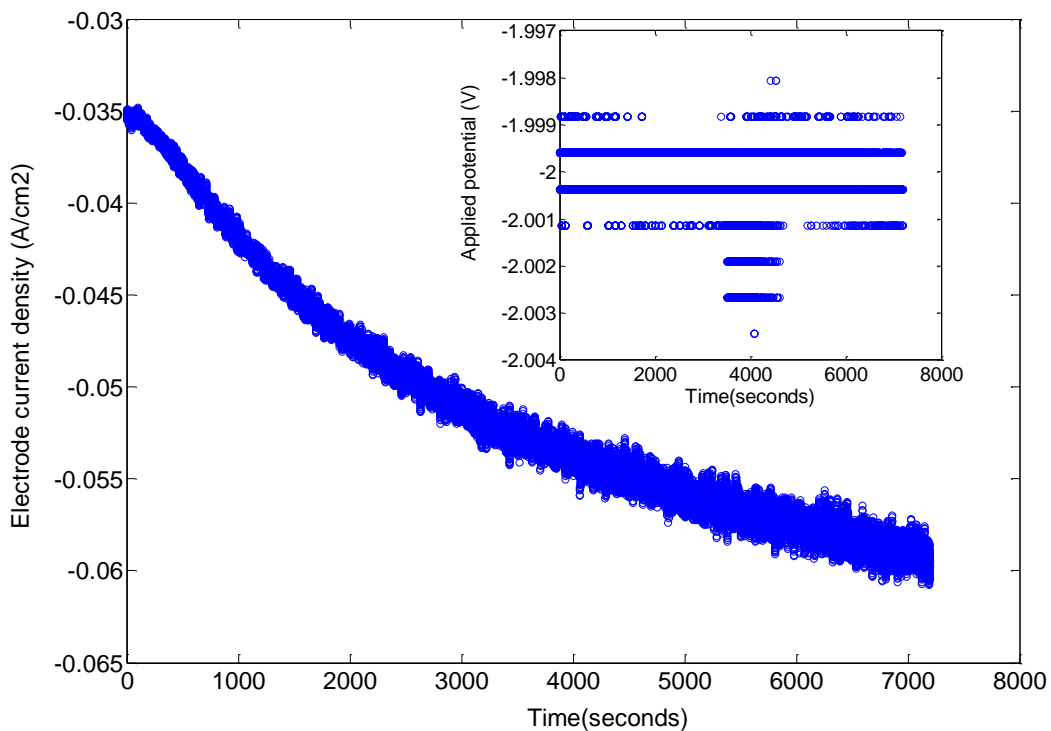


Figure 4-25 *HER* at -2 V for 2 hours on SS mesh in 30 % KOH at 23 °C; inset shows applied voltage

The corresponding Nyquist impedance is shown in Figure 4-26 which indicates reduction in the polarisation resistance after *HER*. Considering Figures 4-21 to 4-24, it is evident that the reaction resistance is slightly reduced by changing polarity of the electrode from *OER* (anodic) to *HER* (cathodic) because this leads to a reduction reaction that removes oxide passivation products from the electrode surface [131-132]. In other words, it is evident that RPC [72] (refer to section 2.3.1) leads to a reduction in overvoltages that is caused by reaction products on the electrode surface.

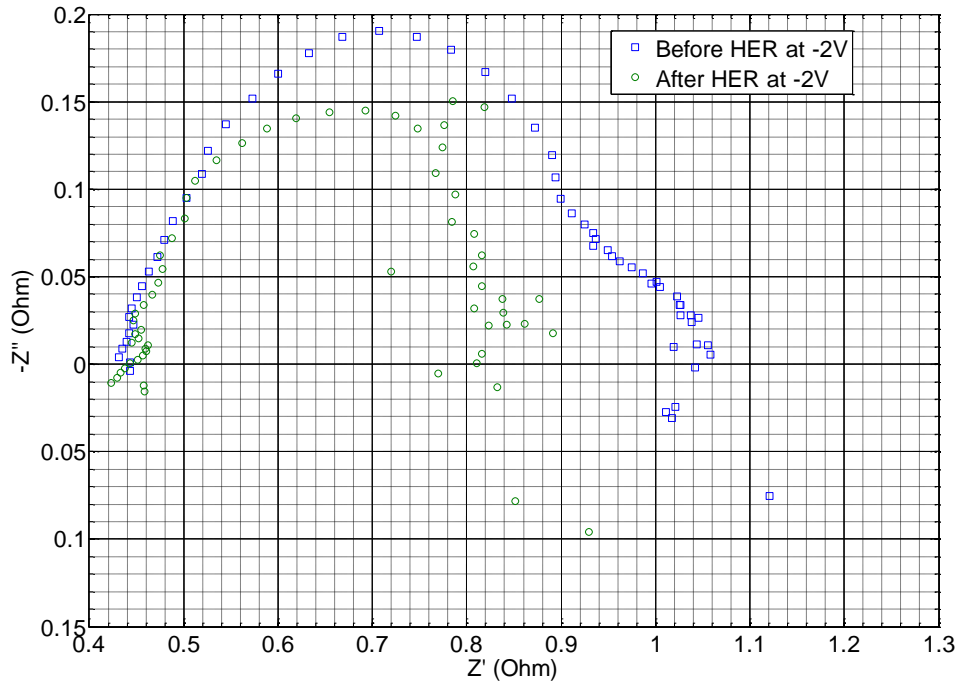


Figure 4-26 Nyquist impedance before and after *HER* at -2 V for 2 hours on SS mesh

Similarly, the *OER* on SS sheet is shown in Figure 4-27 which indicates electrode current density rising up to $\sim 0.03 \text{ A/cm}^2$ at $\sim 2 \text{ V}$.

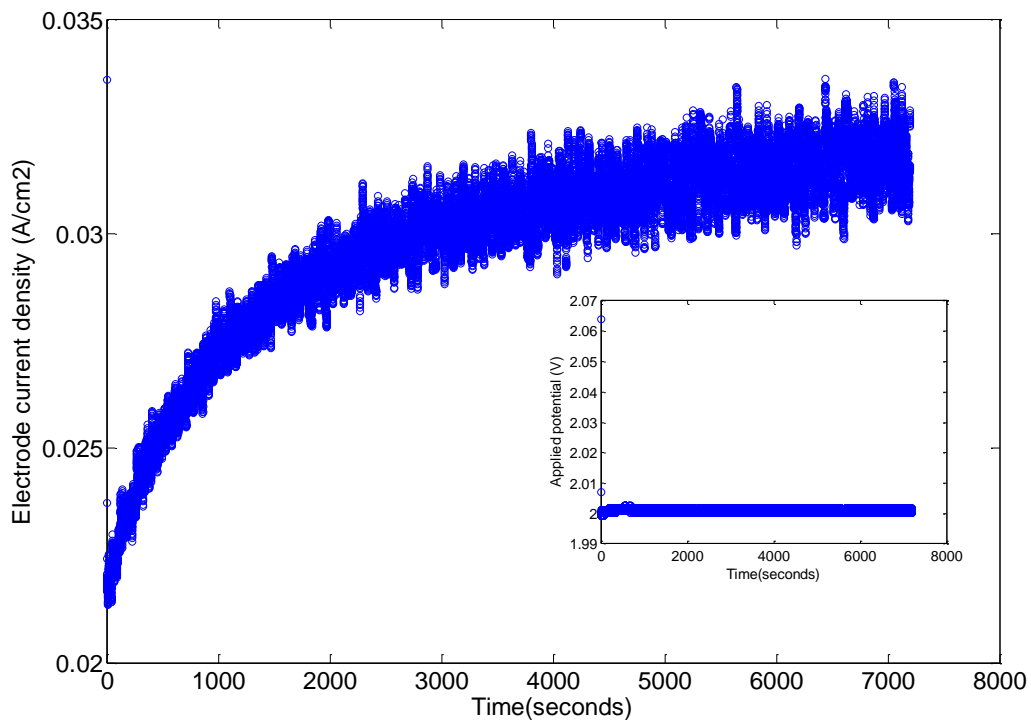


Figure 4-27 *OER* at 2 V for 2 hours on SS sheet in 30 % KOH at 23 °C; inset shows applied voltage

The corresponding impedance is shown in Figure 4-28 which indicates a slight decrease in the reaction resistance and slight increase in the double-layer capacitance after *OER*. The reaction resistance is decreased on SS sheet after some time of electrolysis due to activation of the electrode as also observed in Figure 4-18. As the SS sheet becomes activated, the electrochemical active area is increased which is indicated by an increase in the double-layer capacitance.

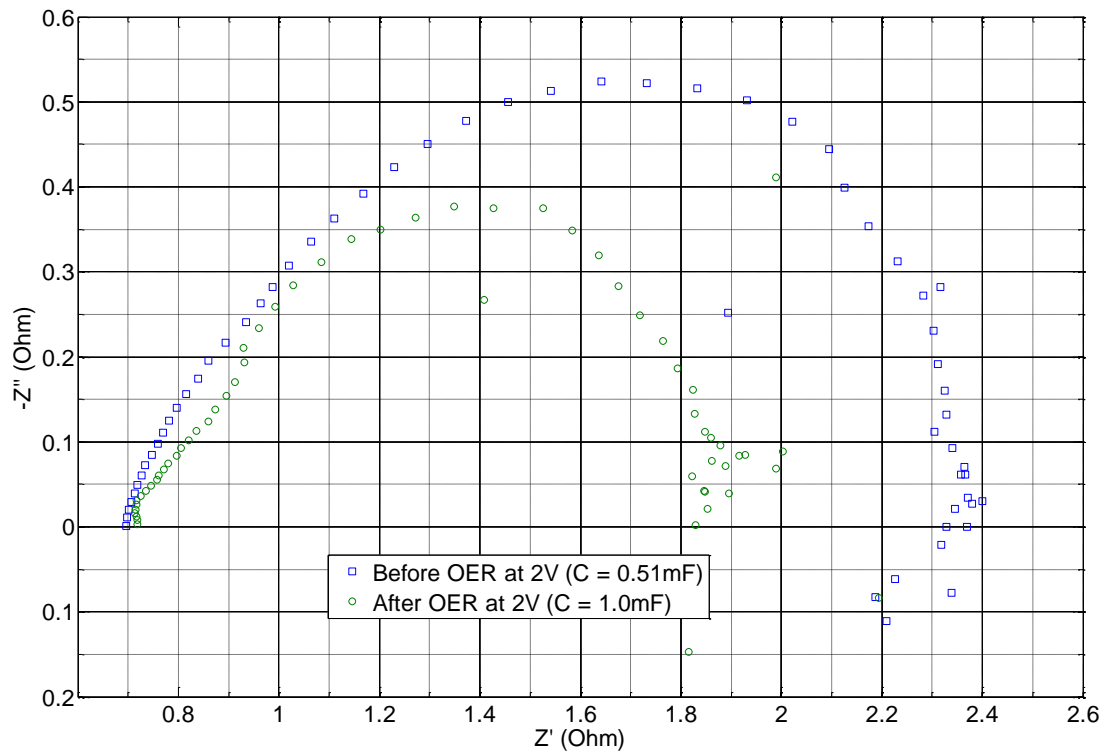


Figure 4-28 Nyquist impedance before and after *OER* at 2 V for 2 hours on SS sheet

As shown in Figure 4-29 the average current density was about 0.0257 A/cm^2 for the *HER* on SS sheet at $\sim 2 \text{ V}$.

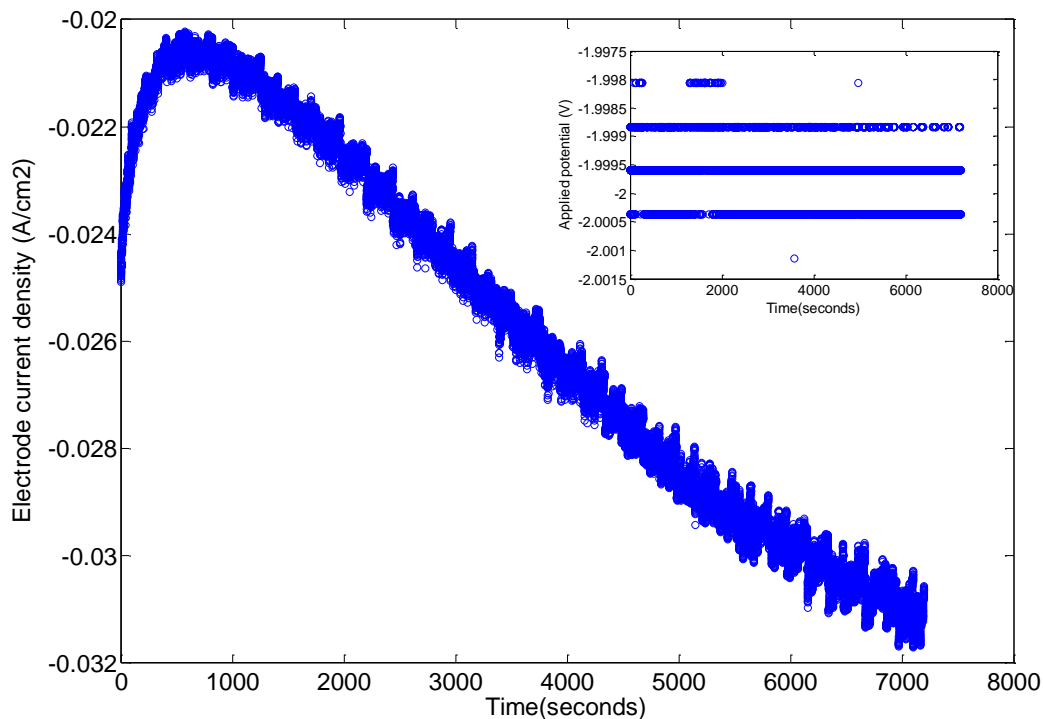


Figure 4-29 *HER* at -2V for 2 hours on SS sheet in 30% KOH at 23°C ; Inset shows applied voltage

The corresponding Nyquist impedance is shown in Figure 4-30 and indicates double capacitive arcs before *HER* due to passivation on the electrode surface. The reaction resistance is almost unchanged after *HER* thereby suggesting permanent passivation of SS sheet by the reaction products. As the SS sheet is non-porous, hydrogen gas bubbles could not penetrate through its surface to effectively neutralise the oxide products that were formed during *OER*. The double-layer capacitance is slightly increased due to activation of SS sheet after some time of electrolysis.

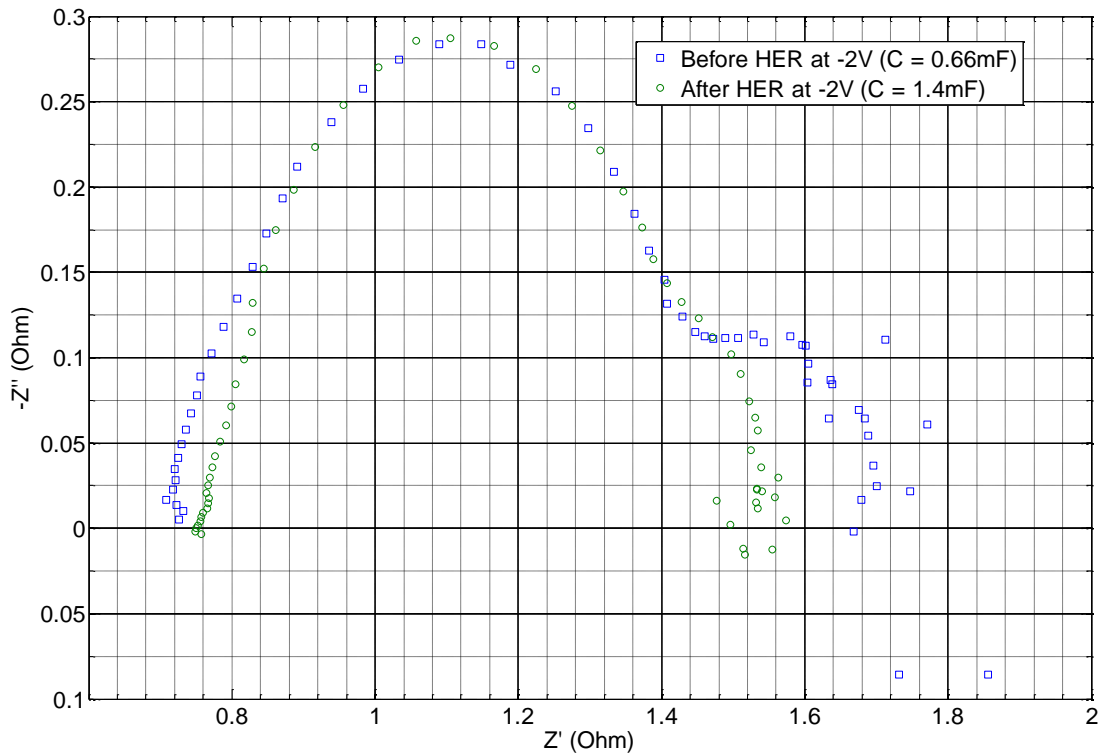


Figure 4-30 Nyquist impedance before and after *HER* at -2V for 2 hours on SS sheet

From Tables 4-2 and 4-3, it can be seen that the current densities for *OER* and *HER* are increased by about 50 % on SS mesh compared with SS smooth sheet. This means that rates of oxygen and hydrogen production are enhanced on SS mesh compared to SS smooth sheet. The rates of *OER* and *HER* are enhanced on SS mesh due to its higher surface area and favourable surface structure.

Table 4-2 Summary of hydrogen (*HER*) and oxygen (*OER*) production rates on SS mesh at 2 V

Electrode reaction	J (A/cm ²)	Evolution rates (l/h)	Electrical Power consumption (W)
<i>OER</i>	0.061	0.025	0.47
<i>HER</i>	0.051	0.041	0.39

Table 4-3 Summary of hydrogen (*HER*) and oxygen (*OER*) production rates on SS smooth sheet at 2 V

Electrode reaction	J (A/cm ²)	Evolution rates (l/hr)	Electrical Power consumption (W)
<i>OER</i>	0.0297	0.0028	0.19
<i>HER</i>	0.0257	0.0052	0.16

Further investigations of the *OER* and *HER* were carried-out under galvanostatic (constant current) mode of operation in order to further understand the effect due to evolved gas bubbles on the electrode surface. The *OER* and *HER* were carried out on SS mesh under constant current load of $\sim 200 \text{ mA/cm}^2$ and $\sim 200 \text{ mA/cm}^2$ for 2 hours respectively. As shown in Figures 4-31 and 4-32, *OER* and *HER* overvoltages were $\sim 2.48 \text{ V}$ and $\sim 2.46 \text{ V}$ respectively on the SS mesh. The *OER* overvoltage is higher due to passivation of the electrode in the oxygen environment.

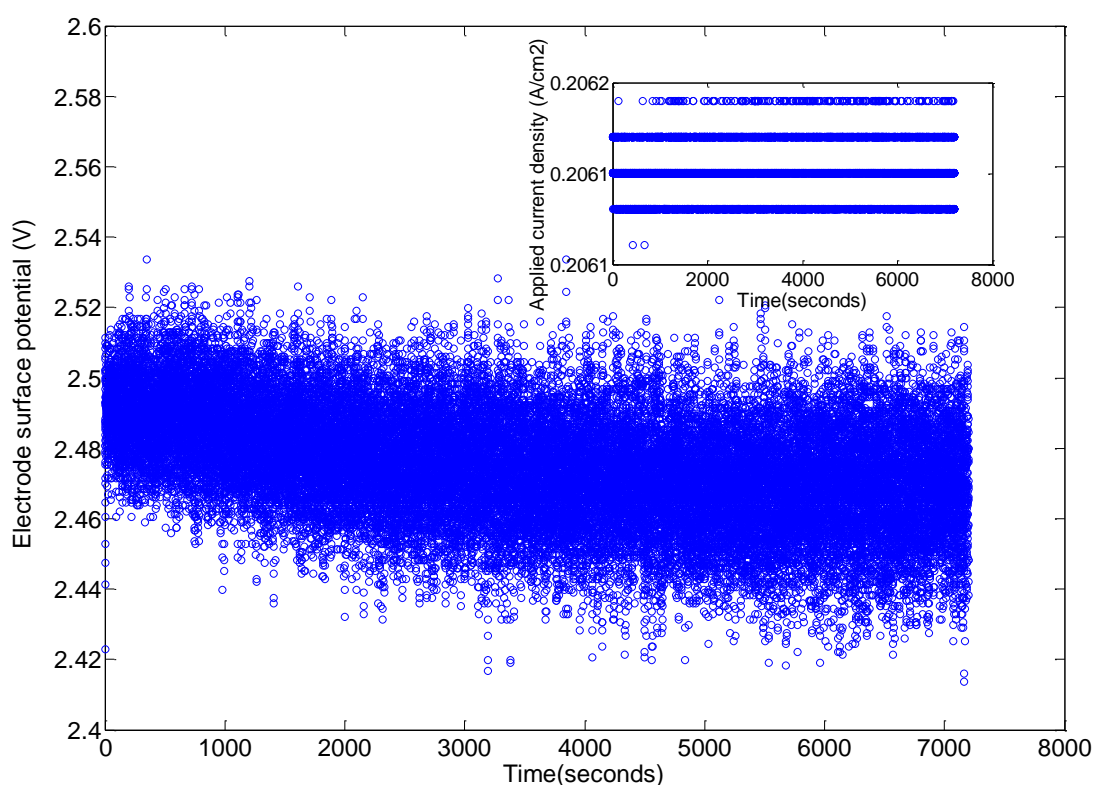


Figure 4-31 *OER* at $\sim 200 \text{ mA/cm}^2$ for 2 hours on SS mesh in 30 % KOH at 23 °C; inset shows applied current load

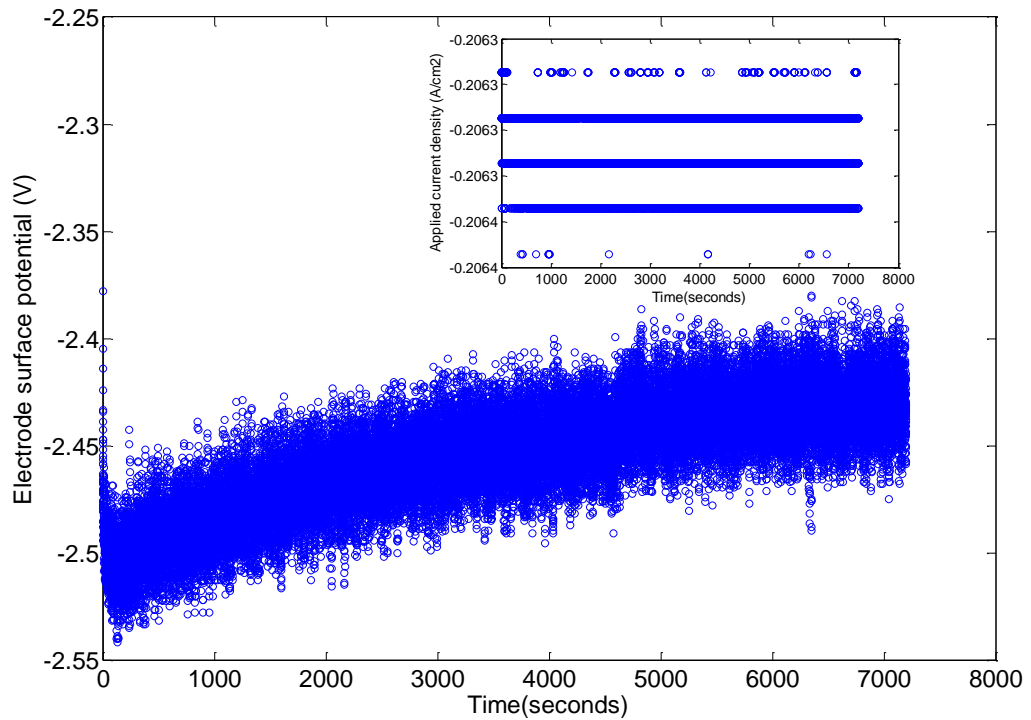


Figure 4-32 *HER* at $\sim -200 \text{ mA/cm}^2$ for 2 hours on SS mesh in 30 % KOH at 23 °C; inset shows applied current load

The reaction resistance and double-layer capacitance are almost unchanged after *OER* that is shown in Figure 4-33. However, as shown in Figure 4-34, the reaction resistance has reduced after *HER* due to removal of oxide passivation products by the reduction reaction, and consequent increase of the capacitance as well as electrochemical active area. This suggests that reversing the polarity of the electrode after some time of electrolysis by continuous *OER* (anodic) and *HER* (cathodic) or RPC (see section 2.3.1) would help to minimise overvoltages that is caused by reaction products on the electrode surface.

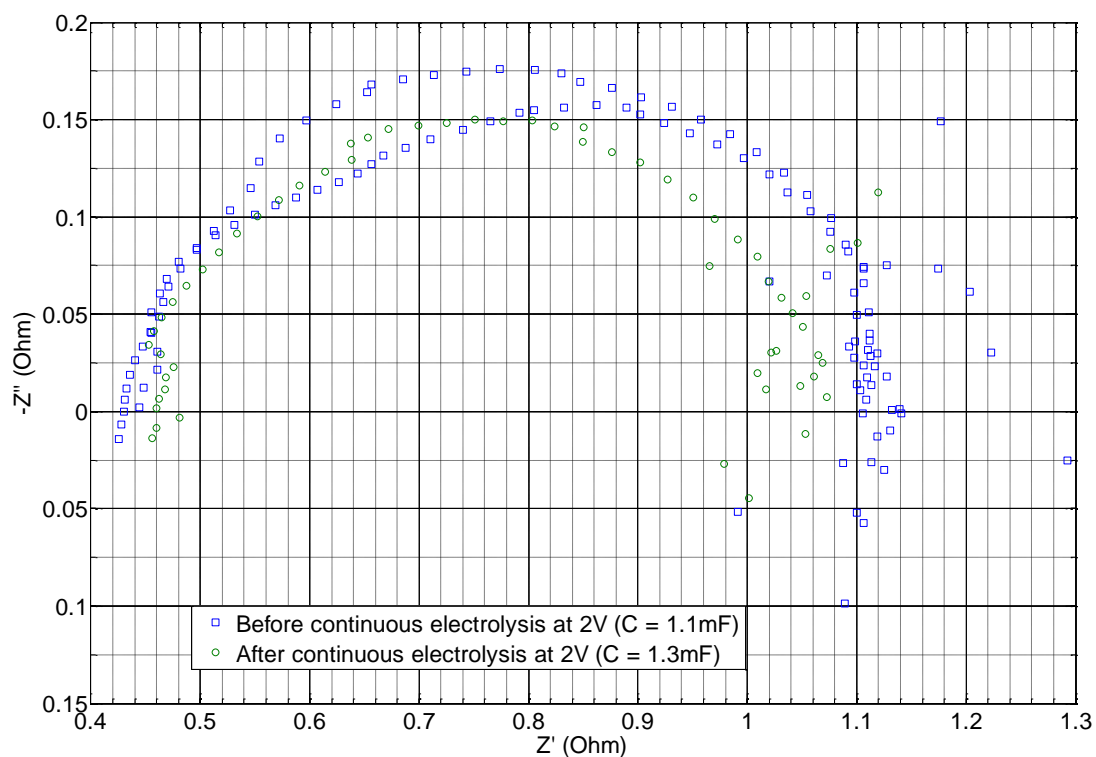


Figure 4-33 Nyquist impedance before and after *OER* at $\sim 200\text{ mA/cm}^2$ for 2 hours on the SS mesh.

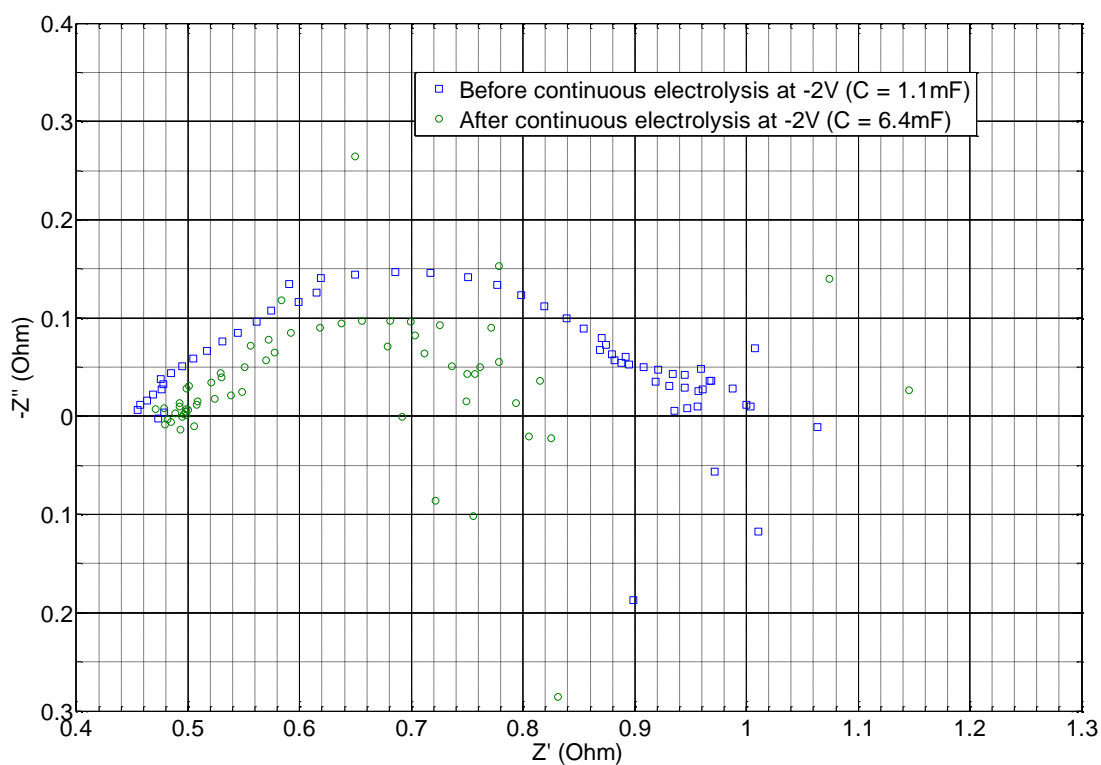


Figure 4-34 Nyquist impedance before and after *HER* at $\sim -200\text{mA/cm}^2$ for 2 hours on SS mesh

Similarly, the *OER* and *HER* were measured on SS sheet under constant current load of about 191 mA/cm^2 , and as shown in Figures 4-35 and 4-36 the *OER* and *HER* overvoltages were about 2.6 V and 2.5 V respectively. The *OER* overvoltage is higher due to passivation of the electrode in the oxygen environment. The current and voltage have fluctuated very rapidly as a result of energy that is exerted on the electrode surface by the evolved gas bubbles.

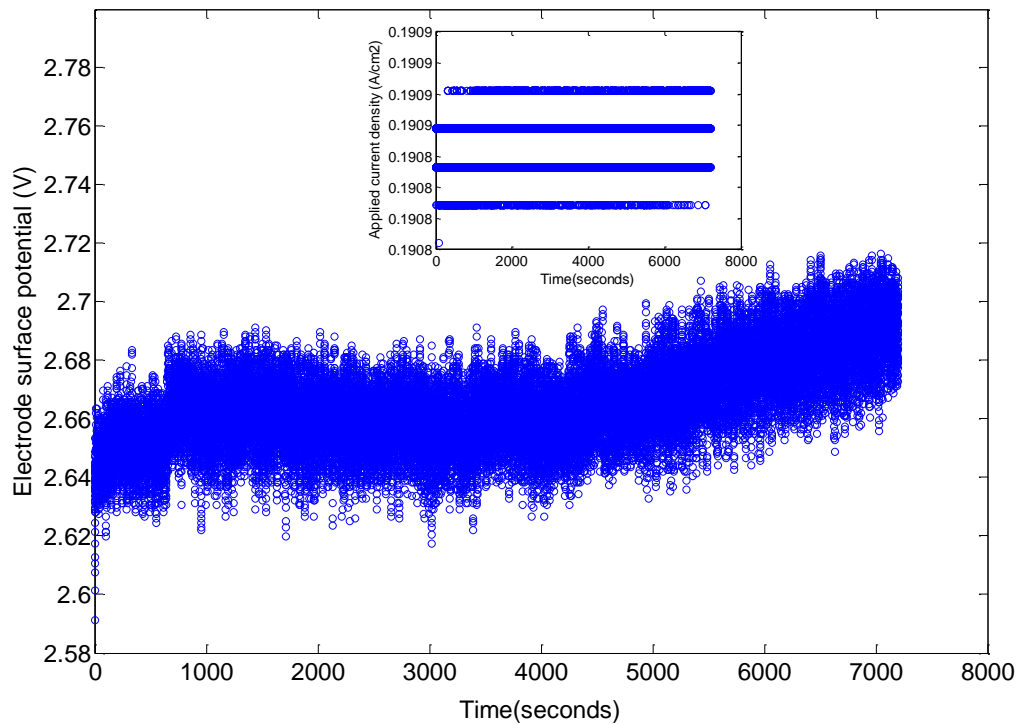


Figure 4-35 *OER* at $\sim 191 \text{ mA/cm}^2$ for 2 hours on SS sheet in 30 % KOH at 23 °C; inset shows applied current load

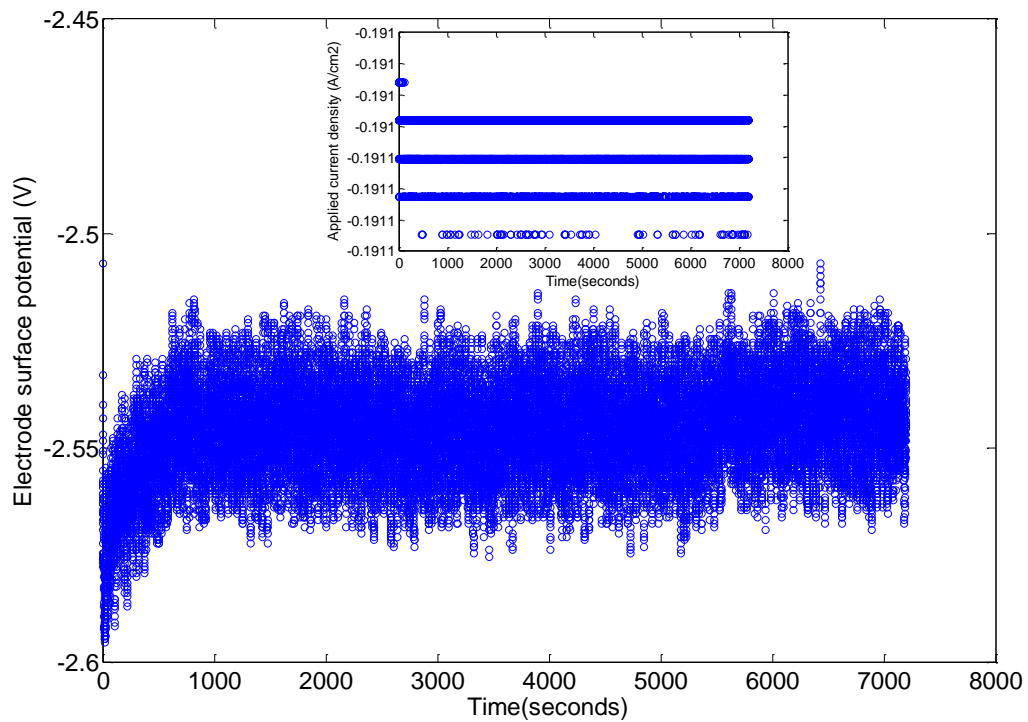


Figure 4-36 *HER* at $\sim -191 \text{ mA/cm}^2$ for 2 hours on SS sheet, inset shows applied current load

In Figure 4-37, the Nyquist impedance suggests slight changes in the reaction resistance after *OER* which might be due to passivation of the electrode in the oxygen environment.

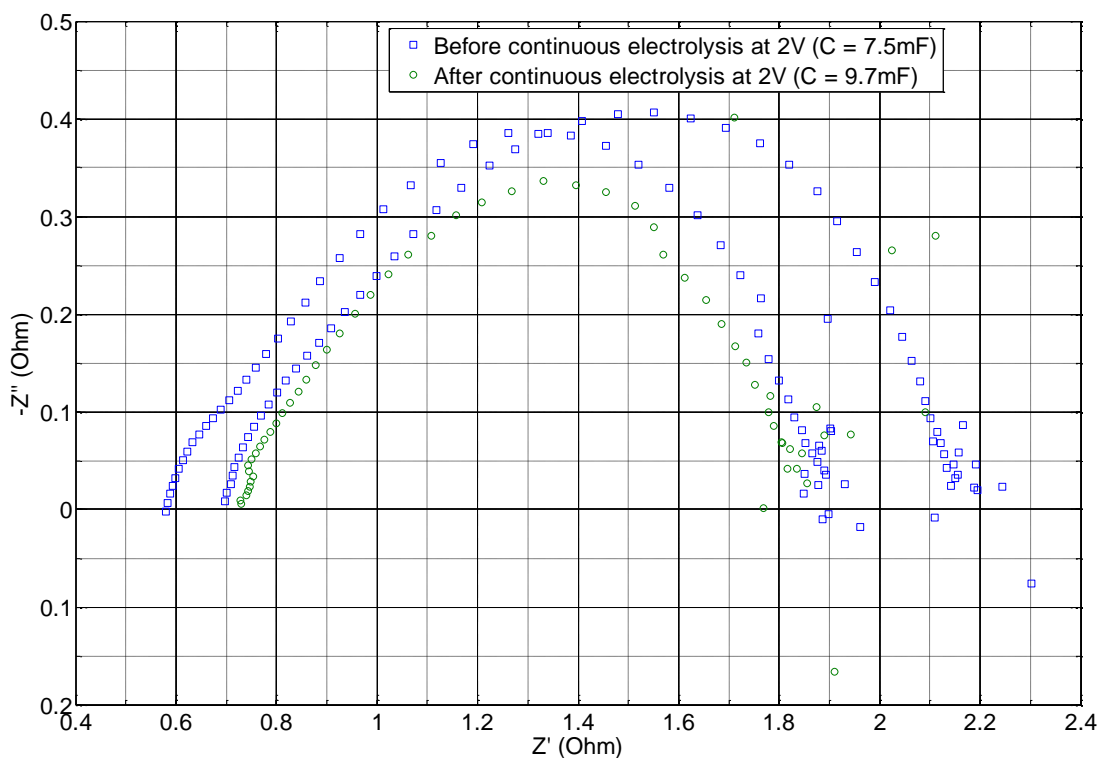


Figure 4-37 Nyquist impedance before and after *OER* at $\sim 191 \text{ mA/cm}^2$ for 2 hours on SS sheet

In Figure 4-38, the Nyquist impedance before *HER* shows a double capacitive arc of which the smaller arc could be attributed to passivation of the electrode surface prior to *HER*. Slight changes in the reaction resistance after *HER* might suggest reduction reaction taking place on the electrode. The double-layer capacitance as well as electrochemical accessible surface area is slightly increased due to activation of the electrode after some time of electrolysis.

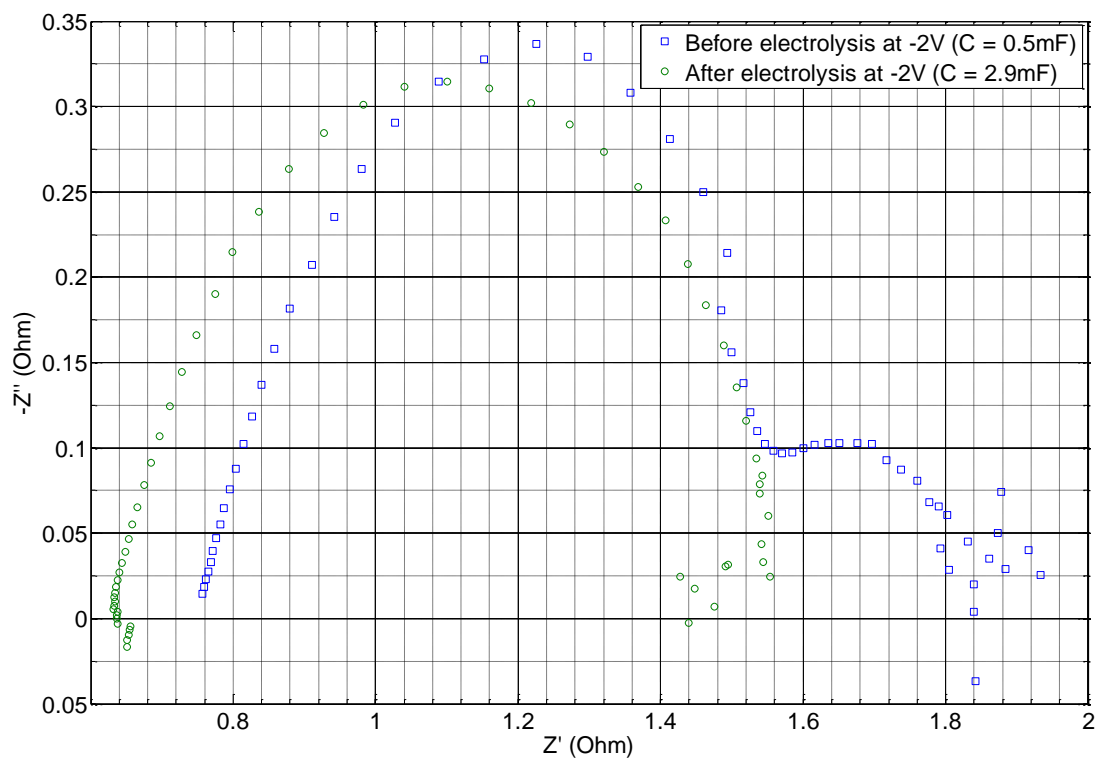


Figure 4-38 Nyquist impedance before and after *HER* at $\sim -191 \text{ mA/cm}^2$ for 2 hours on SS sheet

4.4 Conclusion of Chapter

The kinetic efficiency is higher on SS mesh (type 304) compared to SS sheet (type-304). The SS mesh electrode is robust for continuous *OER* and *HER*. The SS mesh has better efficiency and stability under variable, constant and intermittent electrical power of operation. In contrast, the SS sheet is readily passivated by oxidative reaction products which consequently increase the transport and reaction resistances. The SS sheet exhibit higher impedance at start-up of electrolysis and is readily passivated over extended period of continuous electrolysis.

The SS mesh (type 304) is therefore identified as the best electrode because of its relatively higher efficiency, longer-term stability and manufacturing scalability. The SS mesh (type 304) is low-cost and can be easily fabricated into a suitable size and shape for the alkaline electrolyser cell. For these reasons, the subsequent chapters deal with developing and characterising electro-catalyst based on SS mesh (type 304) for the ambient temperature alkaline electrolyser.

Chapter 5

Fabrication and Characterisation of the Electro-Catalyst

As evidenced in the previous chapter, SS mesh type-304 is the best electrode to enhance efficiency and durability of the ambient temperature alkaline electrolyser. For this reason, this chapter and the next develops the SS mesh type-304 into an electro-catalyst.

5.1 Materials For Electrodeposition of Ni-Mo Catalyst on SS mesh (type 304)

The synthesis method that was reported by Luciana *et al* in section 2.8 has been followed for electrodepositing Ni-Mo on SS mesh. However, in this case the Ni-Mo serves as a catalyst and the SS mesh serves as the current collector or electrode substrate. The preparation of this electro-catalyst was carried-out in two separate plating solutions of pH 4.0 and pH 5.0. Both solutions consisted of the following composition:

800 ml of deionised water

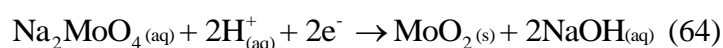
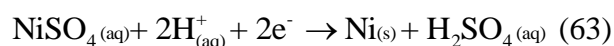
4.71 g of sodium citrate

22.47 g of nickel (II) sulphate

1.9 g of sodium molybdate

Citric acid solution for control of pH

All the chemicals were of analytical grade and were supplied by Sigma-Aldrich [129]. The electrodeposition was done galvanostatically at -30 mA/cm^2 for 2 hours at 23°C with continued stirring of the solution. The basic electrodeposition reactions taking place at the cathode are described in equations 63 and 64.



Considering equations 63 and 64, co-deposition of Ni-Mo is facilitated under acidic conditions. For this reason it was necessary to control and maintain the solution pH of the electroplating bath under acidic conditions by addition of citric acid. Sodium citrate was added as the complexing agent in order to aid co-deposition of Ni-Mo and to achieve homogeneous deposition. Other competing reactions such as water splitting would normally take place and the rate of electrodeposition depends on: composition of the electrolyte bath, temperature, solution pH, electrolyte agitation, current density, time of electrodeposition and cell configuration.

The mass of the electrode was measured before and after electrodeposition and the catalyst loading was determined to be 7.5 mg/cm² for SS-Ni-Mo. The catalyst loading is the mass of deposited catalyst per unit of the geometric active area of the electrode. Table 5-1 shows a comparison of the properties of coated and uncoated SS mesh and indicates that BET surface area is increased by at least 13% for the coated electrode. It appears that, the pH of the plating solution affects the rate and efficiency of electrodeposition.

Table 5-1 Comparison of properties of the electrodeposited SS mesh

S/N	Electrode	pH of plating bath	*BET surface area (m ² /g)	*Micropore size (nm)
0	SS mesh	n/a	2.37	1.85
1	SS-Ni-Mo(1)	4.0	5.85	3.99
2	SS-Ni-Mo(2)	5.0	2.73	2.13

* The BET surface area and pore size were measured using an automatic micromeritics-ASAP 2420 surface area and porosity analyzer.

The SEM micrographs that are shown in Figure 5-1 indicates surface roughening and increase in the apparent surface area of SS mesh due to Ni-Mo catalyst loading.

5.2 SS-Ni-Mo (1) developed at pH 4.0

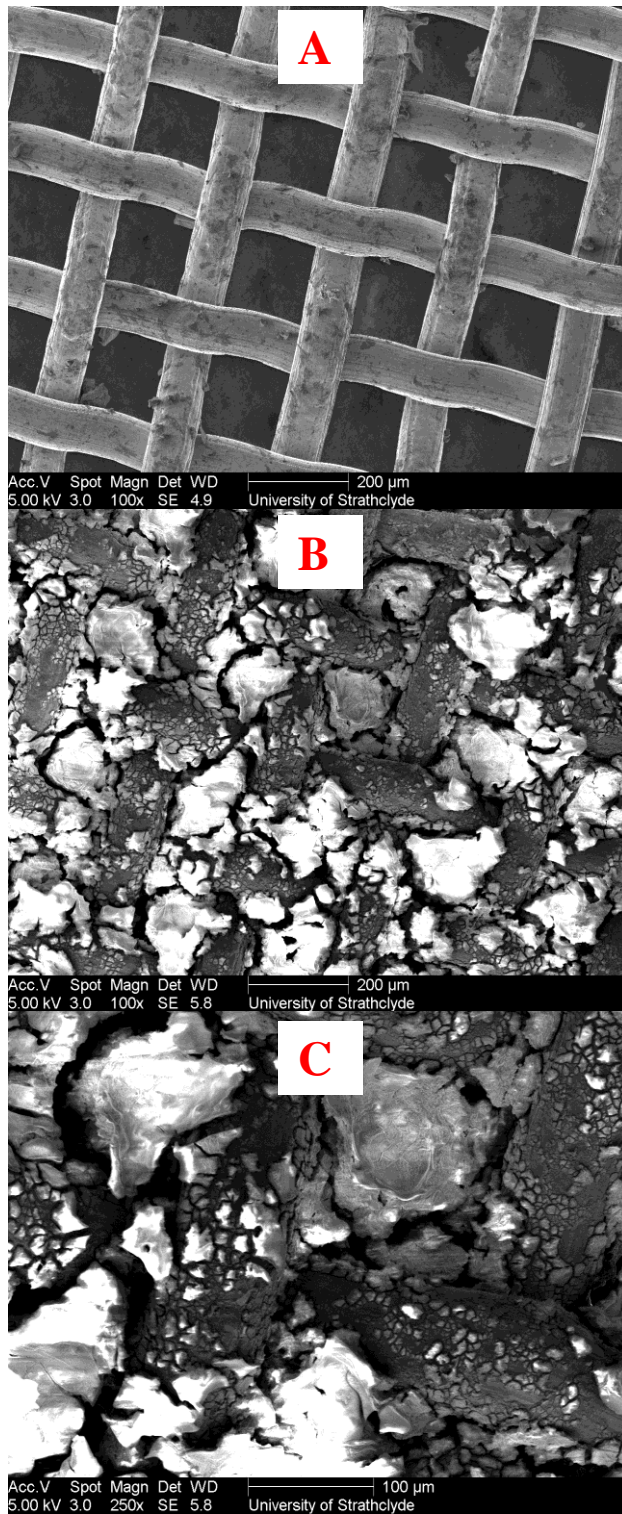


Figure 5-1 SEM micrographs: A. uncoated SS mesh, B. SS-Ni-Mo (1), C. SS-Ni-Mo (1) magnified view

5.2.1 Kinetic Efficiency under Variable Electrical Power of Operation

As shown in Figure 5-2, the kinetic efficiency is slightly increased for hydrogen production on SS-Ni-Mo(1) compared to the uncoated SS mesh. For example at -2 V the current density has increased by 0.02 A/cm² on SS-Ni-Mo(1). Apparently, SS-Ni-Mo(1) is more active for hydrogen production than for oxygen production. The Tafel relation shows extended linearity for hydrogen production, thereby suggesting that the cathodic reactions on SS-Ni-Mo(1) are kinetically controlled. The HER activity is enhanced on SS-Ni-Mo(1) due to relatively higher apparent surface area of the electrode.

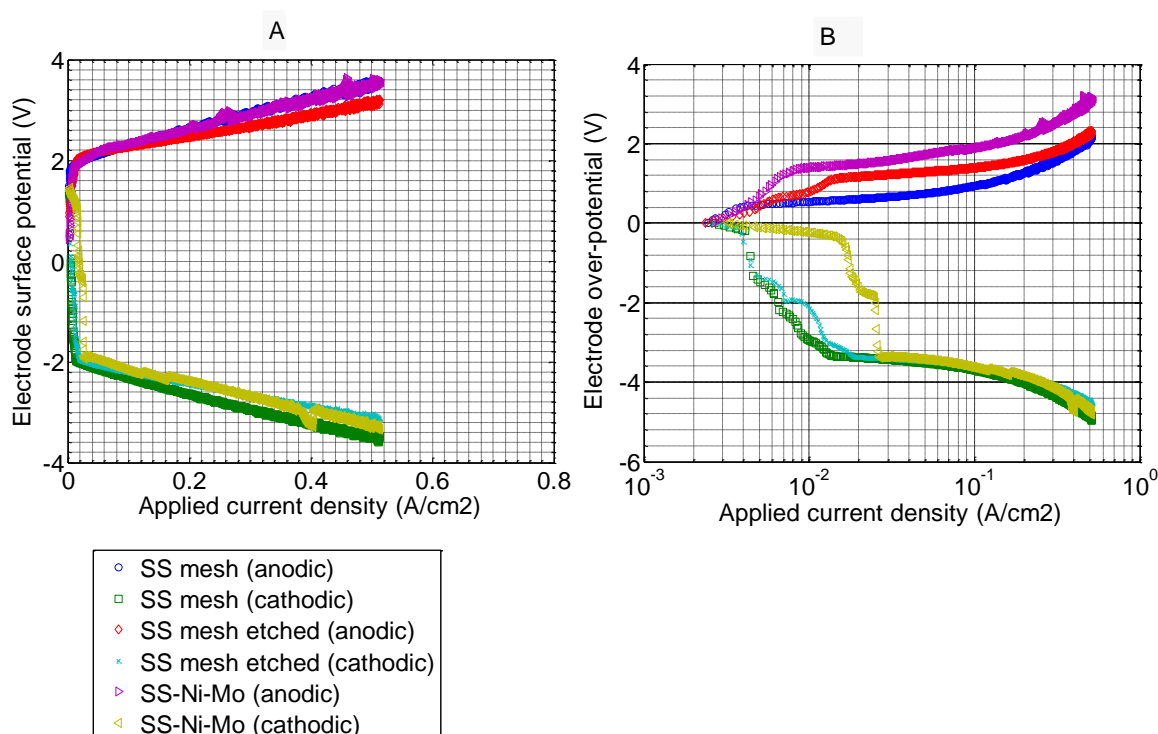


Figure 5-2 Comparison of kinetic efficiency of SS-Ni-Mo(1) and SS mesh in 30 % KOH at 23 °C: A. Polarisation relation, B. Tafel relation

The corresponding Nyquist plot is shown in Figure 5-3 and indicates that the reaction resistance is reduced by about 0.38Ω for hydrogen production on SS-Ni-Mo(1) compared to uncoated SS mesh. The Ohmic resistance is reduced on etched SS mesh due to increased surface roughness and activation of the electrode. The semi-circle is more depressed for SS-Ni-Mo(1) possibly due to its inhomogeneous and rough

surface which also increases the double-layer capacitance as well as electrochemical active area.

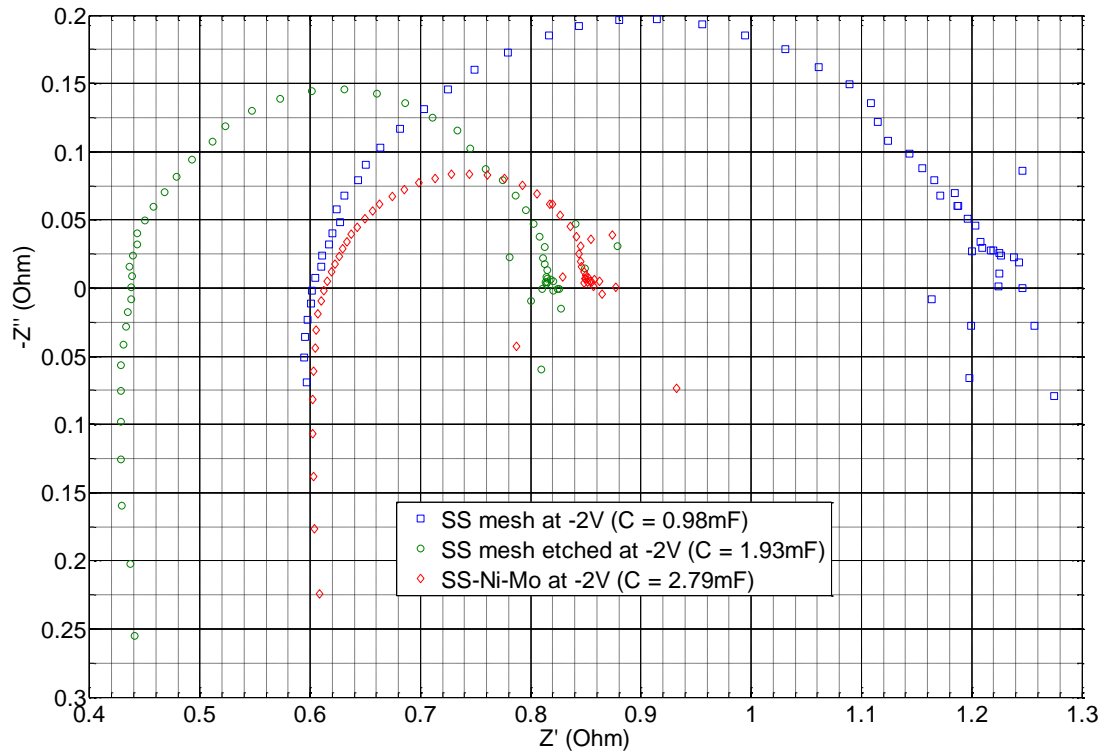


Figure 5-3 Nyquist impedance comparison of SS-Ni-Mo (1) and SS mesh.

As shown in Figure 5-4, the resistance of SS-Ni-Mo(1) varies at different potentials. The Ohmic resistance is unchanged but activation resistance varies with potential. At relatively lower potentials, activation resistance is increased due to gas-bubble coverage on the electrode surface thereby reducing electrochemical active area. However, as the potential is increased, activation resistance is reduced thereby suggesting that sufficient energy has been supplied to facilitate detachment of gas-bubbles from the electrode surface and there is increase in electrochemical active area.

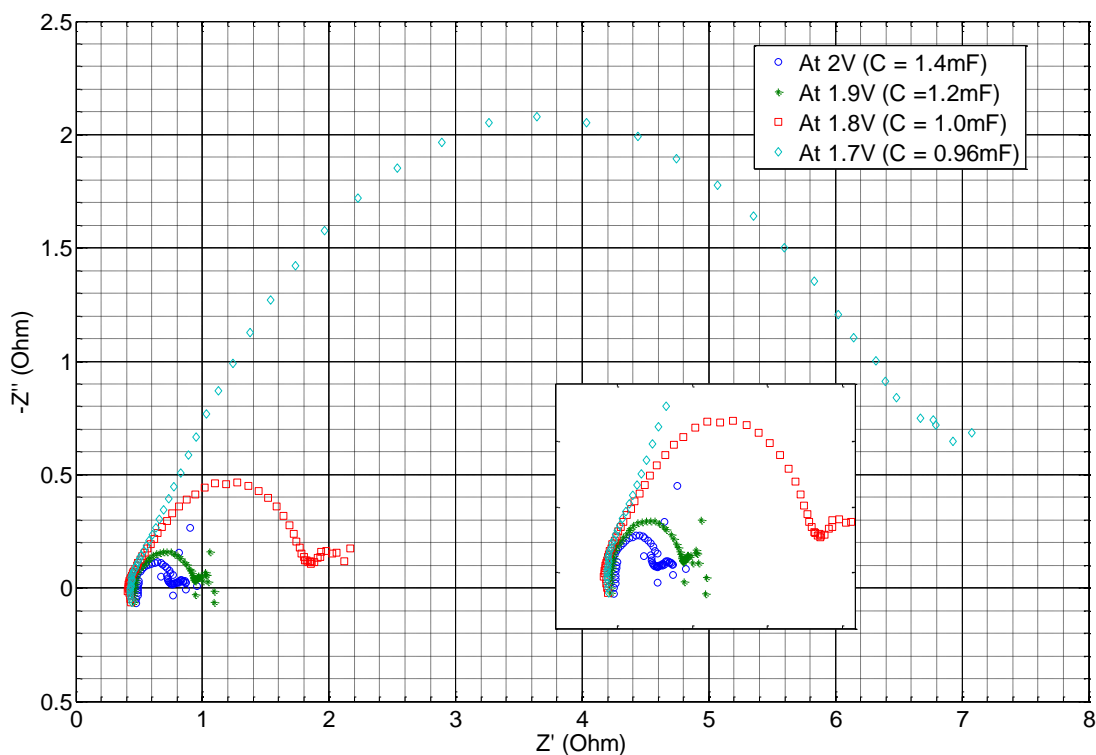


Figure 5-4 Nyquist impedance plot on SS-Ni-Mo (1) at varying potentials; Inset shows slightly zoomed Nyquist impedance plot of the same electrode.

5.2.2 Stability under Intermittent Electrical Power of Operation

From Figure 5-5, it can be seen that under intermittent operation at 200 mA/cm^2 the activity of SS-Ni-Mo(1) is fairly stable as the overpotential is unchanged at an average of 2.5 V. The oxygen overvoltage is reduced by about 0.1 V on SS-Ni-Mo(1) compared to Figure 4-14A for the uncoated SS mesh. This can be attributed to Ni-Mo coatings preventing passivation or formation of surface oxide layers on the underlying SS mesh during *OER*.

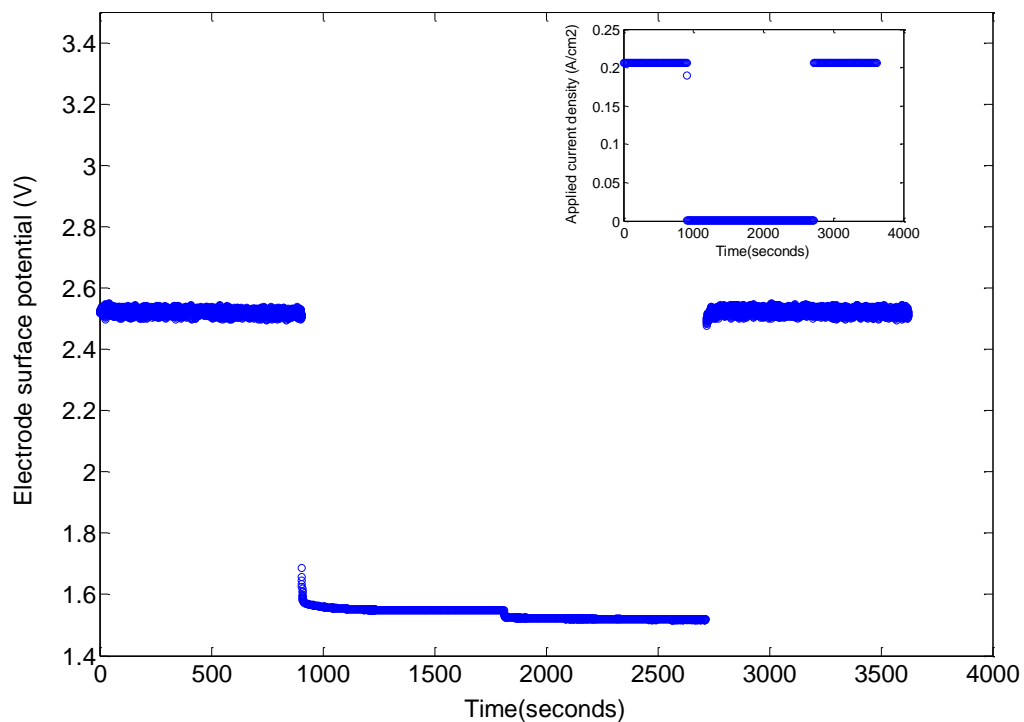


Figure 5-5 Open-circuit test on SS-Ni-Mo (1) in 30% KOH at 23°C; Inset shows applied current load

5.2.3 Stability under Constant Electrical Power of Operation

Figure 5-6 indicates that the SS-Ni-Mo(1) has a lower current density of $\sim 0.026 \text{ A/cm}^2$ for the *OER* at 2V compared to Figure 4-23 for the uncoated SS mesh. This indicates a higher resistance for oxygen evolution on SS-Ni-Mo(1). It appears that *OER* is not favoured on SS-Ni-Mo(1) due to relatively high resistance for oxidation of the underlying SS mesh.

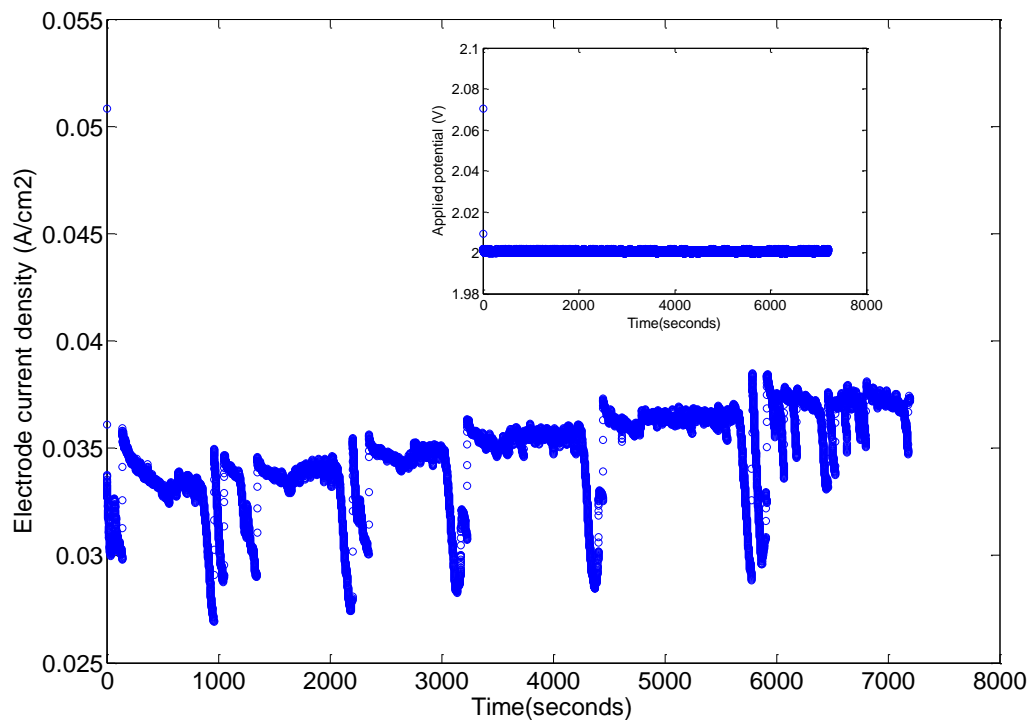


Figure 5-6 *OER* at 2 V for 2 hours on SS-Ni-Mo (1) in 30 % KOH at 23 °C; Inset shows applied voltage

The Nyquist impedance of Figure 5-7 also indicates slight increase in reaction resistance after *OER*. The capacitance however is slightly increased after *OER*, which could be due to several factors such as charge transport, electrode surface roughness, electrolyte conductivity, and gas-bubbles at the electrode/electrolyte interface.

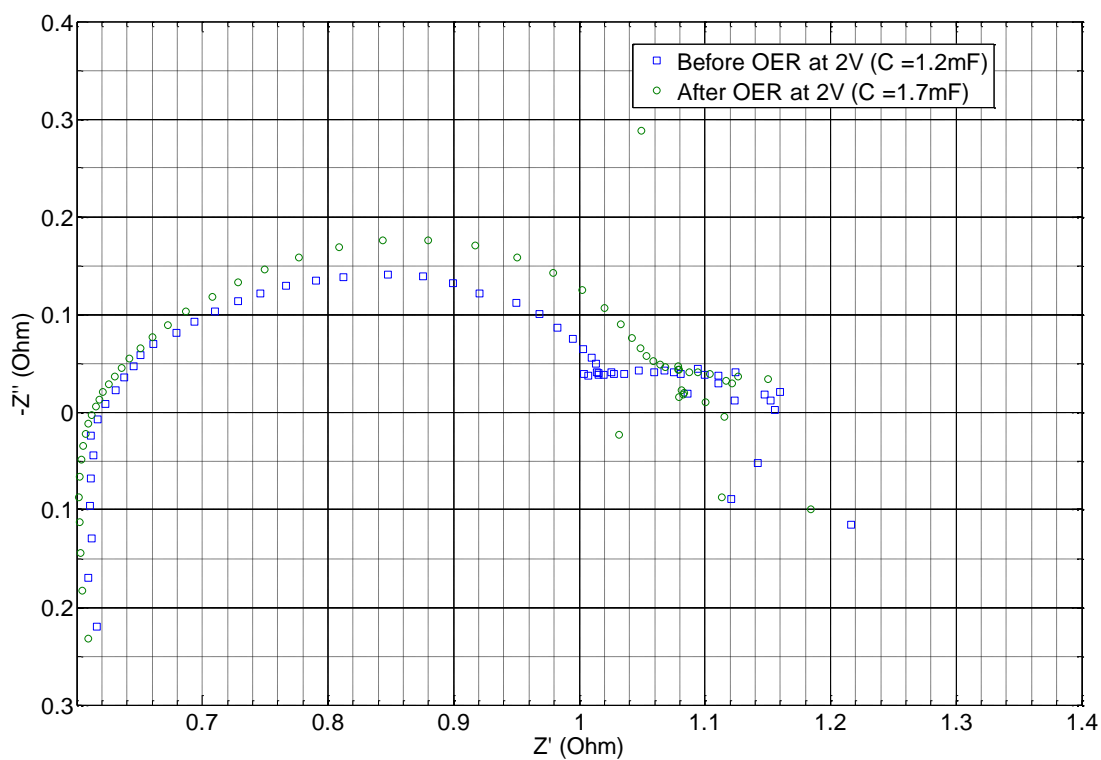


Figure 5-7 Nyquist impedance before and after *OER* at 2 V for 2 hours on SS-Ni-Mo (1)

As shown in Figure 5-8, the *HER* is enhanced on SS-Ni-Mo (1) because the current density is increased by about 0.026 A/cm^2 at -2 V compared with Figure 4-25 for the uncoated SS mesh. The rapid variation of current and voltage is attributed to energy that is exerted on the electrode surface by the movement of gas-bubbles in the ‘zero-gap’ cell configuration.

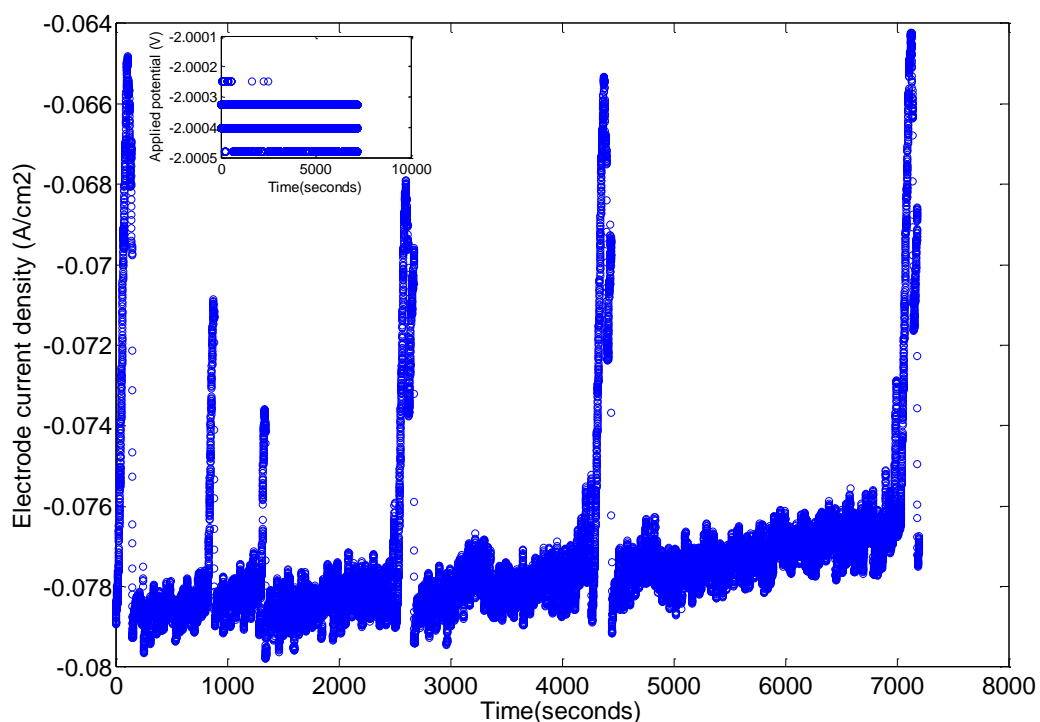


Figure 5-8 *HER* at -2 V for 2 hours on SS-Ni-Mo (1) in 30 % KOH at 23 °C; inset shows applied voltage

The corresponding Nyquist impedance in Figure 5-9 indicates that the reaction resistance is slightly increased and the Ohmic resistance is almost unchanged after *HER*. The reaction resistance is slightly increased by 0.1 Ω after *HER*, which could be due to leaching of Ni-Mo catalyst into the electrolyte solution during electrolysis, and consequently reducing electrochemical active area. The capacitance is slightly increased after *HER*, which could be due to activation of the electrode after some time of electrolysis as well as hydride formation that enhance the electrochemical active area. The existence of capacitance, however, suggests that the *HER* is controlled by charge transfer mechanisms as described under section 2.3.1 [121].

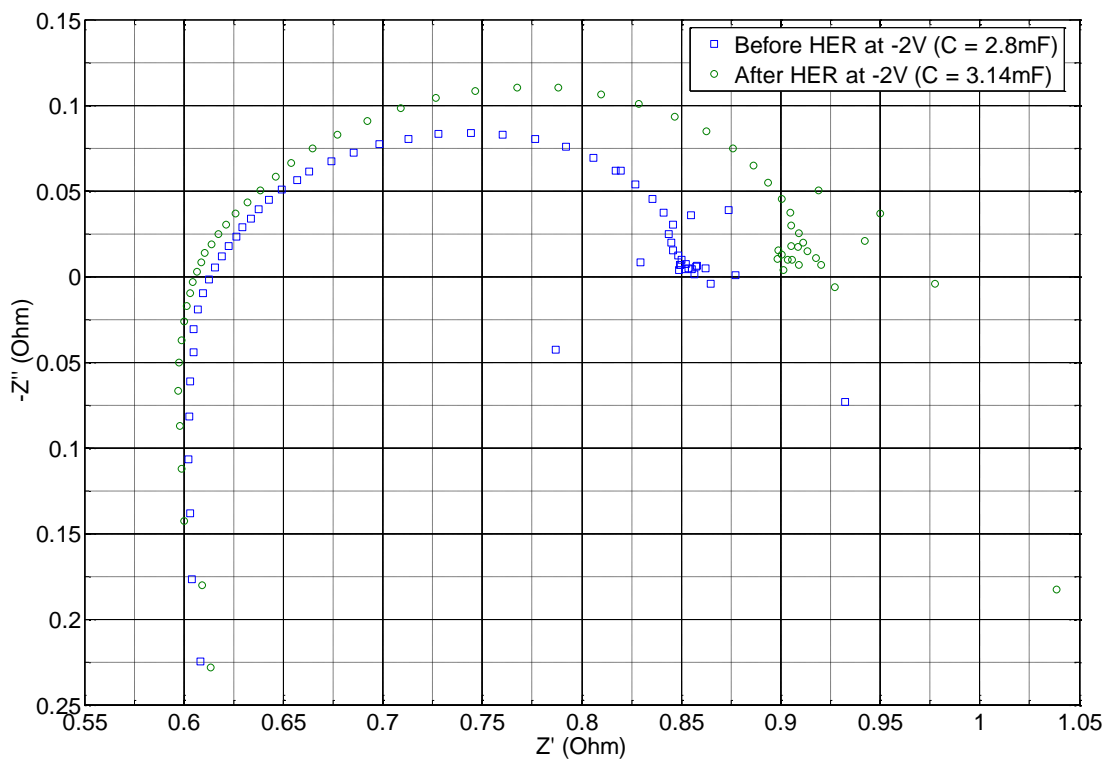


Figure 5-9 Nyquist impedance before and after *HER* at -2 V for 2 hours on SS-Ni-Mo (1)

The activity of SS-Ni-Mo(1) was investigated under constant current load of $\sim 200 \text{ mA/cm}^2$ for the *OER*, and $\sim -200 \text{ mA/cm}^2$ for the *HER*. As shown in Figures 5-10 and 5-11, the *OER* and *HER* overvoltages are 2.49 V and 2.43 V respectively for the SS-Ni-Mo(1), thereby indicating that the electro-catalyst is more active for hydrogen production.

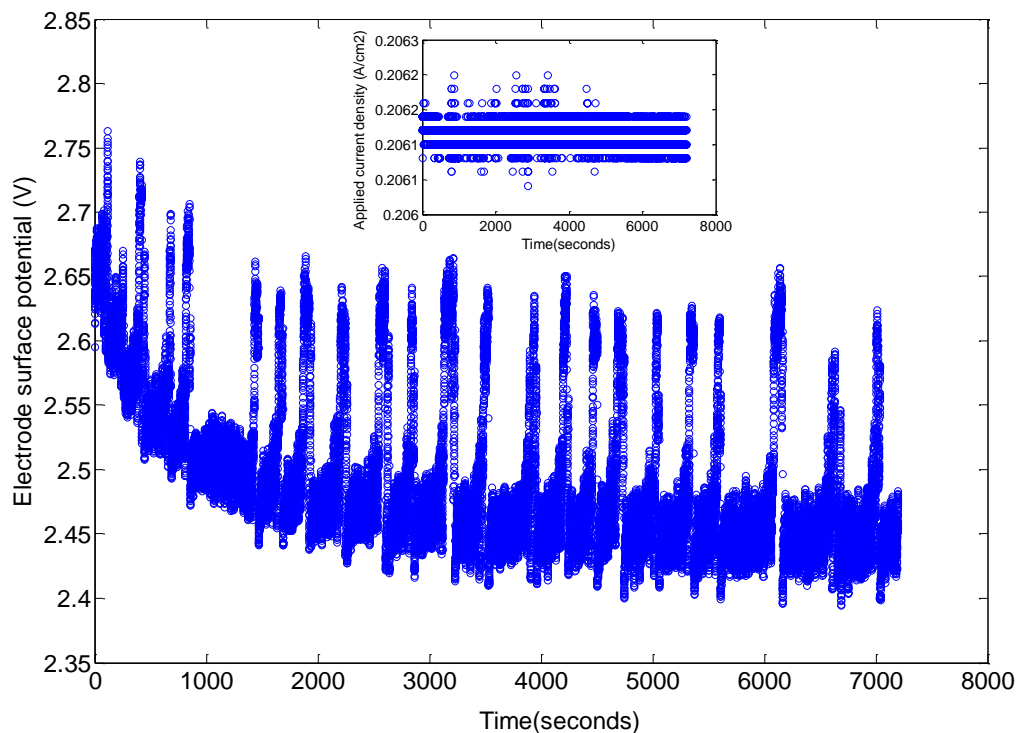


Figure 5-10 *OER* at $\sim 200 \text{ mA/cm}^2$ for 2 hours on SS-Ni-Mo (1) in 30 % KOH at 23 °C; inset shows applied current load

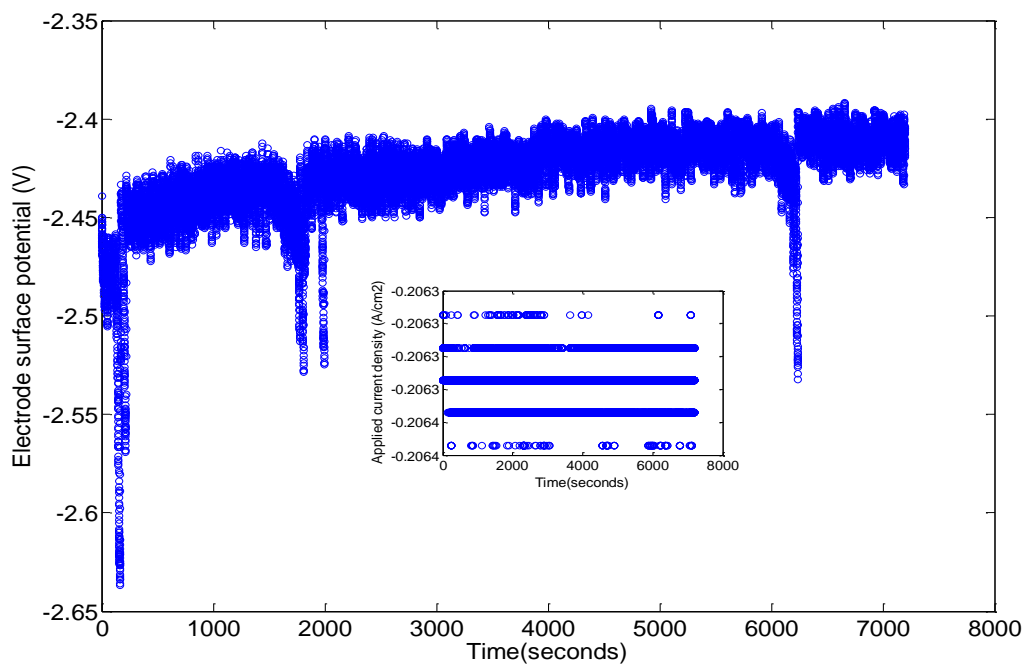


Figure 5-11 *HER* at $\sim -200 \text{ mA/cm}^2$ for 2 hours on SS-Ni-Mo (1) in 30 % KOH at 23 °C; inset shows applied current load

As shown in Figures 5-12 and 5-13, the reaction resistance is significantly reduced after the *OER* and *HER* respectively, which could be due to activation or ‘conditioning’ of the electro-catalyst after some time of electrolysis.

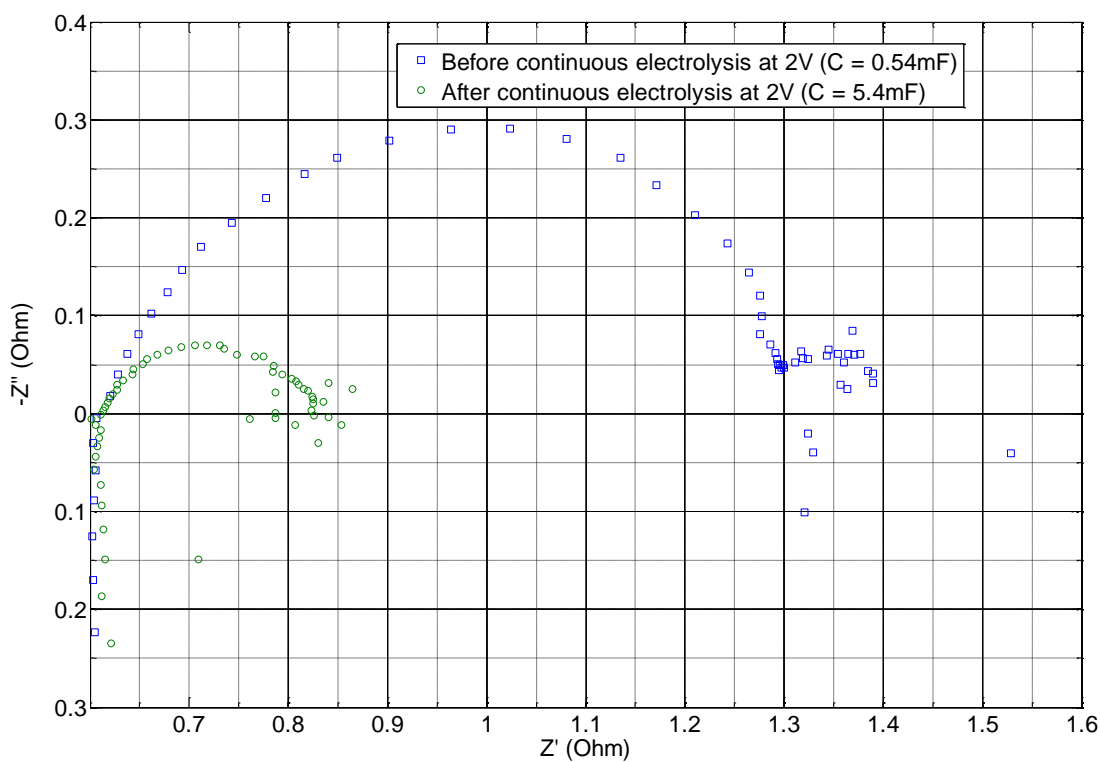


Figure 5-12 Nyquist impedance before and after *OER* at $\sim 200\text{ mA/cm}^2$ for 2 hours on SS-Ni-Mo (1).

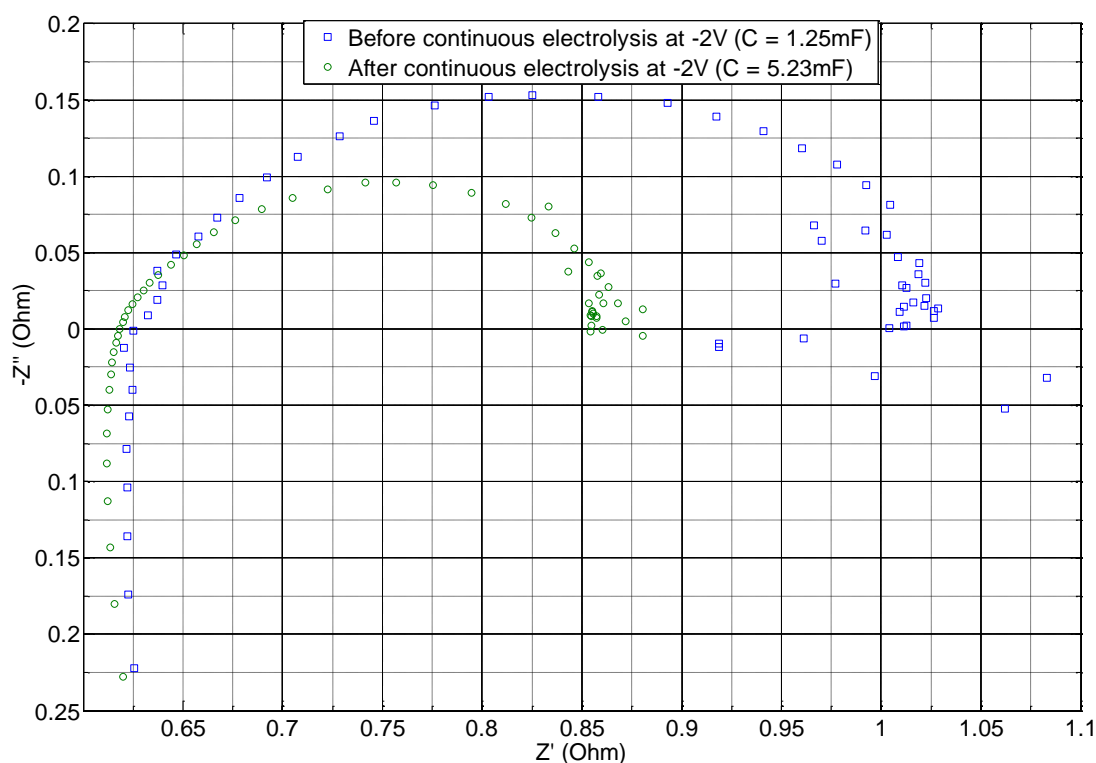


Figure 5-13 Nyquist impedance before and after *HER* at $\sim\sim 200 \text{ mA/cm}^2$ for 2 hours on SS-Ni-Mo (1).

It appears that SS-Ni-Mo(1) is more suitable as a cathode material to enhance the hydrogen production rate. By comparing Figures 5-11 and 4-32, the *HER* overvoltage is 0.03 V lower on SS-Ni-Mo(1), compared with the uncoated SS mesh, thereby indicating that the Ni-Mo catalyst enhances the activity for hydrogen production. Nickel catalyst has the ability to form hydroxides such as Ni(OH)_2 and NiOOH [123] which increase the apparent surface area of the electro-catalyst. However, by comparing Figures 5-10 and 4-31, the *OER* overvoltage is 0.01 V higher on SS-Ni-Mo(1) compared with the uncoated SS mesh, thereby indicating that the Ni-Mo catalyst has a lower activity for oxygen production possibly due to the reduced rate of oxidation of the underlying SS mesh.

The SEM micro-graphs are compared before and after electrolysis (Figure 5-14) and indicate that the Ni-Mo particles have leached out from the SS mesh after electrolysis. This indicates permanent deterioration of the SS-Ni-Mo(1) after some time of electrolysis and agrees with that report in the literature [117-119,122-123] for a similar type of electro-catalyst. As shown in Figure 5-14(A), the SS-Ni-Mo(1) has

inhomogeneous morphology which could be due to poor adhesion of Ni-Mo catalyst on the SS mesh. It is quite obvious that the conditions for electrodeposition have resulted in adsorbed catalyst blocking the pores of the SS mesh. Luciana *et al* [110] have suggested that the solution pH can influence the rate of homogeneous deposition. Therefore electrodeposition was carried-out in the plating bath at a solution of pH 5.0 that produce the SS-Ni-Mo(2).

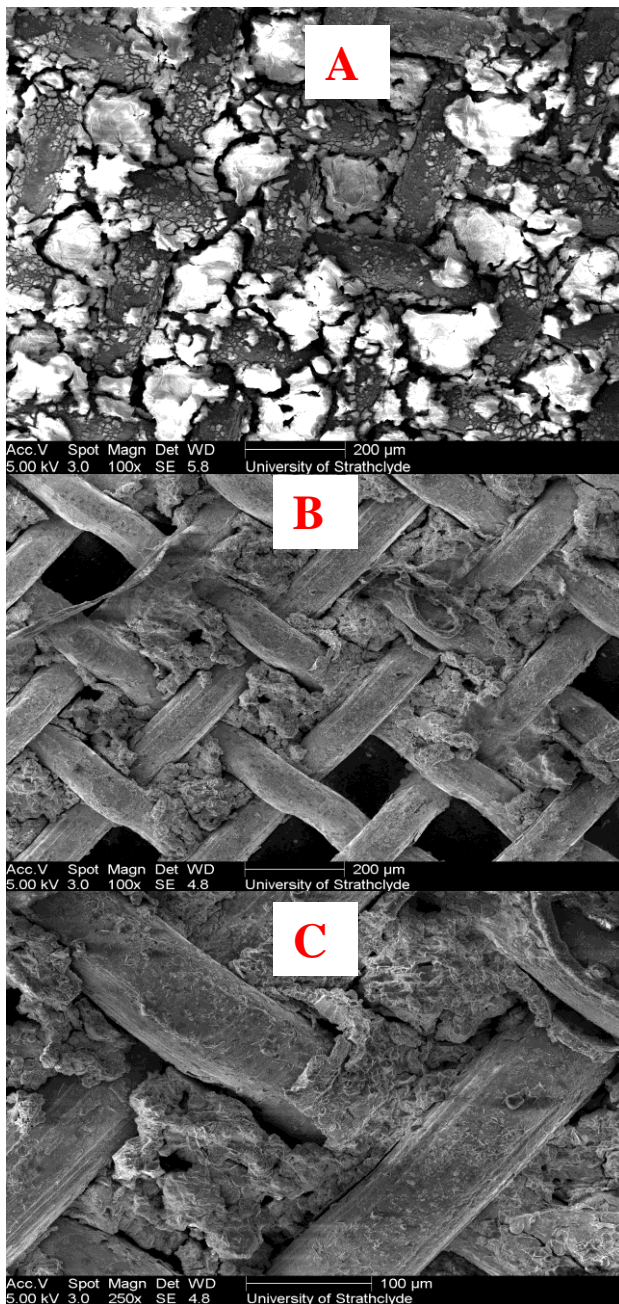
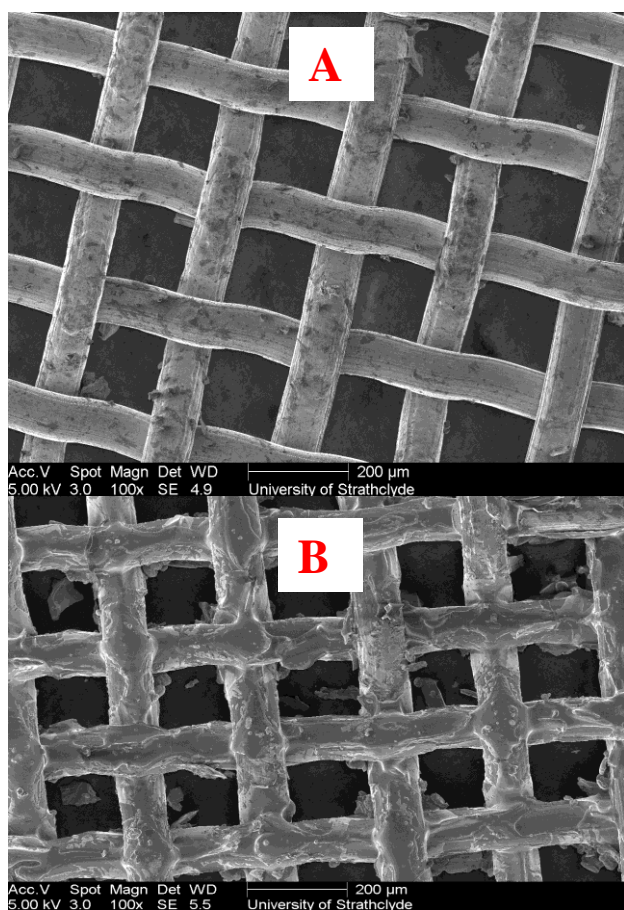


Figure 5-14 SEM micrographs: A. SS-Ni-Mo (1) before electrolysis, B. SS-Ni-Mo (1) after electrolysis, C. SS-Ni-Mo (1) after electrolysis magnified view

From the results it is clear that the SS-Ni-Mo(1) enhances the efficiency of hydrogen production in the ambient temperature alkaline electrolyser. However, the electro-catalyst is unstable over relatively longer period of electrolysis. The Ni-Mo catalyst tends to leach out from the SS mesh during electrolysis. In order to avoid this situation, the solution pH of the electroplating bath was slightly modified in a second experiment that produced the SS-Ni-Mo(2).

5.3. SS-Ni-Mo (2) developed at pH 5.0

As shown in the SEM micrographs of Figure 5-15, it is apparent that SS-Ni-Mo(2) which was developed at pH 5.0, has better adhesion and homogeneous deposition of the Ni-Mo catalyst compared with the SS-Ni-Mo(1). The Ni-Mo catalyst is deposited as skin-like coating on the SS mesh, and it is apparent that the catalyst possesses an internal porous structure that increases apparent surface area of the electrode [133].



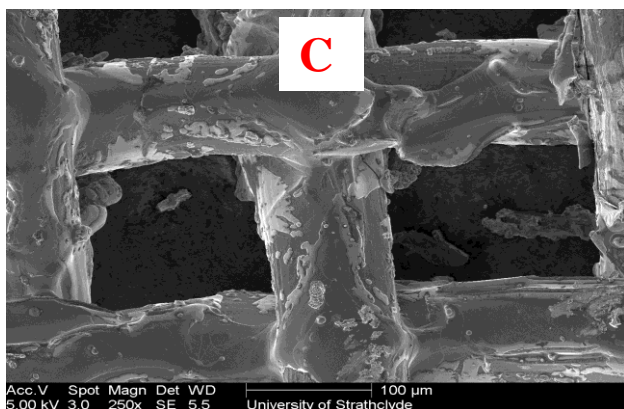


Figure 5-15 SEM micrographs: A. uncoated SS mesh, B. SS-Ni-Mo (2), C. SS-Ni-Mo (2) magnified view

5.3.1 Kinetic Efficiency under Variable Electrical Power of Operation

The polarisation of SS-Ni-Mo(2) is compared to the uncoated SS mesh as shown in Figure 5-16, which indicates that the kinetic efficiency is significantly enhanced on the SS-Ni-Mo(2) for hydrogen and oxygen production. For example at 2V the current density has increased by $0.02\text{A}/\text{cm}^2$, and at -2V the current density has increased by $0.06\text{A}/\text{cm}^2$ on SS-Ni-Mo(2). The oxygen and hydrogen production rates are increased on the SS-Ni-Mo(2) due to its relatively higher apparent surface area and favourable microstructure. The Tafel plots indicate relatively lower activation overvoltages for the anodic and cathodic reactions on SS-Ni-Mo(2). The linearity is well defined for the anodic and cathodic processes on SS-Ni-Mo(2) thereby suggesting relatively better kinetic efficiency of this electro-catalyst in the ambient temperature alkaline electrolyser.

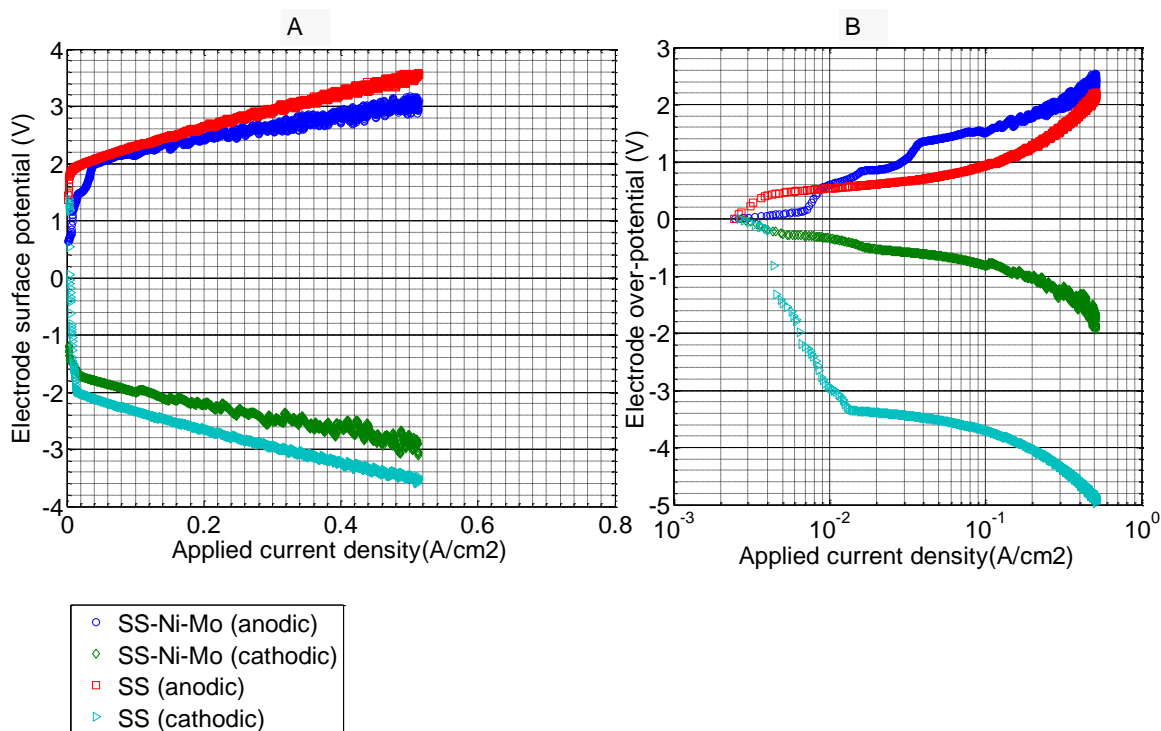


Figure 5-16 Comparison of kinetic efficiency of SS-Ni-Mo (2) and SS mesh in 30 % KOH at 23 °C: A. Polarisation relation, B. Tafel relation

The corresponding Nyquist impedance is shown in Figure 5-17 which indicates reduction in the reaction and Ohmic resistances for anodic and cathodic processes on SS-Ni-Mo(2). The reaction resistance is significantly reduced by 0.3 Ω for the cathodic reaction on SS-Ni-Mo(2) compared to the uncoated SS mesh. The activity is enhanced for *HER* probably due to formation of Ni(OH)₂, and/or NiOOH [133] which increase the apparent surface area. Also, the underlying porous SS mesh facilitates detachment of the hydrogen gas-bubbles thereby reducing gas-bubble coverage on the electrode surface. The double-layer capacitance is also increased on SS-Ni-Mo(2) thereby indicating increase in the electrochemical accessible surface area. The existence of capacitance does indicate that the *HER* and *OER* reactions are governed by charge transfer mechanisms as described under section 2.3.1.

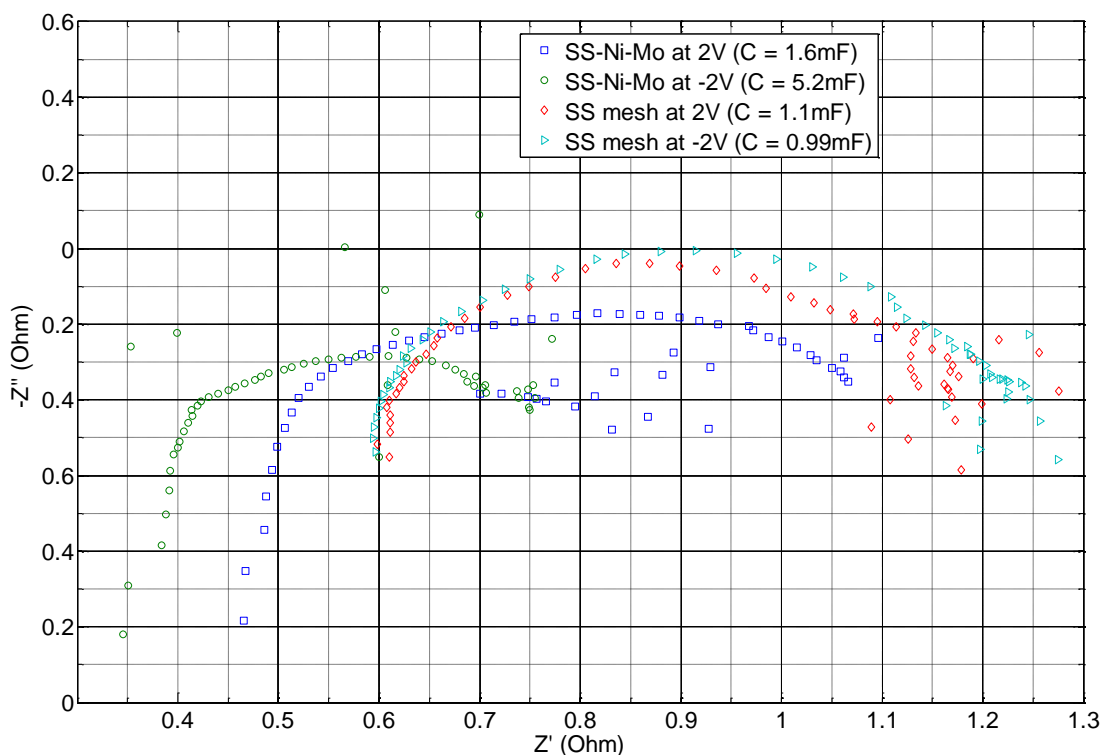


Figure 5-17: Nyquist impedance comparison of SS-Ni-Mo (2) and SS mesh.

5.3.2 Stability under Intermittent Electrical Power of Operation

As shown in Figure 5-18, SS-Ni-Mo(2) is fairly stable under intermittent power of operation since the overpotential is unchanged after open circuit. The *OER* overvoltage is fairly stable at 2.4V which is relatively lower by 0.2V compared to Figure 4-14A for the uncoated SS mesh. This indicates higher activity of SS-Ni-Mo(2) for oxygen production probably due to higher apparent surface area of the electrode.

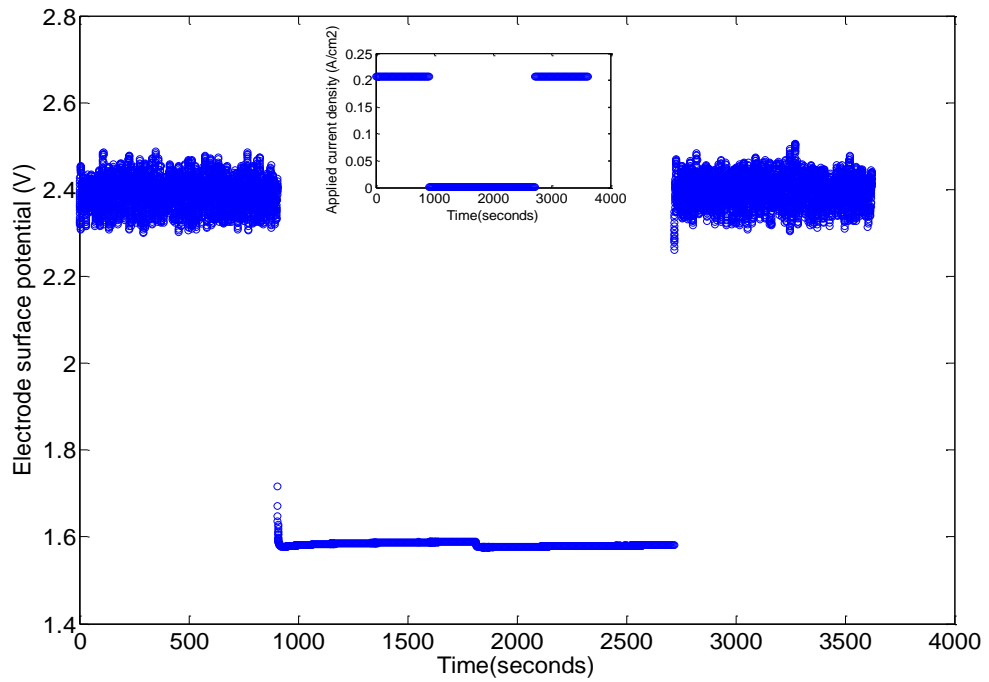


Figure 5-18 Open-circuit test on SS-Ni-Mo (2) in 30 % KOH at 23 °C; Inset shows applied current load

5.3.3 Stability under Constant Electrical Power of Operation

By comparing Figures 4-23 and 5-19, at the *OER* potential of 2 V the average current density is increased by 0.01 A/cm² for SS-Ni-Mo(2) compared to the uncoated SS mesh.

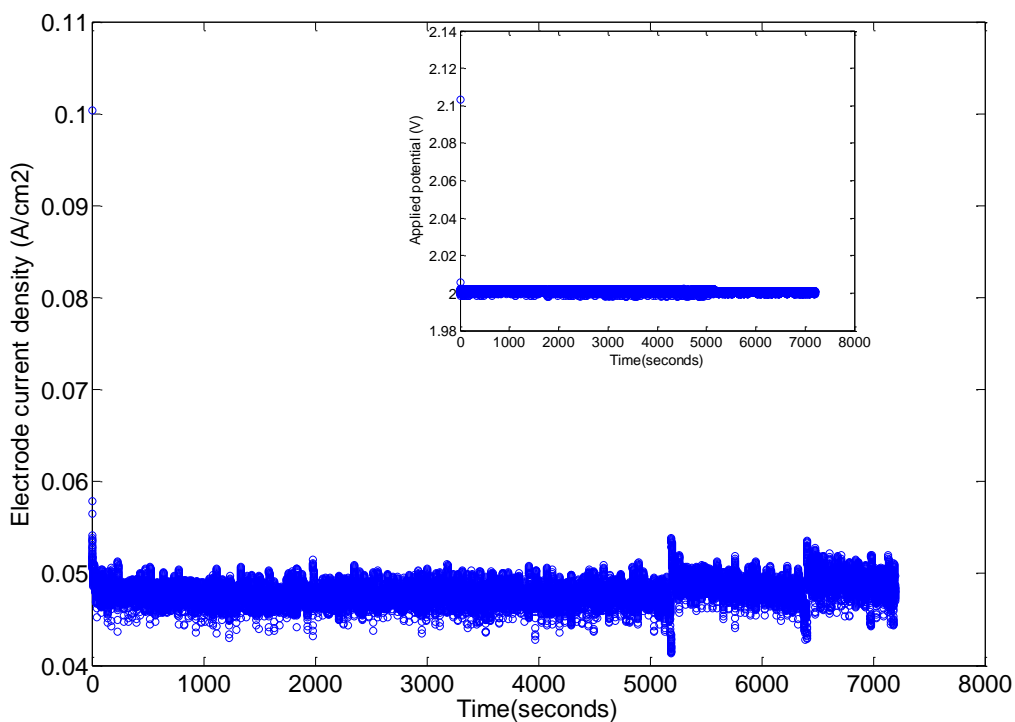


Figure 5-19 OER at 2 V for 2 hours on SS-Ni-Mo (2) in 30 % KOH at 23 °C; Inset shows applied voltage

The corresponding *OER* impedance for SS-Ni-Mo(2) is shown in Figure 5-20 which indicates that the Ohmic and polarisation resistances are slightly reduced after *OER*. This could be attributed to the porous surface structure of the underlying SS mesh which facilitates gas-bubble migration and detachment. As a consequence, the electrochemical surface area is increased after *OER* as indicated by an increase in the double-layer capacitance.

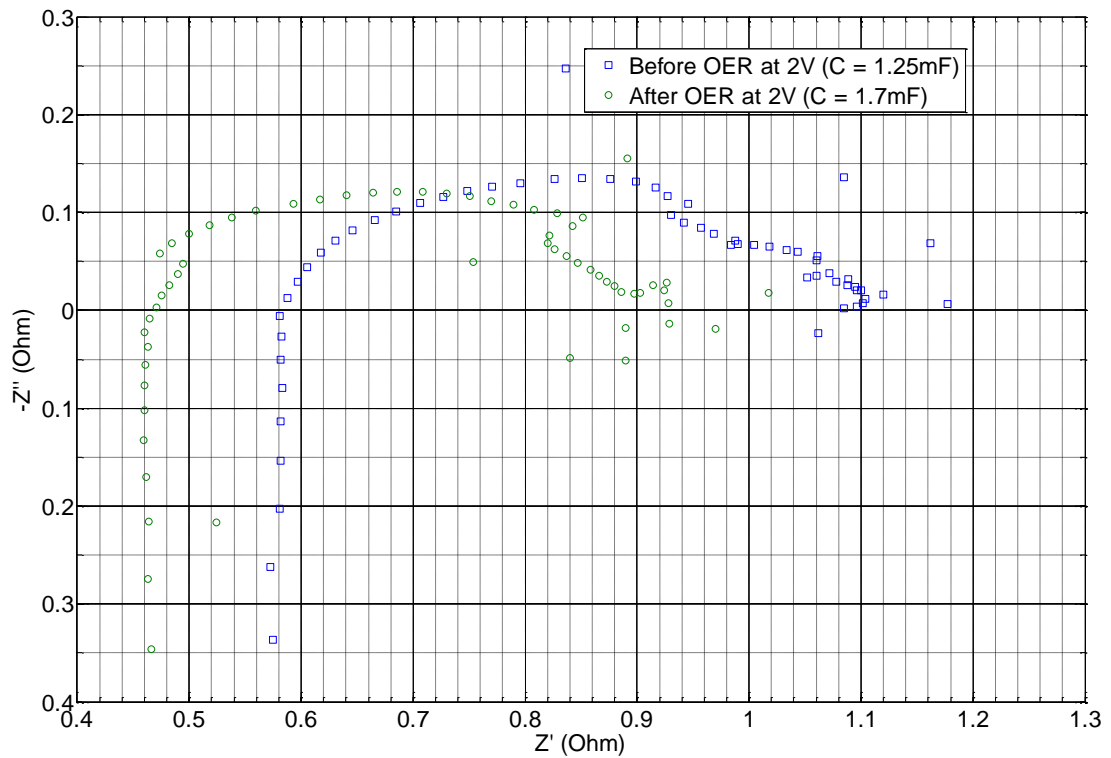


Figure 5-20 Nyquist impedance before and after *OER* at 2 V for 2 hours on SS-Ni-Mo(2)

Similarly, by comparing Figures 4-25 and 5-21, at the *HER* potential of -2V the average current density is increased by 0.1 A/cm^2 for the SS-Ni-Mo(2) compared to the uncoated SS mesh. The current and voltage fluctuate very rapidly due to energy that is exerted on the electrode surface by the movement of gas-bubbles in the ‘zero-gap’ cell configuration.

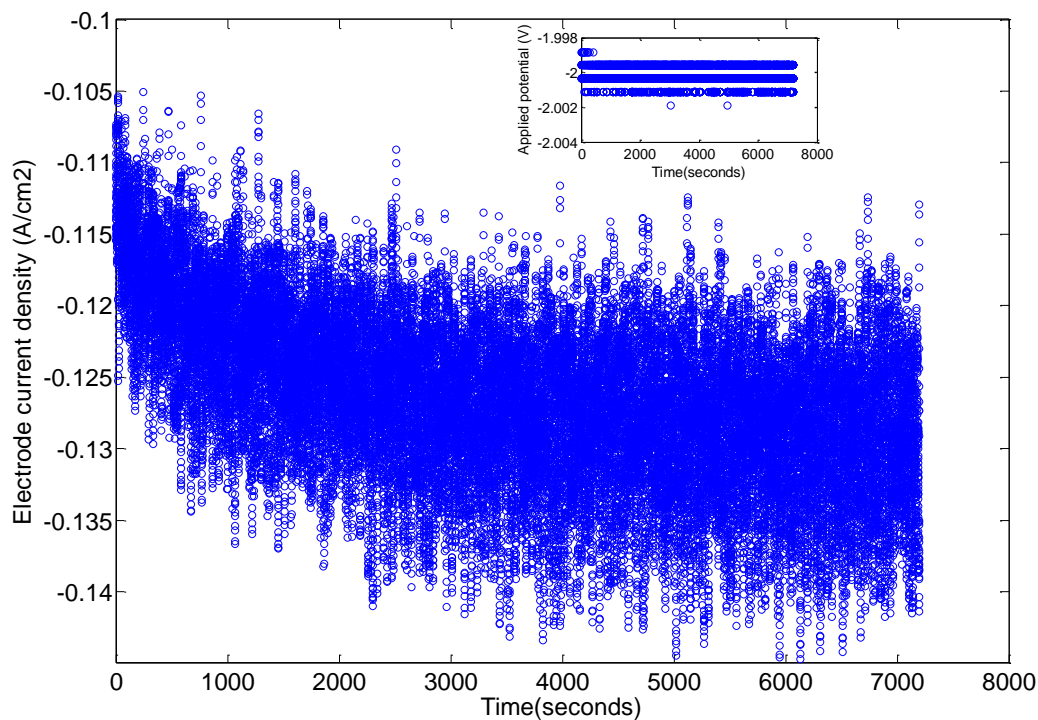


Figure 5-21 *HER* at ~ -2 V for 2 hours on SS-Ni-Mo (2); Inset shows applied voltage

The corresponding *HER* impedance for SS-Ni-Mo(2) is shown in Figure 5-22 which indicates that the reaction and Ohmic resistances are unchanged after *HER*. This can be attributed to the porous surface structure of SS mesh which facilitates gas-bubble detachment, and the Ni-Mo coating which prevents passivation of the underlying SS mesh. The double-layer capacitance is increased after *HER*, which could be due to several factors including hydride formation that increases the electrochemical active area.

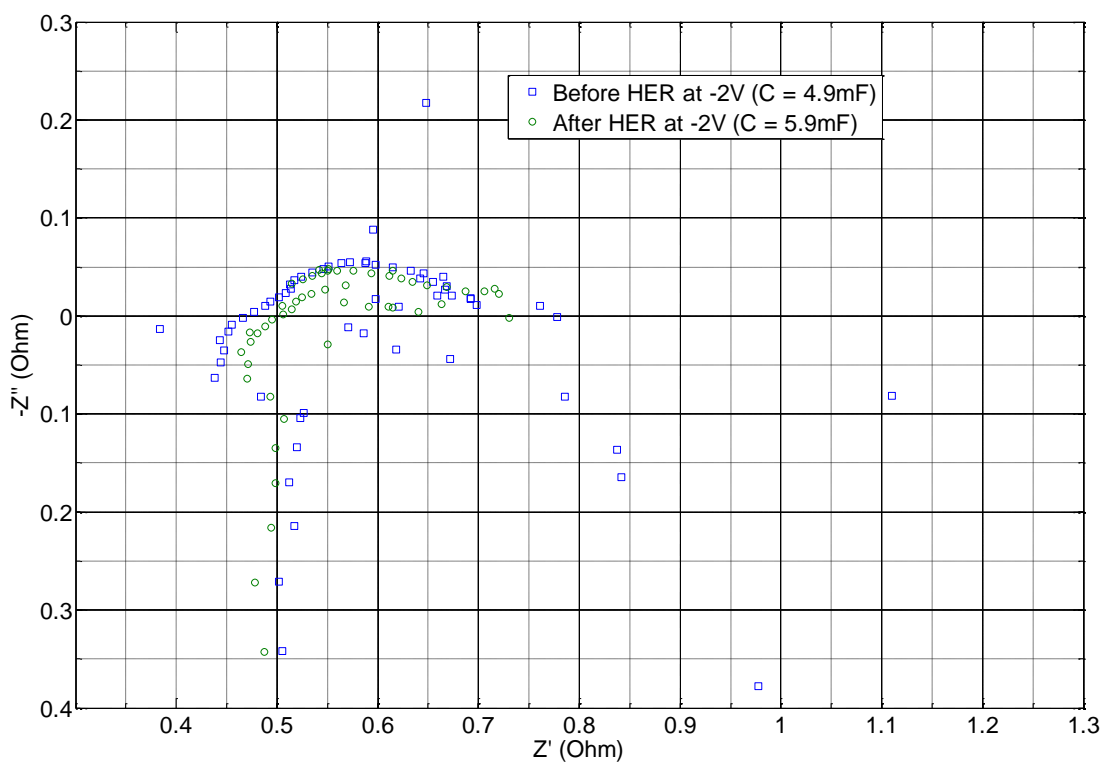


Figure 5-22 Nyquist impedance plot before and after *HER* at -2 V for 2 hours on SS-Ni-Mo (2)

As shown in Figure 5-23, the *OER* was carried out on SS-Ni-Mo(2) at a constant current load of $\sim 129 \text{ mA/cm}^2$ and the average overvoltage was $\sim 2.22 \text{ V}$. The average overvoltage is unchanged for up to 2 hours of continuous electrolysis.

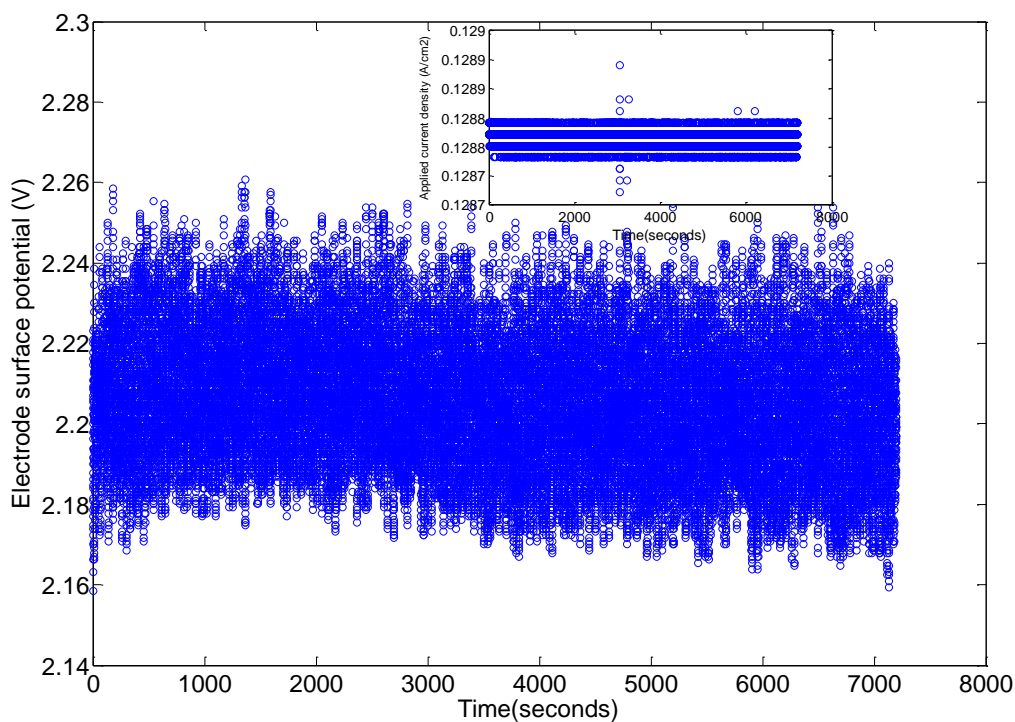


Figure 5-23 *OER* at $\sim 129 \text{ mA/cm}^2$ for 2 hours on SS-Ni-Mo(2) in 30 % KOH at 23 °C; Inset shows the applied current load

Similarly, as shown in Figure 5-24 the *HER* overvoltage is $\sim -2.1 \text{ V}$ at a constant current load of $\sim 163 \text{ mA/cm}^2$ on SS-Ni-Mo(2). The overvoltage is unstable possibly due to ‘conditioning’ of the electrode during electrolysis. The overvoltage seems to rise to relatively lower values over relatively longer period of electrolysis.

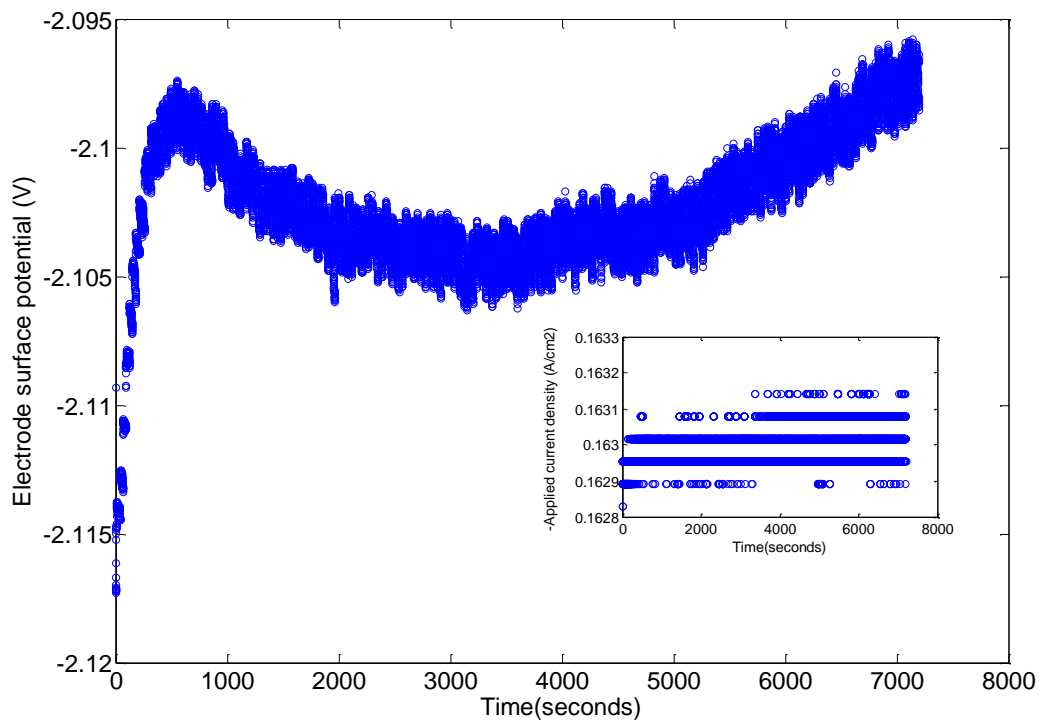


Figure 5-24 *HER* at $\sim 163 \text{ mA/cm}^2$ for 2 hours on SS-Ni-Mo(2) in 30 % KOH at 23 °C; Inset shows applied current load

The Nyquist impedance that is shown in Figure 5-25(A) indicates no significant change in the Ohmic resistance but there is slight decrease in the reaction resistance after the *HER*. Apparently, the SS-Ni-Mo(2) retains its catalytic activity for up to 2 hours of continuous electrolysis.

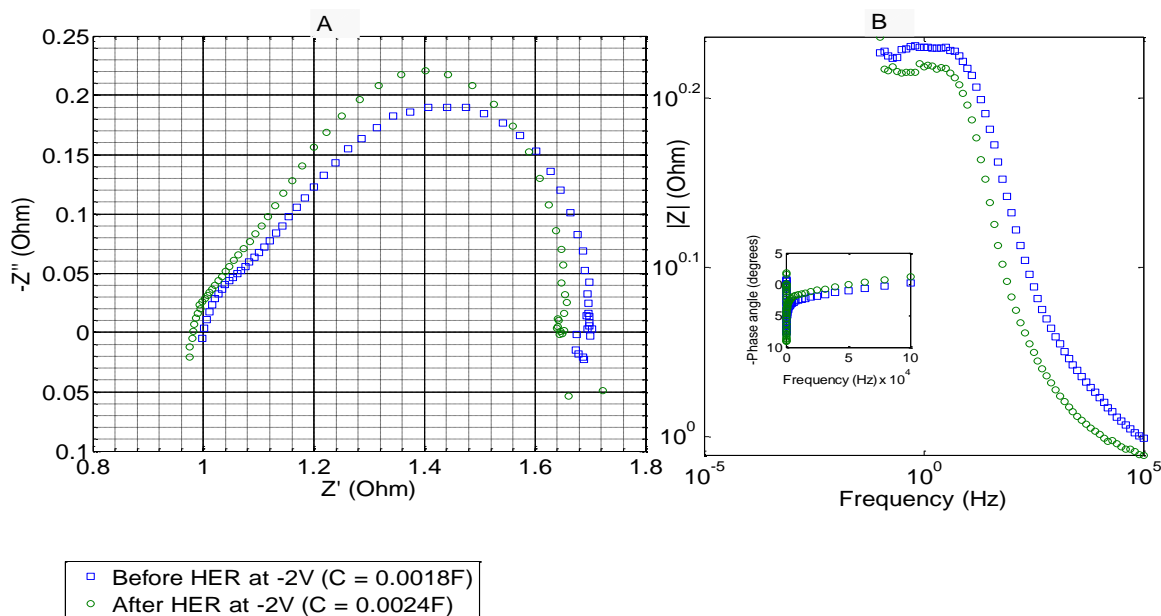


Figure 5-25 Impedance before and after *HER* at $\sim 129 \text{ mA/cm}^2$ for 2 hours on SS-Ni-Mo(2) in 30% KOH at 23°C : (A) Nyquist plot (B) Bode plot

5.4 Comparison of Electro-Catalyst Activity and Effect of pH

The previous sections have dealt with comparing the *HER* and *OER* activities based on the apparent geometric surface area of the electrodes. It is worthwhile, however, to compare the *HER* and *OER* activities based on the ‘real’ surface area of the electro-catalyst in order to account for the electrochemical accessible surface area during electrolysis. The composition and electronic property of Ni-Mo influence on the kinetics for hydrogen and oxygen evolution. For this reason, the intrinsic (real) and geometric (apparent) activities are compared for the SS-Ni-Mo electro-catalyst.

The intrinsic activity depends on the surface roughness factor (R_f). The surface roughness factor accounts for the electrochemical accessible surface area due to deposition of catalyst on the electrode substrate. The surface roughness factor (R_f) is determined based on the ratio of real to geometric active area. A higher surface roughness factor indicates better electro-catalytic behaviour. The real active area is determined by comparing the double-layer capacitance of the electro-catalyst and capacitance of an ideally smooth uncoated electrode substrate as expressed in equation 65[105]:

$$A_{\text{real}} = C_{\text{dl}} (\mu\text{F}) / 20 \mu\text{Fcm}^{-2} \quad (65)$$

As indicated in Table 5-2 surface roughness factor is increased by 9 % and 45 % for the *OER* and *HER* on SS-Ni-Mo(2) respectively. The surface roughness factor is significantly increased for *HER* on SS-Ni-Mo(2), thereby indicating that the electrochemical surface area is increased for hydrogen production.

Table 5-2 Comparison of surface roughness factors for SS-Ni-Mo electro-catalyst

Electrode	$C_{\text{dl } OER}$ (mF) at 2 V, and at 10 kHz-50 kHz	$C_{\text{dl } HER}$ (mF) at -2 V, and at 10 kHz-50 kHz	Anodic (<i>OER</i>) surface roughness factor (R_f)	Cathodic (<i>HER</i>) surface roughness factor (R_f)
SS-Ni-Mo(1) at pH 4.0	14	29	18.0	37.37
SS-Ni-Mo(2) at pH 5.0	15	53	19.33	68.29

Figure 5-26 indicates increase in the apparent activity for *OER* and *HER* on SS-Ni-Mo(2). The Tafel relation also indicates relatively lower overpotential for *HER* and *OER* on SS-Ni-Mo(2) due to its higher apparent activity. In particular, kinetic efficiency for hydrogen production is increased on SS-Ni-Mo(2) due to its relatively higher apparent and intrinsic activities.

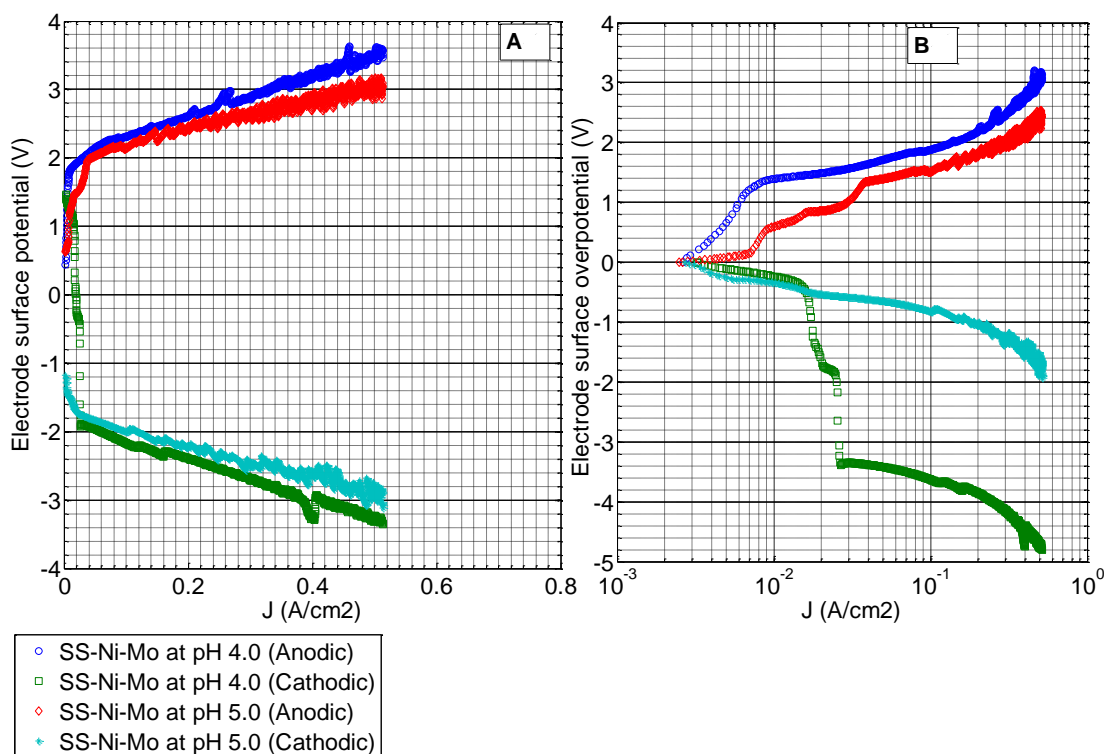


Figure 5-26 DC polarisation of SS-Ni-Mo in 30 % KOH at 23 °C: (A) polarisation comparison for apparent activity (B) Tafel comparison for apparent activity

The hydrogen and oxygen production rates are determined based on the current density at the working voltage of the alkaline electrolyser. As shown in Table 5-3, the oxygen and hydrogen production rates are increased by about 37 % and 64 % respectively on SS-Ni-Mo(2) compared to SS-Ni-Mo(1). This is attributed to increase in the active area and intrinsic activity of the electro-catalyst.

5.4.1 Effect of pH on Electro-Catalyst Activity

It can be seen from Figure 5-26 and in Table 5-3 that the electro-catalyst exhibit significant different properties at slightly varying pH of the electrodeposition bath. This signifies the importance of controlling and maintaining pH of the electrodeposition bath, especially near the electrode surface in order to produce high quality, uniform, homogeneous and porous electrodeposits. The pH of the electroplating bath influence on the current efficiency, and pore formation that takes place due to evolution of hydrogen gas bubbles near the electrode surface. In the electrodeposition of Ni-Mo from citrate bath, the solution pH is usually maintained at acidic conditions [110] in order to facilitate the charge transfer processes

(see equations 64 and 65), promote hydrogen evolution and consequently produce homogenous and porous catalyst coating. However, slight changes in the solution pH especially near the electrode surface could result in significant changes in the characteristics of the electrodeposit. Therefore, it is important to monitor and control the solution pH at a constant acidic condition.

Table 5-3 Hydrogen and Oxygen production rates on SS-Ni-Mo electro-catalyst and effect of pH

Electrode reaction	J_{2V} (A/cm ²)	J_{-2V} (A/cm ²)	*Oxygen production rate (l/hr)	*Hydrogen production rate (l/hr)	Electrical power consumption for <i>OER</i> (W)	Electrical power consumption for <i>HER</i> (W)
SS-Ni-Mo(1) at pH 4.0	0.035	0.077	0.029	0.12	0.27	0.60
SS-Ni-Mo(2) at pH 5.0	0.0479	0.126	0.038	0.20	0.37	0.97

* The oxygen and hydrogen production rates were estimated based on equations 11 and 12 that are described in section 2.2.

5.5 Conclusion of Chapter

The SS-Ni-Mo electro-catalyst can be utilised in the ambient temperature alkaline electrolyser to increase the rates of hydrogen and oxygen production. The kinetics for *HER* and *OER* can be enhanced by utilising the electro-catalyst that has high apparent surface area, high surface roughness as well as possesses the appropriate microporous surface structure. The Ni-Mo catalyst is not only effective in increasing the hydrogen and oxygen production rates but it also protects the underlying SS electrode substrate from passivation thereby enhancing stability and possibly lifetime of the electro-catalyst. In particular, the SS-Ni-Mo is best suited to enhance the *HER* activity and can be employed as cathode in the ambient temperature alkaline electrolyser.

Several attempts in fabricating the SS-Ni-Mo electro-catalyst have revealed that electrodeposition conditions such as control of pH of the electroplating bath determine the quality and characteristics of the electro-catalyst. For this reason, a systematic approach in fabricating and characterising the SS-Ni-Mo electro-catalyst was designed and implemented and is presented in the subsequent chapter.

Chapter 6

Development of SS-Ni-Mo Electro-Catalyst for the Ambient Temperature Alkaline Electrolyser

6.1 Introduction

The ambient temperature alkaline electrolyser is identified as being efficient, durable and relatively low-cost technology for dynamic or continuous (steady-state) operation with renewable energy sources. The ambient temperature alkaline electrolyser is considered for sustainable production of hydrogen and oxygen that can be directly utilised in the alkaline fuel-cell as shown in Figure 2-11. However, the efficiency for hydrogen and oxygen production has to be increased by reducing the overvoltages and simultaneously increasing the operating current density. There are several methods such as: electro-catalysis, optimisation of cell design and operating conditions that can enhance efficiency of the ambient temperature alkaline electrolyser. This chapter however describes fabrication and characterisation of the SS-Ni-Mo electro-catalyst in the ambient temperature alkaline electrolyser to enhance efficiency as well as stability for hydrogen and oxygen production.

The SS-Ni-Mo electro-catalyst was fabricated by electrodeposition and characterised in the ambient temperature alkaline electrolyser. SEM imaging has revealed a rougher morphology of this electro-catalyst. Steady-state polarisation and EIS measurements have revealed increase in activity of the electro-catalyst compared with ordinary stainless steel mesh. The exchange current density increased by 95 % and 35 % for hydrogen and oxygen production respectively, and the electro-catalyst is considerably stable under continuous and intermittent electrolysis for *OER* and *HER*.

6.2 Efficiency of Electro-Catalyst for Hydrogen and Oxygen Production

Electrochemical production of hydrogen and oxygen from water takes place through series of step-wise electron transfer mechanisms. The hydrogen evolution reaction

(*HER*) and oxygen evolution reaction (*OER*) take place at the cathode and anode respectively. The *HER* involves electron transfer mechanisms for adsorption and desorption of hydrogen molecules on the electrode surface [65]. The *OER* also involves electron transfer mechanisms for adsorption of hydroxides, formation of higher oxides and oxygen molecules on the electrode. Equations 66 and 68 describe the Tafel equation for *HER* and *OER* respectively:

$$\eta_{cathode} = 2.3 \frac{RT_K}{\alpha F} \log \frac{i_c}{i_o} \quad (66) \quad \text{Where the cathodic Tafel constant } \beta_c = 2.3 \frac{RT_K}{\alpha F} \quad (67)$$

$$\eta_{anode} = 2.3 \frac{RT_K}{(1-\alpha)F} \log \frac{i_a}{i_o} \quad (68) \quad \text{Where the anodic Tafel constant}$$

$$\beta_a = 2.3 \frac{RT_K}{(1-\alpha)F} \quad (69)$$

The efficiency for *HER* and *OER* can be increased by increasing the exchange current density and reducing the Tafel slope as indicated by the Tafel equations. The electro-catalyst can increase the exchange current density and reduce the Tafel constant. The Tafel constant can be reliably determined from steady-state polarisation measurements while the exchange current density can be reliably determined from EIS measurement of polarisation resistance as expressed in equation 70 [64]:

$$R_p = \left[\frac{RT_K}{nFi_o} \right] \quad (70)$$

The aim of electro-catalysis is to increase the surface area for charge transfer between the electrolyte and electrode. The double-layer capacitance between the electrode and electrolyte can be determined based on the equivalent circuit model for the electrochemical system. For example Figure 6-1 describes the equivalent circuit

model for a smooth electrode that is in contact with the electrolyte such as SS mesh that is in contact with aqueous KOH electrolyte.

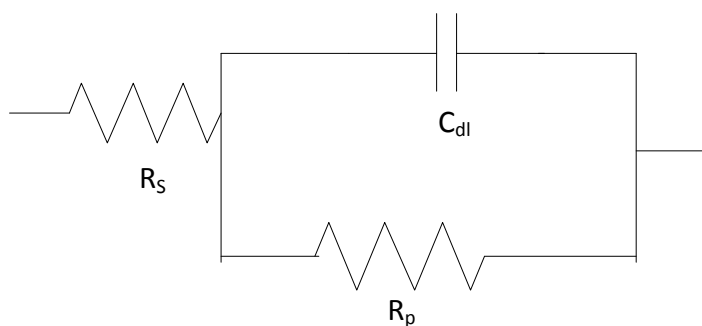


Figure 6-1 Equivalent circuit model for a smooth electrode in contact with electrolyte

The double-layer capacitance of a smooth electrode is determined from the imaginary impedance or reactance based on equation 71:

$$Z'' = \frac{-1}{\omega C_{dl} j} \quad (71)$$

Similarly, Figure 6-2 describes the equivalent circuit model for a rough electro-catalyst that is in contact with the electrolyte, for example SS-Ni-Mo that is in contact with aqueous KOH electrolyte.

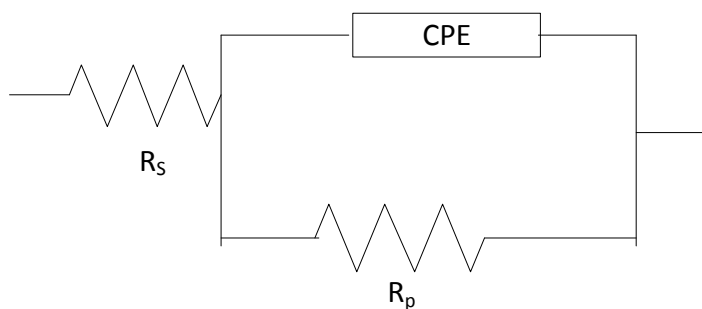


Figure 6-2 Equivalent circuit model for a rough electro-catalyst in contact with electrolyte

It should be noted that in Figure 6-2, the constant phase element (CPE) accounts for several conditions on the electrode such as: surface roughness, varying thickness or composition, non-uniform current distribution, and a distribution of reaction rates

(non-homogeneous reaction rates on the electrode surface) [134]. The CPE impedance is expressed in equation 72 which was originally proposed by Armstrong and Henderson [135-137].

$$Z_{CPE}'' = \frac{-1}{T(j\omega)^P} \quad (72)$$

The double-layer capacitance based on CPE for a rough electro-catalyst surface is described in equation 73 as originally suggested by Brug *et.al* [138].

$$C_{dl} = \left[\frac{T}{(R_s^{-1} + R_p^{-1})^{1-P}} \right]^{\frac{1}{P}} \quad (73);$$

Where P is the CPE co-efficient that characterises the phase shift. For $P = 1 - \gamma$, where $0 < \gamma \leq 0.2$, the CPE corresponds to distortion of the capacitance due to electrode surface roughness or distribution/accumulation of charge carriers, for $P = 0.5 \pm \gamma$, where $0 < \gamma \leq 0.1$, the CPE is related to diffusion, with deviation from the Fick's second law. For $P = 0 \pm \gamma$, where $0 < \gamma \leq 0.2$, the CPE represents distributed resistance. For $P < 0$, the CPE describes inductive energy accumulation [134].

The surface roughness co-efficient essentially is the comparison between double-layer capacitance of the electro-catalyst and capacitance of the smooth uncoated electrode substrate as expressed in equation 74. It describes the electrochemical assessable surface area due to depositing catalyst on the electrode substrate.

$$R_f = \frac{C_{dl} \text{ of electro-catalyst}}{C_{dl} \text{ of the smooth uncoated electrode substrate}} \quad (74)$$

The surface roughness co-efficient is influenced by composition and electronic property of the catalyst deposit. The transition metal alloy such as nickel and molybdenum (Ni-Mo) is reported to have superior *HER* activity due to high surface

roughness causing an increase in apparent and real surface area of the electrode [139–143]. On the basis of the Brewer-Engel bond theory, [108-109] a pronounced synergy takes place by alloying of Ni and Mo. Hence, Ni which has relatively high electron density is alloyed with Mo which has relatively low electron density in order to produce Ni-Mo electro-catalyst that exceeds the catalytic property of Pt at relatively low cost. For this reason, Ni-Mo catalyst is deposited on SS mesh as electro-catalyst in order to enhance efficiency of the ambient temperature alkaline electrolyser.

6.3 Stability of the Electro-Catalyst

The electro-catalyst can increase the efficiency of hydrogen and oxygen production but it might deteriorate or peel off from the electrode substrate during continuous and/or intermittent electrolysis. Instability of the catalyst deposit is largely attributed to poor physico-chemical adhesion of catalyst on the electrode substrate [117,143]. For example Weikang observed [117] that Ni-Mo electro-catalyst was not stable after long period of continuous and intermittent electrolysis due to leaching of Ni and Mo contents in the alkali solution. The Ni and Mo contents have reduced by up to 15 % and 17 % respectively after *OER* in KOH electrolyte at 70°C. The work of Divisek *et al* [118-119] have reported loss in the activity of Raney nickel and Ni-Mo electrodes after long periods of continuous electrolysis due to oxidative dissolution of Al present in the Raney nickel, and Mo respectively. They have observed visible destruction on the electrode surface after electrolysis.

The catalyst activity can reduce over time due to leaching of oxide and hydride products under *OER* and *HER* respectively, and formation of hydroxide products under open-circuit. The current density and time of operation partly determines the rate of electro-catalyst deactivation by reaction products. The current density determines the amount of hydride and oxide products that is formed on the electrode surface and the time of operation determines the rate of formation of reaction products. Under intermittent operation, electrode deactivation could be attributed to formation of reaction products and depolarisation that [117] takes place due to

fuel-cell reactions under open-circuit. In other words, during electrolysis oxide products are formed on the anode and hydride products are formed on the cathode, but during open-circuit, hydroxide products are formed on both electrodes due to depolarisation and reverse current. Leaching of the reaction products largely depend on physico-chemical adhesion of catalyst on the electrode substrate, which is influenced by the nature of the electrode surface. For this reason, adequate pre-treatment of the SS electrode substrate is necessary in order to improve adhesion and stability of the Ni-Mo catalyst.

Stainless steel is difficult to plate substrate because it readily forms a thin naturally protective oxide layer that prevents strong adherence of the catalyst coating. The chromium content in SS readily oxidises in air to form chromium oxide which acts as a protective layer that increases compressive stresses and thereby prevent adherence of the catalyst coating. Some of the pre-treatment methods to improve adhesion of surface coating on stainless steel involve: mechanical roughening, chemical and electrochemical degreasing, pickling or etching in concentrated acid solution, intermediate strike coating and heating after plating. Mechanical roughening of the electrode substrate helps to remove contaminants/impurities on the surface by scratching and also to subsequently promote uniform etching and enhance adhesion of the electrodeposit. The organic based contaminants/ impurities can be effectively removed by dissolution in a suitable organic solvent and/ or electrolytic dissolution in an aqueous alkaline electrolyte. Etching or pickling of the electrode substrate is a form of chemical roughening of the electrode substrate because it results in roughening of the surface for mechanical interlocking or interfingering between the coating and substrate. A thin adherent intermediate coating of the catalyst would serve as base for subsequent coating and thereby improve adhesion. Heating after plating occasionally improves adhesion by promoting rapid diffusion between the coating and substrate [144].

6.4 Experimental

The SS-Ni-Mo was fabricated by electrodeposition and characterised in the ambient temperature alkaline electrolyser that consists of 30 % KOH at 23 °C. Figure 6-3

shows the procedure that was followed for electrodepositing and characterising the electro-catalyst.

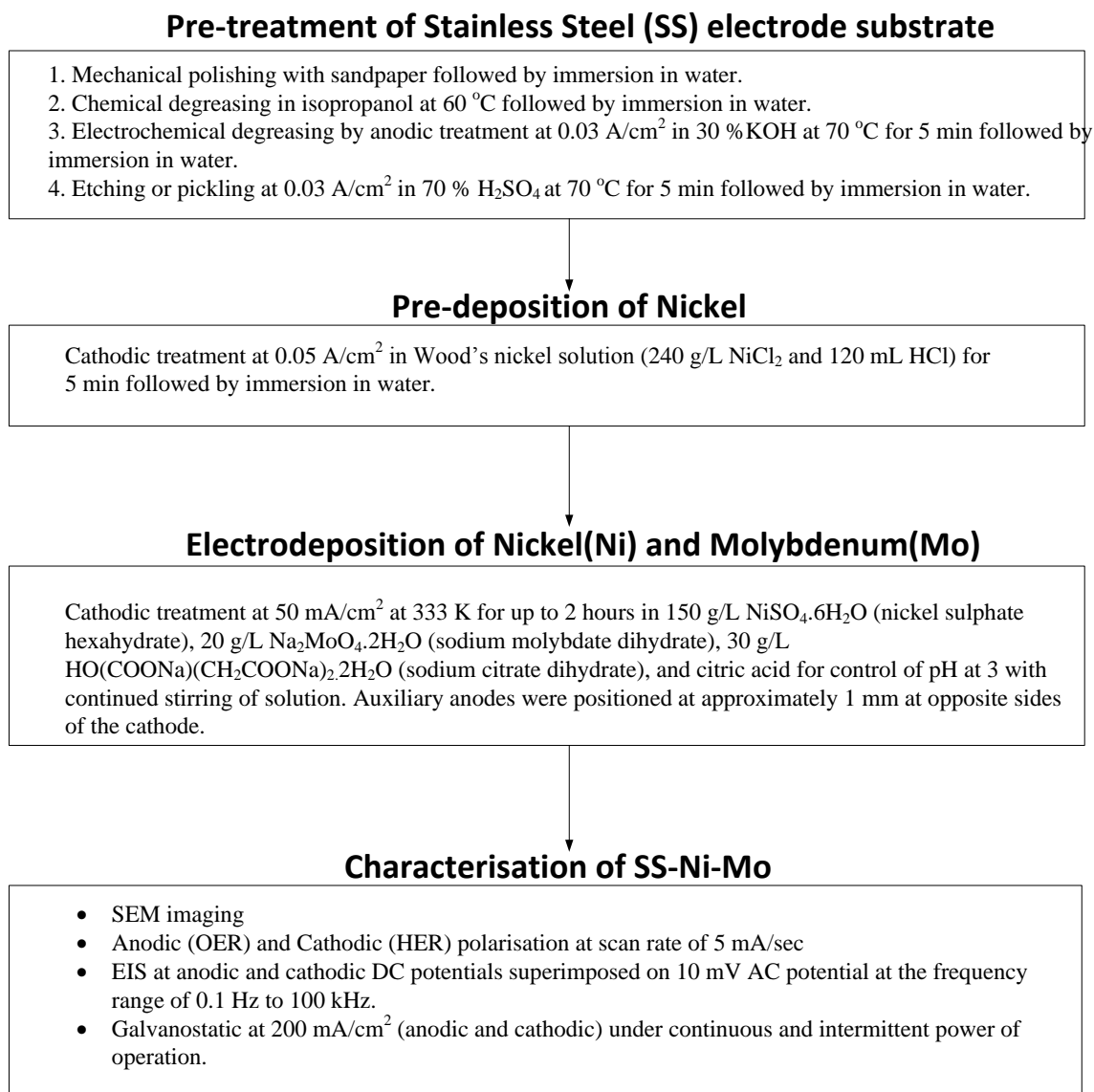


Figure 6-3 Schematic for fabrication and characterisation of SS-Ni-Mo

The separation distance was about 1mm between the working and counter electrodes that are separated by a Celgard® 5550 membrane. The working electrode was either stainless steel (SS) mesh or SS-Ni-Mo that has a geometric active area of about 3.88 cm². The current density was estimated based on this geometric active area. The counter electrode was a smooth SS sheet that has a geometric active area of about 15 cm².

6-5 Discussion of the Results

From Figure 6-4, it can be seen that Ni-Mo is deposited on the SS mesh, although the mesh structure is almost completely covered by high amount of deposited catalyst. Crack formation and rough morphology of the Ni-Mo catalyst however, are evident in Figure 6-5, thereby indicating high apparent surface area of the electro-catalyst. The cathode efficiency in Table 6-1 indicates relatively high rate of electrodeposition of Ni-Mo on the SS mesh.

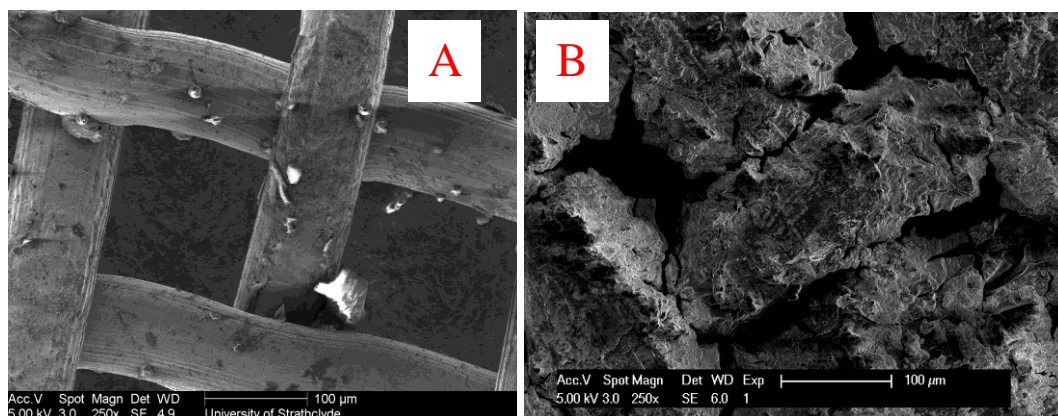


Figure 6-4 SEM images of: (A) SS mesh and (B) SS-Ni-Mo

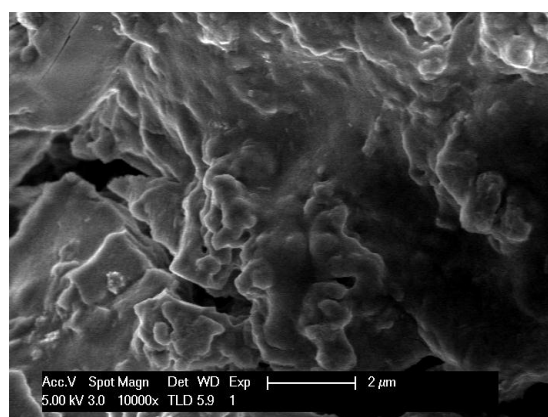


Figure 6-5 Magnified SEM image of SS-Ni-Mo

Table 6-1 Physico-chemical characteristics of the prepared SS-Ni-Mo

Catalyst loading (g/cm^2)	0.016
Cathode efficiency (%)	26
Thickness of deposit (μm)	27.40

Referring to Table 6-1, it should be noted that the thickness of deposit can be determined based on the electrochemical equivalent of the alloy [144] or by taking

cross-sectional SEM imaging of the electrodeposit. In this study, however, the thickness of deposit was determined from the Faraday's relation of equation 75: $T_e = K_e \times J_e \times t_e$ (75), whereby the electrochemical equivalent of the alloy (K_e) was determined based on the electrochemical equivalent of the individual elements of the alloy which were obtained from empirical data in [144].

From Figure 6-6, it can be seen that the overpotential is reduced and current density is increased for hydrogen and oxygen production on SS-Ni-Mo compared with the uncoated SS mesh. For example, for SS-Ni-Mo at -2V, the current density is increased by about 0.1 A/cm² for hydrogen production, while at 2V the current density is increased by about 0.02 A/cm² for oxygen production. Also, for SS-Ni-Mo the Tafel constant is reduced by 4 % and 19 %, while the exchange current density is increased by 33 % and 95 % for *OER* and *HER* respectively. This indicates that *HER* is significantly enhanced on SS-Ni-Mo due to the presence of Ni-Mo catalyst. The Tafel slope for *HER* is in hundreds of millivolts as expected for the reaction mechanism that is governed by charge transfer mechanisms (see section 2.3.1).

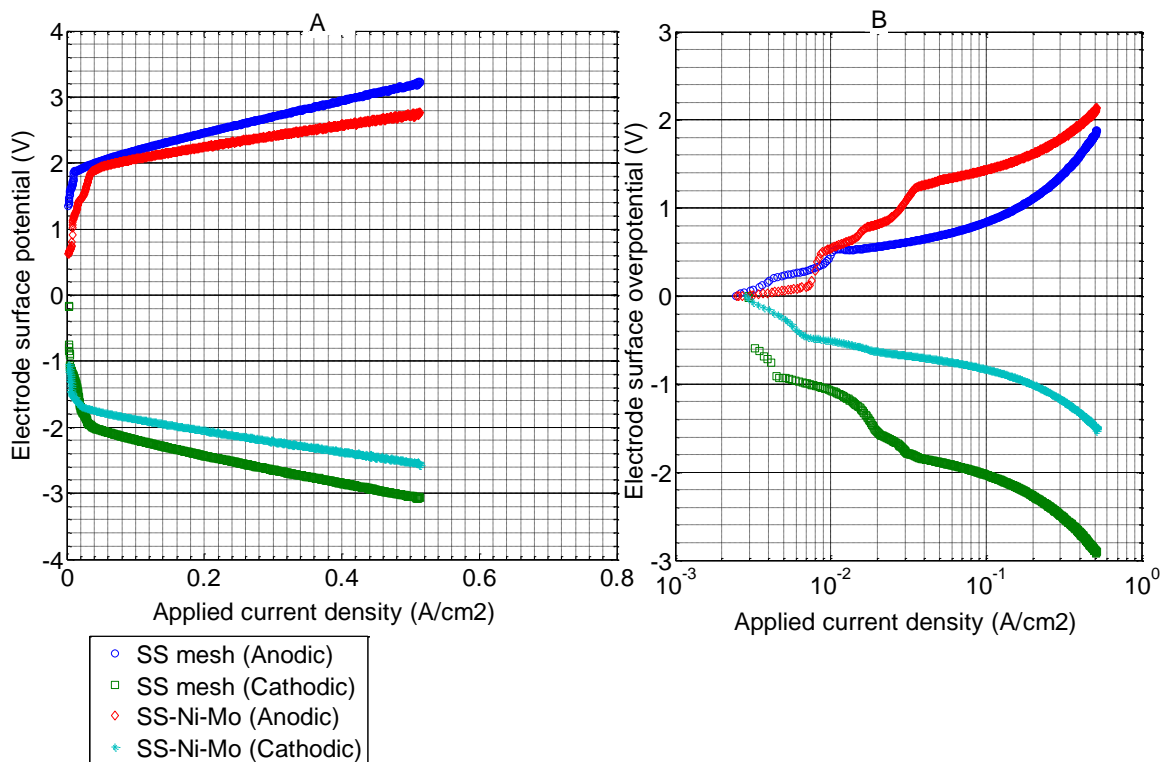


Figure 6-6 (A) Steady-state polarisation and (B) Tafel polarisation for SS mesh and SS-Ni-Mo electro-catalysts in 30 % KOH at 23°C.

The exchange current density is determined from EIS measurement of polarisation resistance as evident in Figure 6-7 and Table 6-2. From Figure 6-7, it can be seen that the semi-circle is more depressed on SS-Ni-Mo. This could be attributed to accumulation of surface charges and the surface roughness [134]. Hence the CPE parameters will be derived for SS-Ni-Mo to elucidate the kinetic processes that take place on this electro-catalyst.

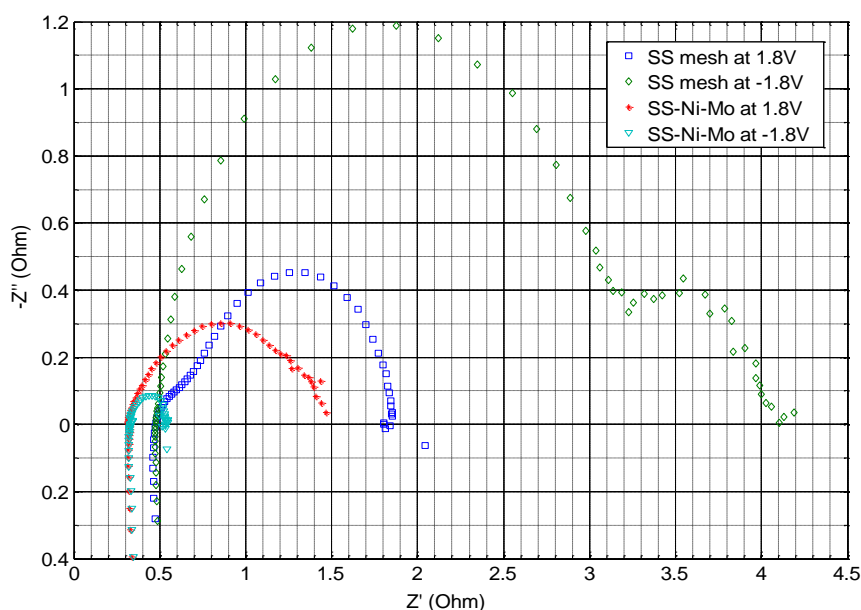


Figure 6-7 Nyquist impedance comparison for SS mesh and SS-Ni-Mo electro-catalyst in 30 % KOH at 23 °C

Table 6- 2 Tafel parameters for SS mesh and SS-Ni-Mo electro-catalyst

Electrode	$ \beta $ (mV)	R_p (Ω)	i_o (mA/cm ²)
SS mesh (anodic)	120.33	1.43	18.0
SS mesh (cathodic)	162.80	2.90	8.96
SS-Ni-Mo (anodic)	115.30	0.96	27.1
SS-Ni-Mo (cathodic)	131.45	0.15	173.3

Impedance measurements were taken for the SS mesh at anodic and cathodic potentials as shown in Figures 6-8 and 6-9 respectively. The Nyquist and Bode plots

are presented, but in this case the Nyquist plot is relevant to derive information about the kinetic processes that take place on the electrode. At all anodic potentials, the Nyquist impedance shows a single capacitive arc which indicates that the electrode reactions are governed only by charge transfer mechanisms. However, at relatively low cathodic potentials, the Nyquist impedance show double capacitive arc which indicates hydrogen gas bubble coverage on the electrode surface. A single capacitive arc, however, is evident at relatively higher cathodic potentials whereby sufficient energy has been supplied to facilitate gas-bubble detachment from the electrode surface. At cathodic and anodic potentials, hydrogen and oxygen gas-bubbles are produced from the electrode respectively. The hydrogen and oxygen gas-bubbles are non-conductive so they increase polarisation resistance by sticking on the electrode surface.

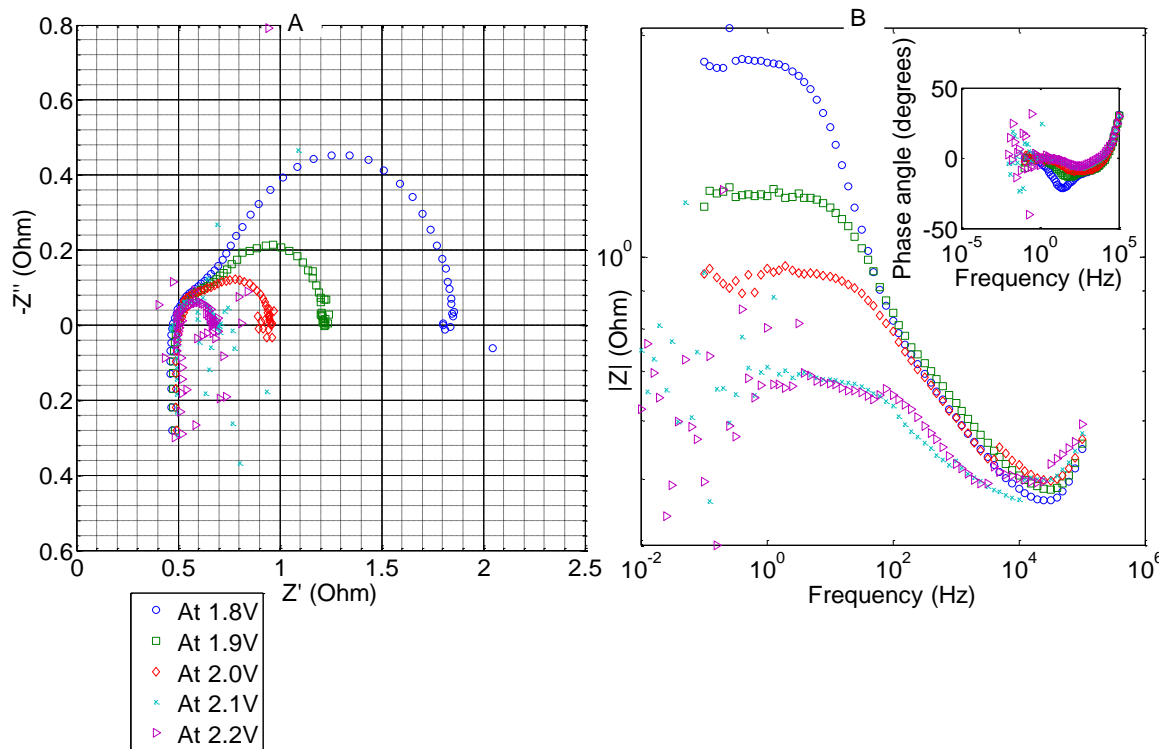


Figure 6- 8 (A) Nyquist and (B) Bode impedance for SS mesh at anodic potentials

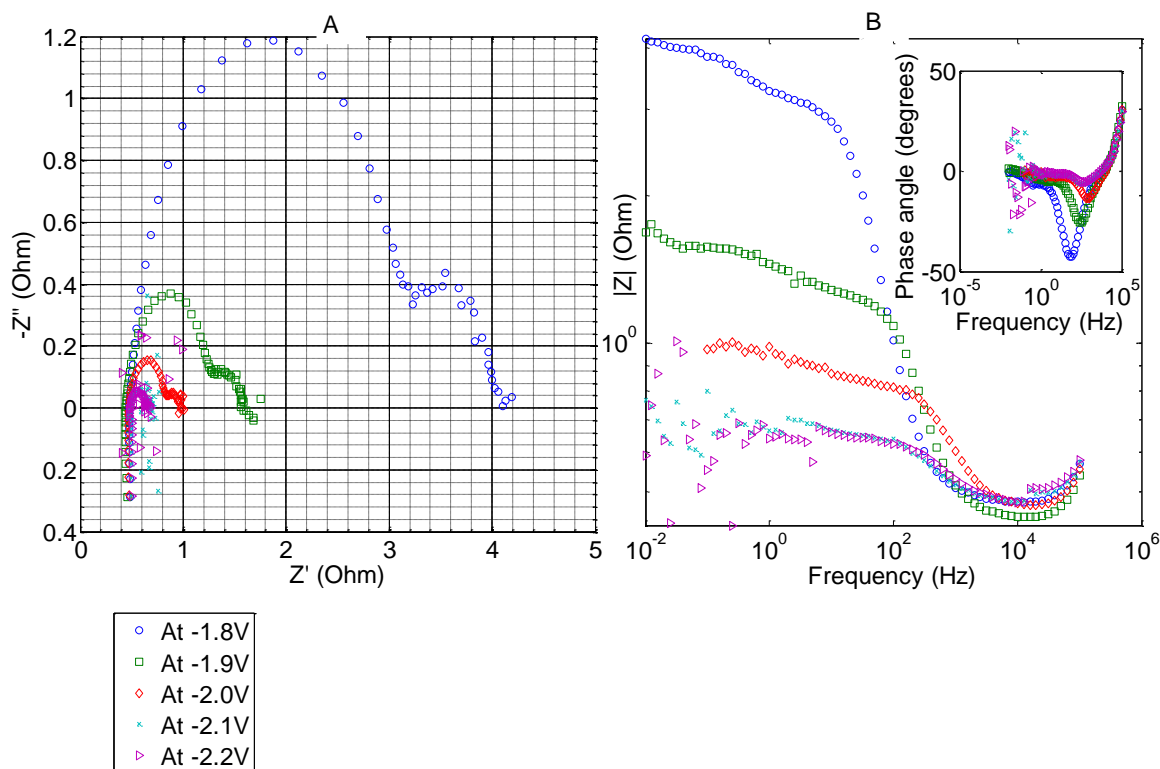


Figure 6-9 (A) Nyquist and (B) Bode impedance for SS mesh at cathodic potentials

As evident in Table 6-3, the double-layer capacitance is reduced as polarisation potential is increased. This is due to increase in the amount of gas-bubbles on the electrode surface, which reduce the electrochemical active area. However, at relatively higher potential for example at ± 2.1 V the double-layer capacitance is increased because sufficient energy is supplied to facilitate detachment of gas-bubbles from the electrode surface. Hence, the electrochemical active area is increased at relatively higher potential. As the potential is increased further, the capacitance as well as electrochemical active area is reduced due to increase in the amount of produced gas-bubbles on the electrode surface. In general, gas bubbles near the electrode surface can result to increase in polarisation resistance, which depends on the cell configuration, operating conditions such as temperature, pressure and electrolyte flow-rate, and operating cell voltage or current density. It should be noted, however, that the reaction rate increases at higher potential as evident by decrease in the reaction time constant that is shown in Table 6-3.

Table 6-3 Resistance and capacitance of SS mesh

Electrode potential	R_s (Ω)	R_p (Ω)	C_{dl} (mF)	* τ (msec)
At 1.8 V	0.568	1.143	5.30	6.058
At 1.9 V	0.590	0.580	3.40	1.972
At 2.0 V	0.543	0.364	2.20	0.801
At 2.1 V	0.504	0.179	6.20	1.110
At 2.2 V	0.507	0.177	5.30	0.938
At -1.8 V	0.500	2.766	2.20	6.085
At -1.9 V	0.468	0.894	1.30	1.162
At -2.0 V	0.498	0.391	0.96	0.375
At -2.1 V	0.505	0.162	4.60	0.745
At -2.2 V	0.508	0.118	3.70	0.437

* The time constant is response of the electrode with respect to electrical load changes and is determined by $\tau = R_p \times C_{dl}$. The reciprocal of time constant is rate constant for the electrode reaction.

Similarly, impedance measurements were taken for SS-Ni-Mo at anodic and cathodic potentials as shown in Figures 6-10 and 6-11 respectively. The Nyquist impedance shows a single capacitive arc at both anodic and cathodic potentials thereby indicating that the electrode reactions are predominantly governed by charge transfer mechanisms. As can be seen from the Nyquist plots, polarisation resistance is increased at relatively low potentials, which could be attributed to the effect of gas-bubbles sticking on the electro-catalyst surface.

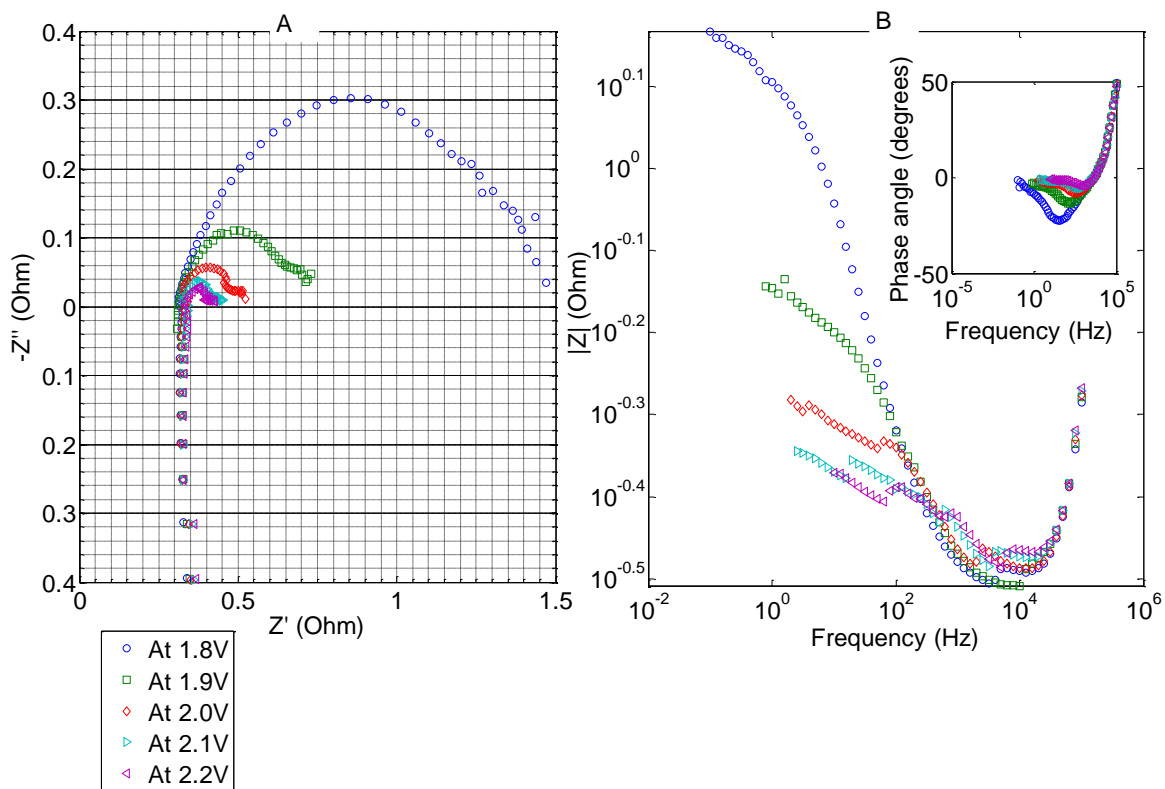


Figure 6-10 (A) Nyquist (B) and Bode impedance for SS-Ni-Mo at anodic potentials

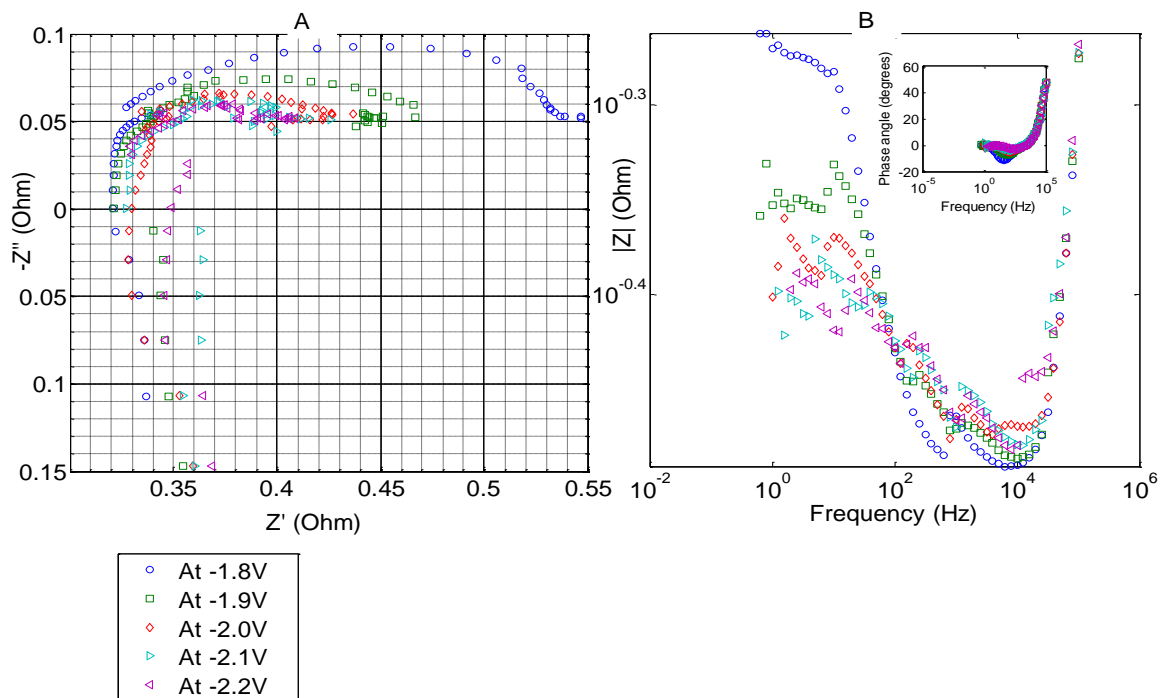


Figure 6-11 (A) Nyquist and (B) Bode impedance for SS-Ni-Mo at cathodic potentials

As shown in Table 6-4, both for the *OER* and *HER*, the double-layer capacitance is reduced as the polarisation potential is increased. By referring to [134] and the CPE exponent derived in Table 6-4, the double-layer capacitance of SS-Ni-Mo is influenced by the electro-catalyst surface roughness, accumulation/distribution of charge carriers and diffusion of the gas-bubbles. At relatively low potentials, the oxygen and hydrogen gas-bubbles stick on the electro-catalyst surface and consequently reduce the electrochemical active area. However, at slightly higher potential the lighter hydrogen gas bubbles are easily removed from the electrode surface. For example at -2.1 V sufficient energy is supplied to facilitate detachment of hydrogen bubbles from the electrode surface, thereby increasing the double-layer capacitance as well as electrochemical active area. As the cathodic potential for *HER* is further increased, the double layer capacitance is reduced possibly due to increase in the amount of hydrogen bubbles on the electrode surface, and accumulation of charge carriers, which consequently reduce the electrochemical active area. The semi-circle is more depressed for SS-Ni-Mo due its rough surface, and it is apparent that surface roughness is higher for *HER* thereby indicating that Ni-Mo is more active for hydrogen production.

Table 6-4 Resistance and capacitance of SS-Ni-Mo electro-catalyst

Electrode potential	R_s (Ω)	R_p (Ω)	$T(\Omega^{-1}s^P)$	P	$C_{dl}(\text{mF})$	R_f	τ (msec)
At 1.8 V	0.30255	1.055	0.057829	0.65728	6.20	1.169	6.541
At 1.9 V	0.30678	0.37425	0.038386	0.69343	4.10	1.206	1.534
At 2.0 V	0.3259	0.16488	0.017468	0.80387	3.80	1.727	0.627
At 2.1 V	0.32487	0.11466	0.041074	0.68797	3.20	0.516	0.367
At 2.2 V	0.33185	0.08233	0.027372	0.73437	2.80	0.528	0.231
At -1.8 V	0.33136	0.21114	0.042613	0.8864	21.90	9.954	4.624
At -1.9 V	0.34056	0.11574	0.034623	0.92433	21.50	16.538	2.488
At -2.0 V	0.34162	0.079506	0.048362	0.86852	20.20	21.042	1.606
At-2.1 V	0.34742	0.062054	0.071418	0.82408	21.70	4.717	1.347
At-2.2 V	0.34594	0.047723	0.052481	0.84202	16.70	4.514	0.797

The activity of SS-Ni-Mo is relatively stable under intermittent electrolysis at 200 mA/cm² for the *HER* and *OER*. As shown in Figure 6-12, the overpotential is fairly stable, even after open-circuit, at an average value of about 2.15 V and 2.25 V for the *HER* and *OER* respectively. The fluctuations in potential and current are due to energy that is exerted by gas-bubbles on the electrode surface. It appears that the Celgard®5550 membrane is suitable in preventing gas-crossover and separating the hydrogen and oxygen gas-bubbles.

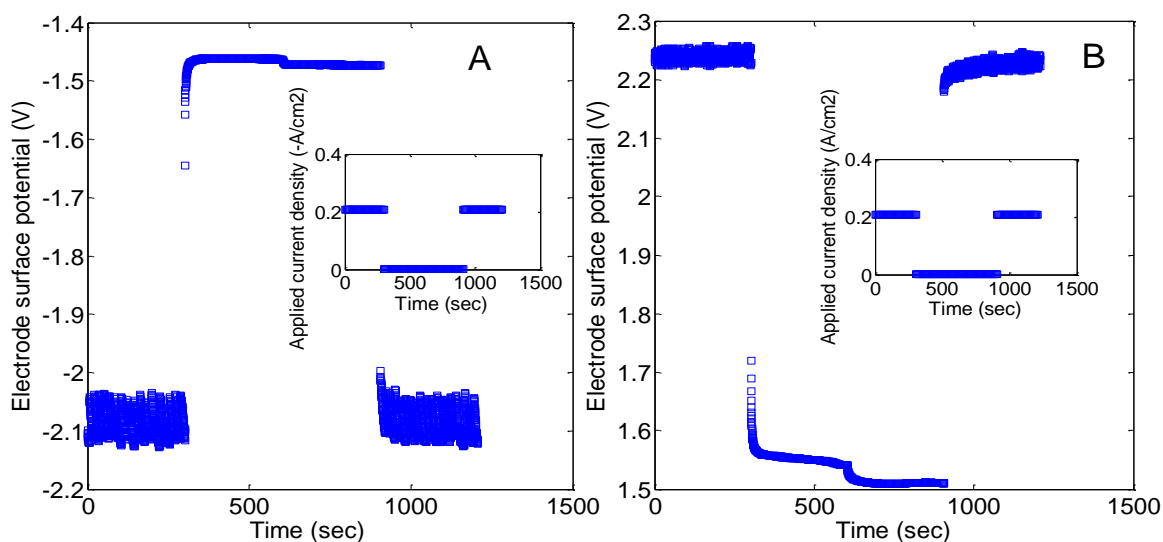


Figure 6-12 Stability of SS-Ni-Mo under intermittent electrolysis at 200mA/cm² for up to 3 cycles for: (A) the *HER* and (B) the *OER*

The activity of SS-Ni-Mo is relatively stable under continuous *OER* at 200 mA/cm² for up to 4 hours. As shown in Figure 6-13(A), the overpotential is almost stable at an average of 2.21 V during electrolysis. The overvoltage is slightly reduced in about 30 minutes of electrolysis possibly due to activation of the electro-catalyst. The current and voltage have fluctuated rapidly due to energy that is exerted by movement of gas-bubbles on the electrode surface. Figure 6-13(B) indicates that polarisation behaviour of SS-Ni-Mo is almost unchanged after *OER*,

but Figure 6-13(C) indicates that the polarisation resistance is reduced by about 0.4Ω after some time of electrolysis. It should be emphasised here that the results indicate that EIS is an effective method to determine slight changes in the activity of the electrode during electrolysis.

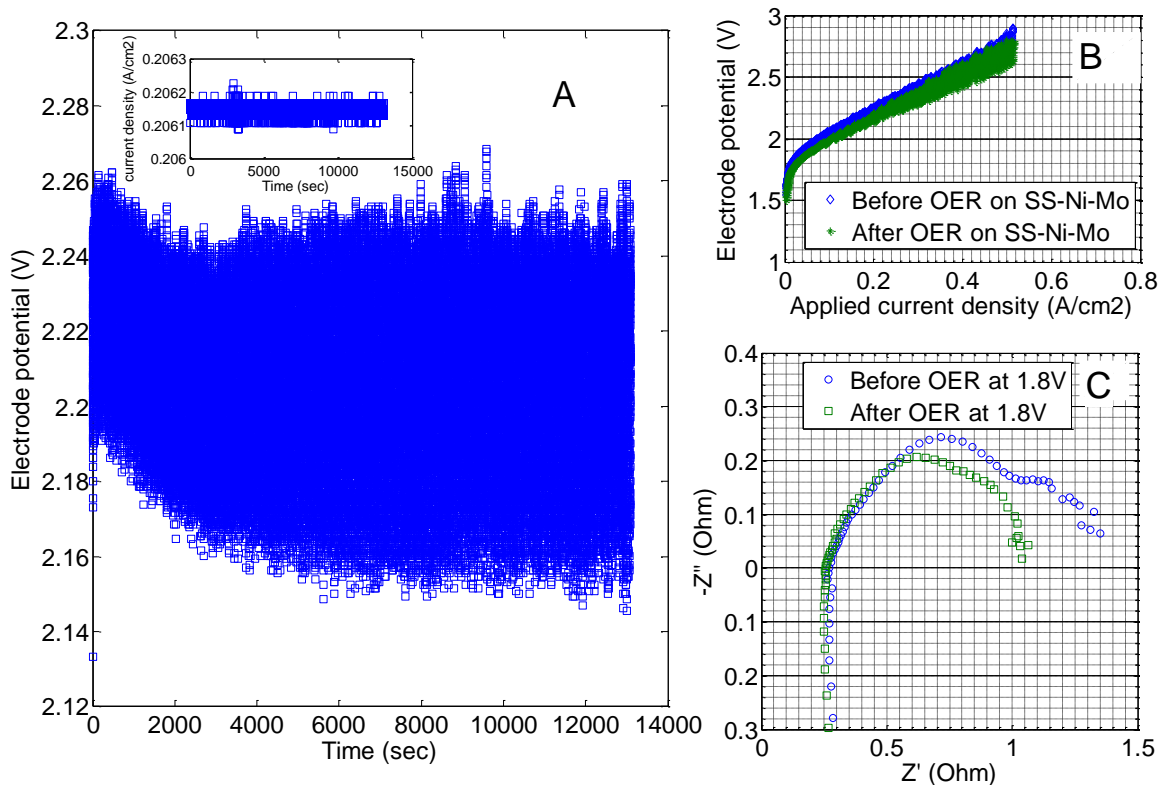


Figure 6-13: (A) Stability of SS-Ni-Mo under continuous electrolysis at 200 mA/cm^2 for the OER; (B) Steady-state polarisation for the OER on SS-Ni-Mo; and (C) Nyquist impedance for the OER on SS-Ni-Mo

The activity and stability of SS-Ni-Mo was investigated under continuous *HER* at 200 mA/cm^2 for up to 24 hours. As shown in Figure 6-14, the overpotential is slightly increased after about 7 hours of continuous electrolysis, which means activity of the SS-Ni-Mo is slightly reduced after about 7 hours of continuous electrolysis. This could be attributed to instability of the Ni-Mo catalyst on the SS mesh.

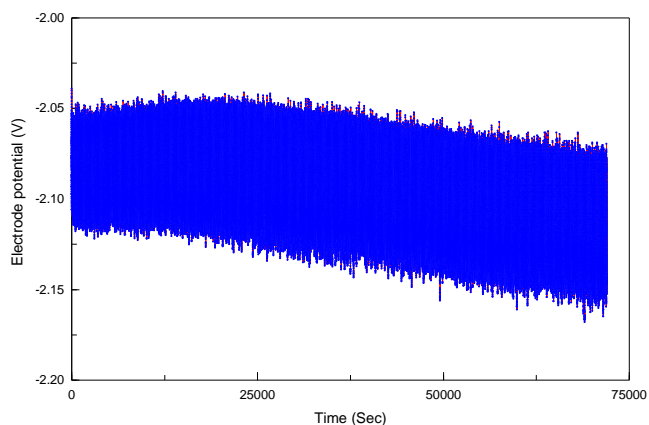


Figure 6-14 Continuous electrolysis on SS-Ni-Mo at 200 mA/cm^2 for the *HER* for up to 24 hours

Figure 6-15(A) indicates no significant change in polarisation after the period of electrolysis but Figure 6-15(B) shows that the polarisation resistance is slightly increased by about 0.089Ω after the period of electrolysis.

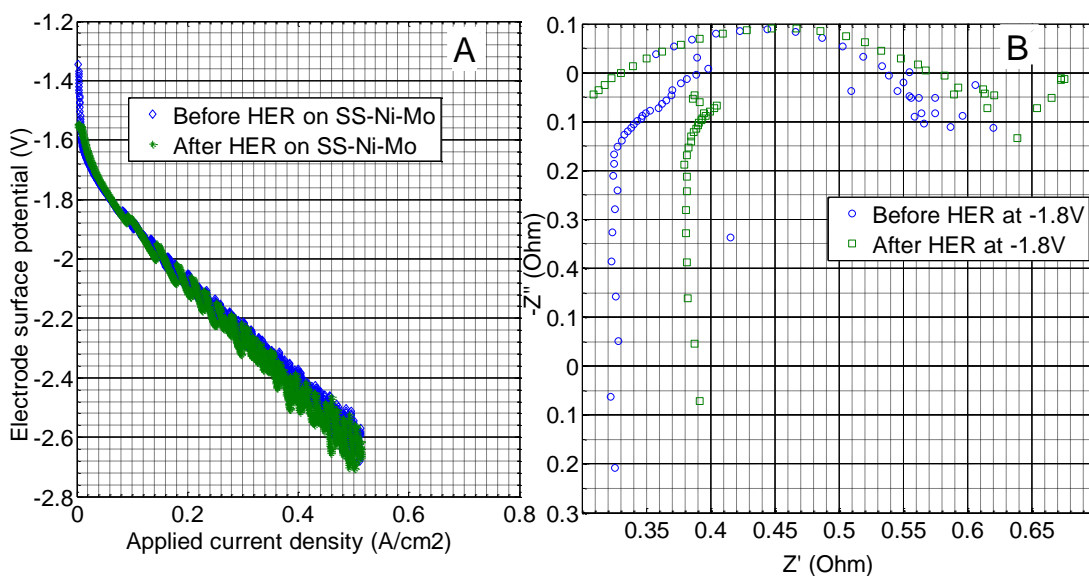


Figure 6-15 (A) Steady-state polarisation for the *HER* on SS-Ni-Mo; **(B)** Nyquist impedance for the *HER* on SS-Ni-Mo

The SEM images of Figure 6-16 indicate that some catalyst materials have been leached out from the electrode substrate after the entire period of variable, intermittent and continuous electrolysis. However, by comparing Figures 6-16 and 6-4(A) it is evident that relatively small amount of Ni-Mo catalyst still remains deposited on the SS mesh after the period of electrolysis. Thus the SS–Ni-Mo slightly retains its activity after the entire period of electrolysis that lasted for up to 24 hours.

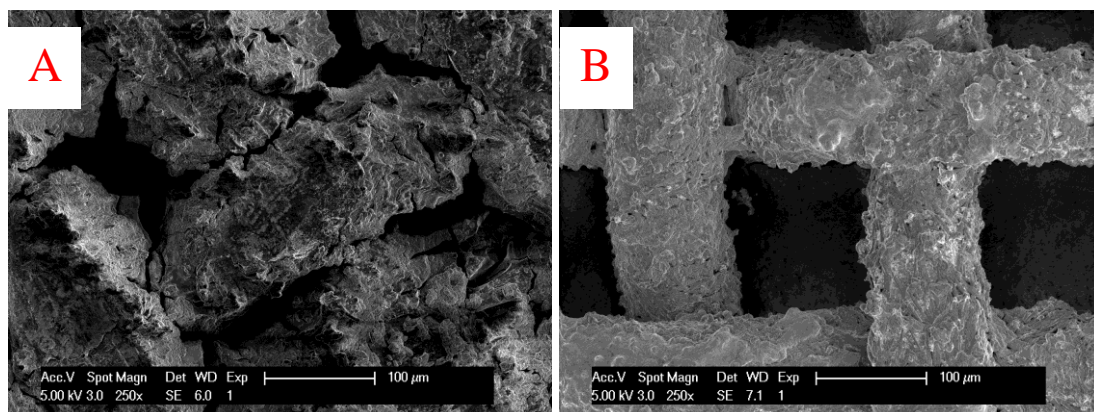


Figure 6-16 SEM images of SS-Ni-Mo: (A) before electrolysis and (B) after electrolysis

In particular from Figure 6-14, it is apparent that activity of SS-Ni-Mo is fairly stable over long period of electrolysis for the *HER*. The SS-Ni-Mo is active for the electron transfer mechanisms of hydrogen adsorption and desorption, although the activity can be slightly reduced due to loss of catalyst material that is accelerated by the generated hydrogen gas-bubbles. There is no doubt however, that adequate pre-treatment of the SS mesh substrate has slightly improved the stability of the Ni-Mo catalyst.

6.6 Conclusion of Chapter

The efficiency for hydrogen production is increased by SS-Ni-Mo electro-catalyst as evident by increase in the exchange current density and decrease in the Tafel constant. It is certain that high surface roughness and intrinsic activity of Ni-Mo catalyst favour the electron transfer mechanisms for hydrogen adsorption and desorption.

The electro-catalyst retains its activity over relatively long period of continuous electrolysis for *OER* and *HER*. However, the activity can be reduced after some time of continuous electrolysis due to loss of catalyst deposits from the electrode substrate. It is demonstrated, however, that stability can be enhanced for the electro-catalyst by adequate pre-treatment of the electrode substrate and by operating in the ambient temperature alkaline electrolyser.

Chapter 7

Construction of the Flow-Cell Ambient Temperature Alkaline Electrolyser for Characterising the Electrode

7.1 Introduction and Description of the Cell Components

The previous chapters have dealt with systematic approaches to fabricate an efficient and stable electrode for the alkaline electrolyser. The next two chapters however deal with design, construction and operation of the alkaline electrolyser cell that consists of the fabricated electrode and electro-catalyst. The alkaline electrolyser cell was designed based on the bi-polar filter press principle that is described in Section 2.6. The cell is manifolded to allow flow of KOH electrolyte across the electrode, and for collecting the product gases. The cell components consist of electrode and electrolyte compartments which are assembled together with end plates. The end plates have an optical ‘Sapphire’ window to enable visual inspection inside the cell. Stainless steel rods, nuts and washers as well as Viton O-rings were used for sealing of the entire cell assembly. The monopolar flow-cell consists of two electrodes whereas the multi-cell configuration consists of four electrodes.

7.1.1 Electrode Compartment

As shown in Figure 7-1, the electrode is sandwiched between two corrosion resistant PVC plates and sealed using stainless steel screws.

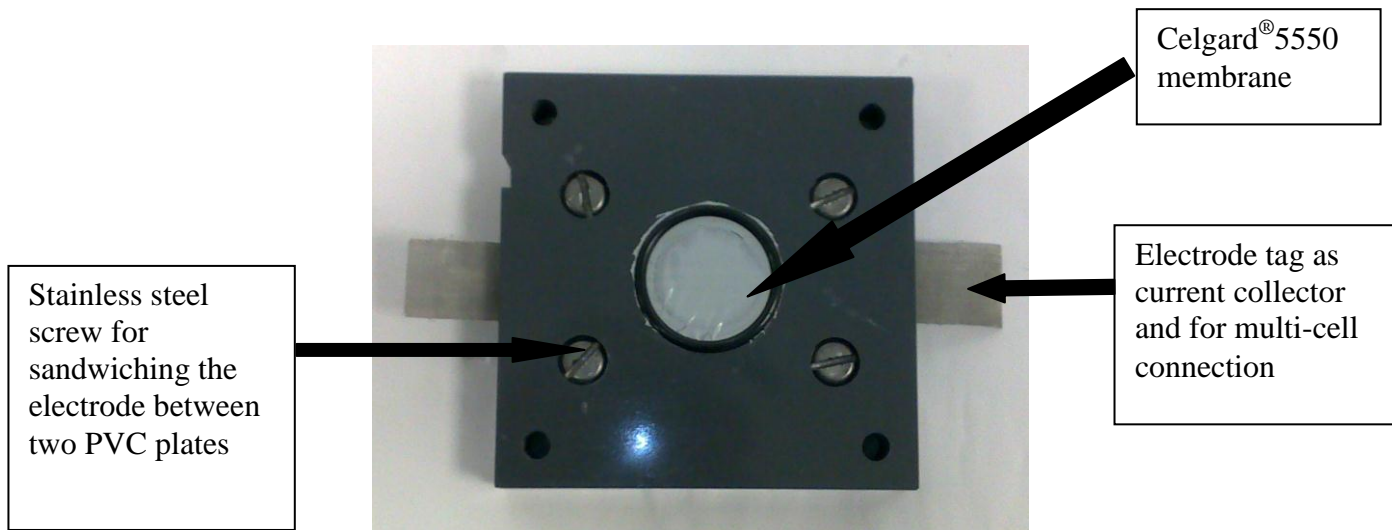
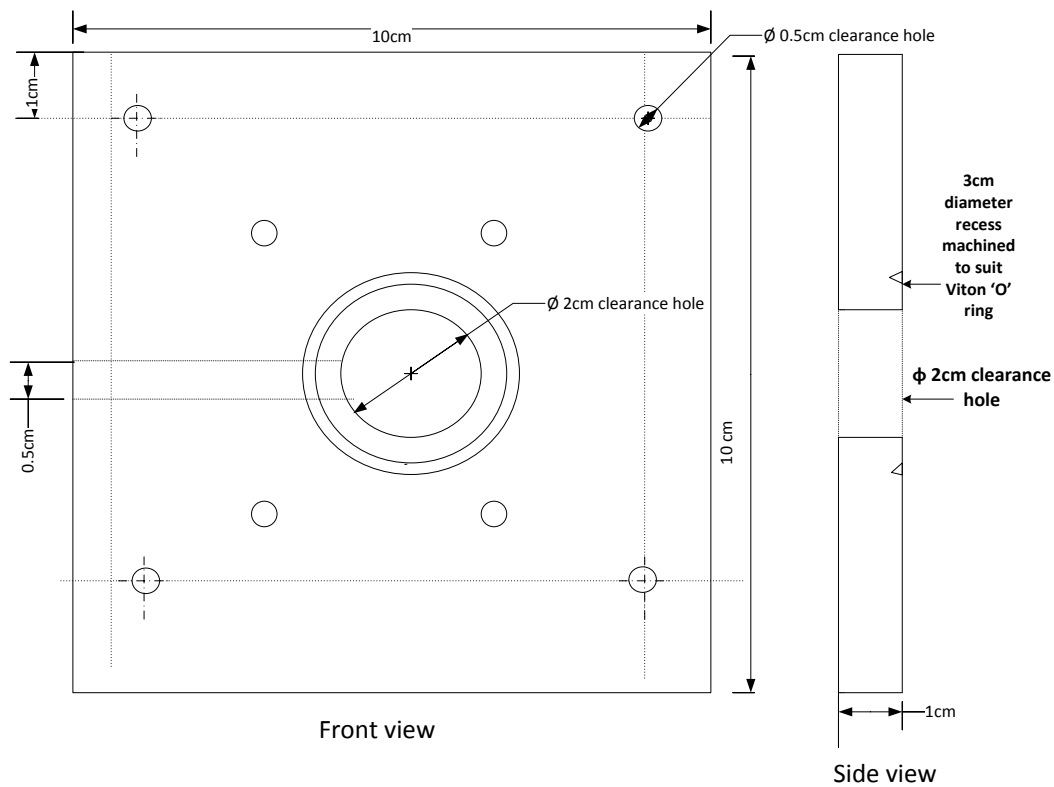


Figure 7-1 Image of electrode compartment of the alkaline electrolyser cell

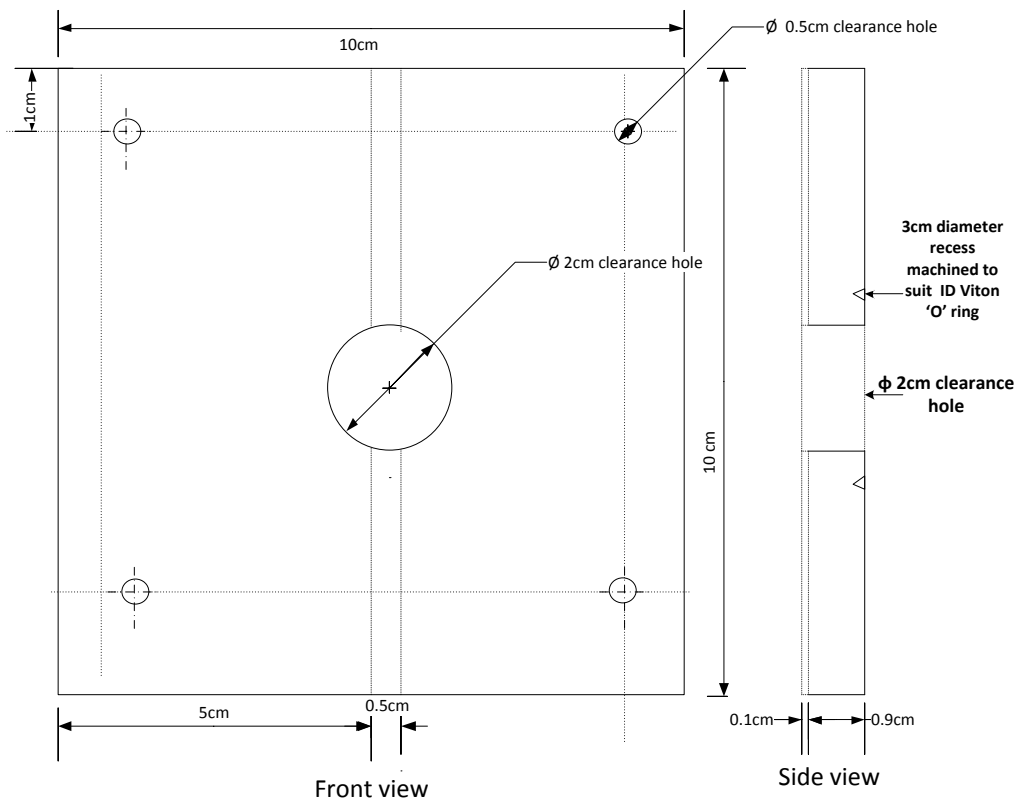
The technical drawings in Figures 7-2 and 7-3 show the two separate parts of the electrode compartment that are screwed together. A 2 cm diameter hole is made in the centre of the compartment in order to create a ‘circular’ shape electrode that has a geometric active area of 3.88 cm². The electrode protrudes from both sides of the compartment to allow for current collection and multi-cell connection. A recess is made in the compartment in order to accommodate the Viton O-ring for sealing of the entire cell. The membrane is sealed with Viton-O ring between the electrode compartments.



PROJECT:H-Delivery Electrode compartment part 1		QTY	SIZE	Checked by	REV;DAT E
DRAWN	T.Douglas	2 off	10cmx10cm		
ISSUED January 2011	SCALE	Material of construction: PVC plastic		SHEET	3 OF 4



Figure 7-2 Technical drawing of electrode compartment-part 1 of the alkaline electrolyser cell



PROJECT:H-Delivery Electrode compartment part 2		QTY	SIZE	Checked by	REV;DATE
DRAWN	T.Douglas	2 off	10cmx10cm		
ISSUED January 2011	SCALE	Material of construction: PVC plastic		SHEET	4 OF 4



Figure 7-3 Technical drawing of electrode compartment-part 2 of the alkaline electrolyser cell

7.1.2 Electrolyte Compartment

The electrolyte compartment is made from PVC plastic and has flow channels on opposite sides as shown in Figure 7-4 and in the technical drawing of Figure 7-5. The flow channels enable inlet and outlet of the KOH electrolyte as well as product gases via PVC tubes. A 2cm diameter hole is made in the centre in order to allow contact of the electrolyte and electrode active area. The electrolyte compartment can contain KOH liquid of up to 2.51cm^3 . A recess is made in the compartment in order to accommodate the Viton-O ring for sealing of the entire cell.

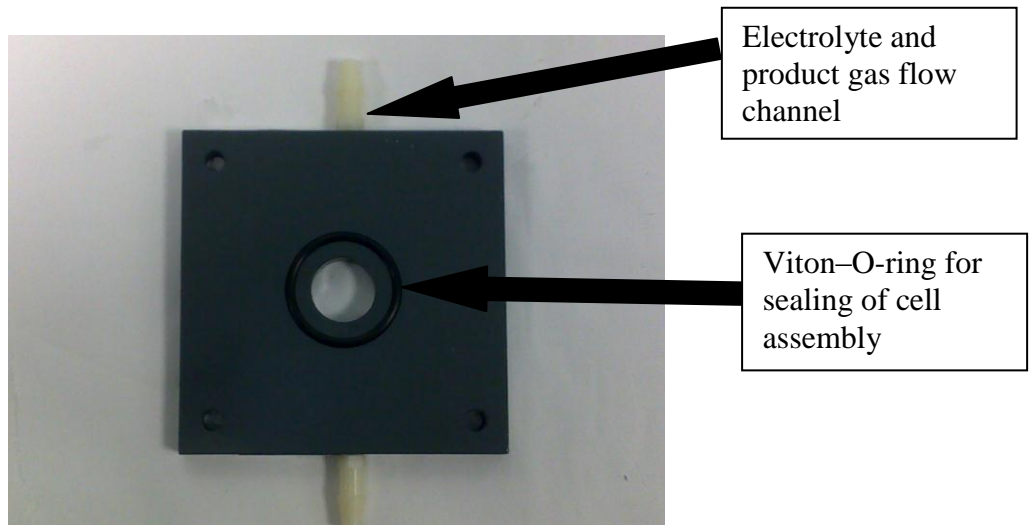
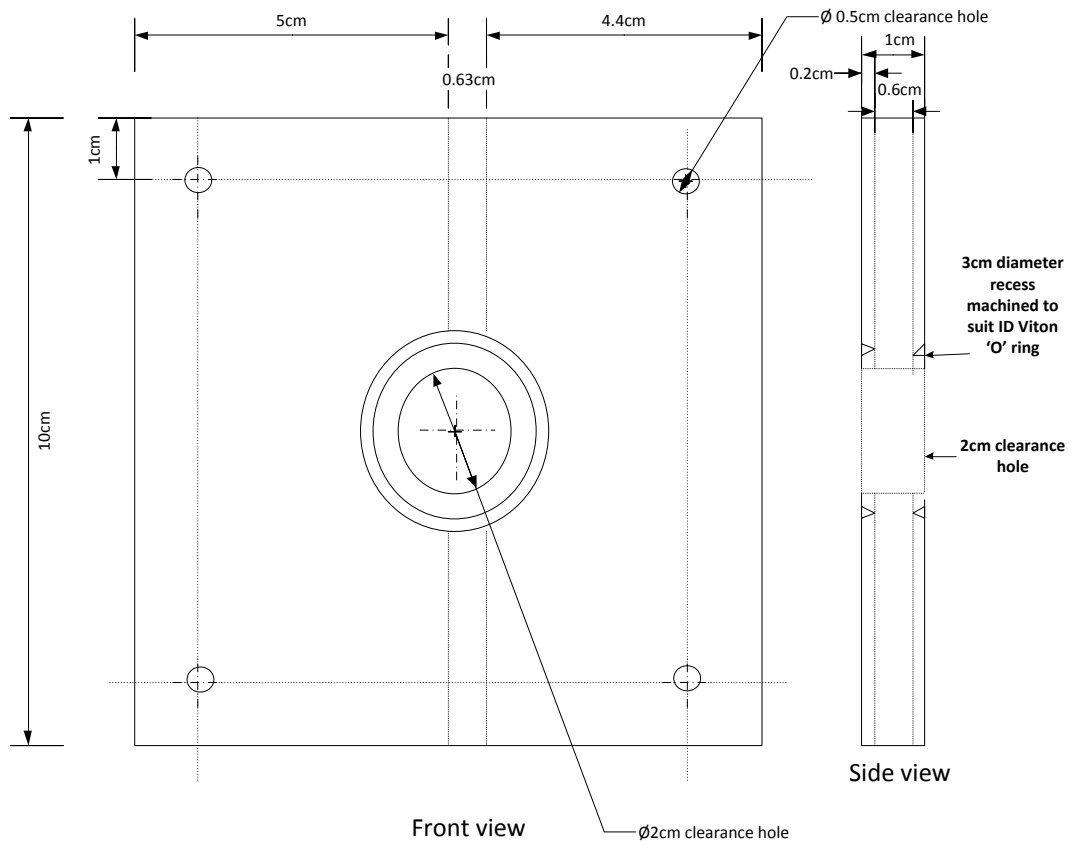


Figure 7-4 Image of electrolyte compartment of the alkaline electrolyser cell



PROJECT: H-Delivery Electrolyte compartment		QTY	SIZE	Checked by	REV; DATE
DRAWN	T. Douglas	X 2 off	10cm x 10cm		
ISSUED January 2011	SCALE	Material of construction: PVC plastic		SHEET	3 OF 4



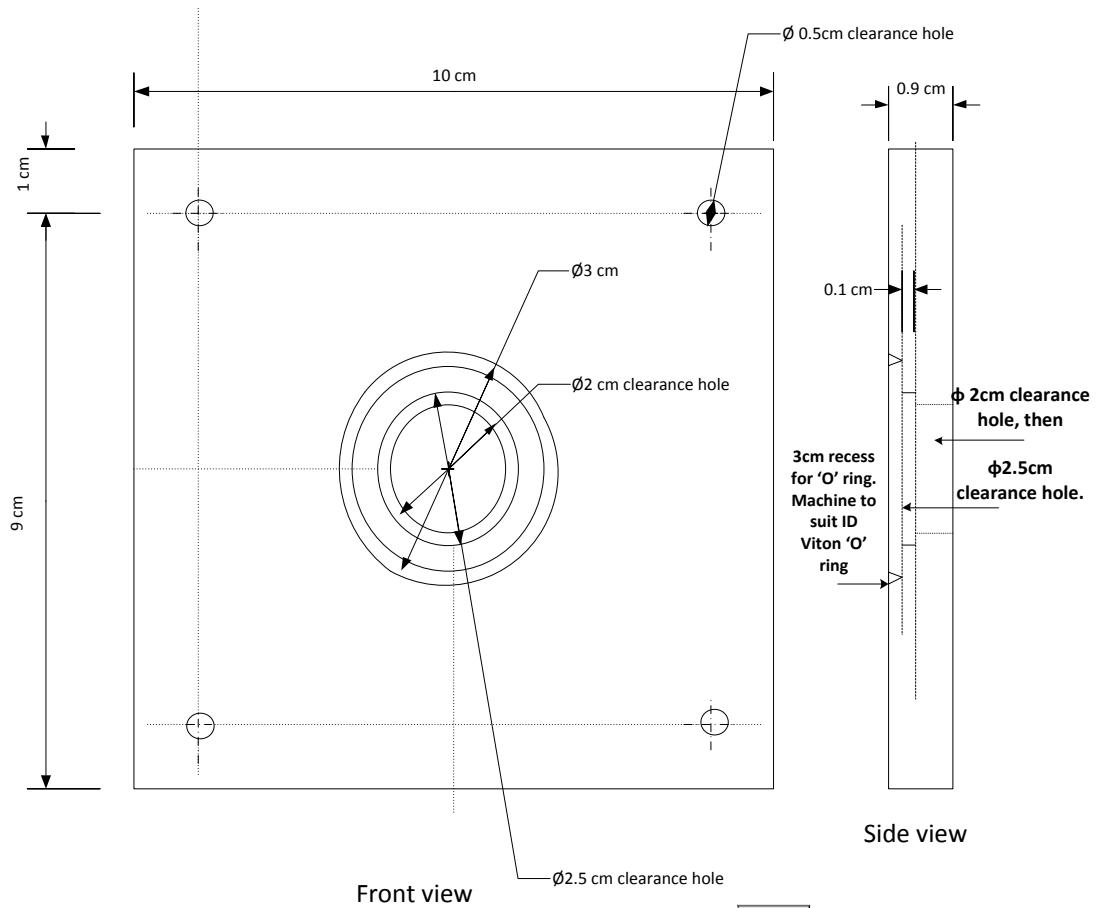
Figure 7-5 Technical drawing of electrolyte compartment of the alkaline electrolyser cell

7.1.3 End Plates and Cell Assembly

A hole was made in the centre of the end plates in order to accommodate the optical ‘Sapphire’ window that allows visual inspection inside the cell. The cell then was assembled and held together using stainless steel rods, nuts and washers as shown in Figure 7-6 and the corresponding technical drawing is shown in Figure 7-7.



Figure 7-6 End plates and cell assembly



PROJECT: H-Delivery End plate		QTY	SIZE	Checked by	REV; DATE
DRAWN T.G. Douglas		2 x off	10cmx10cm		
Issued: Sept; 2010	SCALE	Material of construction: PVC		SHEET	1 OF 4

Figure 7- 7: Technical drawing of end plate of the alkaline electrolyser cell

The assembled cell has a dimension of about 10 cm (L) x 10 cm (W) x 12 cm (H) and weighs up to 10kg. Table 7-1 provides some specific information of the cell.

Table 7-1: Specifications of the flow-cell alkaline electrolyser

Separation distance between the electrodes	Electrical Power Capacity	Type of Membrane
3 cm	1W	Celgard [®] 5550 membrane

7.2 Experimental Measurements and Discussion of the Results

The alkaline electrolyser cell is characterised as electrical load by DC polarisation and EIS measurements. The cell current was varied from 0.1 A to 2 A in step change of 5 mA/sec. The impedance was measured at the frequency range of 100 kHz to 0.1 Hz and at constant AC amplitude of 10 mV. The anode and cathode electrodes have equal geometric active areas of 3.88 cm² and the cell current density is estimated based on this active area. A Celgard[®]5550 membrane was used to separate the electrodes at a separation distance of 3 cm. The multi-cell configuration was designed according to Figure 2-14 such that the middle anode and cathode electrodes were separated at a distance of 1 mm. The KOH electrolyte solution was circulated in the cell at atmospheric pressure.

7.2.1 Monopolar Flow-cell Configuration

As can be seen in Figure 7-8, for the cell that consists of SS mesh type-304 electrode (see Table 4-1 for details of this electrode), the overvoltage increased rapidly after some time of electrolysis at a high current density ($> 0.4 \text{ A/cm}^2$). During this test, the cell overvoltage increased due to over polarisation caused by the relatively low electrode surface area and relatively large separation distance between the electrodes.

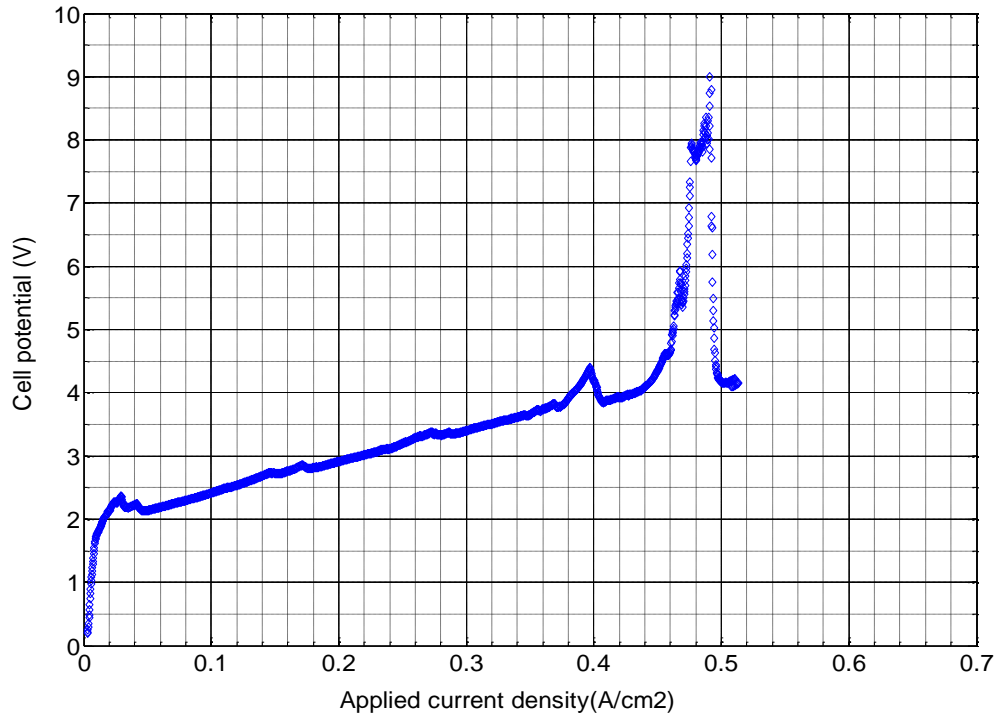


Figure 7-8 Polarisation of SS electrodes in the monopolar flow-cell alkaline electrolyser that consists of 30 % KOH at 23°C

As evident in Figure 7-9, the reaction and Ohmic resistances are relatively high. The reaction resistance increased due to gas-bubble coverage on the electrode thereby reducing the electrochemical surface area. The Ohmic resistance increased due to transport resistance of electro-active ions, and possibly back diffusion of gas-bubbles into the electrolyte solution, which reduce electrolyte conductivity. During electrolysis, if there is no effective method to remove the gas-bubbles, the gas bubbles would stick to the electrode surface and also diffuse into the electrolyte solution i.e. back diffusion; this result in reducing electrochemical active area between the electrode and electrolyte and consequently increase the overpotential.

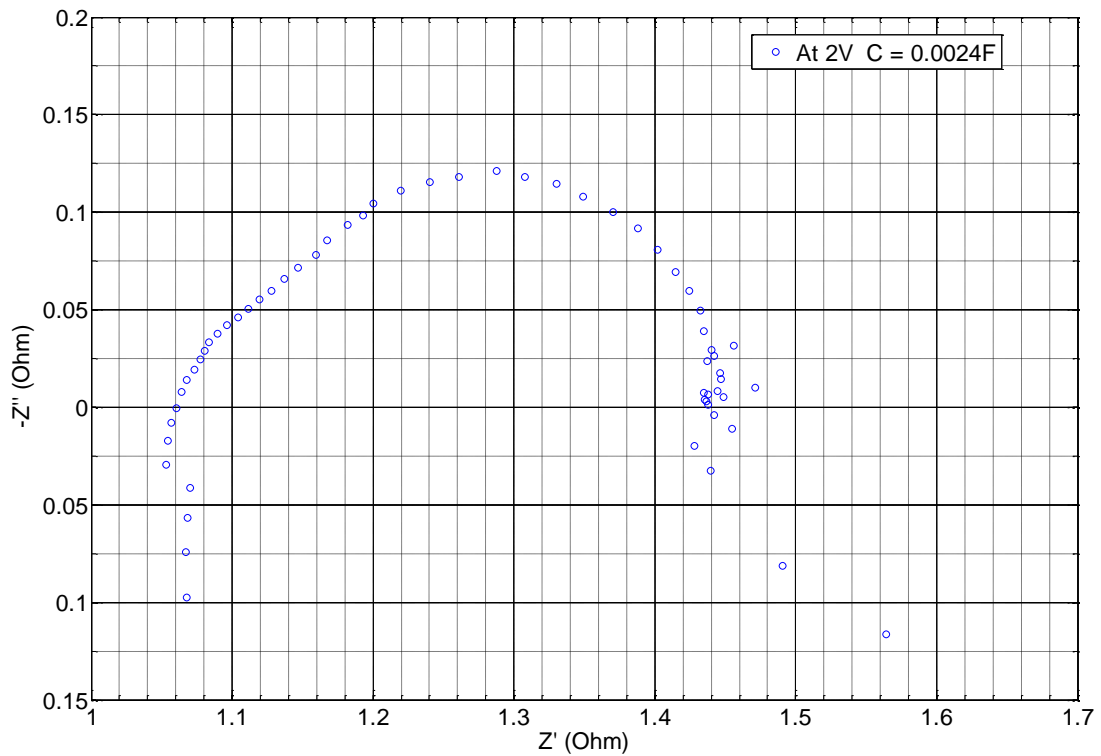


Figure 7-9 Nyquist impedance of SS electrode in the monopolar flow-cell alkaline electrolyser that consists of 30 % KOH at 23 °C.

From Figure 7-10, it can be seen that the Ohmic and reaction resistances are dependent on the applied cell voltage. At relatively low cell voltages, Ohmic and reaction resistances are increased. The Ohmic resistance is increased due to back diffusion of gas-bubbles which reduce electrolyte conductivity. The reaction resistance is increased due to gas-bubble coverage which reduces electrochemical active area of the electrode. At relatively high cell voltages, however, the electrodes are activated so that Ohmic and reaction resistances are reduced. The double-layer capacitance is increased at high cell voltages due to increase in electrochemical active area of the electrode. The gas-bubbles are non-conductive so by increasing the cell voltages the electrodes become activated to facilitate gas-bubble detachment from the surface thereby increasing electrochemical active area.

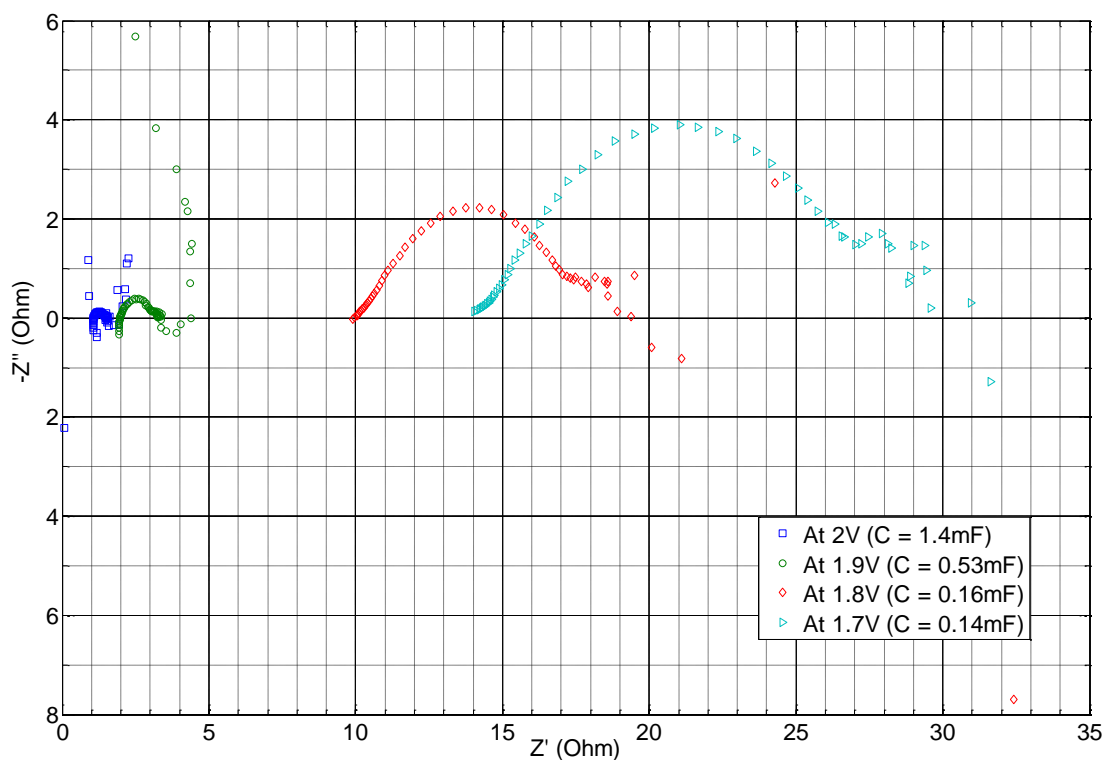


Figure 7-10 Nyquist impedance of the SS electrode in the monopolar flow-cell alkaline electrolyser at varying cell voltages in 30 % KOH at 23 °C.

7.2.2 Bi-polar Multi-cell Configuration

The bi-polar flow-cell was constructed as a multi-cell configuration that is shown in Figures 7-11 and 7-12. The cell components (electrode and electrolyte compartments as well as end plates) were designed and fabricated as described in section 7.1. This bi-polar multi-cell consists of SS-Ni-Mo electrode. The initial DC polarisation and AC impedance measurements that were carried-out on this cell had indicated major over-polarisation and extremely high internal cell resistance. Although it was obvious that there were major problems with the physical set-up, which has led to electrolyte leakage; the contact resistance between the electrode and electrical power source also had a significant influence on the overpotential and cell performance. A current collector was later attached to the cell in order to reduce the contact resistance of the electrical circuit between the electrode and electrical power source.

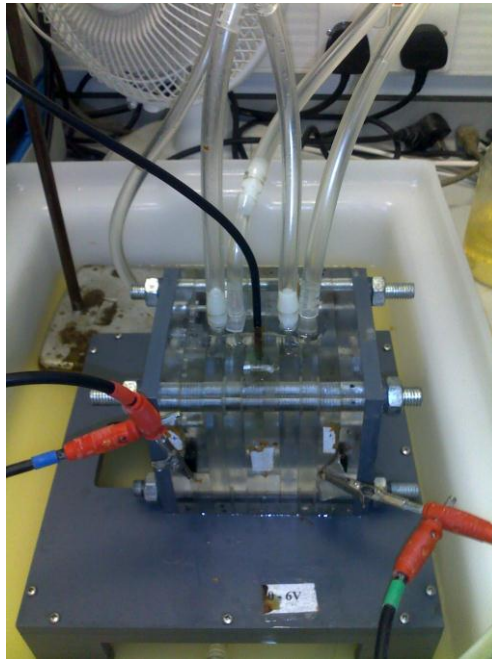


Figure 7-11 Image of the bi-polar multi-cell alkaline electrolyser

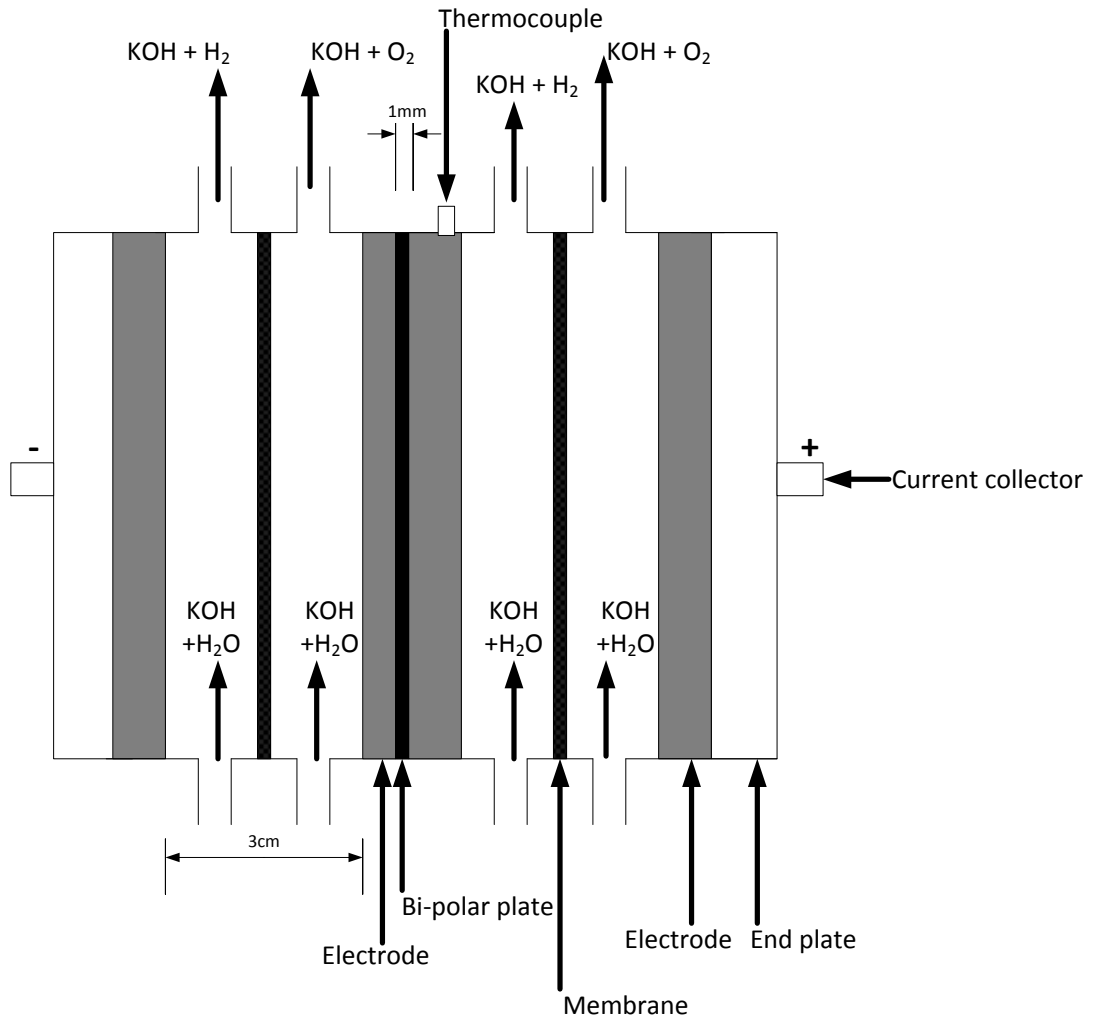


Figure 7-12: Schematic illustration of the bi-polar multi-cell alkaline electrolyser

The internal cell resistance as well as overpotential can be minimised by ‘point-wise’ current collection. As similar with Figure 2-14, Figure 7-12 illustrates the bi-polar flow-cell configuration that consists of ‘point-wise’ current collector in order to reduce electrical resistance of the circuit. Also in Figures 7-13 and 7-14, it is shown the flow-cell configuration that is designed and constructed with ‘point-wise’ current collector. It should be noted that a type-K thermocouple was attached to the electrodes in these cells in order to measure and monitor the cell’s internal temperature. The internal temperature rise of the electrolyte however was determined based on equation 10 in Chapter 2.

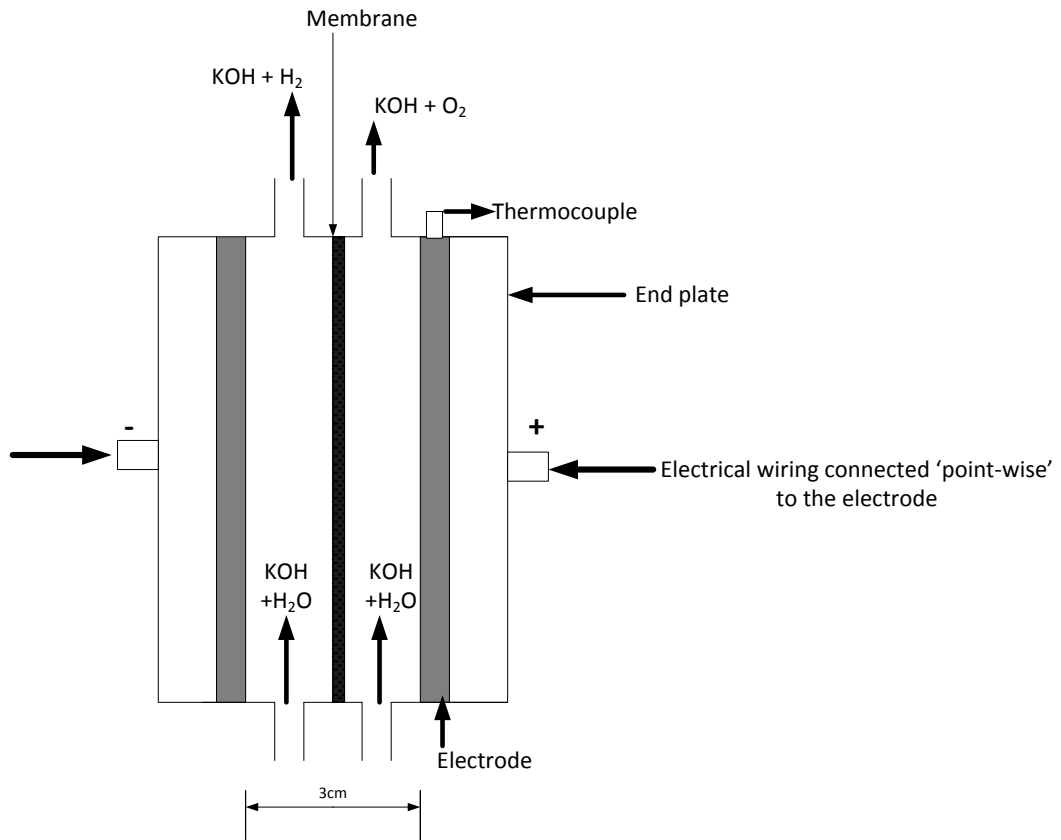


Figure 7-13: Schematic illustration of the flow-cell alkaline electrolyser that is constructed with 'point-wise' current collector

Figure 7-14 shows the flow-cell alkaline electrolyser that consists of 'point-wise' current collector; and as shown in Figure 7-15 the cell voltage is relatively low and varies with current density as expected for a normal working alkaline electrolyser cell.

'Point-wise'
current collector

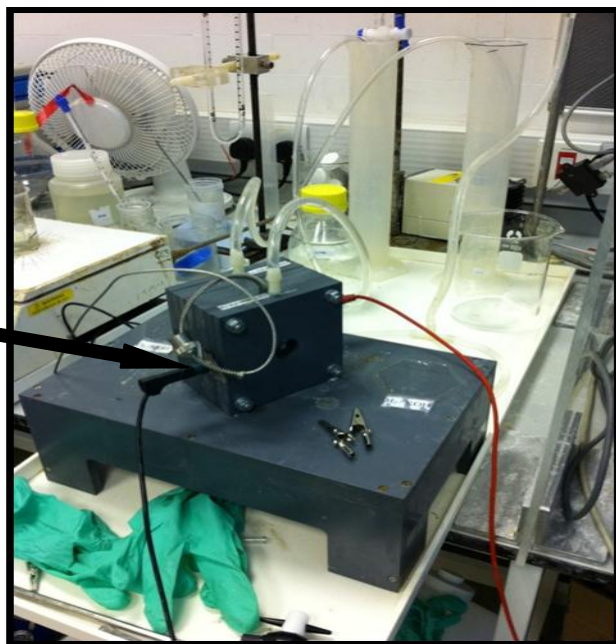


Figure 7-14 Image of the flow-cell alkaline electrolyser that is constructed with 'point-wise' current collector

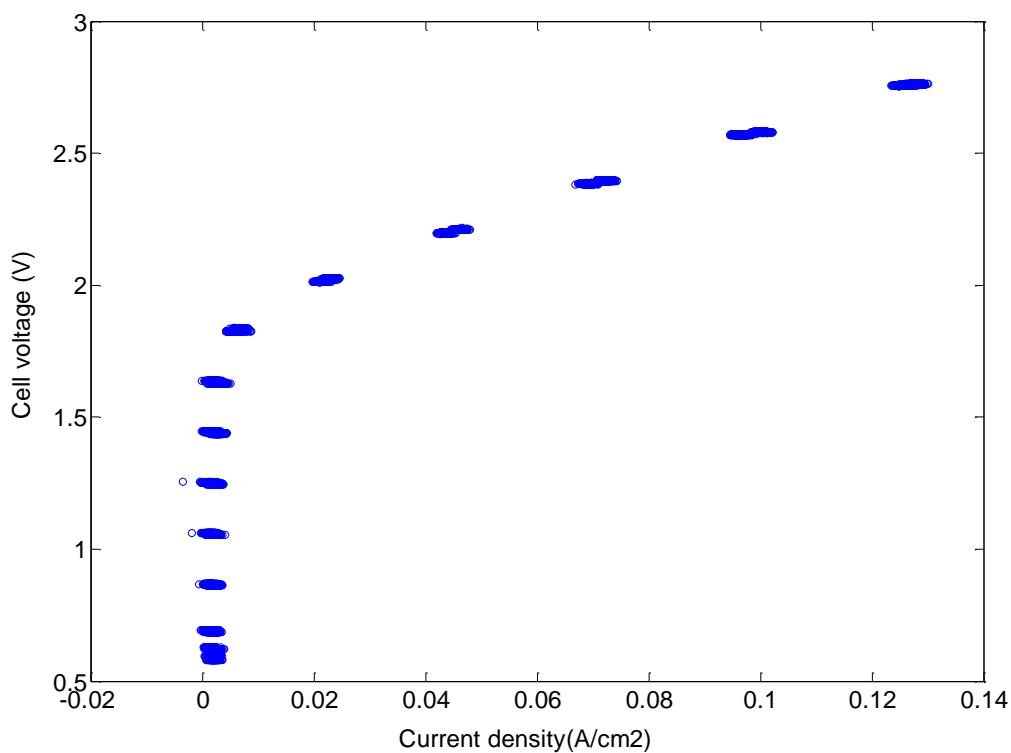


Figure 7-15 Polarisation of the flow-cell alkaline electrolyser that is constructed with 'point-wise' current collector. The cell was operated in 30 % KOH at 23 °C.

The corresponding impedance is shown in Figure 7-16 which indicates relatively low internal resistance for the flow-cell alkaline electrolyser that is constructed with 'point wise' current collector.

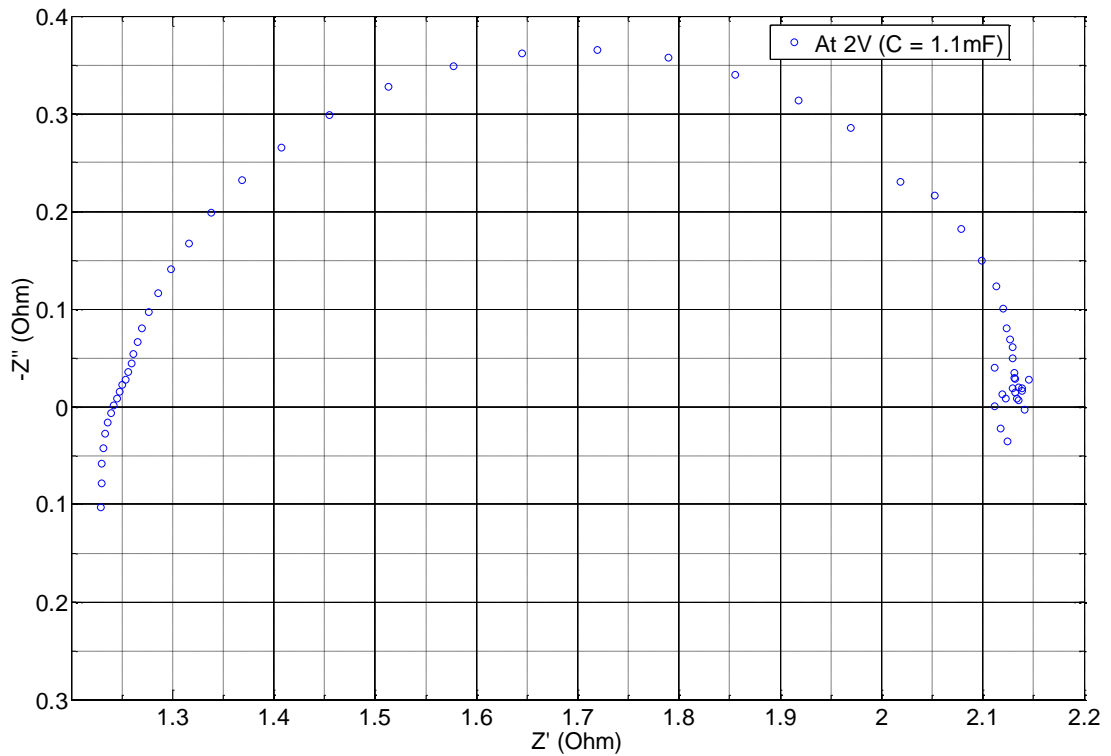


Figure 7-16 Nyquist impedance of the flow-cell alkaline electrolyser that is constructed with 'point-wise' current collector. The cell was operated in 30 % KOH at 23 °C

7.3 Open Circuit Voltage of the Alkaline Electrolyser

The OCV was investigated by charging the cell and leaving it under open-circuit at different times. As can be seen in Figure 7-17, the OCV is not influenced by the duration of charging under electrolysis.

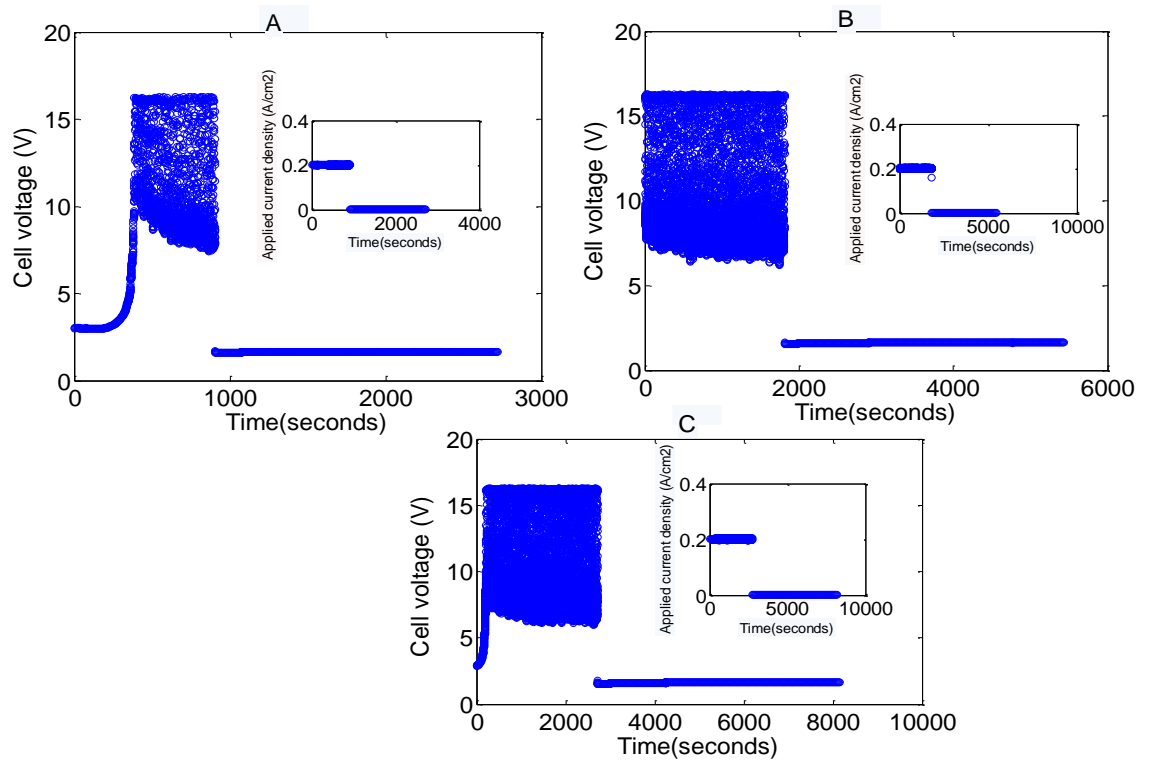


Figure 7-17 OCV of the alkaline electrolyser that consists of 30 % KOH at 23 °C after: A. 16 minutes of charging, B. 33 minutes of charging, C. 41 minutes of charging

However, as shown in Figure 7-18, the OCV is significantly reduced after some time under open-circuit.

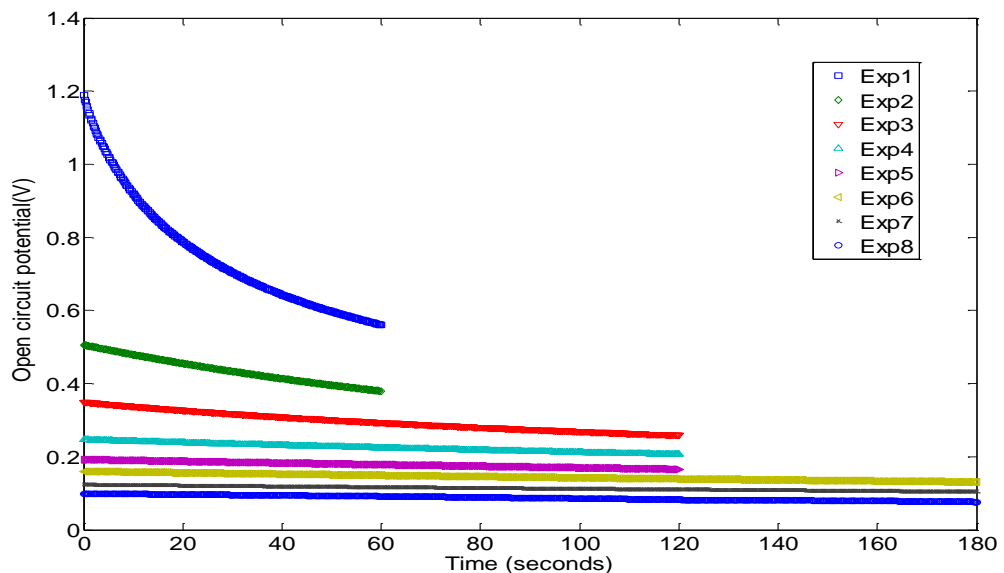


Figure 7-18 OCV of the alkaline electrolyser at discharge time of 3 minutes recorded continuously in separate measurements in 30 % KOH at 23 °C.

The Nyquist plot that is shown in Figure 7-19 indicates high resistance of this cell under open-circuit, thereby suggesting that electrochemical reactions still take place in the alkaline electrolyser that is under open-circuit. The OCV is about 1.45 V and the capacitance is about 0.31 mF, which suggests that electrochemical reactions take place at the double-layer interface between the electrolyte and electrode under open-circuit. By referring to Figure 7-18, at the initial period under open-circuit (see Exp 1 of Figure 7-18), the OCV is high due to ionic charges as well as gas-bubbles that are present at the double-layer interface, but as time elapses during open circuit, the OCV is reduced as there is net migration of ionic charges as well as gas-bubbles at the double-layer interface. The gas-bubbles can migrate by diffusion due to concentration gradient or by natural convection due to buoyancy. The ionic charges will be reduced as there is no flow of electrons from the electrical circuit under open circuit. The OCV is significantly reduced after long period under open-circuit (see Exp 8 of Figure 7-18) as there is significant reduction in ionic charges as well as concentration of hydrogen and oxygen gas-bubbles at the double-layer interface.

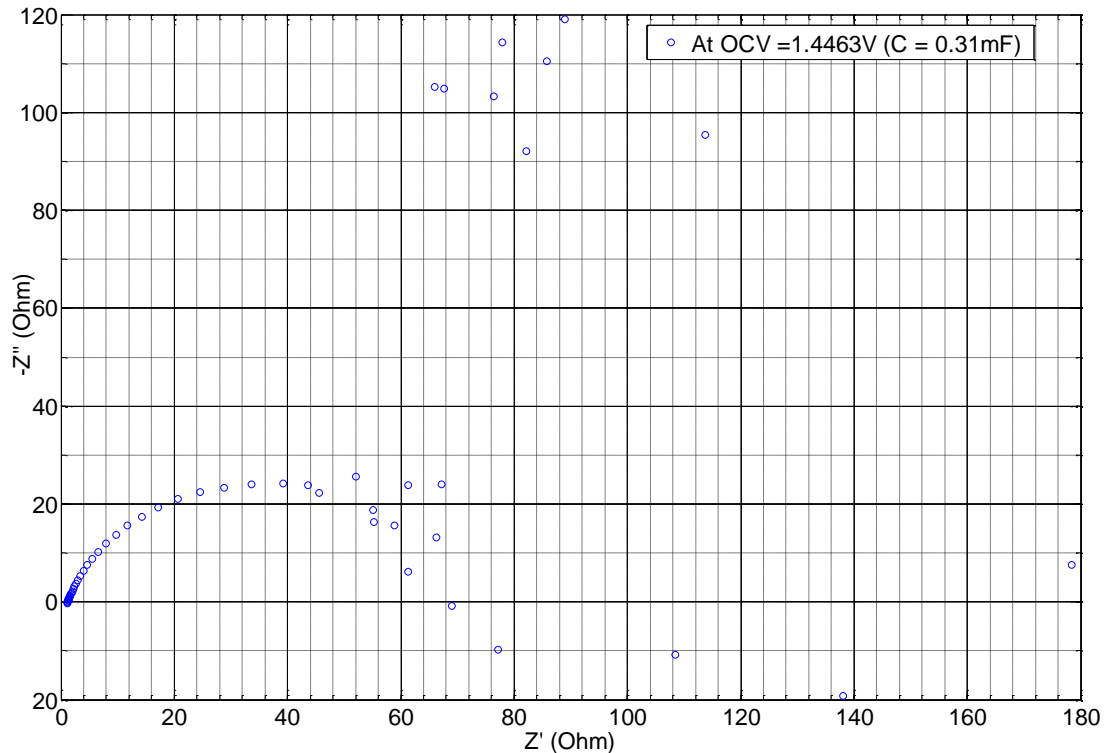


Figure 7-19 Nyquist impedance of the alkaline electrolyser at the OCV in 30 % KOH at 23°C

7.4 Conclusion of chapter

The construction and physical set-up of the alkaline electrolyser cell is seen to influence the efficiency for hydrogen and oxygen production. The Ohmic and polarisation resistances are affected by the mass transport of electrolyte and product gases. The electrical resistance depends on the current collection technique. Therefore, the electrolyte and electrode chambers are critical units of the cell that should be carefully considered in designing and fabricating a highly efficient ambient temperature flow-cell alkaline electrolyser.

Chapter 8

Modelling of Concentration Polarisation and Corrosion Rate of the Electrode

8.1 Background

The internal resistance of the alkaline electrolyser cell is influenced by separation distance between the electrodes, operating temperature, and mass transport of electro-active ions as well as gas-bubbles. This chapter aims to address the conditions that affect internal resistance of the alkaline electrolyser and in particular, concentration of the electrolyte and corrosion rate of the electrode.

Commercial alkaline electrolysers are characterised by current density operation in the region of 200-300 mA/cm² and unit cell voltages at around 1.8-2.1V [6], which corresponds to an energy consumption of about 4.8 kWh/Nm³ H₂ including auxiliary energy consumption. The auxiliary energy consumption is the electricity consumption in auxiliary units such as heaters, heat exchangers, driers, pumps, and deoxidisers. The electrical energy requirement accounts for about 60-80 % of the unit cost of electrolytic hydrogen [6, 28] at comparatively low operational current densities, which makes the technology relatively expensive. The hydrogen production rate is increased as current density is increased. However, at high current density, Ohmic or transport resistance is increased partly due to the electrode surface that is being covered in gas bubbles and gas-void fractions in the electrolyte [80]. The coverage of the electrode surface by gas bubbles reduces the contact between the electrolyte and the active area of the electrode. The generation of gas bubbles at the electrode-electrolyte interface can lead to a concentration gradient of electro-active ions, and consequently to a concentration polarisation.

Aqueous KOH electrolyte is normally added in the electrolyser to increase the conductivity of water by enhancing the mobility of the hydroxyl ions across the electrodes. But at high current densities of operation, electrolyte conductivity can reduce if there is no efficient method to remove the gas bubbles. This is because at

high current density back diffusion of gas bubbles i.e. diffusion of gas-bubbles into the electrolyte solution could result in gas-void fractions in the electrolyte. Also, high current densities of operation can lead to bubble coverage on the electrode surface as well as hydrogen embrittlement [121, 145]. The transport of hydroxyl ions is influenced by concentration gradient, distance of separation between the electrodes, nature of membrane and temperature of the electrolyte.

Concentration gradient occurs due to an unequal distribution of hydroxyl ions between the electrodes. A report by Riegel *et.al* [145] has evaluated the amount of hydrogen and oxygen gas bubbles that is very close to the electrode surface based on the Nernst equation. They have observed dissolved gases near the electrode surface due to the back flow of hydrogen and oxygen gas bubbles at high current densities of operation. The Faraday's law of electrolysis, however, is the effective method to determine the amount of hydrogen and oxygen that is produced from the electrolyser. Nonetheless, the method of Reigel *et.al* is useful and is adopted to evaluate the amount of hydroxyl ions near the electrode surface.

The transport resistance of hydroxyl ions can be reduced by reducing the separation distance between the electrodes [61] and use of appropriate membrane between the electrodes. Nagai *et al* [80] has reported the optimum space of 1-2 mm between the electrodes that is widely recognised [70] as the 'zero-gap' cell configuration in order to reduce transport resistance of electro-active ions at high operational current density ($>0.5\text{A}/\text{cm}^2$). Selective transport of hydroxyl ions is enhanced across the membrane that is hydrophilic, has pore sizes below $10\ \mu\text{m}$ and a porosity of about 50 % [6]. The Celgard[®]5550 membrane is selected because it is hydrophilic, has pore sizes of $0.064\ \mu\text{m}$ and porosity within 50% -55%.

The efficiency of conventional temperature alkaline electrolysers is increased up to ~75 % HHV by raising the temperature of electrolyte. The electrolyte conductivity is increased by 2-3 % per degree Celsius [6]. However, nickel and steel electrodes are less resistant to corrosion in KOH electrolyte at high temperature [6, 146]. Also, the conventional temperature alkaline electrolyser is limited for dynamic and

fast-response of operation with renewable energy systems due to the requirement for heating and cooling of the electrolyte. For example in the experiment that was carried-out by the author using a 550 W laboratory hot-plate, it took almost 10 minutes to raise the temperature of the electrolyser cell from ambient to the conventional operating temperature. Commercial alkaline electrolyser manufacturers can still efficiently heat the electrolyte solution in short time using heaters and heat exchangers but this might incur additional cost of electricity consumption, investments in capital, operating and maintenance costs as illustrated and explained in section 2.5.

8.2 Research Problem and Hypothesis

The polarisation of alkaline electrolyser can be modelled based on equation 76: $V = 0.2i^3 - 0.62i^2 + 1.2i + 1.7$ (76) where the dimensionless variable i is the ratio of anodic current density i_a to ‘limiting current density’ i_L i.e. $i = \frac{i_a}{i_L}$. Equation 76 was derived by curve fitting and extrapolating the steady-state polarisation data of a practical alkaline electrolyser. As shown in Figure 8-1, the model depicts exponential increase in the cell over-potential (see concentration polarisation region) at relatively high current densities of operation.

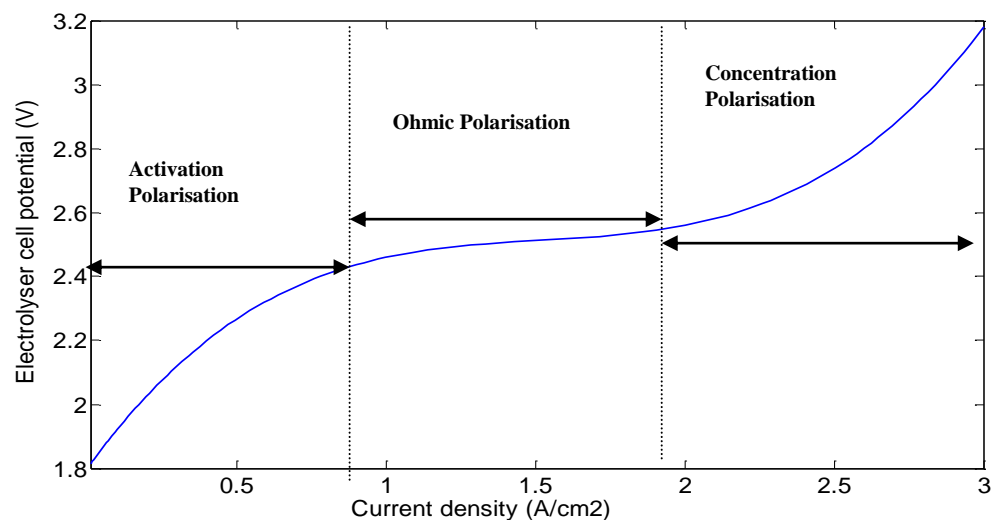
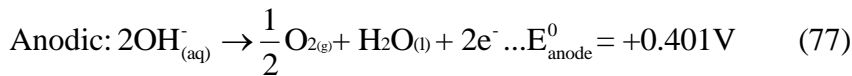


Figure 8-1 Model prediction of concentration polarisation for the electrolyser cell that is operated with 30 % KOH at 293 K

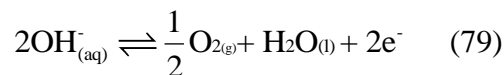
As shown in Figure 8-1, cell over-voltage is increased at relatively high current density ($> 2 \text{ A/cm}^2$) due to concentration polarisation. At high current density of operation, if there is no effective gas bubble removal mechanism such as stirring of the electrolyte solution or forced convection of electrolyte, gas-bubble coverage on the electrode and void-fractions in the electrolyte can result to increases in the Ohmic and reaction overvoltages. The rate of electrolysis will be limited due to the resulting concentration gradient of hydroxyl ions near the anode surface. The electrochemical reaction at the anode essentially involves conversion of hydroxyl ions into oxygen gas and water molecules (see equation 1 above or equation 77 below). However, the concentration of hydroxyl ions is limited compared with water molecules that are in abundant quantity in the alkaline electrolyser. For this reason, concentration polarisation is more likely to take place at the anode due to a concentration gradient of hydroxyl ions.

8.3 Diffusion Model Theory and Assumptions

The reversible half-cell electrode reactions are:



Considering specifically the reversible reaction that takes place at the anode:



The following assumptions can be made:

1. In dynamic electrolysis, migration of hydroxyl ions to the anode is a rate determining step for the overall reaction. This is because concentration of hydroxyl ions (30 %) is lower compared with water molecules (70 %) in the bulk electrolyte solution. The forward and backward processes of equation 79 depend on several factors including the operational current density and rate of

gas–bubble removal. Therefore dynamic equilibrium is established between dissolved molecular oxygen and hydroxyl ions that are present at the anode surface.

2. The concentration of hydroxyl ions near the anode surface can be determined based on the Nernst equation 80 [64]:

$$E_{anode} = E_{anode}^o + 0.0592 \log_{10} C_{OH} \quad (80)$$

3. Only diffusion of hydroxyl ions and oxygen molecules along the electrode surface needs to be considered.
4. The diffusion layer thickness (x_d (m)) of electroactive ions is along the separation distance between the anode and cathode.
5. The solution is initially homogenous and there is no concentration gradient of hydroxyl ions until there is electrolysis.
6. For every hydroxyl ion that is consumed in the process oxygen is formed, that is to say the fluxes of hydroxyl ions and oxygen at the anode surface are equal and opposite i.e. $-J_{OH} = J_{O_2}$.

Based on the above assumptions, equation 81 describes the current density based on diffusion of hydroxyl ions to the anode surface and their subsequent conversion into oxygen [64].

$$i = -nFA_s J_{OH} \quad (81)$$

The diffusion rate of hydroxyl ions depends on the concentration of hydroxyl ions along the separation distance as expressed in equation 82 [64]:

$$J_{OH} = -D_{OH} \frac{dC_{OH}}{dx_d} \quad (82)$$

Considering equation 83, $(C_{OH})^2 = \exp \frac{nF(E_{anode} - E_{anode}^o)}{RT}$ (83);

It is apparent that an increase in anodic overpotential i.e. $E_{anode} \gg E_{anode}^o$ is caused by limited depletion of hydroxyl ions near the anode surface i.e. $(C_{OH})^2 > 0$. The diffusion rate and depletion of hydroxyl ions at the anode surface depends on: the distance of separation between the electrodes, the nature of membrane and operating temperature. Assuming in a ‘zero-gap’ cell configuration, the operating temperature is kept constant and the appropriate membrane is used, the diffusion layer thickness (x_d (m)) is the layer of hydroxyl ions near the anode surface. As the separation distance is reduced, diffusion layer thickness is reduced and hydroxyl ions are depleted near the anode surface. On the other hand, as the separation distance is increased, the diffusion layer thickness is increased and hydroxyl ions are accumulated near the anode surface. The difference between hydroxyl ions near the anode surface and in the bulk electrolyte solution is the concentration gradient of hydroxyl ions, which determines the flux of hydroxyl ions across the electrodes as expressed in equation 84:

$$J_{OH} = -D_{OH} \frac{\Delta C_{OH}}{x_d} \quad (84)$$

$$\text{Where } x_d = (\pi D_{OH} t)^{\frac{1}{2}} \quad (85)$$

Equation 85 means that the diffusion layer thickness increases with time ($t^{\frac{1}{2}}$) in the unstirred electrolyte solution during electrolysis. By substituting equation 84 into equation 81 the ‘limiting current density’ (i_L) can be expressed as equation 86:

$$i_L = nFA_{si} \frac{\Delta C_{OH} D_{OH}}{x_d} \quad (86)$$

The limiting current density is the rate of electrolysis that cannot be exceeded due to subsequently limited depletion of hydroxyl ions at the anode surface. A high limiting current density implies that a greater proportion of hydroxyl ions are depleted or

consumed at the anode surface. On the other hand, a low limiting current density implies that a greater proportion of hydroxyl ions are accumulated near the anode surface. The limiting current density can be increased by raising the electrolyte temperature, increasing surface area of the electrodes, reducing separation distance between the electrodes and stirring or forced convection of the electrolyte solution. The rate of diffusion of electro-active ions is increased by raising the electrolyte temperature, and diffusion layer thickness is reduced by reducing the separation distance between the electrodes. Mass transport of electro-active ions as well as gas-bubbles can be increased by stirring or forced convection of the electrolyte solution. Concentration polarisation can be reduced by increasing the limiting current density as expressed in equation 87 [127].

$$\eta_c = \frac{2.3RT}{nF} \log \left[1 - \frac{i_a}{i_L} \right] \quad (87)$$

8.4 Modelling of Corrosion Rates of the Electrode under Open-circuit

The lifetime and reliability of commercial alkaline electrolyzers can be limited due to corrosion of the electrodes under open-circuit or in stand-by conditions. It is reported that corrosion rates on the electrodes is increased by continuous on/off switching cycles of the alkaline electrolyser [121]. Yet recent proposals have already been made to operate the electrolyser cells with off-peak electricity from renewable energy systems [147]. This means relatively low annual utilisation of the facilities in less than 3000 hours per year and about 5000 hours per year of down time [6]. During down time, the cells are kept on open-circuit and maintained at the operating temperature and pressure by venting of residual gases with nitrogen gas [121]. This results in electrode degradation particularly in the bi-polar cells due to reverse current and mutual depolarisation of the electrodes [6, 117]. Polarisation of the electrodes take place due to flow of current during electrolysis, and depolarisation of the electrodes take place due to flow of reverse current during open circuit. Since in the bi-polar cell the electrodes are not electrically insulated (see Figure 2-12), under open-circuit, reverse current is conducted along the electrodes that are electrically in series thereby causing mutual depolarisation. It appears during open-circuit the

electrodes are still kept in contact with the alkali media and this results in corrosion due to charges that are present at the double-layer as described in the electrochemical reaction (15) in section 2.3.

Corrosion takes place under open-circuit conditions due to electrochemical reactions on the electrode. The electrochemical circuit elements under open-circuit are described in Figure 2-4, while Figure 8-2 shows the behaviour of the electrolyser when it is switched off and on. It can be seen that there are three separate ‘relaxation’ events: (a) the Ohmic relaxation which takes place almost instantaneously when there is no more flow of electrons at shut down; (b) the activation relaxation which takes place slowly due to gas bubble release from the electrode surface; and (c) the activation relaxation which takes place very slowly due to migration of ionic charges from the electrode surface.

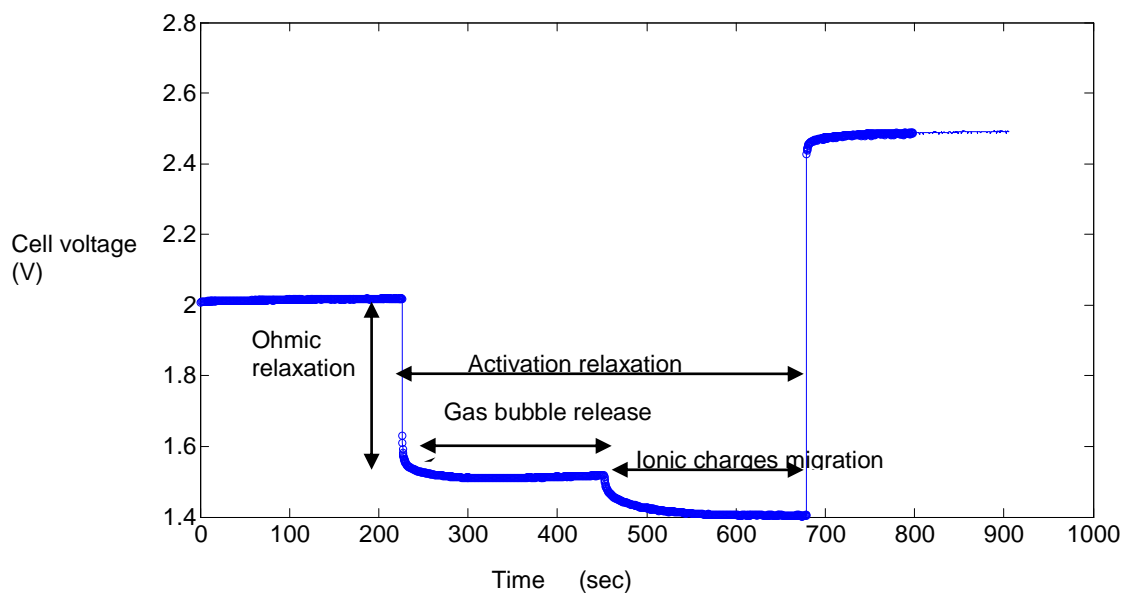


Figure 8-2 Behaviour of the alkaline electrolyser under open-circuit and dynamic power input

Considering the overall cell potential: $E_{cell} = E_{cell}^o + E_{act} + E_{Ohmic}$ (88), for electrolysis at relatively low to medium current densities. Under open-circuit, Ohmic potential relaxation is almost instantaneous thus $E_{Ohmic} = 0$, therefore the overall cell potential is

dependent on the activation potential (E_{act}) and open-circuit potential (E_{cell}^o) as expressed in equation 89.

$$E_{cell} = E_{cell}^o - R_p C_{dl} \frac{dE_{act}}{dt} \quad (89)$$

As shown in Figure 8-2, after about 700 seconds, activation potential is at steady-state so $R_p C_{dl} \frac{dE_{act}}{dt} = 0$, therefore overall cell potential is equal to open-circuit potential as expressed in equation 90.

$$E_{cell} = E_{cell}^o \quad (90)$$

The open-circuit potential leads to corrosion of the electrode due to electrochemical reaction between the electrode and KOH electrolyte. The open circuit potential is influenced by double-layer capacitance which can be described based on the model for constant phase element (CPE) [107, 112, 148] as expressed in equation 91.

$$Z_{CPE}'' = \frac{-1}{T(j\omega)^P} \quad (91)$$

$$\text{Where } T = C_{dl}^P (R_{\Omega}^{-1} + R_p^{-1})^{1-P} \quad (92)$$

For a smooth electrode surface under open-circuit and at steady-state, the total cell potential equals open-circuit potential, and for $P=1$, the CPE impedance can be expressed based on the double-layer capacitance in equation 93. This means the open circuit potential is mainly due to charges carried by ions that are present at the electrochemical double-layer between the electrode and electrolyte.

$$Z_{CPE}'' = \frac{-1}{C_{dl} j\omega} \quad (93)$$

The corrosion current density of electrode can be determined based on polarisation resistance as expressed in equation 94 [127]. The polarisation resistance is the same

as the reaction resistance that is determined by EIS measurements. The polarisation resistance is inversely proportional to the corrosion current density, which means as reaction rate increases corrosion rate also increases.

$$R_p = \left[\frac{\Delta \mathcal{E}}{\Delta J} \right]_{\varepsilon \rightarrow 0} = \frac{\beta}{J_{corr}} \quad (94)$$

Where

$$\beta = \frac{|\beta_a \beta_c|}{2.3(|\beta_a| + |\beta_c|)} \quad (95)$$

Corrosion rates on the electrode under open circuit or in stand-by mode can be minimised by eliminating surface charges at the double-layer interface. The surface charges contribute to open-circuit potential as expressed in equation 96:

$$E_{cell}^o = \frac{Q}{C_{dl}} \quad (96)$$

Where Q accounts for the ionic charge that is present at the double-layer interface.

Some researchers have suggested applying a ‘protective voltage’ on the electrode during stand-by mode in order to minimise corrosion rates. For example Roy has suggested in his PhD thesis [7] to connect super-capacitors in parallel with the electrolyser during standby mode in order to minimise degradation of electrodes. The super-capacitor provides back-up power that keeps the cells slightly running during stand-by mode and thereby prevents open-circuit conditions. However, the energy expended for a ‘protective voltage’ is not a ‘free’ energy as it requires additional capital, operational and maintenance cost investment. During long down-times, however, the electrolyte can be flushed out from the electrolyser by ‘water purging’ in order to prevent build-up of surface charges at the double-layer interface and to eliminate the effect of reverse currents. Corrosion rates can be minimised under open-circuit by diluting the electrolyser with pure water to prevent contact of the electrodes and the corrosive electrolyte solution. Thus the alkaline electrolyser can

be operated with ‘dual-purpose’ flow pump that supplies KOH/H₂O during electrolysis and pure H₂O during stand-by mode or under open-circuit.

8.5 Experimental Set-up and Discussion of the Results

The experimental set-up is the same as shown in Figure 3-2. The SS mesh type-304 that has a geometric surface area of 3.88cm² was investigated as the working electrode and the current density was estimated based on this geometric active area. The separation distance between the electrodes was varied from a 3cm to a 1mm gap and a Celgard[®]5550 membrane was used to separate the electrodes. Magnetic stirrers having lengths of 2cm and 4cm were used to stir the electrolyte solution during electrolysis. No comments are made concerning effects of length of the stirring rod or rotation speed of the stirrer. However, these tests are aimed to investigate operating conditions that influence on electrolyte conductivity, ionic transport and mass transport of gas-bubbles in the alkaline electrolyser.



Figure 8-3 Showing the thermometer and stirring rod that was used for the experiment

8.5.1 Efficiency of Cell in Variable Power of Operation

The polarisation and Tafel plots for the SS electrodes that are separated by a 3cm distance are shown in Figure 8-4. The results indicate slight changes in Ohmic or activation over-potential by stirring the electrolyte solution. It should be noted that

the results for anodic polarisation at 23°C show very rapid fluctuations in the current and voltage, which is attributed to turbulence on the electrode surface by stirring the electrolyte solution.

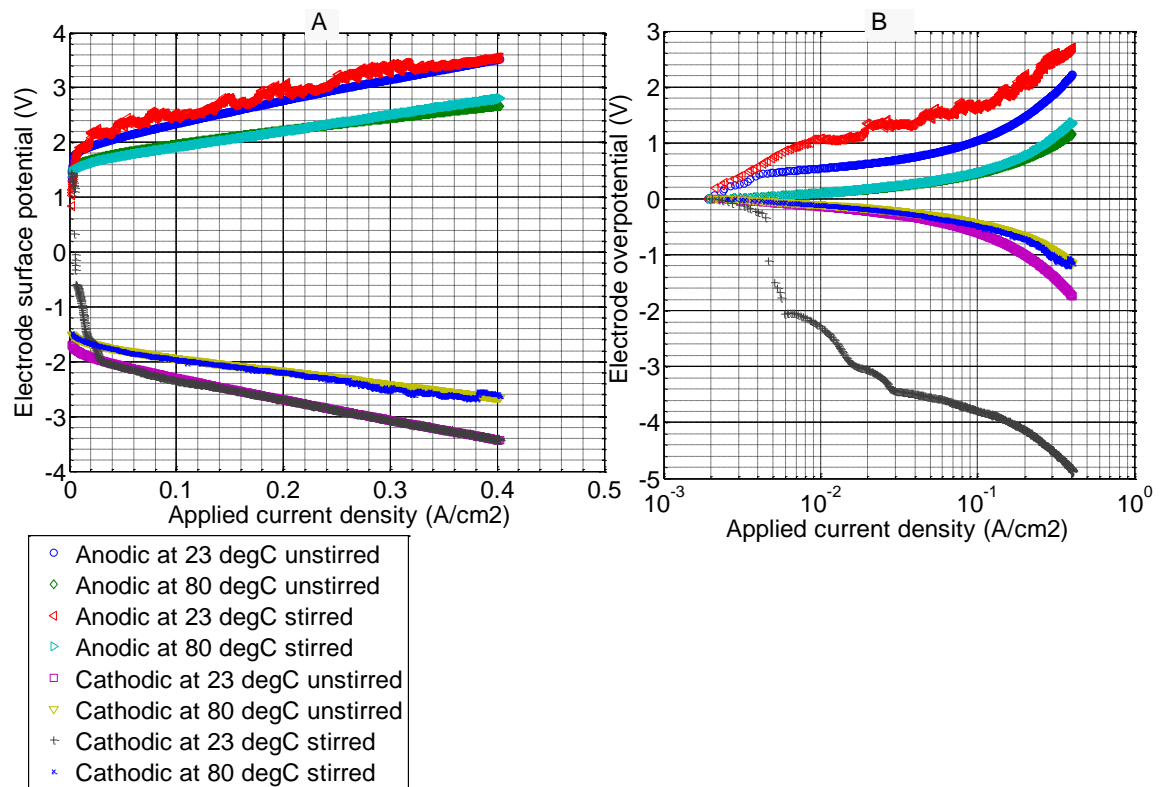


Figure 8-4 Polarisation of SS electrodes separated by a 3cm distance with stirring of electrolyte solution using 2cm length of rod: A. DC polarisation B. Tafel relation

The corresponding Nyquist impedance of Figure 8-5 clearly indicates a slight reduction in Ohmic resistance due to stirring of the electrolyte solution at the ambient and conventional temperatures. Therefore, transport resistance of hydroxyl ions is reduced by stirring of the electrolyte solution.

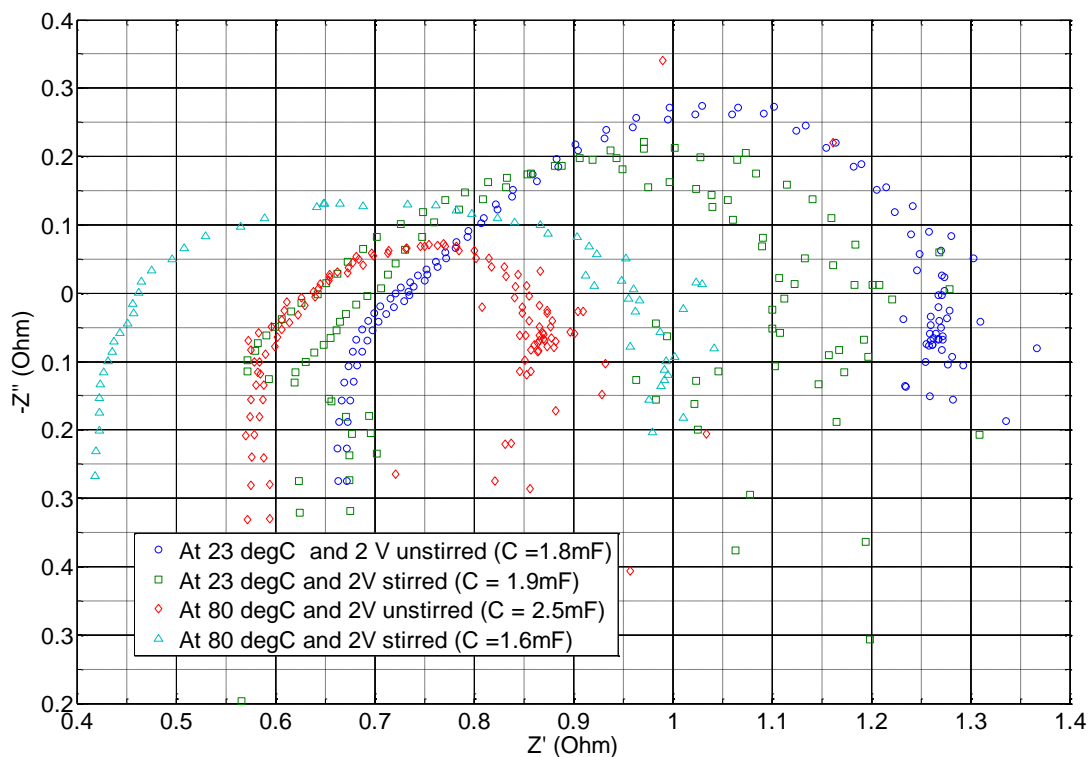


Figure 8-5 Nyquist impedance on SS electrodes separated by a 3cm distance with stirring of electrolyte solution using 2cm length of rod

The polarisation of SS electrodes at ‘zero-gap’ configuration (1mm separation distance) is shown in Figure 8-6.

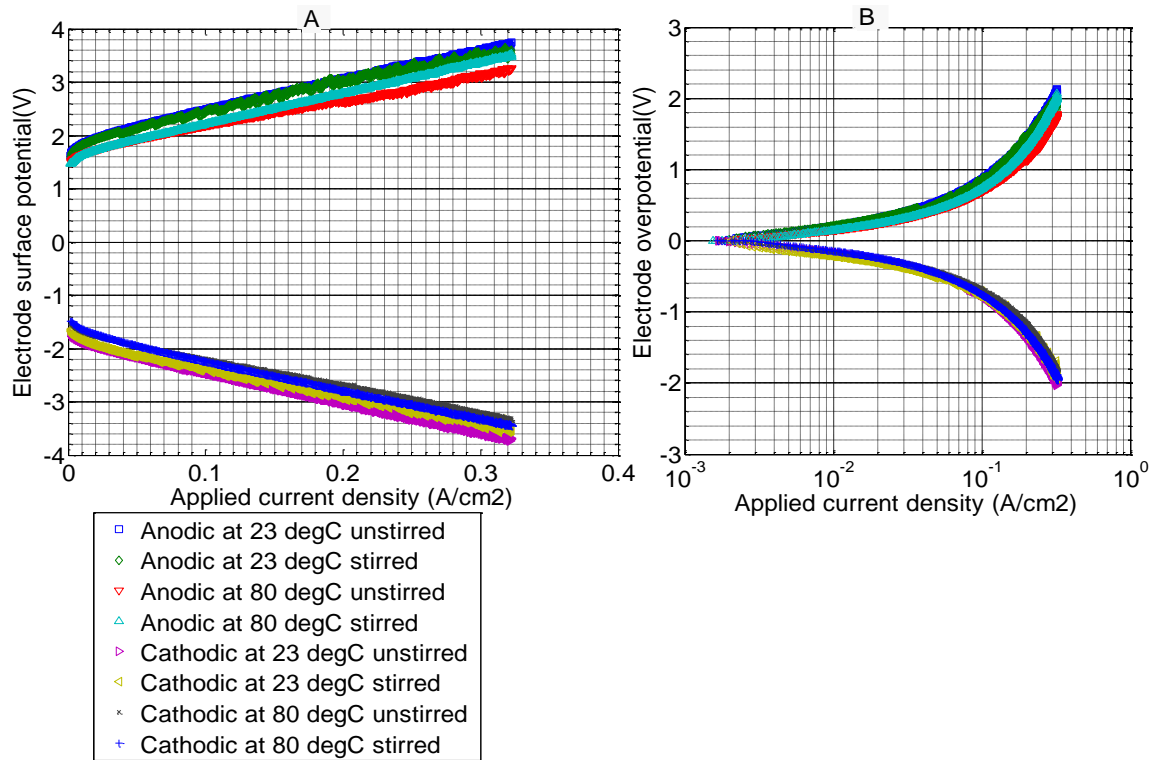


Figure 8-6 Polarisation of SS electrodes at a 1mm separation gap with stirring of electrolyte solution using 4cm length of rod: A. DC polarisation, B. Tafel plot

The cell voltage efficiencies are presented in Table 8-1, which are estimated based on the anodic half-cell potential that is described in equation 97;

$$E_{cell} = E_{cell}^o + \sum \eta_{cell} \quad (97)$$

The results show that efficiency is slightly increased by about 2 % due to stirring the electrolyte solution at the ambient temperature. However, the efficiency is reduced by about 2 % due to stirring the electrolyte solution at the conventional temperature.

Table 8-1 Summary of polarisation results for the SS-type 316 electrodes at 1mm separation gap with stirring of electrolyte solution using 4cm rod

Experimental conditions	* E_{cell}^o (V)	** $\sum \eta_{cell}$ (V)	E_{cell} (V)	*** η_{ELEC} (%)
At 23°C unstirred	1.62	2.13	3.76	39.36
At 23°C stirred	1.61	1.93	3.54	41.80
At 80°C unstirred	1.48	1.77	3.25	45.54
At 80°C stirred	1.48	2.02	3.50	42.28

*The reversible cell voltage was determined from experimental data as the cell voltage under open-circuit i.e. voltage at zero current density.

** The total cell overvoltage was determined based on equation 98; $\sum \eta_{cell} = \eta_{act} + JR_{\Omega}$ (98)

*** Electrolyser efficiency was determined based on equation 7 in section 2.2.

From Figure 8-7, it can be seen that Ohmic or transport resistance is reduced by about 8% due to stirring the electrolyte solution at the ambient temperature.

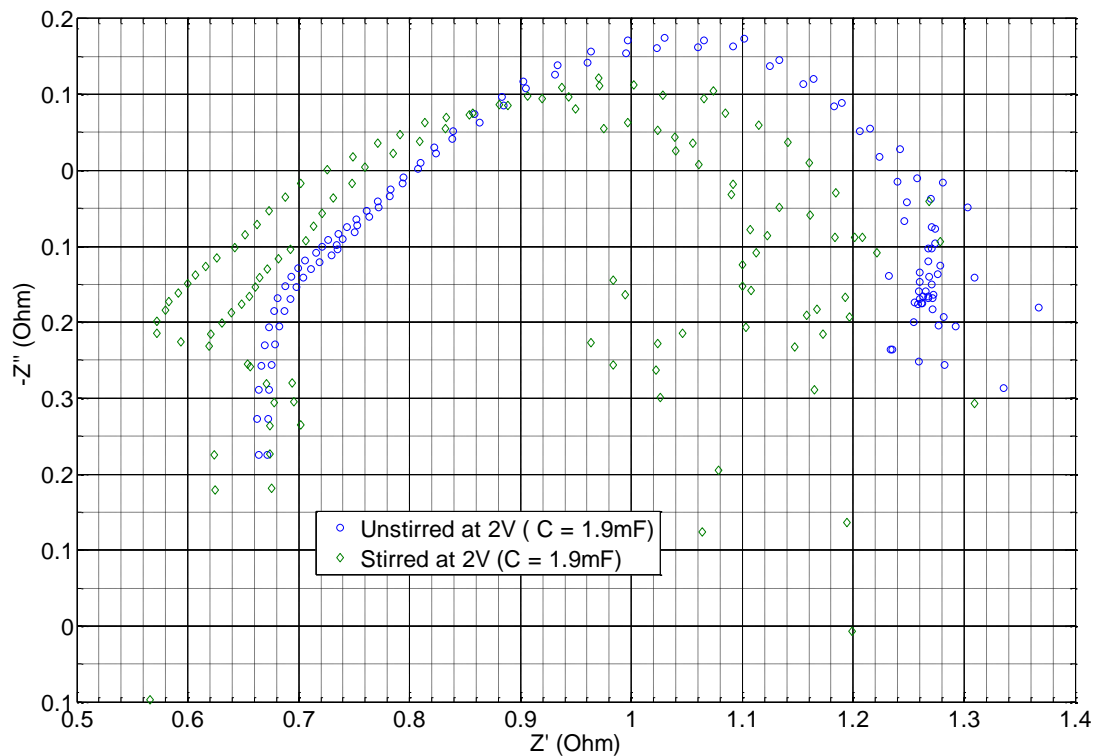


Figure 8-7 Nyquist impedance on SS electrode with stirring of electrolyte solution

Considering Table 8-1, it is apparent that stirring the electrolyte solution has quite the opposite effect at the ambient and conventional temperatures. Stirring the electrolyte solution slightly increases efficiency at the ambient temperature and slightly decreases efficiency at the conventional temperature. This could be attributed to increase in mass transport of gas-bubbles by stirring the electrolyte solution at the ambient temperature thereby minimising gas-bubble coverage on the electrode surface, and/or minimising back-diffusion of gas bubbles into the electrolyte solution. Also, stirring the electrolyte solution reduce the diffusion layer thickness of electro-active ions and thereby prevents concentration polarisation particularly at the anode of the ambient temperature alkaline electrolyser. However, stirring the electrolyte solution at the conventional operating temperature could lead to uniform

distribution of heat, which might slightly reduce the average temperature of electrolyte solution [60] and consequently reduce electrolyte conductivity.

The Ohmic resistance is influenced by the separation distance between the electrodes. As shown in Figures 8-8 and 8-9, Ohmic resistance is reduced by reducing the separation distance between the electrodes. This is because transport resistance of electro-active ions is reduced in the 'zero-gap' cell configuration. Also, the 'zero-gap' cell configuration facilitates gas-bubble detachment from the electrode surface and prevents back diffusion of gas-bubbles thereby minimising resistance of gas void-fractions in the electrolyte.

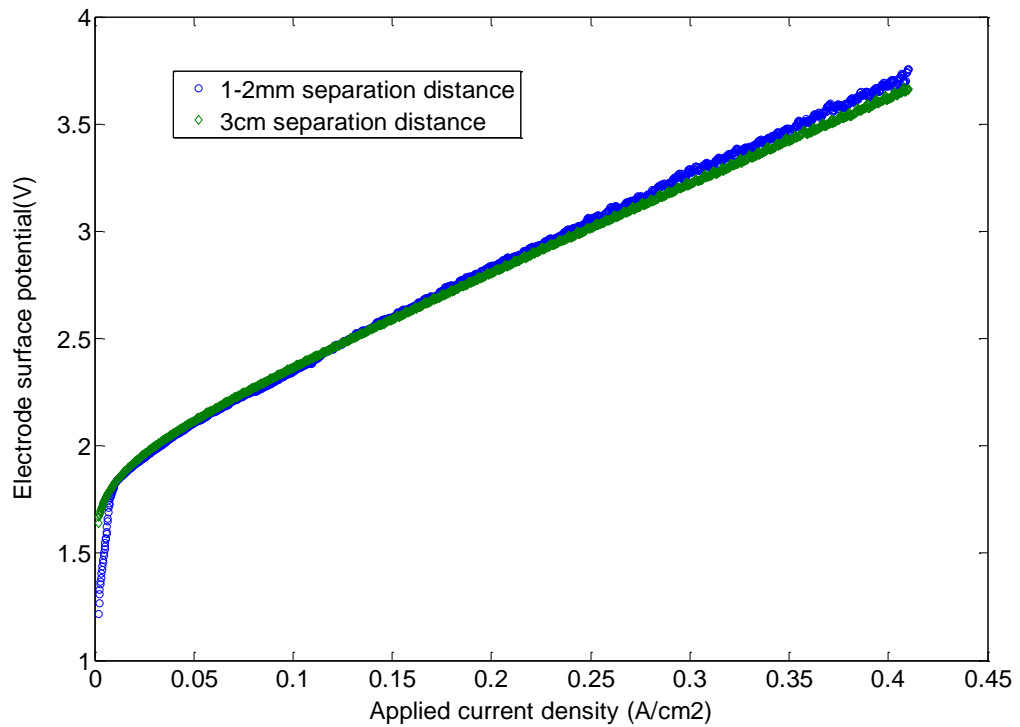


Figure 8-8 Polarisation of SS mesh type-316 electrode at different separation distance in 30% KOH at 23°C

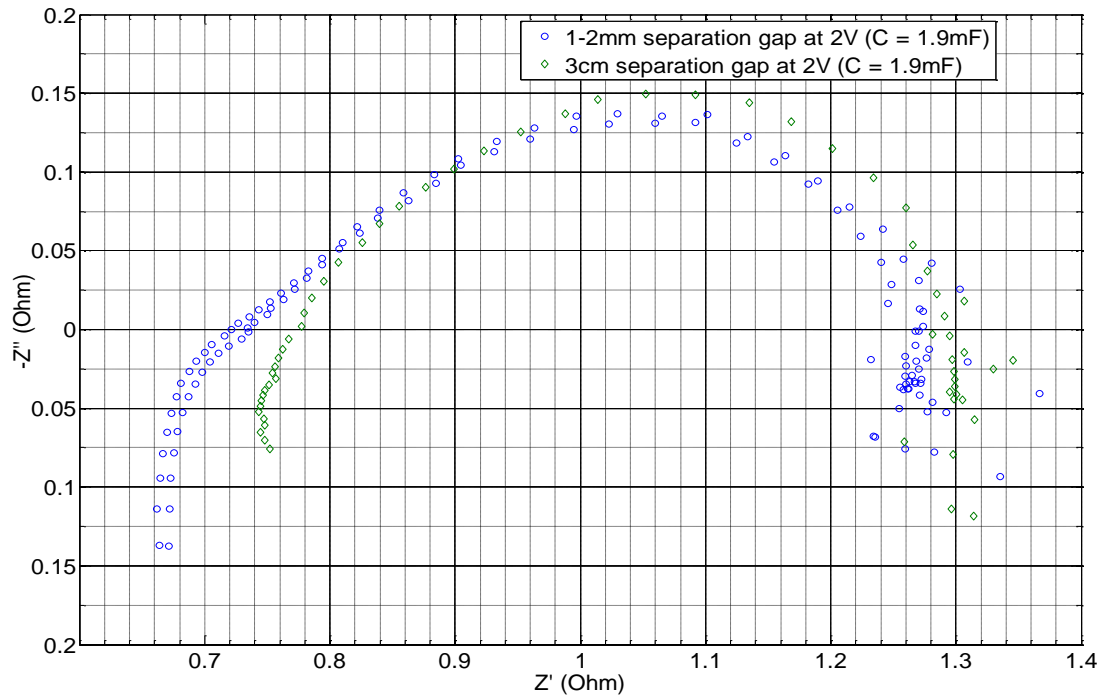


Figure 8-9 Nyquist impedance on SS electrode at different separation distance

It should be noted that from Figure 8-6 (B), the Tafel slopes for SS electrode are determined to be: $\beta_a = +0.03$ V/dec, $\beta_c = -0.03$ V/dec and $\beta = 0.0065$ V/dec. The Tafel parameter (β), in particular, was determined based on equation 95. The Tafel parameters and polarisation resistance are substituted in equation 94 to determine corrosion rates of the electrode.

8.5.2 Determination of Corrosion Rate of the Electrode

The impedance under open-circuit and during electrolysis is compared in Figure 8-10 and indicates that polarisation of the electrode only take place during electrolysis due to the flow of electrons. Under open circuit, the impedance is mainly due to Ohmic resistance, although depolarisation of the electrode might take place under open-circuit due to the flow of reverse current. During electrolysis, the impedance accounts for polarisation resistance, Ohmic resistance and capacitance, but during open-circuit the impedance accounts for capacitance as described in the model of equation 93.

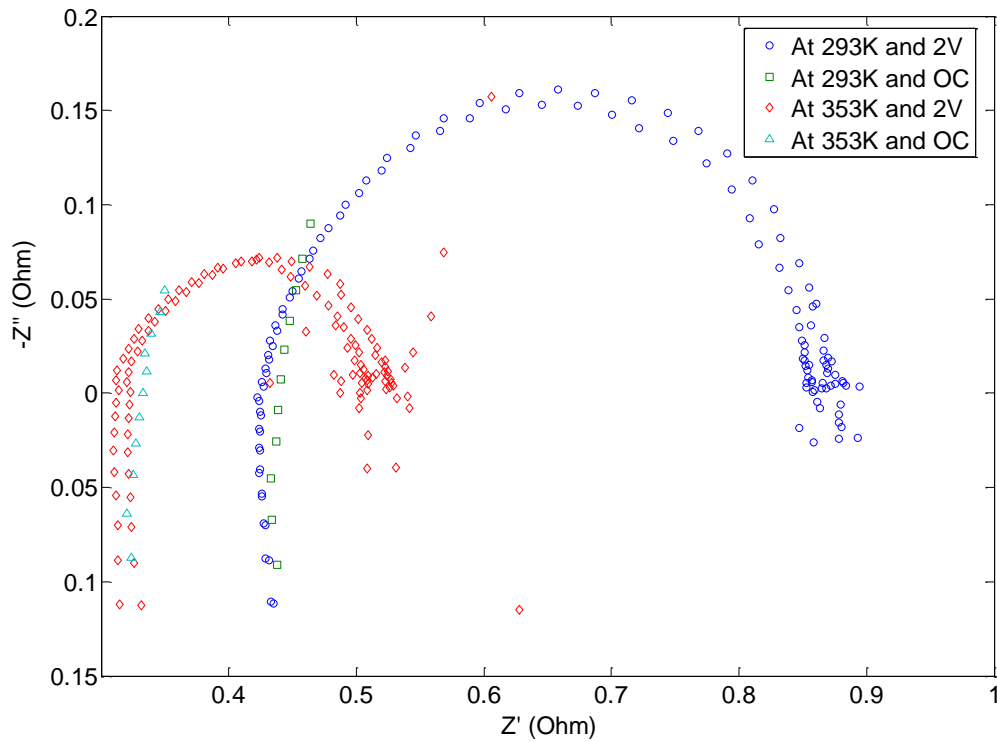


Figure 8-10 Comparison of Nyquist impedance of SS electrode under open-circuit and during electrolysis

From equation 94 and as recorded in Table 8-2, the corrosion rate of the SS electrode is reduced by 50% at ambient temperatures compared with the conventional cell temperature. This observation is in accordance with the literature for the general corrosion behaviour of steel with temperature as described in Figure 2-15 [6].

Table 8-2 Summary of EIS measurements and corrosion rates of SS electrode at 1mm separation distance

Experimental conditions	R_{Ω} (Ω)	R_P (Ω)	J_{corr} (A/cm^2)
At 296K or 23°C	0.67	0.59	0.011
At 353K or 80°C	0.59	0.28	0.023

From Equation 94 and Table 8-2, it is seen that the corrosion rate is reduced as polarisation resistance is increased on the electrode. Polarisation reactions take place during electrolysis by the flow of current. However, depolarisation reactions are caused by reverse current on the electrode under open-circuit and are accelerated in the bi-polar cells due to mutual depolarisation of the electrodes [6]. Thus corrosion is caused by depolarisation reactions on the electrodes under open-circuit. Corrosion

rate however can be reduced under open-circuit by flushing out the KOH electrolyte from the electrolyser cell in order to eliminate surface charges at the double-layer interface. This could be carried out during down-times that last for up to 5000 hours per year [6] when the electrolyser is shut-down for maintenance work or due to electrical power deficit from the electrical grid or the renewable energy source.

8.6 Water Replenishment and Conductivity of KOH Electrolyte

The amount of water that is lost by electrolysis is replenished in the alkaline electrolyser. This is necessary in order to maintain the electrolyte concentration of aqueous KOH solution at the optimum range of 25%-30% [6], where there is the balance of electrical conductivity and corrosion rate of the electrolyte. It is customary to determine the amount of water replenishment based on stoichiometry, thus for every 1 ltr of hydrogen that is produced the equivalent of 1 ltr of water is added into the electrolyser [7]. However, excess dilution of the electrolyte solution would reduce electrolyte conductivity, and consequently increase overvoltage. For example from Figure 8-11, it can be seen that the overvoltage is increased due to excess water replenishment that reduce the concentration of KOH electrolyte. Therefore it is imperative to determine the appropriate amount of water replenishment that is needed to maintain the optimum concentration range of the electrolyte solution in the alkaline electrolyser.

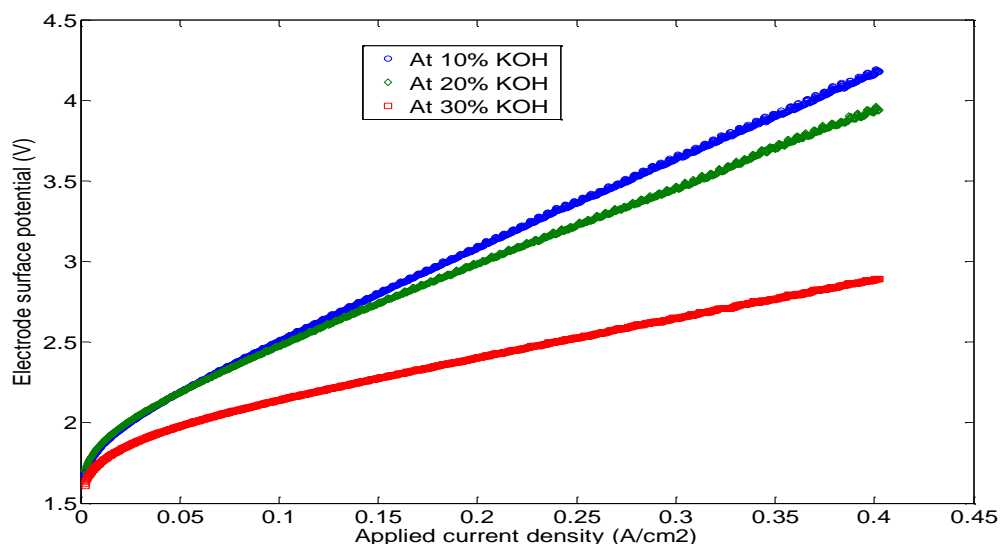


Figure 8-11 Effect of excess water replenishment in the alkaline electrolyser at ‘zero-gap’ separation distance

8.7 Conclusion of Chapter

The diffusion models suggest that concentration polarisation take place in the ambient temperature alkaline electrolyser due to accumulation of hydroxyl ions near the anode surface, transport resistance of electro-active ions and back-diffusion of gas-bubbles. This partly results in higher anodic overpotential compared to cathodic overpotential of the alkaline electrolyser. However, concentration polarisation and internal cell resistance can be minimised at the ambient operating temperature by stirring or forced convection of the electrolyte solution in order to facilitate mass transport of electro-active ions and removal of the gas-bubbles. Although this would enhance efficiency of the ambient temperature alkaline electrolyser, it might add to the cost of auxiliary energy consumption. Thus, in order to justify stirring of the electrolyte solution, the energy savings for electrolysis due to stirring should be greater than the auxiliary energy consumption.

The corrosion rate of SS electrode is minimised by up to 50 % in the ambient temperature alkaline electrolyser. The corrosion rate, however, can be reduced under open-circuit by flushing out the KOH electrolyte in order to eliminate surface charges at the electrochemical double-layer.

Chapter 9

General Conclusions, Contributions to Field and Future Scope of Research

9.1 General Conclusions and Contributions to Field

As the outcome of this work, the contributions to the field of alkaline electrolyser are summarised below, and in the subsequent sections a more detailed account of these findings are presented as evidenced throughout the thesis.

- A thorough analysis of the current state of electrolytic hydrogen production from an integrated renewable energy system is presented, with a view to develop an alkaline electrolyser that is highly efficient, robust, durable, and low-cost for dynamic, intermittent and continuous operation with the electrical grid and renewable energy sources. As a result, this work has identified the ambient temperature alkaline electrolyser to be capable of this aim.
- A systematic approach for fabricating and characterising the electrode and electro-catalyst is presented in view of developing a low cost, durable, robust and highly efficient electrode for the ambient temperature alkaline electrolyser. In particular, efficiency and stability of the electrode are investigated in the ambient temperature alkaline electrolyser.
- By way of theoretical modelling and experimental measurements, proposals were made to improve the electrolyser design and operating conditions in order to minimise over potentials as well as corrosion rates of the electrode, and thereby improve efficiency and durability of the ambient temperature alkaline electrolyser.

9.1.1 Operational Temperature of the Alkaline Electrolyser

The ambient and conventional temperatures alkaline electrolysers have been investigated for sustainable production of hydrogen and oxygen in an integrated renewable energy system. As a result, this research identifies the ambient temperature alkaline electrolyser to be capable of efficient, durable, robust, low-cost, dynamic, intermittent and continuous operation with the electrical grid and renewable energy sources. A comparative analysis of the ambient and conventional temperatures alkaline electrolysers was carried-out and evidenced based on the following contexts:

1. Sustainable production of hydrogen and oxygen
2. Dynamic operation with renewable energy sources
3. Operational and maintenance cost investment
4. Degradation of electrode and electro-catalysts
5. Efficiency and stability of electrode and electro-catalyst

9.1.1.1 Sustainable Production of Hydrogen and Oxygen

The role of an alkaline electrolyser in an integrated renewable energy system is to produce hydrogen and oxygen sustainably as a medium for long or short term energy storage. This application is particularly feasible with the ambient temperature alkaline electrolyser as evident in Chapters 1 and 2 of this thesis. The ambient temperature alkaline electrolyser is compact for distributed production of hydrogen and oxygen; it is relatively low-cost, robust and dynamically responsive to intermittent electricity input. In contrast, the conventional temperature alkaline electrolyser requires additional electricity consumption in auxiliary sub-units such as heaters and heat exchangers, which make it unsuitable for distributed applications, robust, dynamic and intermittent operation with renewable energy sources. In other words, the conventional temperature alkaline electrolyser is limited for distributed applications, low-cost, robust, dynamic and fast-response operation with wind energy sources.

9.1.1.2 Dynamic Operation with Renewable Energy Sources

The ambient temperature alkaline electrolyser is capable of efficient, stable and dynamic operation with renewable energy sources. As described in Chapter 2, this is possible by utilising electro-catalysts, optimising the cell design and configuration and eliminating auxiliary sub-units such as heaters, and heat exchangers that consume ‘auxiliary’ electricity. This means electricity from the wind turbine can be directly inputted into the ambient temperature alkaline electrolyser to produce hydrogen and oxygen, thereby ultimately reducing the system electricity consumption. For this reason, the ambient temperature alkaline electrolyser is potentially capable of operational range within 5 %-100% of the rated electrical power capacity as opposed to 20%-100% operational range for the conventional temperature alkaline electrolyser. Also, the ambient temperature alkaline electrolyser is capable of quicker response operation with renewable energy sources.

9.1.1.3 Operational and Maintenance Cost Investment

As described in Chapter 2, operational and maintenance cost investments are reduced in the hydrogen and oxygen energy system that consists of ambient temperature alkaline electrolyser. Auxiliary utilities such as heater, heat exchangers, and gas driers contribute to the cost of hydrogen in the conventional hydrogen energy system. However, the auxiliary utilities are significantly reduced in the ambient hydrogen and oxygen energy system thereby reducing hydrogen and oxygen production costs. Gas losses are also reduced in the ambient hydrogen and oxygen energy system that eliminate gas driers, thereby increasing hydrogen and oxygen production rates. Moreover, the return on investment is potentially increased since the ambient temperature alkaline electrolyser produce hydrogen and oxygen product gases that can be directly utilised in alkaline fuel cell to generate back electricity.

9.1.1.4 Degradation of Electrode and Electro-Catalysts

As described in Chapters 2, 3 and 8, corrosion rates of electrode and electro-catalysts are reduced by about 50 % at the ambient temperature. This translates to about 50 % increase in the lifetime of electrodes and electro-catalysts in the ambient temperature alkaline electrolyser, and consequently 50 % reduction of its maintenance and service costs. For example, although, commercial manufacturers [54] are able to deliver alkaline electrolysers that can operate continuously for an average of 35 years with cell overhaul every 8 years in order to replace the electrodes, by comparison, however, the ambient temperature alkaline electrolyser can operate continuously for up to 35 years with minimal cell overhaul about every 12 years to replace the electrodes. The maintenance and service cost is reduced by 50% due to a reduction in degradation rates of electrode and electro-catalysts at relatively lower operating temperature.

9.1.1.5 Efficiency and Stability of Electrode and Electro-Catalysts

As evident in Chapter 3, it is clear that efficiency of the electrode is reduced by about 13%, and stability of the electrode is increased by about 50% in the ambient temperature alkaline electrolyser. The efficiency of the electrode, however, can be increased by electro-catalysis in the ambient temperature alkaline electrolyser, which is evident with the development of SS-Ni-Mo electro-catalyst that is described in Chapters 5 and 6. In other words, the electro-catalyst is capable to enhance production rates of hydrogen and oxygen by increasing the exchange current density and reducing the Tafel overvoltage for the electrochemical reactions. Moreover, the electro-catalyst is relatively stable at the ambient temperature as corrosion rates as well as degradation due to reaction products are minimised. Further, the efficiency can be increased by optimising the design and construction of the electrolyser cell in order to reduce cell resistance. This is evident in Chapter 7, which identifies the electrode and electrolyte compartments as critical units of the flow-cell to reduce internal and external cell resistances.

9.1.2 Fabrication and Characterisation of Electrode and Electro-Catalysts

A systematic approach for fabricating and characterising the electrode and electro-catalysts is presented, in view of developing a low-cost, durable, robust and highly efficient electrode for the ambient temperature alkaline electrolyser. The fabrication methods are essentially based on pre-treatment of the electrode substrate followed by electrodeposition of catalyst on the electrode substrate. The characterisation methods involve variable, constant and intermittent electrical power of operation, which are aimed at simulating the alkaline electrolyser that is powered directly either by renewable energy sources such as wind turbine or the electrical grid. In particular, as evident in Chapter 4, the SS type-304 is identified as the best electrode substrate in terms of efficiency, durability and cost. The SS type-304 is further developed into SS-Ni-Mo electro-catalyst as evident in Chapters 5 and 6. The SS-Ni-Mo electro-catalyst is capable to enhance efficiency and durability of the ambient temperature alkaline electrolyser.

9.1.3 Concentration Polarisation and Corrosion Rate of the Electrodes

As evident in Chapter 8, concentration polarisation takes place at the anode of the alkaline electrolyser, which partly explains why anodic overpotential is higher than cathodic overpotential. However, concentration polarisation and anodic overpotential can be minimised by reducing the separation distance between the electrodes, increasing the electrode active area, stirring or forced convection of the electrolyte solution in order to increase mass transport of electrolytic ions and gas bubbles.

Although corrosion rates are reduced by about 50% at the ambient temperature, corrosion takes place in the alkaline electrolyser that is under open-circuit due to surface charges present at the electrochemical double-layer interface. In order to reduce corrosion, the electrolyte solution can be flushed out of the alkaline electrolyser that is under open-circuit. This would eliminate surface charges at the electrochemical double-layer, and thereby extend the lifetime of electrodes and cell components.

9.2 Future Scope of Research

In the future, this research work will concentrate on developing electro-catalysts, design and construction of the cell that can enhance efficiency and durability of the ambient temperature alkaline electrolyser.

9.2.1 Electro-Catalyst Development

Electro-catalysis is the key to improving kinetic efficiency of the ambient temperature alkaline electrolyser. The benefits of electro-catalysts involve reducing costs and increasing hydrogen and oxygen production rates. However, the challenge is to improve stability of the electro-catalyst and based on the outcome of this research it is clear that more attention should be given to pre-treatment of the electrode substrate and electrodeposition conditions in order to improve adhesion and stability of the electro-catalyst. Further work will involve developing electro-catalysts that are highly efficient and stable over longer period of variable, intermittent and continuous electrolysis.

9.2.2 Optimisation of Cell Design and Operation

The aim of optimisation will be to combine maximum electrical efficiency and minimum hydraulic resistance of the electrolyser cell. Uniform supply of electrolyte solution throughout the cell depends on the physical dimensions of the distribution ports. Relatively small cross-sectional area of the distribution ports might result to frictional losses that reduce the distribution rate of electrolyte in the entire stack and ultimately increase the internal cell resistance. Therefore the distribution channels will not be made too small in order to minimise hydraulic resistance, and to allow effective distribution of the KOH electrolyte and collection of the product gases.

The distance of separation has to be optimised in order to reduce Ohmic resistance for transport of electro-active ions and to facilitate the removal of gas bubbles. The monopolar electrolyser cell that was tested has a separation distance of about 3cm between the electrodes, although in the bi-polar flow-cell the distance between the

electrodes was almost 'zero-gap'. The electrolyser cell will be fabricated at an optimum separation distance that improves mass transport of electro-active ions and gas bubbles.

The diffusion models suggest that concentration polarisation takes place in the ambient temperature alkaline electrolyser cell. However, concentration polarisation is minimised at the conventional temperature due to increase in the conductivity of KOH electrolyte and increase in the rate of detachment of gas bubbles from the electrode surface. At relatively high temperature, the gas bubbles are lighter and can easily migrate out of the electrode surface by buoyancy. In contrast, at relatively low temperature, the gas bubbles are heavier so they stick to the electrode surface and consequently result in concentration polarisation. Stirring the electrolyte solution, reducing separation distance and increasing electrode active area are methods to minimise concentration polarisation in the ambient temperature alkaline electrolyser. As such, the author's flow-cell might need further modification in order to incorporate magnetic stirrers or turbulence promoters. However, stirring require additional electricity consumption, hence it might only be possible to optimise the bi-polar 'zero-gap' flow-cell configuration, and fabricate large surface area electrodes for the ambient temperature alkaline electrolyser.

References

- [1] <http://www.decc.gov.uk/> Last checked on 23rd April 2012.
- [2] <http://www.decc.gov.uk/assets/decc/Statistics/publications/brief/78-energyinbrief2009.pdf> Last checked on 23rd April 2012.
- [3] Rupert Gammon, Amitava Roy, John Barton, Matthew Little. <http://ieahia.org/pdfs/HARI.pdf> Last checked on 29th April 2012.
- [4] Aprea J.L. “Hydrogen Energy Demonstration Plant in Patagonia: Description and Safety Issues”. *International Journal of Hydrogen Energy*. Vol. 34, 2009, pp. 4684–91.
- [5] Dutton A. G., Bleijs J. A. M., Dienhart H., Falchetta M., Hug W., Prischichd D., A. J. Rudell. “Experience in the Design, Sizing, Economics, and Implementation of Autonomous Wind Powered Hydrogen Production Systems”. *International Journal of Hydrogen Energy*. Vol. 25, 2000, pp. 705–22.
- [6] Hartmut Wendt. “Electrochemical Hydrogen Technologies: Electrochemical Production and Combustion of Hydrogen”. 1990. *Elsevier Publishing Company*. ISBN: 0444881625.
- [7] Amitava Roy. “Dynamic and Transient Modelling of Electrolysers Powered by Renewable Energy Sources and Cost Analysis of Electrolytic Hydrogen”. 2006. *Doctoral Thesis of the University of Loughborough UK*.
- [8] The Telegraph. “Fears For Global Recovery as Oil hits \$120 mark” <http://www.telegraph.co.uk/finance/oilprices/8427941/Fears-for-global-recovery-as-oil-hits-120-mark.html> Last checked on 23rd April 2012.
- [9] The Telegraph. “Oil Prices”. <http://www.telegraph.co.uk/finance/oilprices/> Last checked on 23rd April 2012.
- [10] Money Week Oil Price Performance Chart at: <http://www.moneyweek.com/news-and-charts/market-data/oil> Last checked on 29th April 2012.
- [11] DECC. “Energy Consumption in the United Kingdom”. <http://www.decc.gov.uk/en/content/cms/statistics/publications/ecuk/ecuk.aspx> Last checked on 23rd April 2012.
- [12] DECC. “Gas Statistics”. <http://www.decc.gov.uk/en/content/cms/statistics/source/gas/gas.aspx> Last checked on 23rd April 2012.

- [13] DECC. “UK Climate Change Sustainable Development Indicator: 2010 Greenhouse Gas Emission, Provisional Figures and 2009 Greenhouse Gas Emission, Fuel Figures by Type and End-use”.
http://www.decc.gov.uk/assets/decc/Statistics/climate_change/1515-statrelease-ghg-emissions-31032011.pdf Last checked on 23rd April 2012.
- [14] “The UK Renewable Energy Strategy”.
http://www.decc.gov.uk/assets/decc/What%20we%20do/UK%20energy%20supply/Energy%20mix/Renewable%20energy/Renewable%20Energy%20Strategy/1_20090715120255_e_@@_TheUKRenewableEnergyStrategyExecutiveSummary.pdf
Checked on 23rd April 2012.
- [15] StART Corporation. “Production of Electrolytic Hydrogen for Methane Supplementation for Residential Space Heating”.
http://www.all-energy.co.uk/UserFiles/File/Peretti_Naskalli.pdf
Last checked on 23rd April 2012.
- [16] Hydrogen Fact Sheet, Hydrogen Production- Steam Methane Reforming (SMR).
<http://www.scribd.com/doc/54181313/Hydrogen-Production-Steam-Methane-Reforming>
Last checked on 28th March 2013.
- [17] World Resources Institute. “Carbon Capture and Storage”.
<http://www.wri.org/project/carbon-dioxide-capture-storage>
Last checked on 29th April 2012.
- [18] Hydro. “The Utsira Wind-Hydrogen Project”.
http://www.iphe.net/docs/Meetings/Brazil_3-05/Norway_Utsira_Wind_H2.pdf
Last checked on 23rd April 2012.
- [19] ‘Potential for Hydrogen as a Fuel for Transport in the Long Term (2020-2030)’.
<http://ftp.jrc.es/EURdoc/eur21090en.pdf> Last checked on 23rd April 2012.
- [20] P. P. Edwards, V. L. Kuznetsov, W. I. F. David, N. P. Brandon. “Hydrogen and Fuel Cells: Towards a Sustainable Energy Future”. *Energy Policy*. Vol. 36, 2008, pp. 4356–4362.
- [21] National Research Council and National Academy of Engineering. “The Hydrogen Economy, Opportunities, Costs, Barriers, and R&D Needs”. 2004. *National Academies Press*. ISBN: 0-309-09163-2.
http://www.nap.edu/catalog.php?record_id=10922 Last checked on 29th April 2012.
- [22] European Commission Research and Innovation.
“Fuel Cell and Hydrogen (FCH) Energy Technologies”.

http://ec.europa.eu/research/energy/eu/research/fch/index_en.htm

Last checked as at 23rd April 2012.

[23] “Electrification of Future Mobility-National Programs and Activities in Germany. Hydrogen & Fuel Cells and Battery Technologies”.

http://www.hydrogen.energy.gov/pdfs/review09/6_bonhoff_2009_amr.pdf

Last checked on 23rd April 2012.

[24] The US DoE Hydrogen and Fuel Cells Program.

<http://www.hydrogen.energy.gov/>

<http://www1.eere.energy.gov/hydrogenandfuelcells/mypp/#>

Checked on 23rd April 2012.

[25] Canadian Hydrogen and Fuel Cell Association. <http://www.h2fcc.ca/>

Checked as at 23rd April 2012.

[26] World Energy Network.

http://www.ena.or.jp/WE-NET/contents_e.html Checked as at 23rd April 2012.

[27] Marcello Contestabile. “Critical Review of the State of the Art and International Development Targets for Selected Hydrogen Production and Delivery Technologies”.

<http://www.standrews.ac.uk/media/M3.1%20Review%20of%20state%20of%20the%20art%20and%20targets%20Dec%202009.pdf> Checked on 29th April 2012.

[28] Ki DTU, Risoe DTU, DONG Energy. “Pre-Investigation of Water Electrolysis”. <130.226.56.153/rispubl/NEI/NEI-DK-5057.pdf> Webpage no longer available.

[29] Timothy Lipman. “An Overview of Hydrogen Production and Storage Systems with Renewable Hydrogen Case Studies”.

<http://www.cleanenergystates.org/assets/2011-Files/Hydrogen-and-Fuel-Cells/CESA-Lipman-H2-prod-storage-050311.pdf> Checked on 23rd April 2012.

[30] Worldwide Hydrogen Fuelling Stations.

<http://www.fuelcells.org/info/charts/h2fuelingstations.pdf>

Checked on 23rd April 2012

- [31] Government-Grants.co.uk. “15% of Total Energy from Renewables by 2020”.
<https://www.government-grants.co.uk/wind-turbines.shtml>
Checked on 23rd April 2012.
- [32] Hugh Sharman, Incoteco, John Constable. “Electricity Prices in the United Kingdom Fundamental Drivers and Probable Trends”.
<http://www.ref.org.uk/attachments/article/139/jc.hs.pricing.22.05.08.pdf>
Checked on 29th April 2012.
- [33] Leonard Wagner. “Overview of Energy Storage Methods”.
<http://www.moraassociates.com/publications/0712%20Energy%20storage.pdf>
Website no longer available.
- [34] R. Gazey, S. K. Salman, D. D. Aklil-D’Halluin. “A Field Application Experience of Integrating Hydrogen Technology with Wind Power in a Remote Island Location”. *Journal of Power Sources*. Vol. 157, 2006, pp. 841–847.
- [35] Øystein Ulleberg, Torgeir Nakken, Arnaud Ete´.
“The Wind/Hydrogen Demonstration System at Utsira in Norway: Evaluation of System Performance using Operational Data and updated Hydrogen Energy System Modeling Tools”.
International Journal of Hydrogen Energy. Vol. 35, 2010, pp. 1841-1852.
- [36] Agbossou K., Chahine R., Hamelin J., Laurencelle F., Anouar A., St-Arnaud J.M., Bose T.K. “Renewable Energy Systems based on Hydrogen for Remote Applications”. *Journal of Power Sources*. Vol. 96, 2006, pp. 168–72.
- [37] Gazey R., Salman S.K., Aklil-D’Halluin D.D. “A Field Application Experience of Integrating Hydrogen Technology with Wind Power in a Remote Island Location”. *Journal of Power Sources*. Vol. 157, 2006, pp. 841–847.
- [38] Harrison K.W., Kroposki B., Pink C. “Characterising Electrolyser Performance for use in Wind Energy Applications”.
<http://www.nrel.gov/hydrogen/pdfs/40100.pdf> Last checked on 29th April 2012.
- [39] Harrison K.W., Martin G. D. “Renewable Hydrogen: integration, Validation, and Demonstration”. <http://www.nrel.gov/docs/fy08osti/43114.pdf>
Last checked on 29th April 2012.
- [40] Varkaraki E., Tzamalis G., Zoulias E. “Operational Experience from the RES2H2 Wind-Hydrogen Plant in Greece”.
<http://www.whec2008.com/abstract/305.asp> Last Checked on 29th April 2012.
- [41] The Hydrogen Road of Norway (HyNor). <http://hynor.no/en/>
Checked on 23rd April 2012.

- [42] European Fuel Cell Forum.
<http://www.efcf.com/reports/E04.pdf..round> Checked on 25th April 2012.
- [43] Colleen S. Spiegel. "Designing & Building Fuel Cells". 2007. New York: *McGraw Hill*. ISBN: 0-07-148977-0.
- [44] Etienne Bernier, Jean Hamelin, Kodjo Agbossou, Tapan Bose. "Electric Round-Trip Efficiency of Hydrogen and Oxygen-based Energy Storage". *International Journal of Hydrogen Energy*. Vol. 30, 2005, pp. 105-111.
- [45] IEA. "World Energy Outlook".
<http://www.worldenergyoutlook.org/> Last checked on 24th April 2012.
- [46] Johanna Ivy. "Summary of Electrolytic Hydrogen Production".
<http://www.nrel.gov/hydrogen/pdfs/36734.pdf> Last checked on 29th April 2012.
- [47] Leanne M. Crosbie. "Hydrogen Production by Nuclear Heat".
<http://www.mpr.com/news-and-publications/white-papers/H2-from-Nuclear.pdf>
Checked as at 24th April 2012.
- [48] Hydrogenics. "HyLYZER" Product Literature.
<http://www.hydrogenics.com/> Checked as at 24th April 2012.
- [49] Frank Menzl. "Windmill-Electrolyser System for Hydrogen Production at Stralsund".
<http://www.docstoc.com/docs/47170281/WINDMILL---ELECTROLYSER-SYSTEM-FOR-HYDROGEN-PRODUCTION-AT-STRALSUND>
Checked as at 24th April 2012.
- [50] National Renewable Energy Laboratory. "Technology Brief: Analysis of Current-Day Commercial Electrolysers".
<http://www.nrel.gov/docs/fy04osti/36705.pdf> Checked as at 24th April 2012.
- [51] Elektrolyse Technik. "Pressure Electrolyser based on the Lurgi System".
<http://www.elektrolyse.de/vkp/modules.php?name=Content&pa=showpage&pid=3>
Checked on 24th April 2012.
- [52] Oliver Weinmann. "Hydrogen-The Flexible Storage for Electrical Energy". *Power Engineering Journal*. Vol. 13, 1999, pp. 164-170.
- [53] S. Stucki, G. G. Scherer, S. Schlagowski and E. Fischer. "PEM Water Electrolysers: Evidence of Membrane Failure in 100kW Demonstration Plants". *Journal of Applied Electrochemistry*. Vol. 28, 1998, pp. 1041-1049.
- [54] Hydrogen Technologies. "World Leader in Electrolysis for Hydrogen Solutions". <http://www.rtsafrica.co.za/StatoilHydro.pdf>
Checked on 24th April 2012

- [55] Richard Bourgeois P.E. “Advanced Alkaline Electrolysis”.
http://www.hydrogen.energy.gov/pdfs/review06/pd_8_bourgeois.pdf
Checked on 29th April 2012.
- [56] Ph. Vermeiren, W. Adriansens, J. P. Moreels, R. Leysen. “Evaluation of the Zirfon® Separator for use in Alkaline Water Electrolysis and Ni-H₂ Batteries”.
International Journal of Hydrogen Energy. Vol. 23, 1998, pp. 321-324.
- [57] Dana Swalla. “Advanced Alkaline Electrolysis”.
http://www.hydrogen.energy.gov/pdfs/review08/pdp_14_swalla.pdf
Checked on 29th April 2012.
- [58] N. Lymberopoulos. “Hydrogen Production from Renewables”.
http://ec.europa.eu/energy/efficiency/studies/doc/industry/res_hydrogen.pdf
Checked on 5th September 2011.
- [59] Varkaraki E., Lymberopoulos N., Zoulias E., Kalyvas E., Christodoulou C., Vionis P., Chaviaropoulos P. “Integrated Wind-Hydrogen Systems for Wind Parks”.
http://www.storiesproject.eu/docs/Integrated_Wind-H2_Systems_for_Wind_Parks.pdf Checked on 29th April 2012.
- [60] Øystein Ulleberg. “Modeling of Advanced Alkaline Electrolysers: A System Simulation Approach”. *International Journal of Hydrogen Energy*. Vol. 28, 2003, pp. 21-33.
- [61] Kai Zeng, Dongke Zhang. “Recent Progress in Alkaline Water Electrolysis for Hydrogen Production and Applications”.
Progress in Energy and Combustion Science. Vol. 36, 2010, pp. 307-326.
- [62] Bird R.B., Stewart W.E., Lightfoot E.N. “Transport Phenomena”. 2nd ed, 2001. New York: *John Wiley & Sons*. ISBN: 0471410772.
- [63] Oldham K. B., Myland J. C. “Fundamentals of Electrochemical Science”. 1st ed, 1993. San Diego: *Academic Press*. ISBN: 0125255454.
- [64] Philip H. Rieger. “Electrochemistry”. 1987. NJ: *Prentice-Hall International*. ISBN: 0-13-249138-9.
- [65] R. L. Le Roy. “Advanced Unipolar Electrolysis”.
International Journal of Hydrogen Energy. Vol. 6, 1981, pp. 589-599.
- [66] Milica P., Marceta Kaninski, Snezana M. Miulovic, Gvozden S. Tasic, Aleksandar D. Maksic, Vladimir M. Nikolic. “A Study on the Co–W Activated Ni Electrodes for the Hydrogen Production from Alkaline Water Electrolysis – Energy Saving”. *International Journal of Hydrogen Energy*. Vol. 36, No. 9, 2011, pp. 5227-5235.

- [67] C. A. C. Sequeira, D. M. F. Santos, P. S. D. Brito. “Electrocatalytic Activity of Simple and Modified Fe–P Electrodeposits for Hydrogen Evolution from Alkaline Media”. *Energy*. Vol. 36, No. 2, 2011, pp. 847-853.
- [68] Milica P. Marceta Kaninski, Djordje P. Saponjic, Ivana M. Perovic, Aleksandar D. Maksic, Vladimir M. Nikolic. “Electrochemical Characterisation of the Ni–W Catalyst formed in situ during Alkaline Electrolytic Hydrogen Production—Part II”. *Applied Catalysis A: General*. Vol. 405, No. 1–2, 2011, pp. 29-35.
- [69] Kinoshita K. “Electrochemical Oxygen Technology”. 1st ed, 1992. New York: *John Wiley & Sons*. ISBN: 9780471570431
- [70] Derek Pletcher, Xiaohong Li. “Prospects for Alkaline Zero Gap Water Electrolysers for Hydrogen Production”. *International Journal of Hydrogen Energy*. Vol. 36, No. 23, 2011, pp. 15089-15104.
- [71] J. Balajka. “The Testing of Electrodes for Alkaline Solution Water Electrolysis”. *International Journal of Hydrogen Energy*. Vol. 8, No. 10, 1983, pp. 755-762.
- [72] I. ArulRaj, V.K.Venkatesan. “Characterisation of Nickel-Molybdenum and Nickel-Molybdenum-Iron Alloy Coatings as Cathodes for Alkaline Water Electrolysers”. *International Journal of Hydrogen Energy*. Vol. 23, No. 4, 1988, pp. 215-223.
- [73] Gamry Instruments. “Basics of Electrochemical Impedance Spectroscopy”. <http://www.gamry.com/assets/Application-Notes/Basics-of-EIS.pdf>
Last checked on 27th April 2012.
- [74] “Electrochemical Impedance Spectroscopy (EIS): A Powerful and Cost-Effective Tool for Fuel Cell Diagnostics”. <http://www.scribner.com/files/tech-papers/Scribner%20Associates%20-%20Electrochemical%20Impedance%20Spectroscopy%20for%20Fuel%20Cell%20Research.pdf> Last checked on 27th April 2012.
- [75] Norsk hydro A. S. Commercial brochure. “How you can produce hydrogen by electrolysis”. <http://www.nel-hydrogen.com/home/?pid=80>
Last checked on 30th April 2012.
- [76] K. Christiansen and T. Gundt. “Large Scale Hydrogen Production”. *Electrochemical Society*. Vol. 78, No. 4, 1978.
- [77] H. Wullenweber and J. Muller. “Lurgi Pressure Electrolysis”. *Electrochemical Society*. Vol. 78, No. 4, 1978.

- [78] H. Hofmann, G. Luft, H. Wendt. "Advanced Alkaline Water Electrolysis at Enhanced Pressures and Temperatures". Commission European Communities, Report EUR 9406 EN (1984).
- [79] Nunes S. P., Peinemann K. V. "Membrane Technology". 2nd ed, 2007. Weinheim: *John Wiley & Sons*. ISBN: 3527608591.
- [80] Nagai N., Takeuchia M., Kimurab T., Okaa T. "Existence of Optimum Space between Electrodes on Hydrogen Production by Water Electrolysis". *International Journal of Hydrogen Energy*. Vol. 28, 2003, pp. 35-41.
- [81] Celgard. <http://www.celgard.com/specialty-membranes.aspx>
Last checked on 1st September 2012.
- [82] D. P. Gregory, K. F. Blurton and N. P. Biederman. "Economic Criteria for the Improvement of Electrolyser Technology". *Electrochemical Society*. Vol. 78, No. 4, 1978, pp. 54.
- [83] A. J. Appleby, G. Crepy, and J. Jacquelin. "High Efficiency Water Electrolysis in Alkaline Solution". *International Journal of Hydrogen Energy*. Vol. 3, 1978, pp. 21.
- [84] John O' M. Bockris. "Electrochemical Processes" in "Comprehensive Treatise of Electrochemistry". Vol. 2, 1981. *Plenum Press*. ISBN: 0306405032
- [85] M. H. Miles. "Evaluation of Electrocatalysts for Water Electrolysis in Alkaline Solutions". *Electroanalytical Chemistry and Interfacial Electrochemistry*. Vol. 60, 1975, pp. 89 -96.
- [86] Advent Research Materials, <http://www.advent-rm.com/contact/>
Last checked on 30th April 2012.
- [87] M. Pourbaix. "Atlas of Electrochemical Equilibrium in Aqueous Solutions". 1974. Houston: *NACE International*. ISBN: 0915567989.
- [88] P. W. T. Lu and S. Srinivasan. "Advances in Water Electrolysis Technology with Emphasis on use of the Solid Polymer Electrolyte". *Journal of Applied Electrochemistry*. Vol. 9, No. 3, 1979, pp. 269 -283.
- [89] R. L. LeRoy, M. B. I. Janjua, R. Renaud, and U. Leuenberger. "Analysis of Time-Variation Effects in Water Electrolysers". *Journal of Electrochemical Society*. Vol. 126, No. 10, 1979, pp. 1674 -1682.
- [90] P. W. T. Lu and S. Srinivasan. "Electrochemical-Ellipsometric Studies of Oxide Film Formed on Nickel during Oxygen Evolution". *Journal of Electrochemical Society*. Vol. 125, No. 9, 1978, pp. 1416-1422.

- [91] R. L. LeRoy. "Industrial Water Electrolysis: Present and Future". *International Journal of Hydrogen Energy*. Vol. 8, No. 6, 1983, pp. 401-417.
- [92] C. Bailleux. "Advanced Water Alkaline Electrolysis: A two year running of a test plant". *International Journal of Hydrogen Energy*. Vol. 6, 1981, pp. 461-471.
- [93] D. E. Brown, M. N .Mahmood, A. K. Turner, S. M. Hall and P. O. Fogarty. "Low Voltage Electrocatalysts for Hydrogen Evolving Electrodes". *International Journal of Hydrogen Energy*. Vol. 7, 1982, pp. 405- 410.
- [94] J.Z .O. Stachurski, D. Pouli, J. A. Ripa, G. F. Pokrzyk. "Low Overvoltage Hydrogen Cathodes". US. Patent 4,354,915, Oct 19, 1982.
- [95] J. Balej. "Electrocatalysts for Oxygen Evolution in Advanced Water Electrolysis". *International Journal of Hydrogen Energy*. Vol. 10, 1985, pp. 89-99.
- [96] D. E. Hall. "Electrodes for Alkaline Water Electrolysis". *Journal of Electrochemical Society*. Vol. 128, No. 4 ,1981, pp. 740.
- [97] N. Wakabayashi, E. Torikai, Y. Kawami, and H. Takenaka. "Advance Hydrogen Energy 2". *Hydrogen Energy Progress*. Vol. 1, 1981, pp. 59.
- [98] J. Divisek, J. Mergel and H. Schmitz. "Improvement of Water Electrolysis in Alkaline Media at Intermediate Temperatures ". Proceedings of the 3rd World Hydrogen Energy Conference, Tokyo, Japan, Vol. 1, 1980, pp. 209-221.
- [99] Jason C. Ganley. "High Temperature and Pressure Alkaline Electrolysis ". *International Journal of Hydrogen Energy*. Vol. 34, 2009, pp. 3604-3611.
- [100] Chubb T. "Production of Excited Surface States by Reactant Starved Electrolysis". <http://www.lenr-canr.org/acrobat/ChubbTAproduction.pdf>
Last accessed on 30th April 2012.
- [101] A. Garat and J. Gras. "Corrosion Study of Nickel for Alkaline Water Electrolysis". *International Journal of Hydrogen Energy*. Vol. 8, No. 9, 1983, pp. 681- 688.
- [102] A. J. Salkind and U. Falk. "Alkaline Storage Batteries". 1970. New York: *John Wiley & Sons*. ISBN: 0471253626.
- [103] A. C. C. Tseung, J. Botejue. "Some Fundamental and Practical Aspects of Electrocatalysis for Water Electrolysis". *International Journal of Hydrogen Energy*. Vol. 11, No. 2, 1986, pp. 125-127.

- [104] G. E. Stoner and P. J. Moran. In “Proceedings of the Symposium on Industrial Water Electrolysis”. 1978. Princeton, NJ: *The Electrochemical Society*.
- [105] G. L. Cahen, Jr. P. J. Moran, L. L. Scribner, and G. E. Stoner. “Investigation of Nickel Whisker Networks as Electrodes for Hydrogen and Oxygen Evolution”. *Journal of Electrochemical Society*. Vol. 128, No. 9, 1981, pp. 1877- 1880.
- [106] A. J. Appleby, G. Crepy, and J. Jacquelin. “High Efficiency Water Electrolysis in Alkaline Solution”. *International Journal of Hydrogen Energy*. Vol. 3, No. 1, 1978, pp. 21- 37.
- [107] F. Rosalbino, D. Maccio, E. Angelini, A. Saccone, S. Delfino. “Electrolytic properties of Fe-R (R= rare earth metal) Crystalline Alloys as Hydrogen Electrodes in Alkaline Water Electrolysis”. *Journal of Alloys and Compounds*. Vol. 403, 2005, pp. 275-282.
- [108] M. M. Jaksic, M. M. Jakšić. “Electrocatalysis of Hydrogen Evolution in the light of the Brewer—Engel Theory for Bonding in Metals and Intermetallic Phases”. *Electrochimica Acta*. Vol. 29, No. 11, 1984, pp. 1539-1550.
- [109] M .M. Jakšić. “Advances in Electrocatalysis for Hydrogen Evolution in the light of the Brewer-Engel Valence-Bond Theory”. *International Journal of Hydrogen Energy*. Vol. 12, No. 11, 1987, pp. 727-752.
- [110] Luciana S. Sanches, Sergio H. Domingues, Ademir Carubelli and Lucia H. Mascaró. “Electrodeposition of Ni-Mo and Fe-Mo alloys from Sulfate-Citrate Acid Solutions”. *Journal of Brazilian Chemical Society*. Vol. 14, 2003, No. 4, pp. 556-563.
- [111] Podlaha E. J., Landolt D. “Induced Co-deposition”. *Journal of Electrochemical Society*. Vol.143, 1996, pp. 885.
- [112] Podlaha E. J., Landolt D. “Induced Co-deposition”. *Journal of Electrochemical Society*. Vol.143, 1996, pp. 893.
- [113] Podlaha E. J., Landolt D. “Induced Co-deposition”. *Journal of Electrochemical Society*. Vol.144, 1997, pp. 1672.
- [114] Zeng Y., Zelin L., Ming M., Shaomin Z., Yue Zeng, Zelin Li, Ming Ma, Shaomin Zhou. “In situ Surface Raman study of the Induced Codeposition Mechanism of Ni–Mo Alloys”. *Electrochemistry Communications*. Vol. 2, No. 1, 2000, pp. 36-38.
- [115] Chassaing E., Quang K. V., Wiart R. “Mechanism of Nickel-Molybdenum Alloy Electrodeposition in Citrate Electrolytes”. *Journal of Applied Electrochemistry*. Vol. 19, No. 6, 1989, pp. 839 – 844.

- [116] E. Gómez, E. Pellicer, E. Vallés. “Electrodeposited Cobalt-Molybdenum Magnetic Materials”. *Journal of Electroanalytical Chemistry*. Vol. 517, No. 1–2, 2001, pp. 109-116.
- [117] Weikang Hu. “Electrocatalytic Properties of new Electrocatalysts for Hydrogen Evolution in Alkaline Water Electrolysis”. *International Journal of Hydrogen Energy*. Vol. 25, 2000, pp. 111-118.
- [118] J. Divisek, J. Mergel, H. Schmitz. “Advanced Water Electrolysis and Catalyst Stability under Discontinuous Operation”. *International Journal of Hydrogen Energy*. Vol. 15, No. 2, 1990, pp. 105-114.
- [119] J. Divisek, H. Schmitz, B. Steffen. “Electrocatalyst Materials for Hydrogen Evolution”. *Electrochimica Acta*. Vol. 39, No. 11–12, 1994, pp. 1723-1731.
- [120] Milica P. Marceta Kaninski, Djordje P. Saponjic, Vladimir M. Nikolic, Dragana L. Zugic, Gvozden S. Tasic. “Energy Consumption and Stability of the Ni-Mo Electrodes for the Alkaline Hydrogen Production at Industrial Conditions”. *International Journal of Hydrogen Energy*. Vol. 36, 2011, No. 15, pp. 8864-8868.
- [121] Amitava Roy, Simon Watson, David Infield. “A Novel Design of a Low Cost, Robust, Efficient and Dynamic Electrolyser Optimised for Fluctuating and Intermittent Renewable Energy Powered Operation”. http://www.rehydrogen.com/publications_reports.html Last accessed 30th April 2012.
- [122] Ramazan Solmaz, Ali Doner, Gulfeza Kardas. “Preparation, Characterisation and Application of Alkaline Leached CuNiZn Ternary Coatings for Long-Term Electrolysis in Alkaline Solution”. *International Journal of Hydrogen Energy*. Vol. 35, 2010, pp. 10045-10049.
- [123] Ramazan Solmaz, Ali Doner, I. Sahin, A. O. Yuce, G. Kardas, B. Yazici, M. Erbil. “The Stability of NiCoZn Electrocatalyst for Hydrogen Evolution Activity in Alkaline Solution during Long-Term Electrolysis”. *International Journal of Hydrogen Energy*. Vol. 34, 2009, pp. 7910-7918.
- [124] Qing Han, Kuiren Liu, Jianshe Chen, Xujun Wei. “Preparation of the Composite LaNi_{3.7}Al_{1.3}/Ni-S-Co Alloy Film and its HER Activity in Alkaline Medium”. *International Journal of Hydrogen Energy*. Vol. 34, 2009, pp. 71-76.
- [125] Reza Karimi Shervadini, Amir Hossein Alinoori and Ali Reza Madram. “Electrocatalytic Activities of Nickel-Phosphorus Composite Coating Reinforced with Codeposited Graphite Carbon for Hydrogen Evolution Reaction in Alkaline Solution”. *Journal of New Materials for Electrochemical Systems*. Vol. 11, 2008, pp. 259-265.

- [126] H. B. Sufferedini, J. L. Cerne, F. C. Crnkovic, S. A. S. Machado, L. A. Avaca. "Recent Developments in Electrode Materials for Water Electrolysis". *International Journal of Hydrogen Energy*. Vol. 25, 2000, pp. 415-423.
- [127] Denny A. Jones. "Principles and Prevention of Corrosion". Second ed., 1996. NJ: *Prentice-Hall International*. ISBN: 0-13-3599930-0.
- [128] <http://www.astm.org/> Last accessed on 7th August 2012.
- [129] Sigma-Aldrich UK. <http://www.sigmaaldrich.com/united-kingdom.html> Last accessed on 30th April 2012.
- [130] Eddy Current Technology Inc. <http://www.eddy-current.com/condres.htm> Last checked as at 8th September 2011.
- [131] Solmaz R., Döner A., Kardas G. "The Stability of Hydrogen Evolution Activity and Corrosion Behaviour of NiCu Coatings with Long-Term Electrolysis in Alkaline Solution". *International Journal of Hydrogen Energy*. Vol. 34, 2009, pp. 2089-2094.
- [132] Solmaz R., Döner A., Şahin I., Yüce A. O., Kardas G., Yazıcı B., M.Erbil. "The Stability of NiCoZn Electrocatalyst for Hydrogen Evolution Activity in Alkaline Solution During Long-Term Electrolysis". *International Journal of Hydrogen Energy*. Vol. 34, 2009, pp. 7910-7918.
- [133] N. V. Krstajić, V. D. Jović, Lj. Gajić-Krstajić, B. M.jović, A. L. Antozzi, G. N. Martelli. "Electrodeposition of Ni-Mo Alloy Coatings and their Characterisation as Cathodes for Hydrogen Evolution in Sodium Hydroxide Solution". *International Journal of Hydrogen Energy*. Vol. 33, 2008, pp. 3676-3687.
- [134] Stoynov Z, Vladikova D. "Differential Impedance Analysis". 2005. Bulgaria: *Marin Drinov Academic Publishing House*.
- [135] Armstrong R.D., Henderson M. "Impedance Plane Display of Reaction with an Adsorbed Intermediate". *Journal of Electroanalytical Chemistry*. Vol. 39, 1972, pp. 81-90.
- [136] Lasia A., Rami A. "Kinetics of Hydrogen Evolution on Nickel Electrodes". *Journal of Electroanalytical Chemistry*. Vol. 294, 1990, pp. 123-41.
- [137] Birry L., Lasia A. "Studies of the Hydrogen Evolution Reaction on Raney Nickel-Molybdenum Electrodes". *Journal of Applied Electrochemistry*. Vol. 34, 2004, pp. 735-749.

- [138] Brug G.J., Vandeneeden A.L.G., Sluytersrehabach M., Sluyters J.H. “The Analysis of Electrode Impedances Complicated by the Presence of a Constant Phase Element”. *Journal of Electroanalytical Chemistry*. Vol. 176, 1984, pp. 275-95.
- [139] J. Kubisztal, A. Budniok, A. Lasia. “Study of the Hydrogen Evolution Reaction on Nickel-based Composite Coatings containing Molybdenum Powder”. *International Journal of Hydrogen Energy*. Vol. 32, No. 9, 2007, pp. 1211-1218.
- [140] Omar Aaboubi. “Hydrogen Evolution Activity of Ni–Mo Coating Electrodeposited under Magnetic Field Control”. *International Journal of Hydrogen Energy*. Vol. 36, No. 8, 2011, pp. 4702-4709.
- [141] S. Martinez, M. Metikoš-Huković, L. Valek. “Electrocatalytic Properties of Electrodeposited Ni–15Mo Cathodes for the HER in Acid Solutions: Synergistic Electronic Effect”. *Journal of Molecular Catalysis A: Chemical*. Vol. 245, No. 1–2, 2006, pp. 114-121.
- [142] Divisek J., Schmitz H., Balej J. “Ni and Mo coatings as hydrogen cathodes”. *Journal of Applied Electrochemistry*. Vol. 19, No. 4, 1989, pp. 519-530.
- [143] Gala J., Małachowski A., Nawrat G. “Electrolytic Nickel—Molybdenum—Vanadium Alloy Coatings as a Material with a Decreased Hydrogen Overvoltage”. *Journal of Applied Electrochemistry*. Vol. 14, No. 2, 1984, pp. 221- 230.
- [144] Yuliy D. Gamburg, Giovanni Zangari. “Theory and Practise of metal Electrodeposition” 2011. New York: *Springer*. ISBN: 978-1-4419-9668-8.
- [145] H. Reigel, J. Mitrovic, K. Stephan. “Role of Mass Transfer on Hydrogen Evolution in Aqueous Media”. *Journal of Applied Electrochemistry*. Vol. 28, 1998, pp. 10-17.
- [146] A. V. Nikiforov, I. M. Petrushina, E. Christensen, A. L. Tomas-Garcia and N. J. Bierrum. “Corrosion Behaviors of Construction Materials for High Temperature Steam Electrolysers”. *International Journal of Hydrogen Energy*. Vol. 36, 2011, pp. 111-119.
- [147] H. G. Eickhoff, D. Martinsen and M. Walbeck. “A Market Potential and Economic Aspects of a Future Hydrogen Supply for the F.R.G”. *International Journal of Hydrogen Energy*. Vol. 9, 1984, pp. 233-242.
- [148] G. J. Brug, A. L. G. Van den Eeden, M. Sluyters-Rehbach, J. H. Sluyters. “The Analysis of Electrode Impedances Complicated by the Presence of a Constant Phase Element”. *Journal of Electroanalytical Chemistry and Interfacial Electrochemistry*. Vol. 176, No. 1–2, 1984, pp. 275-29

Appendix A

List of Publications, Posters and Presentations

Journal Publications

1. Tamunosaki Graham Douglas, Andrew Cruden, David Infield, Peter Hall, Amitava Roy. "Investigation of molybdenum-(resorcinol-formaldehyde) (Mo-RF) electrode for alkaline electrolyser operation". *International Journal of Hydrogen Energy*. Vol. 36, 2011, pp. 7791-98.
2. Tamunosaki Graham Douglas, Andrew Cruden, David Infield. "Development of an Ambient Temperature Alkaline Electrolyser for Dynamic Operation with Renewable Energy Sources". *International Journal of Hydrogen Energy*. Vol. 38, 2013, pp. 723-739.
3. Andrew Cruden, David Infield, Mahdi Kiaee, Tamunosaki Graham Douglas, Amitava Roy. Development of new materials for alkaline electrolysers and investigation of the potential electrolysis impact on the electrical grid. *Journal of Renewable Energy*. Vol.49, 2013, pp.53-57.

Conference Publication

1. Tamunosaki Graham Douglas, Andrew Cruden, David Infield, Peter Hall, Amitava Roy. "Investigation of molybdenum-(resorcinol-formaldehyde) (Mo-RF) electro-catalyst for alkaline electrolyser reaction". HYSYDAYS 3rd World congress, Turin Italy, October 2009.

Posters

1. Dr.Andrew Cruden, Prof.David Infield, Mahdi Kiaee, Tamunosaki Douglas. Hydrogen production with electrolysers. All Energy Conference and Exhibition, Aberdeen, May 2010.
2. Dr.Andrew Cruden, Prof.David Infield, Mahdi Kiaee, Tamunosaki Douglas, Daniel Chade. Alkaline electrolysers and their role in the performance improvement of electrical grid. SuperGen Hydrogen-delivery industry day, Birmingham, September 2011.

External presentations and reports

1. Tamunosaki Douglas. Interim presentation on project objectives. SuperGen Hydrogen-delivery consortium meeting, Leeds, May 2009.
2. Tamunosaki Douglas. Sustainable hydrogen by alkaline water electrolysis. SuperGen Hydrogen-delivery consortium meeting, Glasgow, September 2009.

3. Tamunosaki Douglas. Low temperature electrolysis development. Scottish Hydrogen and fuel cell consortium meeting, St Andrews, February 2010.
4. Tamunosaki Douglas and Mahdi Kiaee. Investigation of low-cost and high performance electrode catalyst material for alkaline electrolyzers and the impact of alkaline electrolyzers on the electrical grid. SuperGen Hydrogen-delivery consortium meeting, Cardiff, May 2010.
5. Tamunosaki Douglas. Development of alkaline electrolyzers (Comparing between closed and open system of operation). SuperGen Hydrogen-delivery consortium meeting, Cambridge, September 2010.
6. Tamunosaki Douglas. Development of efficient alkaline electrolyzers and investigation of their impact on the electrical grid. SuperGen Hydrogen-delivery consortium meeting, St Andrews, June 2011.
7. Tamunosaki Douglas. Development of the alkaline electrolyser for dynamic operation with renewable energy systems. SuperGen Hydrogen-delivery consortium meeting, London, March 2012.

Appendix B

How to Calculate Geometric Surface Area of the Mesh Electrode and Electrical Resistance of the Wires

The physical dimensions of a stainless steel (SS) mesh can be provided by a commercial supplier as:

Product code	Name-type	Form	No of mesh per inch	Description/Physical dimensions
FE6210	SS-304	Mesh	100	1550 sq.cm, Wire diameter 0.1mm, Aperture 0.15mm, Open area 37%, Purity 99%.

If $n = 100$ mesh per inch

It should be noted that n means there are 100 wires in one linear inch (25.4 mm) of the mesh. Thus there are 99 ($n - 1$) numbers of holes in one linear inch of the mesh.

Let wire diameter $d1 = 0.1$ mm

Length of wire in one linear inch of the mesh is;

$$l = n \times d1 = 10 \text{ mm} \dots\dots\dots 1$$

Size of one hole in one linear inch of the mesh is;

$$H = \frac{(25.4 - l)}{(n - 1)} = 0.155 \text{ mm} \dots\dots\dots 2$$

Therefore linear distance of one wire and one hole is;

$$L1 = d1 + H = 0.255 \text{ mm} \dots\dots\dots 3$$

Based on equation 4 this is equivalent to 39.20 cm which is also numbers of wires and hole in 1cm linear distance of the mesh.

$$L2 = \frac{10 \text{ mm}}{L1} = 39.20 \text{ cm} \dots\dots\dots 4$$

The density of wire is determined based on equation 5 which is total numbers of wires per unit area of the mesh.

$$D = \frac{2 \times L2}{cm^3} = \frac{78.43 \text{ wires}}{cm^2} \dots\dots\dots 5$$

Assuming the circular shape mesh electrode has diameter of 20mm, wire length $L3 = 20 \text{ mm}$. Surface area of one strand of wire is estimated based on equation 6 which is area of half side of a cylinder excluding its top and bottom sections.

$$A1 = \pi \times \left(\frac{d1}{2}\right) \times L3 = 3.143 \text{ mm}^2 \dots\dots\dots 6$$

Therefore geometric surface area of 1 cm^2 of mesh is product of surface area of one strand of wire and density of wire as expressed in equation 7.

$$A2 = D \times A1 \text{ (in cm}^2\text{)} = 2.465 \text{ cm}^2 \dots\dots\dots 7$$

Assuming resistivity is $\rho = 6.897 \text{E-}04 \text{ } \Omega\text{-mm}$ for the SS metal. Electrical resistance of one strand of wire is estimated based on equation 8.

$$R1 = \frac{\rho(\Omega\text{-mm}) \times L3(\text{mm})}{A1(\text{mm}^2)} = 0.0044 \text{ } \Omega \dots\dots\dots 8$$

Therefore electrical resistance of 1 cm^2 of SS mesh is product of density of wire and resistance of one strand of wire as estimated in equation 9.

$$R2 = D \times R1 = 0.345 \text{ } \Omega / \text{cm}^2 \dots\dots\dots 9$$

